UNIVERSITY OF SOUTHAMPTON
Faculty of Engineering and Applied Science
Department of Electronics and Computer Science

Adaptive Full Response Digital Modulation for Wireless Communication Environments

by

Jeffery Mark Torrance
B.Sc., M.Sc.

A Doctoral Thesis submitted in partial fulfilment of the requirements for the award of Doctor of Philosophy at the University of Southampton

March 1997

SUPERVISOR: Dr. Lajos Hanzo
M.Sc., Ph.D, SMIEEE

UNIVERSITY OF SOUTHAMPTON

ABSTRACT

FACULTY OF ENGINEERING AND APPLIED SCIENCE
DEPARTMENT OF ELECTRONICS AND COMPUTER SCIENCE

Doctor of Philosophy

Adaptive Full Response Digital Modulation for Wireless Communication Environments

by Jeffery Mark Torrance

In this thesis the performance of coherently detected Binary Phase Shift Keying (BPSK), Quaternary Phase Shift Keying (QPSK) as well as Square 16 and 64 Quadrature Amplitude Modulation (QAM) are considered as benchmark transmission schemes, and are referred to as fixed modulation schemes. Their performance is evaluated over narrow-band channels, with and without the presence of interference. Interference cancellation is considered for the interfered scenarios. The fixed schemes are compared with an adaptive modulation scheme that switches between various transmission modes depending upon the channel conditions. The transmission modes are 'No Transmission', BPSK, QPSK, Square 16 and 64 QAM and it is proposed that the channel conditions are estimated exploiting the reciprocal nature of a slow fading Time Division Duplex (TDD) channel. An optimised adaptive scheme yields up to 7 dB E_b/N_0 and 18 dB E_b/N_0 benefit over fixed modulation schemes across slow Rayleigh fading channels for Bit Error Rates (BER) of 1×10^{-2} and 1×10^{-4}, respectively, in the absence of interference. It is shown that when latency is constrained to 30 ms and a statistical multiplex algorithm is deployed, the adaptive scheme can support 25% more multi-media users than a fixed modulation scheme, with an additional reduction in BER by as much as 1.5 orders of magnitude.

By exploiting adaptive modulation and cancellation of the interference from a single co-channel interferer, it is shown that average BERs of 1×10^{-2} and 1×10^{-4} may be achieved over slow Rayleigh fading channels in the presence of 10 and 20 dB Signal to Interference Ratio (SIR), respectively, for average channel SNRs from 0 to 50 dB. A modified TDD technique, incorporating passive reception, is detailed. This strategy would allow adaptive modulation to be incorporated into the proposed third generation Universal Mobile Telecommunications System (UMTS) protocols. It is shown that Adaptive modulation, in an indoors environment, would achieve its upper-bound performance for mobile speeds below 4.5 ms^{-1}.

Acknowledgements

I would like to thank my supervisor Dr. Lajos Hanzo for his continual help, enthusiasm and encouragement during my research and during the preparation of this thesis. I am also grateful to all my colleagues in the Communications Group for their friendship and their help. In particular the following members of staff: Professor Raymond Steele for providing interesting input on the direction of mobile radio research, Mr. David Stewart and Dr. Hristo Strelouhov for their interest and guidance upon radio issues, and Mr. Steve Braithwaite for being a source of information regarding practical communication systems. I would also particularly like to thank the following fellow students: Thomas Keller for providing channel measurements and generally discussing modulation issues, Terry Mitchell and Jason Woodard for the help they gave me with some of the mathematical problems I encountered, Juergen Streit and Peter Cherriman for computer support, and finally Micky Mehta and Chris Hayler for their thoughts on communications in general.

Thanks to Stephanie and Thomas for their considerable assistance in the preparation of this thesis and doing all the things that *Linux-Ispell* cannot manage.

I must also thank the Engineering and Physical Science Research Council (EPSRC) for their financial support of my work and the members of the ACTS-FIRST consortium who gave such useful feedback about my research.

Finally thanks to my parents, Joy and Chris, for all their support during my studies.

List of Publications

The following publications have been made as a result of this research:

1. **J. M. Torrance and L. Hanzo** "Comparative study of Pilot Symbol Assisted Modem Schemes", in the Proceedings of the IEE Sixth International Conference on Radio Receivers and Associated Systems, Bath on 26-28 September 1995, pages 36-41.

2. **J. M. Torrance, T. Keller and L. Hanzo** "Multi-level modulation in the indoors leaky feeder environment", in the Proceedings of the IEEE 46^{th} Conference on Vehicular Technology, 28 April - 1 May 1996 Atlanta, pp 1554-1558.

3. **J.P. Woodard, J. M. Torrance and L. Hanzo** "A Low-Delay Multi-mode Speech Terminal", in the Proceedings of the IEEE 46^{th} Conference on Vehicular Technology, 28 April - 1 May 1996 Atlanta, pp 213-217.

4. **J. M. Torrance and L. Hanzo** "On the upper-bound performance of adaptive modulation in a slow Rayleigh fading channel", IEE Electronics Letters, April 1996, pp 169-171.

5. **J. M. Torrance and L. Hanzo** "Optimisation of Switching Levels for Adaptive Modulation in a Slow Rayleigh Fading Channel", IEE Electronics Letters, June 1996, pp 1167-1169.

6. **J. M. Torrance and L. Hanzo** "Demodulation Level Selection in Adaptive Modulation", IEE Electronics Letters, September 1996, pp 1751-1752.

7. **J. M. Torrance and L. Hanzo** "Performance Upper Bound of Adaptive QAM in Slow Rayleigh Fading Environments", in the Proceedings of IEEE ISPACS 96, Singapore, on 25-29 October 1996, pages 6153-1657.

8. **J. M. Torrance and L. Hanzo** "Adaptive modulation in slow Rayleigh fading Channel", in the Proceedings of IEEE PIMRC 96, Taipei, Taiwan, ROC on 15-18 October 1996, pages 497-501.

9. **J. M. Torrance, D Didascalou and L. Hanzo** "The potential and limitations of Adaptive modulation over slow Rayleigh fading Channel", in the Proceedings of IEE Colloquium on The Future of Mobile Multimedia Communications, Digest Number 1996/248 on 6 December 1996, pages 10/1-10/6.

10. **J. M. Torrance and L. Hanzo** "Latency Considerations for Adaptive Modulation in Slow Rayleigh fading Channel", in the Proceedings of IEEE VTC 97, Phoenix, Arizona on 4-7 May 1997.

11. **J. M. Torrance and L. Hanzo** "Statistical Multiplexing for Mitigating Latency in Adaptive Modems", submitted to the Proceedings of IEEE PIMRC 97, to be held in Helsinki, Finland in September 1997.

12. **J. M. Torrance and L. Hanzo** "Latency and Networking Aspects of Adaptive Modems over Slow Indoors Rayleigh Fading Channels", submitted to the IEE Proceeding on Communications.

13. **J. M. Torrance and L. Hanzo** "Interference Cancellation for adaptive modems in slow Rayleigh fading Environments", submitted to the IEEE Transactions on Vehicular Technology.

Contents

Abstract i

Acknowledgements ii

List of Publications iii

1 Introduction 7

1.1 Introduction 7

1.2 Mobile Radio Communications 7

1.2.1 First Generation 9

1.2.2 Second Generation 9

1.2.3 Third Generation 9

1.3 Organisation of Thesis 10

1.4 Associated Issues 12

2 Mobile Radio Channels 14

2.1 Introduction 14

2.2 Receiver Noise 16

2.3 Path Loss 16

2.3.1 Outdoors 17

2.3.2 Indoors 17

2.3.2.1 Bellcore Model 17

2.3.2.2 Ericsson Model 19

2.4 Fast Fading . . . 19
2.4.1 Rayleigh Fading . . . 20
2.4.1.1 Rayleigh Distribution . . . 20
2.4.1.2 Rician Distribution . . . 21
2.4.1.3 Spectrum of Fading Channel . . . 23
2.4.1.4 Autocorrelation . . . 24
2.4.1.5 Level Crossing Rate . . . 24
2.4.1.6 Average Fade Duration . . . 24
2.4.1.7 Systems . . . 24
2.4.2 Simulation of Rayleigh Fading . . . 25
2.4.2.1 Jakes' Method . . . 25
2.4.2.2 Quadrature Noise Source . . . 26
2.4.2.3 Comparison of Jakes' Method with Quadrature Noise Simulation . . . 27
2.5 Wide-band Channels . . . 37
2.5.1 Typical Wide-band Channels . . . 37
2.5.2 Measurement of Wide-band Channels . . . 37
2.5.3 Simulation of Dispersion . . . 38
2.6 Leaky Feeders . . . 38
2.6.1 Experimental Measurements . . . 39
2.6.2 Modelling . . . 39
2.6.2.1 Post Processing Results . . . 41
2.6.2.2 Calculation of Mean delay, D and RMS delay spread, Δ . . . 45
2.7 Conclusions . . . 45

3 Coherent and Non-coherent Modulation **47**

3.1 Introduction . . . 47
3.1.1 Square Constellations . . . 48
3.1.2 Star Constellations and Differential Encoding . . . 48

3.2 Modulation Performance in Gaussian Channels 50
3.2.1 Coherent Detection 50
3.2.2 Non-coherent Detection 51
3.2.2.1 Decision Directed 53
3.2.2.2 Reduced Minimum Distance Constellation 53
3.3 Block Codes 53
3.4 Coherent Modulation in Rayleigh Channels 55
3.4.1 PSAM Overview 57
3.4.2 Comparison of PSAM Techniques 58
3.4.2.1 Linear Interpolation 60
3.4.2.2 Low-pass Interpolation 60
3.4.2.3 Polynomial Interpolation 60
3.4.2.4 Cavers Interpolation 61
3.4.3 Simulation Lengths 63
3.4.4 Simulation Parameters 65
3.4.5 Results and Discussion 66
3.4.6 Transparent Tone In Band 72
3.5 Non-coherent Modulation in Rayleigh Channels 73
3.6 Conclusions 74

4 Adaptive Modulation - Numerical **76**

4.1 Introduction 76
4.2 System Overview 77
4.2.1 Transmission Integrity versus Capacity 79
4.3 Upper-bound Performance 81
4.3.1 Assumptions 81
4.3.2 Development of Theory 83
4.3.2.1 Solution of BER integrals 83
4.3.3 Average upper-bound performance in Rayleigh fading 84

4.3.4 Upper-bound Performance in Rician Fading 87
4.3.5 Upper-bound Performance in a Gaussian channel 92
4.3.6 Level Switching 93
4.4 Comparison with Fixed Schemes 100
4.4.0.1 Fixed Modulation 103
4.4.0.2 Adaptive modulation 103
4.4.0.3 Dual mode air interface 104
4.5 Conclusions 105

5 Interference **107**
5.1 Introduction 107
5.2 Band-limited Signalling 108
5.2.1 Impulse Response Truncation 111
5.3 Multi-user Interference - Fixed Modulation Schemes 114
5.3.1 Co-Channel Interference 114
5.3.1.1 Gaussian Channel 116
5.3.1.2 Fading Signal and Fading Interference 124
5.3.2 Adjacent Channel interference 125
5.3.3 Comparison of ACI and CCI in Fixed Modulation Schemes 130
5.3.3.1 Gaussian Channel 130
5.3.3.2 Rayleigh Channel 132
5.4 Multi-user Interference - Adaptive Modulation Schemes 135
5.4.1 Impact of interference upon channel estimate 135
5.4.2 Re-optimisation 140
5.4.2.1 Intuitive Threshold Adjustment 146
5.5 Interference Cancellation 148
5.5.1 Introduction 148
5.5.2 Principle of Operation 148
5.5.3 Fixed Schemes 149

5.5.3.1 Theoretical performance of BPSK with interference cancellation 150
5.5.3.2 Theoretical performance of QPSK with interference cancellation 152
5.5.3.3 Simulated Performance with channel estimation 153
5.5.3.4 Rayleigh Channel Performance using channel estimation . . 155
5.5.4 Adaptive Schemes 159
5.6 Channel Capacity 164
5.7 Conclusion 166

6 Network Layer Considerations **169**

6.1 Introduction 169
6.2 Buffering 169
6.3 Simulation Model 170
6.4 Experimental Frame-work 175
6.5 Single Slot performance 175
6.6 Frequency Hopping 179
6.7 Statistical Multiplexing 180
6.7.1 Implementation 182
6.8 Burst Capture and Assisted Capture 189
6.9 Comparison with fixed modulation, using block coding 191
6.9.1 Background 191
6.9.2 Fixed Scheme 192
6.9.2.1 Interleaved Block-codes 193
6.9.2.2 Performance Evaluation 193
6.9.3 Adaptive Scheme 194
6.9.3.1 Performance Evaluation 195
6.10 Conclusions 200

7 Modulation Scheme Selection and Signalling **202**

7.1 Introduction 202

7.2 Modulation Scheme Selection 202
7.2.1 Channel variation between estimation and transmission 203
7.2.2 Channel measurement 206
7.2.2.1 Error Detection 208
7.3 Pre-decoding frame type decision 209
7.3.1 Single PSK Symbol 209
7.3.2 Majority Decision 210
7.3.3 Discrete Walsh Codes 212
7.3.4 Uneven Error Protection 214
7.3.4.1 Optimisation 214
7.4 Conclusions 218

8 Conclusions and Suggestions for Further work **221**
8.1 Introduction 221
8.2 Summary and Conclusions 221
8.3 Suggestions for further work 225

Glossary **226**

Bibliography **231**

Chapter 1

Introduction

1.1 Introduction

This introductory Chapter gives an overview of mobile communications, where it is coming from, and some of the possible future developments. An outline of the research work reported in this thesis is then discussed, in terms of how it may be seen in the context of the future of mobile radio communications. Clearly, the scope for investigation is enormous and this introductory Chapter defines the bounds of the research. Furthermore, it highlights issues that could be considered particularly relevant to the material covered in the thesis that were not explored during the course of the research.

1.2 Mobile Radio Communications

Mobile radio communications is an umbrella for a gamut of services. These various services, from a user's perspective, have characteristics which make them differ each from other. The characteristics include the type of information that is transmitted, the direction of the information flow, the portability in terms of mobile velocity, coverage area and the security of the information that is transmitted; they are discussed briefly and exemplified below:

- **Speech, Audio, computer data or video:** Cellular radio telephony is an example of a speech service, although in modern cellular services, for example GSM, computer data transfer is also possible. Hifi quality audio is carried by the European Digital Audio Broadcasting system and, at least in principle, a television service could be received in a slowly time-variant mobile environment.

- **Simplex, half duplex, balanced full-duplex or un-balanced duplex:** Broadcast radio can be considered as a simplex service, Citizen's Band radio as a half duplex service and cellular radio telephony as a balanced full-duplex service. Future mobile radio schemes may transmit requests for data, these requests may be approximately 100 bytes pointing to a file in a database. The reply could be of the order of MBytes; such a system would support nomadic Web browsing.

- **Portable, slow or fast moving:** Wireless Local Area Networks (LAN) represent an example of a portable mobile radio service, indoors cordless telephony would be an example of a service that would be required to operate in a slow moving environment and broadcast radio an example of a service required to operate in a fast moving environment.

- **Indoors, Local, National, Continental or Global radio coverage:** Indoors coverage may include future services for data, speech or video transmission either in an office environment or over the floors of a manufacturing plant. Local radio coverage is the sort of service required by taxi cab companies, which could cover a greater metropolitan area, or a town and neighbouring villages. The service offered by early cellular providers was generally approaching national coverage in countries like the United Kingdom. Later cellular services, for example GSM, have been standardised for use in many countries and future telephony services may offer coverage globally.

- **Secure and Insecure Service:** Some mobile radio services require security, mobile telephony for example, while others are intended to be insecure, in the sense that as many people will receive them as possible, for example commercial broadcast radio stations.

Users view the apparatus or system that delivers one service quite separately from another, because the features that characterise each of the services are different. However, from a mobile radio engineer's perspective, if all the characteristics listed above could be incorporated into one standard, then one intelligent piece of apparatus could support global mobile radio multi-media communications. There would be many benefits from such a convergence of systems compared with the current ad hoc combinations of analogue and digital telephony and broadcast, satellite and terrestrial systems. Examples of such benefits would include the proliferation of novel mobile radio services and global economies of scale associated with mobile and network apparatus manufacture.

The standardisation of all mobile radio communication services may be ten to fifteen years away, however, the convergence of mobile cellular telephony systems is the subject of considerable research in Europe, Japan and the United States of America. These telephony systems will support voice communications but also other forms of information and it is a sub-set of this future system with which this thesis is concerned. In order to understand this, so-called third generation systems and the earlier first and second generation [1] systems are discussed.

1.2.1 First Generation

First generation systems included, among others, Total Access Communications System (TACS) for use in the UK and Advanced Mobile Phone System (AMPS) in the USA. These systems transmitted analogue speech using analogue Frequency Modulation (FM). They used Frequency Division Duplex (FDD) and Frequency Division Multiple Access (FDMA). The coverage of the first generation systems was largely restricted to one country and there was very little capacity to transmit anything other than speech. TACS was introduced to the UK in about 1985 and is still operating, although the system capacity may now be reduced so that the radio spectrum can be used by second generation systems.

1.2.2 Second Generation

Second generation systems include the Global System for Mobile communications (GSM) that was developed in Europe, as well as Digital AMPS (DAMPS) and Qualcomm Code Division Multiple Access (CDMA) that were developed in the USA. These systems use Digital Signal Processing (DSP) algorithms to code the speech digitally and they exploit digital modulation techniques. Both GSM and DAMPS utilise Time Division Multiple Access (TDMA) and the Qualcomm system uses CDMA. All of the systems use Frequency Division Duplex (FDD). Because the speech is transmitted digitally in the second generation systems, there is the possibility of transmitting digital data, other than speech.

1.2.3 Third Generation

The third generation of cellular systems is referred to as either Universal Mobile Telecommunications System (UMTS) or Future Public Land Mobile Telephone Service (FPLMTS), in Europe or the USA, respectively. While it is not sure what this future system will offer, it is likely to deliver speech and other forms of data, including broad-band services to mobile hand-sets that can be used all over the world. It is likely that the system will be intelligent

enough to determine whether the propagation conditions favour CDMA, FDMA, TDMA, FDD or Time Division Duplex (TDD) at the air-interface. The modulation, and source- and channel-coding schemes are likely to be adaptive on the basis of the nature of the information being transmitted and type of radio coverage and traffic that exists at a particular place at a particular time. UMTS is likely to be standardised before the end of the 20^{th} century and be developed to be backwardly compatible with GSM and allowing flexibility for expansion of functionality as communications and micro-processor technology advance.

Currently a series of pan-European consortia, under the auspices of the Advanced Communications Technologies and Services (ACTS) programme are striving towards UMTS. These include the Future Radio Wide-band Multiple Access Systems (FRAMES) project [2, 3] that is considering the air-interface of the future system. The FRAMES proposals, to date, have been based around the results of two Research in Advanced Communications Equipment (RACE) projects, namely Advanced Time Division Multiple Access [4] (ATDMA) and COde DIvision Test-bed [5] (CODIT). ATDMA proposed using a flexible TDMA air-interface, employing TDD or TDMA depending upon the cell classification. It also proposed changing the modulation scheme based in the channel conditions. CODIT investigated CDMA and FRAMES considers an adaptive air-interface that switches between an ATDMA and CODIT type air-interface.

1.3 Organisation of Thesis

This thesis addresses the issues associated with incorporating a burst-by-burst adaptive modulation scheme into a third generation air-interface. The results presented contribute towards the University of Southampton's involvement in the ACTS Flexible Integrated Radio Systems Technology (FIRST) project. It has already been stated that the UMTS air-interface is likely to vary on the basis of the channel conditions and user requirements. The modulation techniques discussed in this thesis are proposed for inclusion within a UMTS modulation tool box, that is a UMTS radio will be capable of using them, however, will only do so, when it is deemed that they are the most suitable for the given scenario.

- **Chapter 2:** The well known statistics of Rician and Rayleigh channels are presented and two computer simulation methods for the generation of band-limited Rayleigh fading are compared. A more specific channel, that of a leaky feeder to a single antenna in an indoor environment is then considered. A model is proposed for simulating the channel and this is compared with measurements taken and generously made available

by Thomas Keller and Prof. Steele.

- **Chapter 3:** The performance of multi-level modulation with coherent and non-coherent detection is discussed. Initially the Bit Error Rate (BER) performance of differentially and non-differentially encoded modulation schemes are compared over a Gaussian channel with perfect clock recovery and carrier recovery assumed. Results achieved by simulation correspond well to established analytical results. The results of simulating Pilot Symbol Assisted Modulation (PSAM) through Rayleigh fading channels are also presented in Chapter 3. Different interpolation techniques are investigated for estimating the channel between pilot symbols and the results of each technique, over a range of pilot separations and buffer lengths, are given.

- **Chapter 4:** Adaptive coherent modulation is introduced. The chapter develops a novel numerical estimate of the upper-bound performance of such a scheme in a narrow-band Rician channel. The numerical performance in a Rayleigh channel, time-invariant for the duration of a transmission burst, corresponds extremely well to the upper-bound performance achieved by simulation through a Rayleigh fading channel, at pedestrian velocities. The switching thresholds for the adaptive modulation are optimised by using another novel technique. This allows adaptive modulation schemes to be optimised for particular applications, for example speech or computer data transmission. The performance of such schemes was evaluated for the channel over which the optimisation was performed, as well as for other channels. The effect of the optimisation upon the underlying characteristics of the modulation scheme is investigated and the bandwidth efficiency is given.

- **Chapter 5** The effect of band-limiting a Quadrature Amplitude Modulation (QAM) is discussed and the appropriate Nyquist filters for obtaining the band-limiting are investigated. The effects of co- and adjacent-channel interference are evaluated for various QAM schemes, numerically and by simulation, in Gaussian and Rayleigh channels. Adjacent-channel interference is considered for an ATDMA-type system, when fixed or adaptive modulation are employed. The adaptive modulation schemes discussed in Chapter 4 are modified to withstand co-channel interference. This is followed by the introduction of interference cancellation, for a single interferer, with numerical and simulated results. The performance gain for QAM schemes employing interference cancellation, compared to those without cancellation, is given. Finally, the performance of adaptive modulation and fixed modulation are compared when interference cancellation is employed for both.

- **Chapter 6** The latency introduced as a result of employing adaptive modulation in slow fading channels is characterised. The effects of the normalised Doppler frequency, average channel SNR and adaptive switching levels are illustrated. Frequency Hopping and Statistical Multiplexing are proposed to mitigate system latency. The Chapter is concluded with a comparison of the performance of fixed and adaptive modulation assuming a FRAMES-type burst structure, block coding and Statistical Multiplexing without Frequency Hopping.

- **Chapter 7** Channel estimation is evaluated, in terms of how it affects the BER of adaptive modulation. Traditional TDD is considered and compared with a novel approach, referred to as slot-TDD with passive reception. Signalling of the mode of operation in which the adaptive modem is operating is reviewed, with a novel signalling strategy proposed and evaluated.

1.4 Associated Issues

Section 1.2 gives the background to the work that is presented in this thesis and Section 1.3 outlines what research has been conducted. The research presented in this thesis, as outlined in Section 1.3, contributes to one specific area in the field of Mobile Radio Communications. There are many other areas that must be considered. The areas which are most closely related to the research are briefly described below, with appropriate references:

- **Clock Recovery:** Clock recovery obtains the timing of the transmitted symbols such that the received signal level is measured at the most appropriate instant. Failure to sample at the correct time manifests an increase in BER for a given SNR. This issue is addressed in considerable depth by Webb and Hanzo in Reference [6], Chapters 6 and 12, however, throughout this thesis it is assumed that clock recovery is perfect.

- **Carrier Recovery:** Carrier recovery is obtaining the phase reference with which a received signal is to be demodulated. Chapter 3 discusses how the BER performance varies between coherent detection and, non-coherent detection of differentially encoded schemes. However, while pilots are proposed for mitigating the effects of channel fading, the effects of drifting in the local oscillator are not considered.

- **Wide-band Channels and Equalisation:** In Chapter 2 wide-band channels are discussed. However, the performance of the fixed and adaptive modems described in this thesis is considered in narrow-band channels. The performance of fixed QAM in wide-band channels is discussed in Reference [6].

- **Linear Amplification:** Multilevel QAM schemes are dependent upon linear amplification as non-linear amplification results in different amplitude constellation points experiencing different levels of amplification. Power-inefficient linear amplification is particularly undesirable in a mobile environment due to battery life constraints. Further, non-linear amplification results in the spectrum of the transmitted signal spreading, which results in increased adjacent channel interference. More efficient techniques to overcome the non-linear amplification involve pre- or post-distortion [7, 8] or Cartesian feedback amplifiers [9].

Chapter 2

Mobile Radio Channels

2.1 Introduction

According to Jenkins [10], in 1621 Snell announced what is essentially the law of refraction for visible light in an unpublished paper. By 1802 Thomas Young [11] demonstrated diffraction and superposition of visible light. In 1865 Maxwell [12] augmented understanding of electricity and magnetism when he presented the Maxwell equations. In 1905 Einstein [13] showed that the well known but previously unexplained photoelectric effect could be understood, and experimental results precisely modelled, by assuming that electromagnetic radiation possessed particle as well as wave properties. Using the fundamental models of electromagnetism and by understanding fully the propagation environment it is, theoretically, possible to predict the characteristics of a radio communication channel within the confines of the uncertainty principle. However, the positions of every reflector, diffractor or refractor of the radio signal are rarely known. Moreover, the positions of such obstacles are likely to change and complicate the propagation model further. Because of the complexity of a complete model to characterise a mobile radio channel, approximations and assumptions are made.

Throughout this work reciprocity will be assumed for all communication channels. Therefore, if there is a transmitter at a position (X_1, Y_1, Z_1) and a receiver at another position (X_2, Y_2, Z_2), the effect of the channel upon the transmitted radiation is the same as if the receiver was positioned at (X_2, Y_2, Z_2) and the transmitter positioned at (X_1, Y_1, Z_1). This, however, is not the same as assuming that the interference at (X_1, Y_1, Z_1) is the same as that at (X_2, Y_2, Z_2).

Electromagnetic radiation is likely to take many paths from the transmitter to the receiver,

with the radiation from each path arriving at a different time. All the paths will be superimposed with each having different relative phase and amplitude to the others. In extreme cases the receiver would have to move only a small distance and the received signal might vary by 60dB. If the received signal level is considered as a random variable, the auto-correlation of that variable is a function of the mobile velocity.

The fluctuation in received signal [1], resulting from a mobile roaming in an area where there is superposition of electromagnetic radiation from many paths, is referred to as fast fading. There is also slow fading which results from a significant physical obstruction between the transmitter and the receiver. In order to reveal the slow fading the signal power at the receiver must be averaged. This is typically achieved by considering the received power at the mobile as it travels along a path of length between 20 and 200 λ, where λ is the wavelength of the transmitted radio wave. Aggregating the received power over a shorter window would result in the likelihood of fast fading masquerading as slow fading and exploiting a longer window could lead to averaging the effects of the slow fading. Averaging the effect of the fading allows the identification of the path-loss, where the path-loss is an effect of the separation between transmitter and receiver.

Path-loss, fast and slow fading are a function of the position of the transmitter and the receiver and these positions are a function of time in a mobile scenario. Therefore, path-loss and both types of fading can be represented by a single complex variable

$$\eta(t) = f(t) \cdot s(t) \cdot p(t), \tag{2.1}$$

where the path-loss, the fast and the slow fading are individually represented by $p(t)$, $f(t)$ and $s(t)$, respectively. Other mobile effects can be included in the effective mobile velocity of this complex base-band model.

A crucial metric in communications is the relative level of received signal energy to the noise energy at the demodulator, refered to as the Signal to Noise Ratio. This could be computed instantaneously or, more usefully, as the average of a time ensemble. This is dependent upon the channel characteristics, the amplitude of the noise $n(t)$ at the receiver and the transmitted signal amplitude, $l(t)$ and is defined as

$$\gamma = \frac{\langle |l(t-d)|^2 \cdot |\eta(t)|^2 \rangle}{\langle |n(t)|^2 \rangle}. \tag{2.2}$$

The value d is the time delay for the propagation of the electromagnetic radiation from the transmitter to the receiver. The $\langle\rangle$ operator represents the average of the time ensemble. The duration of the ensemble for the calculation of γ is dependent upon what type of SNR

measure is required. Generally it should be sufficiently long for means of both $f(t)$ and $n(t)$ to be taken into account but sufficiently short that variations of $s(t)$ do not have a significant effect on the average calculation. This is considered more deeply in Chapter 6.

Increasing the SNR improves the quality of a communications channel. The transmitted signal level $l(t)$, however, cannot be increased beyond a particular level because of amplifier non-linearities, excessive electromagnetic radiation which can result in biological damage, restricted battery life and the excessive co-channel interference that would be generated in a cellular system. It is, therefore, desirable to characterise the fading and noise features carefully and devise techniques to maximise the data rate and minimise the error rate while preserving bandwidth and avoiding an escalation of system complexity and excessive network infrastructure costs.

The Shannon-Hartley theorem presented in [14] states that for a Gaussian channel the data capacity is directly related to the bandwidth and the SNR by,

$$C = W \cdot \log_2 [1 + \gamma], \tag{2.3}$$

where C is the channel capacity in bits per second, and W is the bandwidth in Hz.

2.2 Receiver Noise

Noise is predominantly generated in two places in a receiver by the thermal excitation of electrons. Initially, noise is generated in the receiving antenna. This noise is amplified in the front end of the receiver and is compounded by the intrinsic noise of the amplifier. The noise is assumed to be uncorrelated and complex normally distributed. For simulation purposes the Box Muller algorithm, published in [15], is used.

2.3 Path Loss

A path loss model is not always important when simulating various modulation schemes. This is because the path loss can often be abstracted into the SNR measurement. However, under certain circumstances, it is useful to have a path loss model. The most simple approximation for signal level path loss in a mobile radio simulation is the free space model,

$$p(r) \propto \frac{\lambda}{4\pi r}. \tag{2.4}$$

The variable for time, t, has been exchanged for r, which is the distance between the transmitter and the receiver. However, accurate representation of the path loss requires a more

sophisticated model. The path loss is dependent upon the propagation environment as well as the radio bearer frequency.

This work focuses on microwave frequencies although recently, millimetre waves [16, 17, 18] have been investigated for high data-rate mobile services. The indoor and outdoor scenarios are considered separately because of the obvious difference in mobility and magnitude of outdoor obstructions, for example mountains and indoor obstructions, for example furniture.

2.3.1 Outdoors

Outdoor loss is dependent upon many diverse parameters. Antenna height can be altered to either reduce the cell size and increase the frequency reuse or to increase the cell size [19]. The propagation terrain can result in heavy and multiple shadowing of certain areas and the radio frequency bearer also has a significant effect upon the path loss. These and other factors have been reviewed recently by Bertoni [20].

2.3.2 Indoors

Motley [21] shows that radio coverage in an office block environment is significantly lower at 1700MHz than it is at 900MHz. Hashemi [22] reviewed the work conducted upon the indoor mobile radio channel and two of the models in his review are investigated. The two models considered here were based upon measurements at around 2GHz.

2.3.2.1 Bellcore Model

Devasirvatham [23] proposed what will be referred to as the Bellcore model. This approach adds an attenuation coefficient, α, to a free space type model. The model is a truncated Gaussian distribution where the mean path loss, $p(r)$, at distance, r, is given by,

$$p(r) = \left[r \cdot 10^{\left(\frac{\alpha \cdot r}{20} + 1.925\right)}\right]^{-1}, \tag{2.5}$$

where α may take values of 0.3, 0.5 or 0.7. The standard deviation, σ, is given by

$$\sigma = 0.2 \cdot p(r) \tag{2.6}$$

and the truncation of the Gaussian distribution is at $\pm 2\sigma$. Figure 2.1 illustrates the mean and $\pm 2\sigma$ range of the Bellcore model for all three values of α.

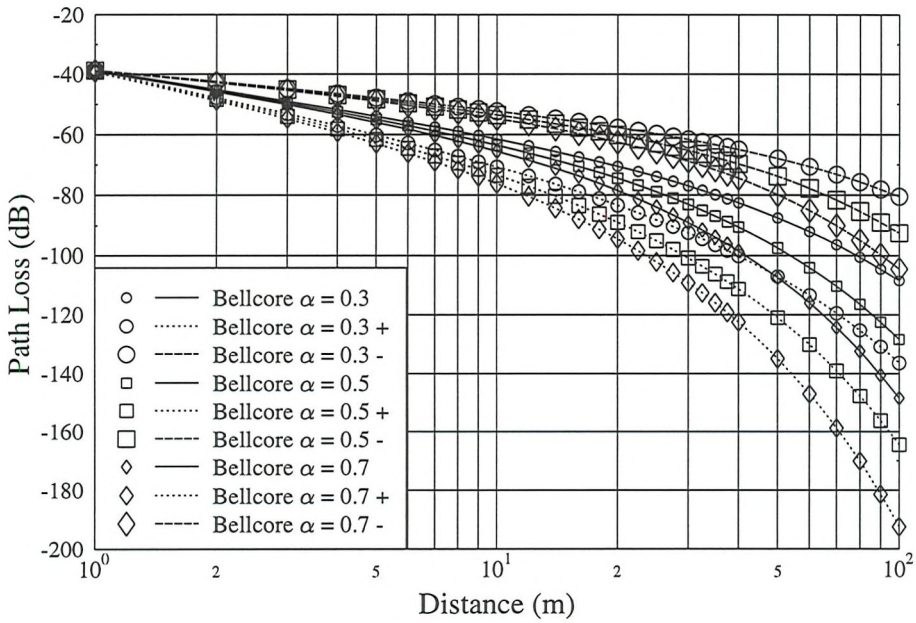

Figure 2.1: Path loss characteristics for Bellcore indoor propagation model at the mean and ± 2 standard deviations for values of $\alpha = 0.3$, 0.5 and 0.7.

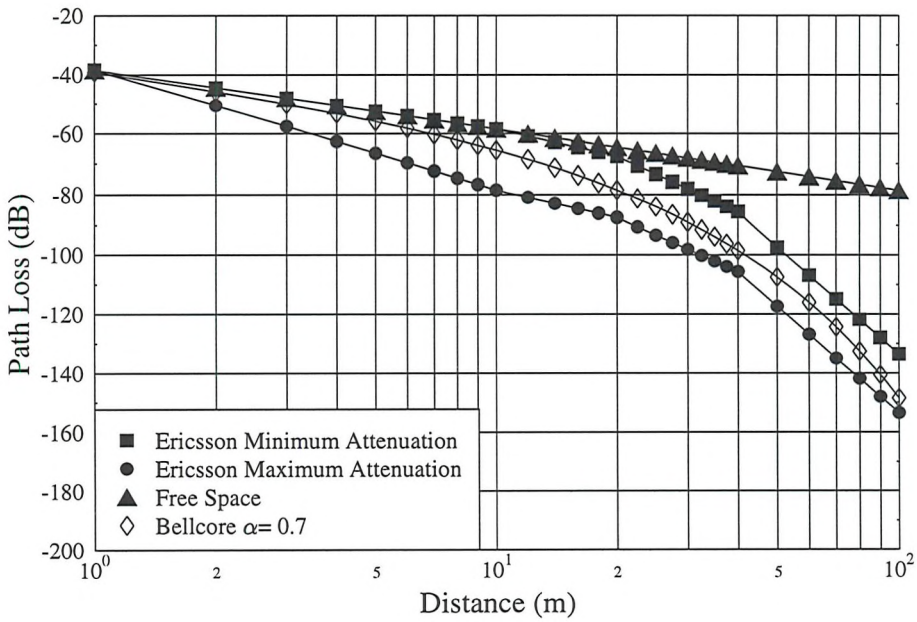

Figure 2.2: Path loss characteristics for upper and lower bounds of the Ericsson indoor propagation model, free space propagation and the Bellcore indoor propagation model mean with α=0.7.

Distance (m)	Min Amp. Path loss	Max Amp. Path loss
$1 < r < 10$	$10^{-1.925} \cdot r^{-1}$	$10^{-1.925} \cdot r^{-2}$
$10 < r < 20$	$10^{-1.425} \cdot r^{-1.5}$	$10^{-2.425} \cdot r^{-1.5}$
$20 < r < 40$	$10^{0.525} \cdot r^{-3}$	$10^{-0.475} \cdot r^{-3}$
$r > 40$	$10^{5.325} \cdot r^{-6}$	$10^{4.325} \cdot r^{-6}$

Table 2.1: The maximum and minimum amplitude path loss as a function of distance for the Ericsson model.

2.3.2.2 Ericsson Model

The Ericsson model was proposed by Akerberg [24] and is illustrated in Table 2.1. Akerberg proposed upper and lower bounds for indoor path losses for the ranges 1m - 10m, 10m - 20m and 20m - 40m. The model is based on measurements taken at 2GHz and Figure 2.2 shows the path losses of the upper and lower bounds for distances 1m - 100m. The free space model is also shown, which is an optimistic estimate. It should be noted that the mean of the Bellcore model with $\alpha = 0.7$ is a good estimate of the centre of the region between the upper and lower bounds of the Ericsson model.

2.4 Fast Fading

The resultant received power of an ensemble of different propagation paths from transmitter to receiver can be statistically evaluated. Initially, a case where all members of the ensemble arrive in a period very much shorter than the symbol period, T, is considered; this is referred to as a narrow-band channel or a frequency non-selective channel. A Rician parameter K can be defined as the ratio of the power in the dominant member of the ensemble to the power of the remaining members, hence,

$$K = \frac{\text{Power in dominant path}}{\text{Power in remaining paths}}. \tag{2.7}$$

As all the radiation tends to travel along the same path, K tends to ∞. This is the least hostile transmission channel and is referred to as a Gaussian channel. When K approaches zero the channel is classified as a Rayleigh channel and the fluctuations in the received signal are most hostile.

2.4.1 Rayleigh Fading

Perfect Gaussian or Rayleigh fading channels are unlikely to exist in reality but they represent an upper and lower bound for narrow-band multi-path channels. The Gaussian channel involves complex additive corruption at the receiver by white Gaussian noise, as discussed in Section 2.2. The Rayleigh fading is complex multiplicative corruption between the transmitter and the receiver. In order to characterise the Rayleigh fading channel fully, the theoretical statistical properties of the channel are considered.

2.4.1.1 Rayleigh Distribution

The sum of the squares of N_f independent Gaussian Random Variables X_i gives a Chi-Squared distribution with N_f degrees of freedom [25]. Therefore, Y is a Chi-Squared Distributed random variable with N_f degrees of freedom if

$$Y = \sum_{i=1}^{N_f} X_i^2. \tag{2.8}$$

The Rayleigh distribution is related to the Chi-Squared distribution with only two degrees of freedom where

$$\overline{X_1} = \overline{X_2} = 0 \tag{2.9}$$

and

$$\sigma^2 = \sigma_{X_1}^2 = \sigma_{X_2}^2; \tag{2.10}$$

$\overline{X_n}$ and $\sigma_{X_n}^2$ denote the mean and variance of X_n, respectively. A complex random variable R can be defined as

$$R = X_1 + jX_2, \tag{2.11}$$

where the amplitude of R is Rayleigh distributed and given by

$$|R| = \sqrt{X_1^2 + X_2^2} \tag{2.12}$$

and the phase of R,

$$\angle R = \arctan\left[\frac{X_2}{X_1}\right]. \tag{2.13}$$

The Probability Distribution Function (PDF) $P_{|R|}(r)$ and the Cumulative Distribution Function (CDF) $C_{|R|}(r)$ of the Rayleigh distribution can be shown to be

$$P_{|R|}(r) = \frac{r}{\sigma^2} \cdot e^{-r^2/2\sigma^2}, r \geq 0, \tag{2.14}$$

$$= 0, r < 0 \tag{2.15}$$

and

$$C_{|R|}(r) = 1 - e^{-r^2/2\sigma^2}, r \geq 0, \tag{2.16}$$

$$= 0, r < 0. \tag{2.17}$$

The PDF for the phase of R can be shown to be uniform:

$$P_{\angle R}(r) = \frac{1}{2 \cdot \pi}, \ -\pi < r \leq \pi. \tag{2.18}$$

A Rayleigh fading channel results in the received signal amplitude being Rayleigh distributed and uniform phase rotation. Therefore, R is a random variable that represents a type of fading found in a Rayleigh mobile radio channel. The k^{th} statistical moment of $|R|$ is given by [25] as,

$$E(|R|^k) = (2\sigma^2)^{k/2}\Gamma(1 + \frac{k}{2}) \tag{2.19}$$

where $\Gamma(p)$ is the gamma function defined as

$$\Gamma(p) = \int_0^\infty t^{p-1} \cdot e^{-t} dt, \ p > 0. \tag{2.20}$$

Equations 2.19 and 2.20 can be used to show that the mean of $|R|$, $\overline{|R|}$ and the variance of $|R|$, $\sigma^2_{|R|}$ are given by

$$\overline{|R|} = \frac{\sqrt{2\pi}\sigma}{2} \tag{2.21}$$

and

$$\sigma^2_{|R|} = (2 - \frac{\pi}{2}) \cdot \sigma^2, \tag{2.22}$$

where σ originates in Equation 2.10.

2.4.1.2 Rician Distribution

A more general distribution of fading that is experienced in a mobile radio channel is Rician fading [26]. Rayleigh fading was defined by $K = 0$, from Equation 2.7, and is a special case of Rician fading. For general Rician fading the constraint of Equation 2.9 is removed. That is, $\overline{X_1}$ or $\overline{X_2}$ do not have to be equal and neither have to be 0. However, Equation 2.10 holds true. A variable, s, may be defined as

$$s^2 = \overline{X_1}^2 + \overline{X_2}^2. \tag{2.23}$$

Considering Equation 2.7, s^2 can be considered as the power in the dominant path and $2\sigma^2$ as the power in the other paths. Therefore, K can be defined mathematically as

$$K = \frac{s^2}{2\sigma^2}. \tag{2.24}$$

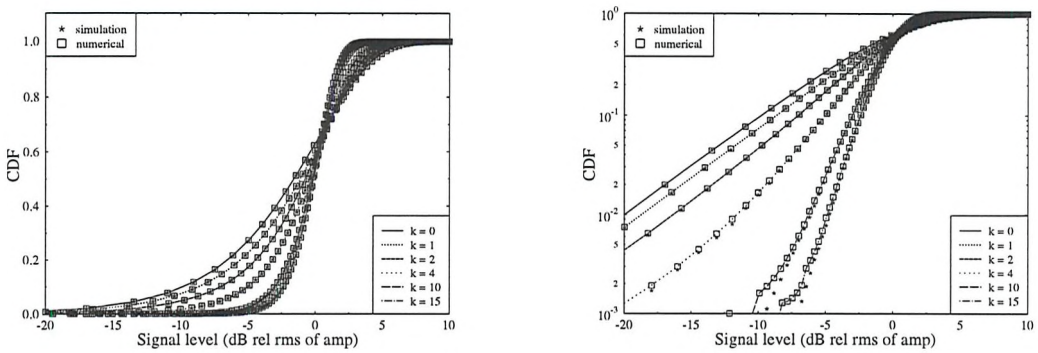

(a) Linear CDF

(b) Log_{10} CDF

Figure 2.3: CDF of Rician fading for target K factors of 0, 1, 2, 4, 10 and 15 which correspond to actual K factors of 4.014×10^{-6}, 0.999, 1.996, 3.987, 9.962 and 14.939

Proakis [25] shows that if R and $|R|$ are defined as in Equations 2.11 and 2.12 then the PDF and CDF of $|R|$ become,

$$P_{\angle R}(r) = \frac{r}{\sigma^2} \cdot e^{-\frac{r^2}{2*\sigma^2}} \cdot^{-K} \cdot I_0\left(\frac{r}{\sigma}\sqrt{2K}\right) \tag{2.25}$$

$$C_{|R|}(r) = 1 - e^{\left(K+\frac{r}{2\sigma^2}\right)} \sum_{m=0}^{\infty} \left[\left(\frac{\sigma\sqrt{2K}}{r}\right)^m \cdot I_m\left(\frac{r\sqrt{2K}}{\sigma}\right)\right], \tag{2.26}$$

where $I_m(x)$ is the m^{th} order modified Bessel function of the first kind. Proakis [25] also shows that the k^{th} moment of $|R|$ is given by,

$$E(|R|^k) = (2\sigma^2)^{\frac{k}{2}} \cdot e^{-K} \cdot \Gamma\left(\frac{2+k}{2}\right) \cdot_1 F_1\left(\frac{2+k}{2}, 1; K\right) \tag{2.27}$$

where, ${}_1F_1\left(\alpha, \beta; x\right)$ is the confluent hyper-geometric function defined as

$${}_1F_1\left(\alpha, \beta; x\right) = \sum_{k=0}^{\infty} \frac{\Gamma(\alpha+k)\Gamma(\beta)x^k}{\Gamma(\alpha)\Gamma(\beta+k)k!} \quad \beta \neq 0, -1, -2, \ldots \ . \tag{2.28}$$

To verify Equation 2.26 uncorrelated Rician channels were generated with 100000 values and target K factors of 0, 1, 2, 4, 10 and 15. Checking of the generated channels revealed that the actual K factors were, 4.014×10^{-6}, 0.999, 1.996, 3.987, 9.962 and 14.939. The CDFs of the amplitude of these signals were computed. The theoretical CDFs were generated for actual K factors using Equation 2.26, where the infinite series was truncated so that the last term of the summation had less than 0.1% contribution. All CDFs were normalised to the

Root Mean Squared (RMS) of $|R|$, which was evaluated as the $\sqrt{E(|R|^2)}$; again the infinite series was truncated so that the last term of the summation had less than 0.1% contribution. The RMS may have been more simply calculated as the square-root of the total of the power in the dominant and remaining paths. From 2.7 and 2.24 the RMS of the fading envelope, $|R|_{RMS}$ can be derived as,

$$|R|_{RMS} = \sigma\sqrt{2 + 2K}. \tag{2.29}$$

Figure 2.3:a indicates good correspondence between numerical and simulated CDFs for all the simulated Rician K factors. Higher K factors indicate less variation in the channel, that is, a more Gaussian channel. From Figure 2.3:b, the same data displayed with a logarithmic CDF, discrepancies can be noted for larger K factors at the lower probabilities. Initially this was attributed to insufficient data points in the simulated results, however, increasing the number of points did nothing to reduce the discrepancy. Therefore, it was concluded that the discrepancies were a consequence of computational inaccuracies in the evaluation of the numerical CDF.

2.4.1.3 Spectrum of Fading Channel

The rate at which a mobile station moves from a point of constructive to destructive interference in a multi-path propagation environment is obviously a function of the mobile velocity[1]. Lee [27] shows that this is related to the Doppler effect and introduces the maximum Doppler frequency, f_d. The value of f_d defines the highest frequency component of the Rayleigh fading and is defined by

$$f_d = \frac{v}{\lambda} \tag{2.30}$$

where v is the mobile velocity and λ is the carrier wavelength. Assuming that incident radiation is equally likely from all horizontal directions (and assuming that the mobile velocity takes into account the environmental mobility), the Classical Power Spectral Density (PSD), D(f), may be derived for various antennae as shown in Table 2.2, and in all cases $D(f) = 0$ for $|f| > f_d$. The type of mobile radio communications considered generally utilise vertical mono-pole antennae. All the following calculations assume vertical mono-pole antennae, unless otherwise stated.

[1] As mentioned in section 2.1, reciprocity is assumed at all times therefore the fading would have the same effect upon either a received or transmitted signal

Antenna	D(f)
Vertical Mono-pole	$\frac{3}{2\pi\sqrt{f_d^2-f^2}}$
Vertical Loop in plane perpendicular to vehicle motion	$\frac{3}{2\pi f_d^2}\sqrt{f_d^2-f^2}$
Vertical Loop in plane of vehicle motion	$\frac{3f^2}{2\pi f_d^2\sqrt{f_d^2-f^2}}$

Table 2.2: Various Doppler Filters [27]

2.4.1.4 Autocorrelation

The Wiener-Khinchin theorem states that the Fourier transform pair of the PSD of a signal is the autocorrelation of that signal. The standard Bessel integral,

$$J_n(x) = \frac{(-j)^n}{\pi}\int_0^\pi e^{jx\cos\psi}\cdot\cos(n\psi)d\psi, \tag{2.31}$$

can be exploited to show that the autocorrelation of the Rayleigh fading for a vertical mono-pole antenna is given by

$$\rho(\tau) = J_0(2\pi f_d\tau). \tag{2.32}$$

2.4.1.5 Level Crossing Rate

Lee [27] shows that the amplitude of Rayleigh fading, normalised to $2\sigma^2$, crosses a given level l, $n(l)$ times per second in a positive direction where

$$n(l) = \sqrt{2\pi}f_d l e^{-l^2}, \tag{2.33}$$

and this statistic is referred to as the Level Crossing Rate (LCR).

2.4.1.6 Average Fade Duration

The average fade duration, $\overline{n}(l)$, at a level, l which is normalised to $2\sigma^2$, is given by [27]

$$\overline{n}(l) = \frac{e^{l^2}-1}{\sqrt{2\pi}f_d l}. \tag{2.34}$$

2.4.1.7 Systems

The normalised Doppler frequency is defined as the product of the Doppler frequency, f_d, and the symbol period, T. Equation 2.30 is used to calculate f_d for several popular digital

System type	Signal rate	Typical velocity range	Nominal carrier frequency	Maximum normalised Doppler frequency	Reference
	kBd	ms^{-1}	MHz	Hz	
IS 54	20	0-25	850	3.356×10^{-3}	[28]
DECT	1152	0-2.5	1900	1.375×10^{-5}	[29]
GSM	271	0-25	900	2.769×10^{-3}	[30]
DCS 1800	271	0-25	1800	5.539×10^{-4}	[31]

Table 2.3: Signal rate, typical velocity range, vicinity of carrier frequency and computed values of maximum normalised Doppler frequencies for several popular digital mobile radio systems

mobile radio systems and the resulting normalised Doppler frequencies are shown in Table 2.3.

2.4.2 Simulation of Rayleigh Fading

Fast fading simulation is an integral part of simulating communication channels [27, 1, 32] and because of the equivalence of baseband and passband systems described in [6], it need only be simulated at baseband frequencies. Rayleigh fading is considered here and two methods of simulation are compared. The first is described by Jakes [33] and the second is conceptually outlined by Arredondo [34] and will be referred to as Quadrature Noise Source (QNS) simulation of Rayleigh fading. Both methods are described and their performance in terms of the statistics introduced in Section 2.4.1, are compared.

2.4.2.1 Jakes' Method

Jakes [33] describes, and Casas et al [35] implements in hardware, a technique referred to as 'sum of sinusoids' for simulating Rayleigh fading using the summation of several low frequency sinusoids with regularly spaced phase differences. Jakes shows the derivation of 2.35 and 2.36:

$$x_1(t) = 2\left[\sum_{n=1}^{N_O} \cos\beta_n cos\omega_n t\right] + \sqrt{2}\cos\frac{\pi}{4}\omega_m t \tag{2.35}$$

$$x_2(t) = 2\left[\sum_{n=1}^{N_O} \sin\beta_n cos\omega_n t\right] + \sqrt{2}\sin\frac{\pi}{4}\omega_m t \tag{2.36}$$

N_O is the number of low frequency sinusoids used, t is time and β_n ensures uniform distribution of phases by being defined as,

$$\beta_n = \frac{n \cdot \pi}{N_O}. \tag{2.37}$$

$$\omega_n = 2\pi f_d \cdot \cos\left[\frac{2\pi n}{N}\right]. \tag{2.38}$$

Jakes then shows that if

$$r(t) = x_1(t) + jx_2(t) \tag{2.39}$$

and there are enough oscillators[2], $r(t)$ will be a good approximation to the random variable R in Equation 2.11.

2.4.2.2 Quadrature Noise Source

An alternative approach performs complex addition of two quadrature band-limited Additive White Gaussian Noise (AWGN) sources as shown in Figure 2.4. Such a simulator has been implemented using analogue noise sources by Arredondo et al [34], discrete logic by Comroe [38], digital pseudo random sequences by Ball [39], a microprocessor by Agusti et al [40] and a Digital Signal Processing (DSP) microprocessor by Goubran et al [41]. This is a direct implementation of Equation 2.11 where $X'(t)$ and $Y'(t)$ are merely band-limited replacements for X_1 and X_2. Kay [42] shows that both $X'(t)$ and $Y'(t)$ remain Gaussian if the band-limiting is introduced via a linear network and if the time sequence is long enough.

When implementing such a method in software, the major complexity is involved in realising the band-limiting. This is because f_d is often a small fraction of the sampling frequency of the channel[3], f_s, and therefore a long impulse response would be required to implement the filter accurately as a Finite Impulse Response (FIR) filter. To avoid this the QNS was implemented using fast convolution. The Fourier Transform pair of AWGN is AWGN and this can be exploited. This prevents the need to perform a time to frequency transformation upon the uncorrelated noise. The complex frequency domain noise may be multiplied with the required frequency response, given by Equation 2.30 and Table 2.2. Singletons algorithm described in [15] is a very long inverse Fast Fourier Transform (FFT) algorithm, that utilises external storage. This can be implemented to obtain the band-limited time domain Gaussian sources. The mean and standard deviation of the Gaussian signals are then normalised to one and zero respectively.

[2]Jakes cites [36] and [37] quoting that at $N_O \geq 6$ quite good Rayleigh distributions can be obtained

[3]The sampling frequency of a channel is the same as the symbol rate for the system it simulates

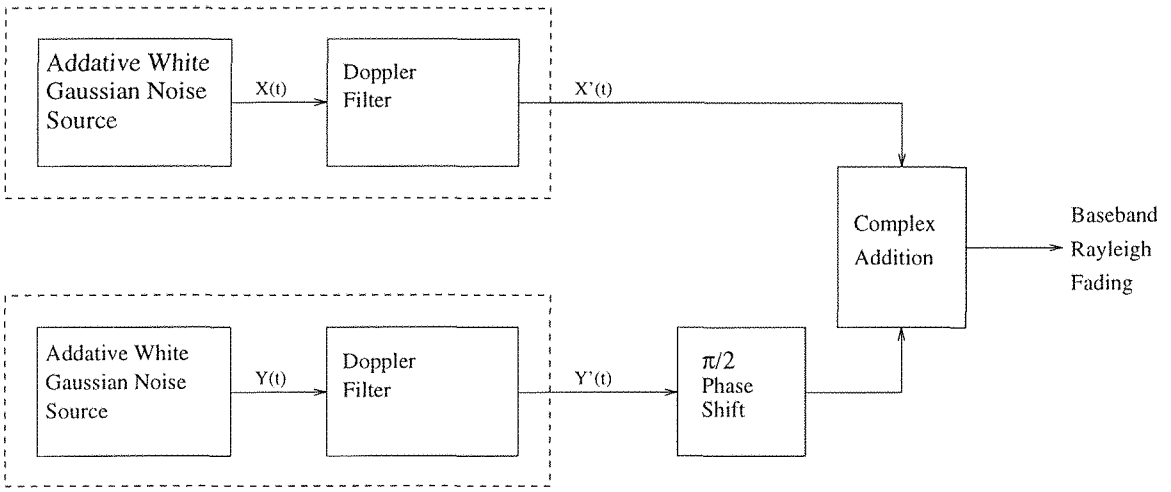

Figure 2.4: Baseband Rayleigh fading simulator using quadrature additive white Gaussian noise sources

2.4.2.3 Comparison of Jakes' Method with Quadrature Noise Simulation

Figures 2.6 - 2.15 show the results of a comparison between Jakes' method and the QNS simulation of two Rayleigh fading channels. The normalised Doppler frequencies of the channels are 4.16955×10^{-3} and 4.16955×10^{-4}. These represent channels with a 20 kBd symbol rate and carrier frequency of 1.8GHz with mobile velocities of 50 kmh^{-1} and 5 kmh^{-1} respectively. The channel generated using Jakes' method had $N_O = 6$ and 2^{22} complex channel points were calculated. These were normalised such that the mean and standard deviation of the real and imaginary Gaussian signals were zero and one respectively. For the QNS method the inverse FFT length was set to 2^{22} so that the same number of channel points were generated for each method. Amplitude PDFs for both the theoretical distribution and the Jakes' and QNS methods, were generated with 80 bins evenly separated in the $\log_{10}$ domain between -60dB and 20dB, where 0dB was at σ. This results in uneven bin widths and consequently alters the shape of the distribution such that the maximum PDF value is no longer at 0 dB. However, employing this technique gives a better insight into the amplitude PDF. The phase PDF was generated with 80 evenly spaced bins between $-\pi$ and π radians.

The theoretical mean and standard deviation of the resulting Rayleigh distribution are given by Equations 2.21 and 2.22 where the theoretical values in this case are 1.2533 and 0.65514. From Table 2.4 it is clear that the first order statistics are closer to the theoretical values for the QNS method compared with Jakes' method.

The use of the χ^2 statistic [15] was considered as a technique for distribution testing when comparing the theoretical and experimental histograms. However when using the incomplete

gamma function to compute the probability, for both simulation methods, at both normalised Doppler frequencies, χ^2 significances were below 1×10^{-40}. This required further explanation.

In Section 2.4.2.2 it was assumed that processing a Gaussian signal with a linear network would result in another Gaussian signal if the signal was long enough. An experiment was conducted on a signal of 2^{19} AWGN points. These points were then band-limited using fast convolution and a rectangular transfer function at various normalised Doppler frequencies. A histogram was then generated for each filtered output, the χ^2 statistic computed and the significance calculated using the incomplete gamma function. Figure 2.5 shows that there is a general trend towards large reduction in statistical significance as the channel bandwidth is reduced. Therefore, at the velocities and radio bearer frequencies encountered in terrestrial mobile radio channels, there is insufficient independence between sample to employ the χ^2 statistic for testing the statistical significance of a Rayleigh channel generator. Because of this the deviations from the theoretical PDF for the QNS and the Jakes' method were measured and compared. The Mean Absolute Error (MAE) between each of the experimental PDF bin values and the theoretical PDF bin values was used to measure the deviation.

Considering the amplitude PDFs in Figures 2.6 and 2.7, it can be seen that generally both methods produce a channel with largely correct amplitude PDFs at both normalised Doppler frequencies. Table 2.4 shows the MAE between the theoretical and the experimental amplitude ($|R|$ PDF MAE) and phase ($\angle R$) PDF PDF bins. Results for both normalised Doppler frequencies and both the Jakes' and the QNS methods are given. Considering the deviation in amplitude PDF it can be seen that the QNS method out performs Jakes' method at both normalised Doppler frequencies. However, at the lower normalised Doppler frequency the difference is eroded as the QNS method deteriorates. Because the quality measure of Jakes' method remained approximately the same, the reduction in quality with the QNS method is not a result of there being a factor ten fewer fades (3.5×10^3 rather than 35×10^3) at the lower normalised Doppler frequency; Jakes' method has a relative improvement over the QNS technique at lower normalised Doppler frequencies given that all other parameters are the same.

On close inspection there appears to be a point at zero dB amplitude, at both Doppler frequencies, where the PDFs generated using Jakes' method changes from being consistently below the theoretical curve to being above it. This suggests a consistent, although relatively small, deviation from the theoretical distribution with Jakes' method.

Now considering the phase PDFs in Figures 2.8 and 2.9, it is clear that the phase has a more uniform distribution in the case with the higher normalised Doppler frequency irrespective of the simulation method deployed. Again the MAE are given in Table 2.4. The MAE quality

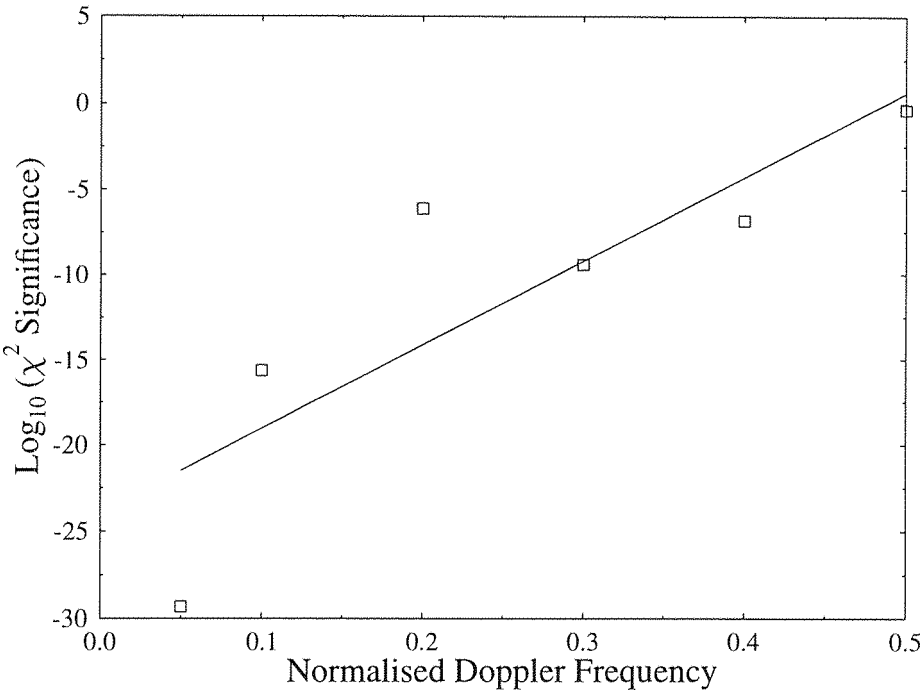

Figure 2.5: χ^2 significance statistic for various normalised Doppler frequencies on Gaussian inputs of 2^{19} data points.

Channel Simulation	$\|R\|$ PDF MAE	$\angle R$ PDF MAE	$\overline{\|R\|}$	$\sigma_{\|R\|}$
QNS, $f_d \cdot T = 4.16955 \times 10^{-3}$	355	1404	1.253923	0.653971
Jakes, $f_d \cdot T = 4.16955 \times 10^{-3}$	8785	1522	1.275320	0.611194
QNS, $f_d \cdot T = 4.16955 \times 10^{-4}$	4746	2560	1.255731	0.650491
Jakes, $f_d \cdot T = 4.16955 \times 10^{-4}$	8777	2336	1.275392	0.611045

Table 2.4: The Mean Absolute Error (MAE) between the theoretical and experimental phase and amplitude PDFs and the Mean and Variance of the experimental amplitudes.

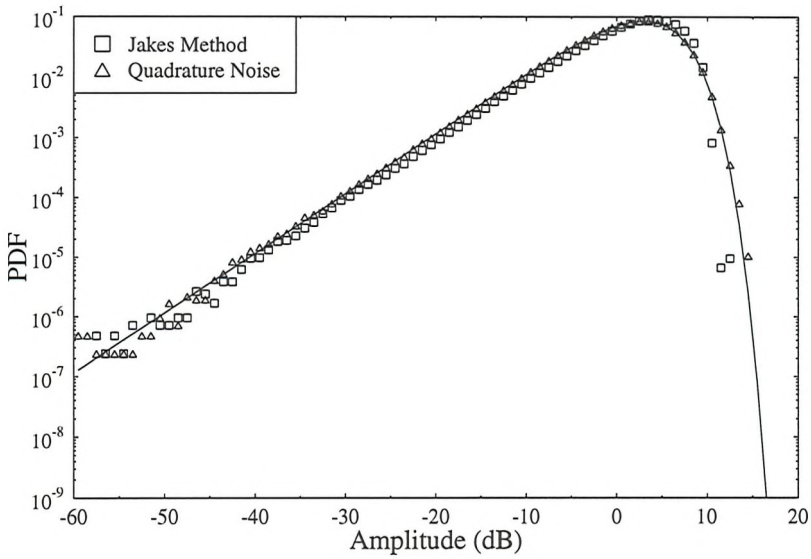

Figure 2.6: Amplitude PDF, calculated with variable bin widths, of fading file generated with Jakes' method and quadrature noise sources for $f_dT = 4.16955 \times 10^{-3}$ and 2^{22} data points

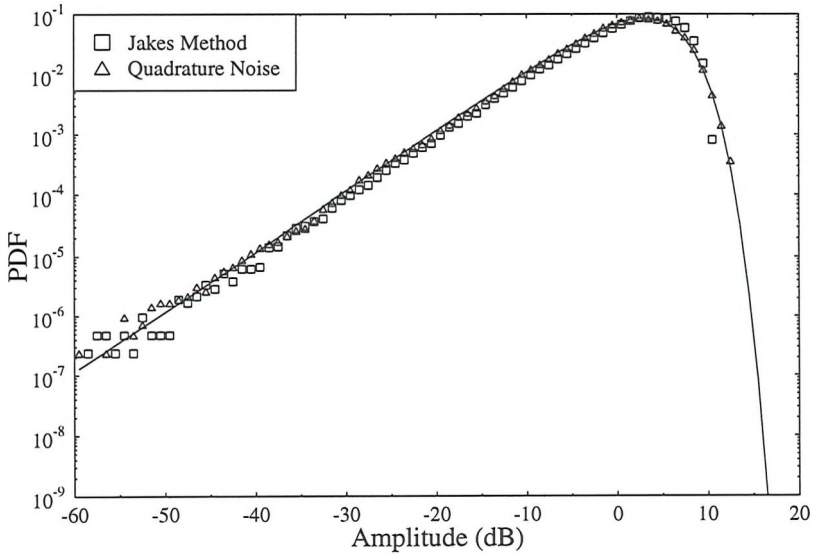

Figure 2.7: Amplitude PDF, calculated with variable bin widths, of fading file generated with Jakes' method and quadrature noise sources for $f_dT = 4.16955 \times 10^{-4}$ and 2^{22} data points

measure is approximately the same for both methods and the consistent reduction in quality with reduction in the number of fades suggests that, unlike with the amplitude PDFs, the phase PDFs exhibit noise effects due to the factor of ten reduction in the number of fades.

Figure 2.10 shows that for fades from −35dB to fades up to 5dB the level crossing rate is close to the theoretical for both models and at both normalised Doppler frequencies. Only the QNS method manages to generate constructive superposition above 10dB at the higher normalised Doppler frequency and the measured level of these is very close to the theoretical curve. Very close scrutiny of the graph reveals that the QNS is marginally closer to the theoretical value than Jakes' method. Further confidence in both simulation methods can be obtained by noting that there is exactly one order of magnitude in the vertical axis between the curves of different normalised Doppler frequencies. The relationship between the LCR and the MFD makes it unsurprising that the observations from Figure 2.10 apply equally well to Figure 2.11.

The explicit spectral properties of the channels are displayed in Figures 2.12 and 2.13. The spectra of the channels were calculated by taking 2^{18} complex values from each channel, windowing them with a Blackman window and then performing an FFT. The two sided PSD is displayed where the zero dB point was initially set to the DC frequency bin. However, it was clear that this normalisation was unsuitable so the normalisation was manually adjusted to give the best comparison to the theoretical curves. The theoretical curves were plotted using the mono-pole equation in Table 2.2.

The Doppler frequency in Figure 2.12 is 83.39Hz and in Figure 2.13 it is 8.339Hz; the frequency axis is scaled with the same 10 : 1 ratio ie, ±100Hz and ±10Hz for the respective graphs. It is clear that the QNS method confines the energy of the channel within $\pm f_d$ much more effectively than Jakes' method for both normalised Doppler frequencies. However, the difference is less significant at the lower normalised Doppler frequency. Within the passband the QNS has a greater resemblance to the PSD given in Table 2.2 than Jakes' method, however, the difference again appears to be eroded at the lower normalised Doppler frequency. Considering the passband in Jakes' method alone it can be seen, particularly at the higher normalised Doppler frequency, that there are 12 harmonic peaks, these relate to N_O being set to 6 in Equations 2.35 and 2.36.

The autocorrelation plots in Figures 2.14 and 2.15, were calculated with 500001 Blackman windowed data points. Figure 2.14 shows the autocorrelation calculated for 1000 points and Figure 2.15 shows ten times as many samples in order to illustrate the same number of fades. These figures support the observations made about Figures 2.12 and 2.13 because of the Wiener-Khinchin theorem. It can be seen that below $\tau \cdot T$ equals 0.05 the QNS method is a

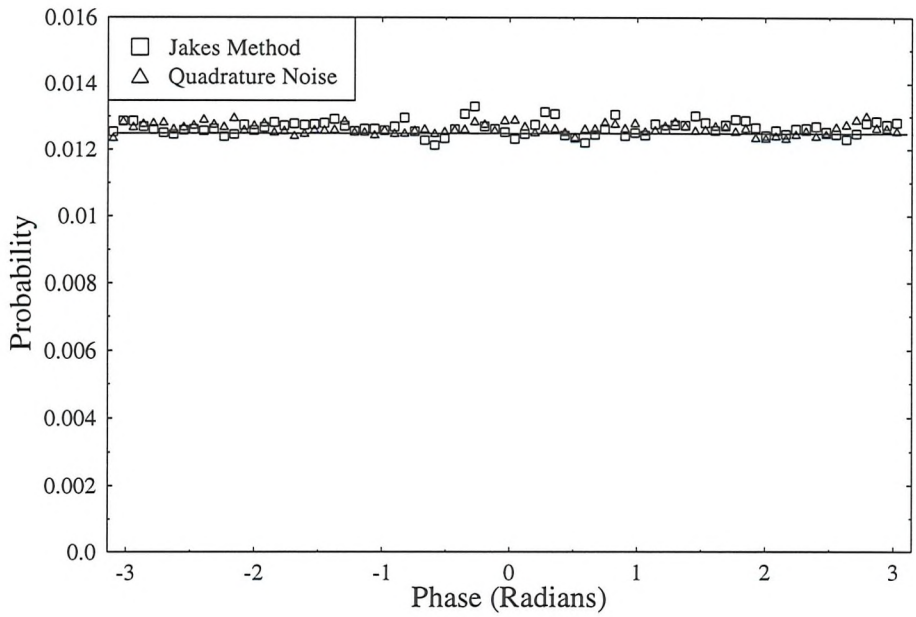

Figure 2.8: Phase PDF of fading file generated with Jakes' method and quadrature noise sources for $f_dT = 4.16955 \times 10^{-3}$ and 2^{22} data points

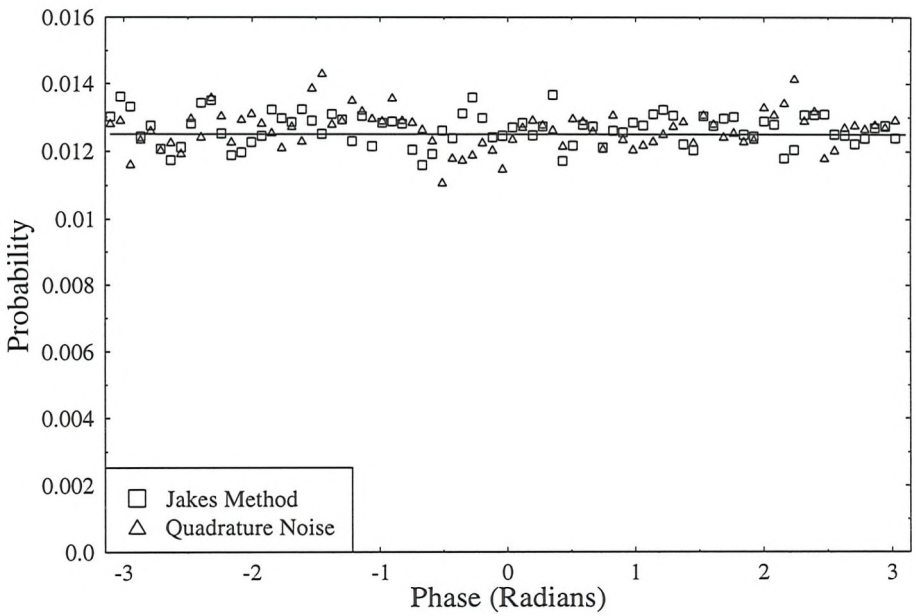

Figure 2.9: Phase PDF of fading file generated with Jakes' method and quadrature noise sources for $f_dT = 4.16955 \times 10^{-4}$ and 2^{22} data points

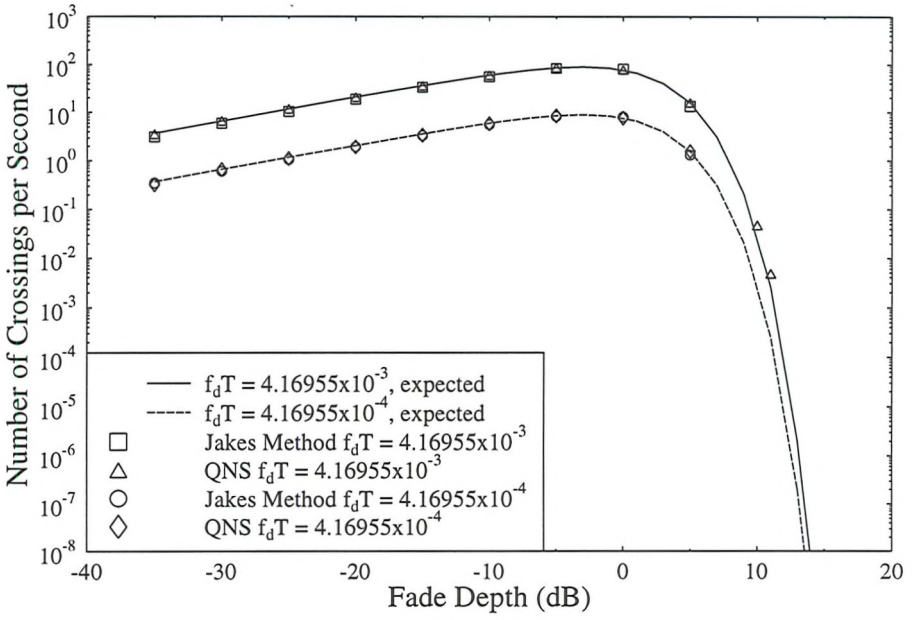

Figure 2.10: Level crossing rate for Rayleigh fading amplitude generated with 2^{22} data points

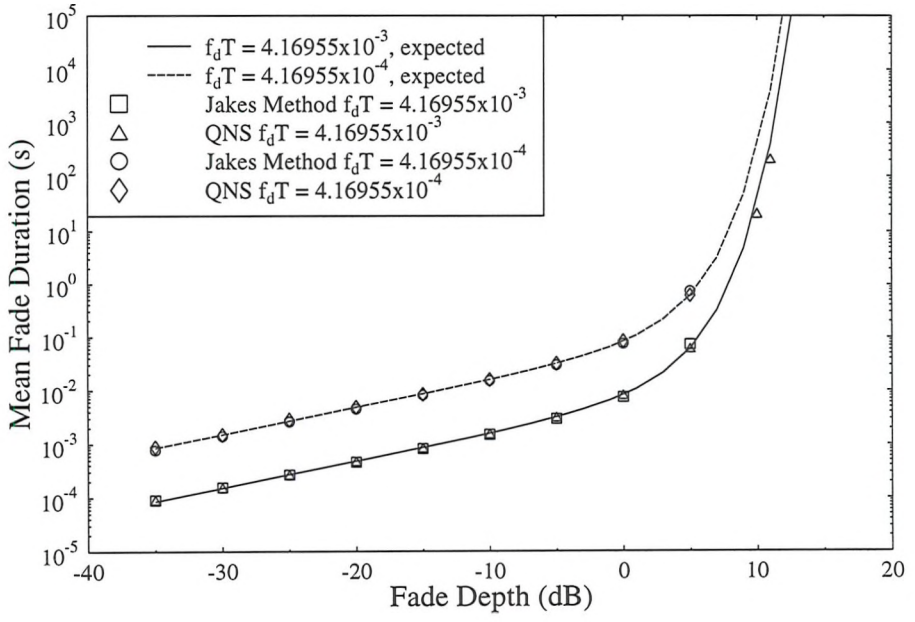

Figure 2.11: Mean fade duration for Rayleigh fading amplitude generated with 2^{22} data points

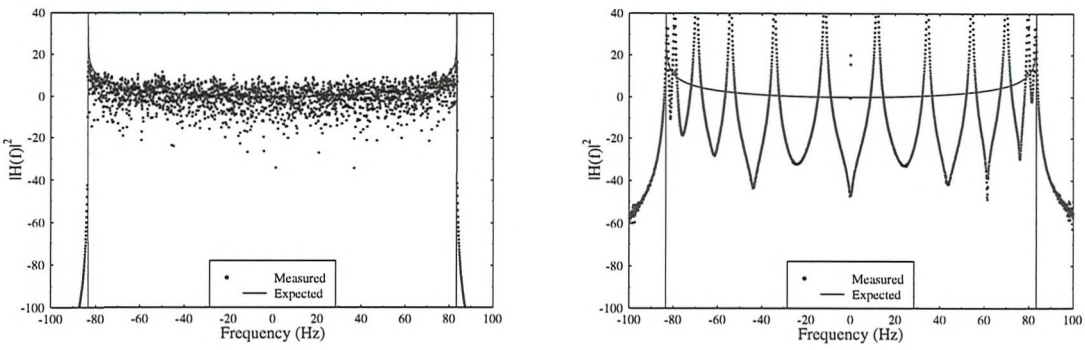

(a) QNS

(b) Jakes' Method

Figure 2.12: Magnitude FFT of 2^{18} complex channel points, Blackman windowed; Rayleigh channel, $f_d = 83.39$Hz, $f_s = 20$kHz

good approximation to the theoretical autocorrelation for both values of normalised Doppler frequency. However, the error between the theoretical values and the values generated using Jakes' method is much less over this range for the lower normalised Doppler frequency. It is clear from figures 2.12 and 2.13 that the first zero crossing of the autocorrelation function is at $\frac{1}{2}f_d$. It can be seen that in Figure 2.14 the QNS experimental curve completely follows the theoretical curve, corresponding to the very sharp cutoff at $\pm f_d$ in Figure 2.12(a). Jakes' method's experimental curve follows the theoretical closely but deviates before the first point of inflection, corresponding to the less sharp cutoff at $\pm f_d$ in Figure 2.12(b). Similar observations may be made concerning figure 2.15. The QNS experimental curve deviates at a lower value of $\tau \cdot T$, which is equivalent to the less tight cutoff at $\pm f_d$ in Figure 2.13(a). Jakes' method in this case deviates before the first inflection point which is also equivalent to the less tight cutoff.

Hoeher [43] and Crespo et al [44] investigate other aspects of these models and conclude that Jakes' method is less computationally demanding and when implemented in hardware, low normalised Doppler frequencies could lead to numerical instabilities with the QNS technique. However, the purpose of simulating these channels within the scope of this work requires the simulation to be performed ahead of time and stored on magnetic media to be recalled during modulation simulation. Therefore the superior accuracy of the QNS method that was presented above out-weighs the processing time penalty. Furthermore as channels are simulated on a personal computer and written in 'C' virtually all numerical instability problems

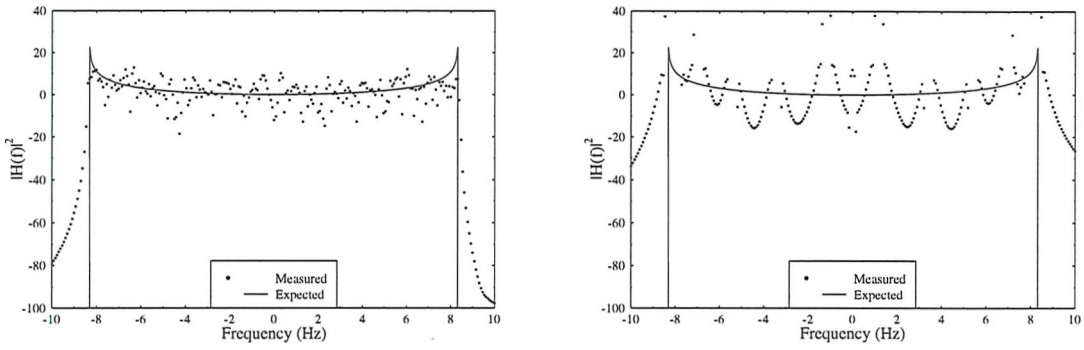

(a) QNS

(b) Jakes' Method

Figure 2.13: Magnitude FFT of 2^{18} complex channel points, Blackman windowed; Rayleigh channel, $f_d = 8.339$Hz, $f_s = 20$kHz

are eliminated.

Crespo et al [44] and Wesolowski [45] recommend employing multi-rate DSP techniques and decimating the in-phase and quadrature components of the fading in order to reduce the storage requirements. The merit of this is clear; the highest frequency component of the channel which is of interest is significantly less than half the sampling frequency. Therefore from a sampling theory point of view it is unnecessary to sample the channel at such a high rate. The problem with this approach is that the channel samples generated at the required signalling rate would have to be reconstructed by interpolation when used in a modulation simulation. This would increase the run time of modulation simulations.

The QNS method of simulation implemented using fast convolution has a further potential drawback over Jakes' method. Channel fading is generated in blocks and when more of these blocks are joined together there are likely to be abrupt discontinuities between them. This is very unlike the real fading characteristic that is being simulated. However, for modulation simulation on a personal computer this not a problem because more than 2^{22} channel points are rarely required. On the occasion that they are required the first and last 1000 points can be linearly manipulated to enable the rewinding of the channel without abrupt discontinuity. This approach was adopted for this work and had no noticeable effect on any of the statistics discussed. It should be noted that Jakes' method, however, does have advantages for TDMA type work because it can be calculated on the fly.

A final comparison between the two methods, shows that QNS gives more accurate results,

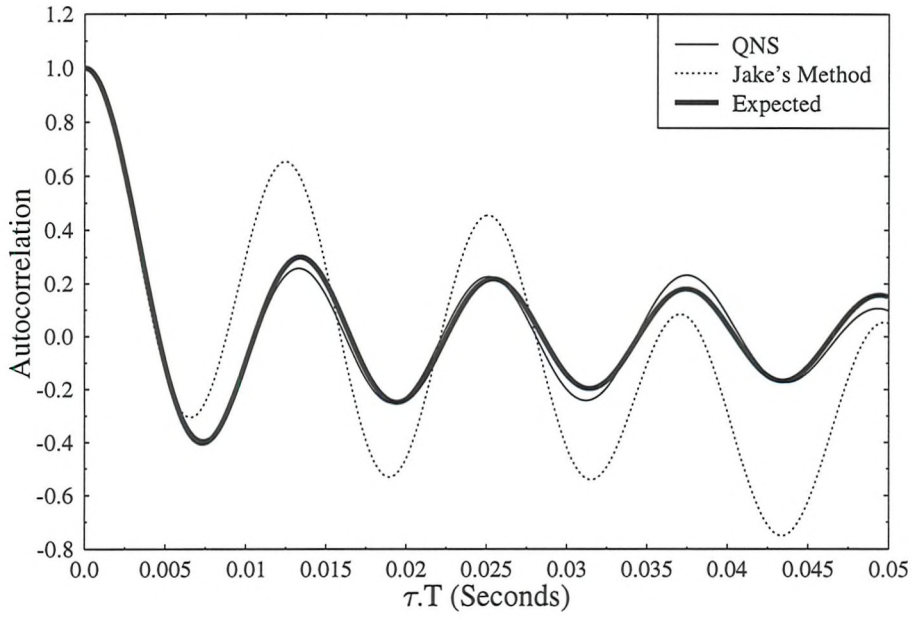

Figure 2.14: Autocorrelation for Rayleigh fading, Blackman windowed 500001 data points, $f_d = 83.39$Hz

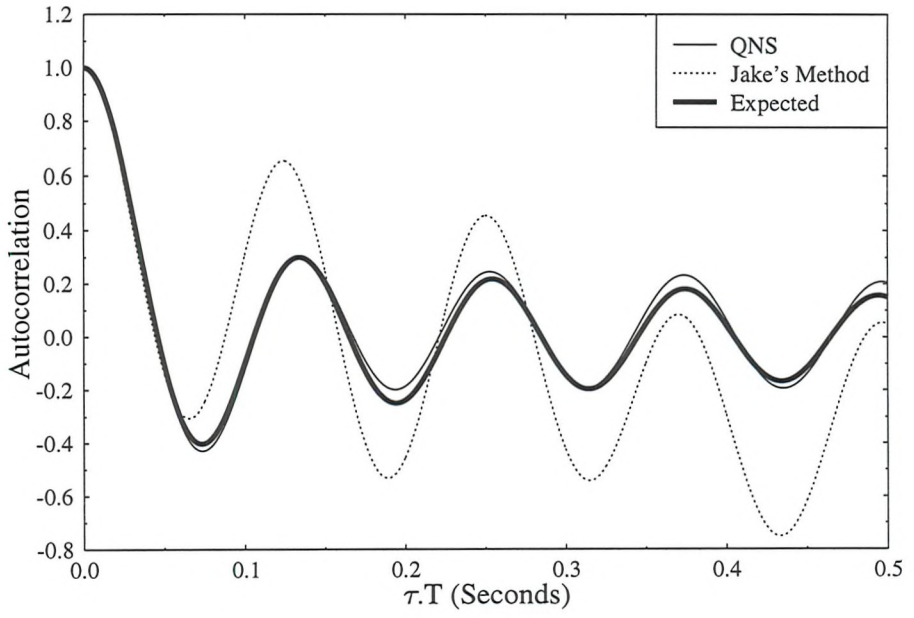

Figure 2.15: Autocorrelation for Rayleigh fading, Blackman windowed 500001 data points, $f_d = 8.339$Hz

particularly at higher normalised Doppler frequencies. At lower normalised Doppler frequencies QNS does not support sufficient frequency domain passband contributors. This results in insufficient non-zero frequencies after the fast convolution operation. The advantage associated with Jakes' method is that only the passband contributors are simulated. This is the explanation for the relative improvement of Jakes' method at the lower normalised Doppler frequencies. The zero and first order statistics, namely the mean and standard deviation, give a reasonable measure of how close a simulated channel is to the theoretical. Jakes' method is largely advantageous in real time simulations when computational requirements are critical and there are strict criteria for floating point accuracy. Within the scope of the work presented in this thesis the QNS method is preferred.

2.5 Wide-band Channels

Until now the discussion has been limited to narrow-band channels, where the time between the arrival of the first and final propagation paths has been very small relative to the symbol period. Wide-band channel conditions are encountered as the symbol rate is increased. A wide-band channel is characterised by the impulse response of the channel, $h(t)$.

2.5.1 Typical Wide-band Channels

Wide-band channels vary with the physical environment. They tend to be characterised as 'typical indoor', 'typical rural', 'typical hilly' or 'typical urban'. Steele [1] illustrates the typical impulse responses that are defined in the GSM system.

Each of the elements of the impulse response acts as an independent narrow-band channel. The obvious disadvantage is that multiple copies of each transmitted symbol are received causing Inter-Symbol Interference (ISI). There is scope to utilise each separated path as a form of diversity and improve the performance of a modulation scheme, when a channel equaliser is employed.

2.5.2 Measurement of Wide-band Channels

It is difficult to measure the impulse response of a channel directly, however, a measurement can be achieved using a Swept Time Delay Cross Correlator (STDCC) [46]. A measure of the width of the impulse response, $h(t)$, is the RMS delay spread, Δ, defined as the square-root

of the second central moment [47] where

$$\Delta = \left[\frac{\int_{-\infty}^{\infty} (t - D)^2 \cdot h(t) dt}{\int_{-\infty}^{\infty} h(t) \cdot dt} \right]^{\frac{1}{2}} \tag{2.40}$$

where D is the mean delay,

$$D = \frac{\int_{-\infty}^{\infty} t \cdot h(t) \cdot dt}{\int_{-\infty}^{\infty} h(t) \cdot dt}. \tag{2.41}$$

The normalised delay spread, Λ, is defined as

$$\Lambda = \frac{\Delta}{T}. \tag{2.42}$$

The effect of wide-band channels upon portable radio systems are discussed to some length by Chuang [48] for values of $\Lambda \leq 0.2$.

2.5.3 Simulation of Dispersion

Caples et al [49] documents a hardware wide-band channel simulator that utilises a Surface Acoustic Wave Device to simulate the relative delay of the separate paths. Software implementation involves convolving independent fast fading channels with relative weighting and delay related to the impulse response being simulated.

2.6 Leaky Feeders

Leaky feeders form a family of distributed antennae. The one considered here was constructed from coaxial cable where the outer shielding is perforated with a plethora of holes. The coaxial cable can be of the order of several hundred metres long and can weave through buildings offering radio illumination in a way that would require many individual antennae. Fabrication costs are relatively low and deployed intelligently, leaky feeders can reduce network infrastructure costs.

Leaky feeders were originally conceived to provide subterranean radio propagation, particularly for analogue speech transmission, for example, in train tunnels [50, 51, 52] and coal mines [53]. As an alternative to conventional antennae for indoor micro-cells, they have only been considered more recently [54, 55, 56, 57, 58, 59]. This section of work is concerned with illustrating how the impulse response of the propagation channel from a leaky feeder to a single receiver antenna can be modelled in an indoor propagation environment. It also quantifies the correspondence between the model and measurements. This is achieved without considering the effect of the detailed geometry of the building upon the radiation from each

slot of the leaky feeder. The model is restricted to two dimensions and only the relative signal strength is considered.

2.6.1 Experimental Measurements

The leaky feeder[4] was constructed of a 0.5" diameter copper foil outer and a foam polyethylene dielectric inner. It had transversal slots pseudo-randomly distributed with a minimum and maximum spacing of 0.01 m and 0.3 m, respectively. The feeder's specified linear axial attenuation κ was 0.15dB/m at a frequency of 2GHz, the relative phase velocity β was 0.88 and the input signal had a frequency of 1.8GHz. The transmitted power was +30dBm or 1W. The cable was laid out on the floor in the centre of a 60 m x 1.4 m corridor that runs through the centre of the top level of a modern four-storey office building of concrete and steel construction. The building has a rectangular shape of 10 m x 60 m. An $m = 511$-bit maximal-length pseudo-random bit PN sequence was transmitted from the leaky feeder at a chip rate of 50 Mbit/sec. This permitted impulse response measurements to be taken around the top floor of the building using a vertically polarised disc-cone receiver antenna attached to a Swept Time Delay Cross-Correlator (STDCC). A delay range of $511/(50 \cdot 10^6) \approx 10\mu$s and a resolution of $1/(50 \cdot 10^6) \approx 20$ns was achieved.

2.6.2 Modelling [61]

The leaky feeder was modelled as a group of radiating short dipoles [62] lying on the $y = 0$ axis of a two dimensional plane, with the input at $x = 0$ and N number of slots at coordinates $(D(n), 0)$ for $n = 1, 2, ..., N$. Let $P = Ae^{j\phi}$, an idealised impulse of amplitude A and phase ϕ, propagate along the leaky feeder from $x = 0$ at a velocity of $c \cdot \beta$, where c is the speed of light in free space. The impulse will take $t_1(n) = D(n)/(\beta c)$ to travel to slot n. The attenuated and phase-rotated impulse at this point can be described as in Equation 2.43, where λ is the free space wavelength:

$$S(n) = 10^{\frac{-D(n)\kappa}{20}} Ae^{j(\phi + (\frac{2\pi\beta D(n)}{\lambda}))}. \tag{2.43}$$

The propagation distance from the n^{th} slot to a receiver at (R_x, R_y) is given by Equation 2.44 for $n = 1, 2, ..., N$.

[4]Gratitude is expressed to Dipl.-Ing. Davies at RFS Hanover for the supply of the leaky feeder cable and Dipl.-Ing. Thomas Keller for conducting the physical experiments, results of which may be found in Reference [60].

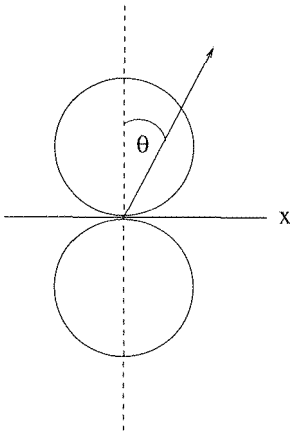

Figure 2.16: Directivity diagram of ideal dipole antenna

$$R(n) = \sqrt{(R_x - D(n))^2 + R_y^2}. \tag{2.44}$$

A free space propagation velocity is assumed once the impulse has left the cable and hence the impulse takes $t_2(n) = \frac{R(n)}{c}$ to travel from the n^{th} slot to (R_x, R_y). This assumes that the delay from reflections inside the building are negligible compared to those in the leaky feeder.

Treating each slot as an independent dipole it can be assumed that the radiation pattern of each slot relates the transmitted power in a given direction to the cosine of the angle, θ, between the direction of propagation and a perpendicular to the cable as shown in Figure 2.16. It can be seen that the received impulse at the antenna is given by Equation 2.45, where $P(r)$ is the amplitude path loss at r and r is the distance from slot n to the receiver antenna:

$$Q(n) = S(n) \cdot cos(\theta) \cdot P(R(n)) \cdot e^{j\frac{R(n)}{c\lambda}}. \tag{2.45}$$

In order to explore the range of propagation scenarios the three different indoor models discussed above were considered, namely free space model, the Ericsson Model [24] and the Bellcore model [23]. The Bellcore model was considered with the model constant set to $\alpha = 0.7$.

Using a similar technique to [63] for taking the sum of an ensemble of paths and letting t represent time, it can now be seen that the impulse response is given by

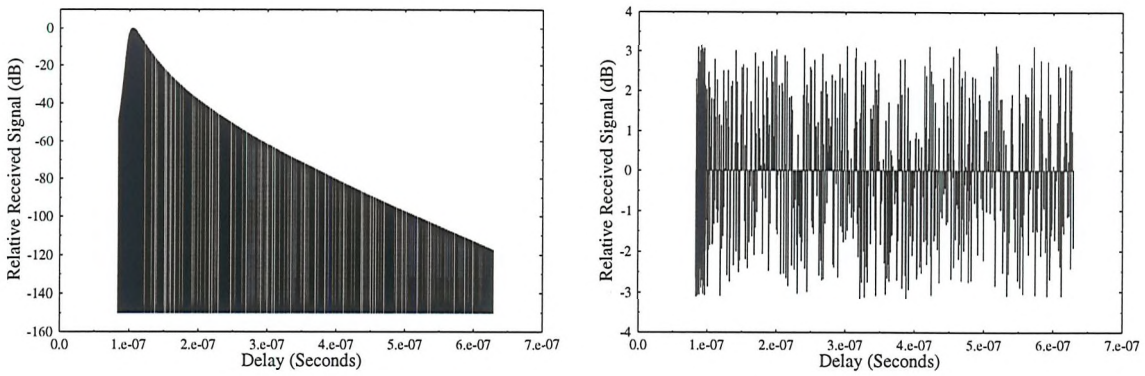

(a) Relative Power (b) Phase

Figure 2.17: Simulated impulse response at coordinate (25,3)

$$h(t) = \begin{cases} \mathrm{Q(n)} & \text{if } t = t_1(n) + t_2(n) \\ 0 & \text{otherwise.} \end{cases} \tag{2.46}$$

2.6.2.1 Post Processing Results

Figure 2.17 shows the impulse response calculated using Equation 2.46 with much greater resolution than that which can be measured. The phase information is also available. In order to compare the simulated results with those measured, the simulated impulse response must be post-processed. Since the PN sequence's average autocorrelation $\psi'(n)$ is not an ideal impulse-like autocorrelation function, it follows from Reference [64] that the STDCC's estimated output signal is given by

$$y(t) = \sum_{k=-\infty}^{+\infty} h(k) \cdot \psi'(t-k). \tag{2.47}$$

The average auto-correlation is used because in reality the STDCC receiver will not be perfectly aligned with the transmitter and this will result in the receiver's sampling points not always falling on the auto-correlation peaks. The STDCC receiver partly avoids this problem by taking the average of every two measurements. The post processing must take this into account. From [46] we can arrive at Equation 2.48 which is an expression for the autocorrelation of the PN sequence $\psi(k)$.

$$\psi(k) = \begin{cases} m - (m+1) \cdot k & \text{if } |k| \leq 1 \\ \text{-1} & \text{otherwise.} \end{cases} \tag{2.48}$$

From here we assume that $\psi'(k)$ is given by

$$\psi'(k) = \frac{\psi(k) + \psi(k+1)}{2}. \tag{2.49}$$

Finally, as the STDCC has a resolution of 20 ns, the simulated impulse response is averaged into 20 ns bins, which allows the generation of a comparable number of sample points for both the simulated and measured results.

Figures 2.18 and 2.19 show the measured impulse responses and simulated impulse responses after post-processing, using the free space path loss, the Ericsson Minimum and Maximum path loss margins, as well as the mean of the Bellcore model, where $\alpha = 0.7$. The Figures portray comparisons at (R_x, R_y) equal to (15,3)m and (25,3)m, respectively. For an impulse response attenuation of less than approximately 40dB very good agreements were registered but for higher attenuation both the model and the measured results were affected by a number of ameliorating factors. The free space model predicts in both cases an impulse response with a higher delay spread than that measured, while all the other models follow the measured result more closely. Further comparisons between the measured and modelled scenarios showed that when the receiver was very close (less than 1 metre) to the cable the agreement between them was less close. This was due to *near field* effects.

Ideally, the Ericsson Minimum and Maximum models would surround the measured impulse response. This is more the case with the receiver at (15,3)m than at (25,3)m. A possible explanation for this may be that all the models used a statistically similar distribution of slots to that of the real leaky feeder, as opposed to the absolute exact position of each of the slots. Furthermore, a single slot may be considered to have a radiation pattern of a dipole, however close slots will interact with one another to modify this radiation pattern. The slots in the cable were on one side only and the direction that they were facing was likely to affect the radiation pattern; this was neglected in the model.

By using either of the Ericsson models or the mean of the Bellcore model with $\alpha = 0.7$, it was found that a good approximation to the impulse response measured by the STDCC could be achieved, for receiver distances greater than 1 metre from the cable. This was possible without having to implement vastly complex algorithms to model each of the many sources.

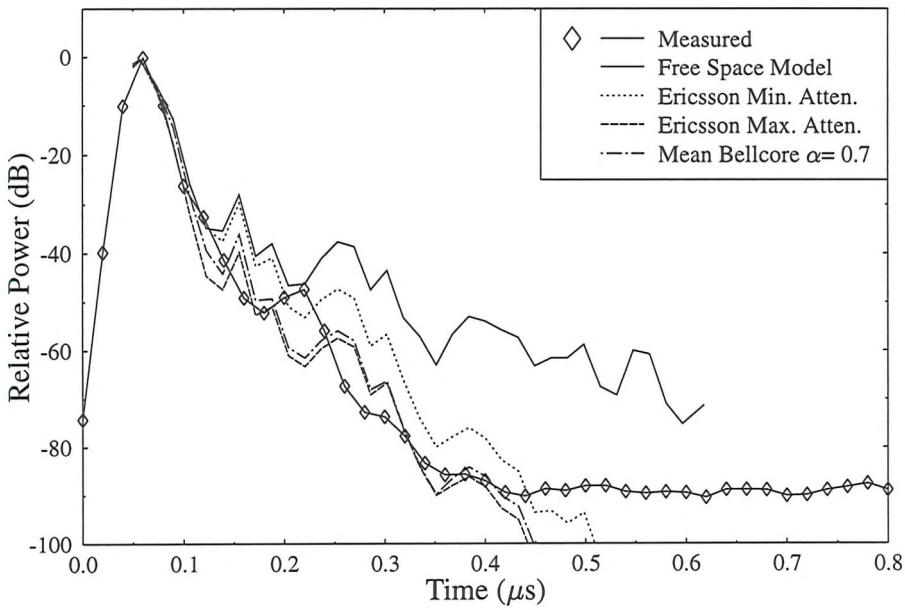

Figure 2.18: Measured and simulated impulse responses at position (15,3)

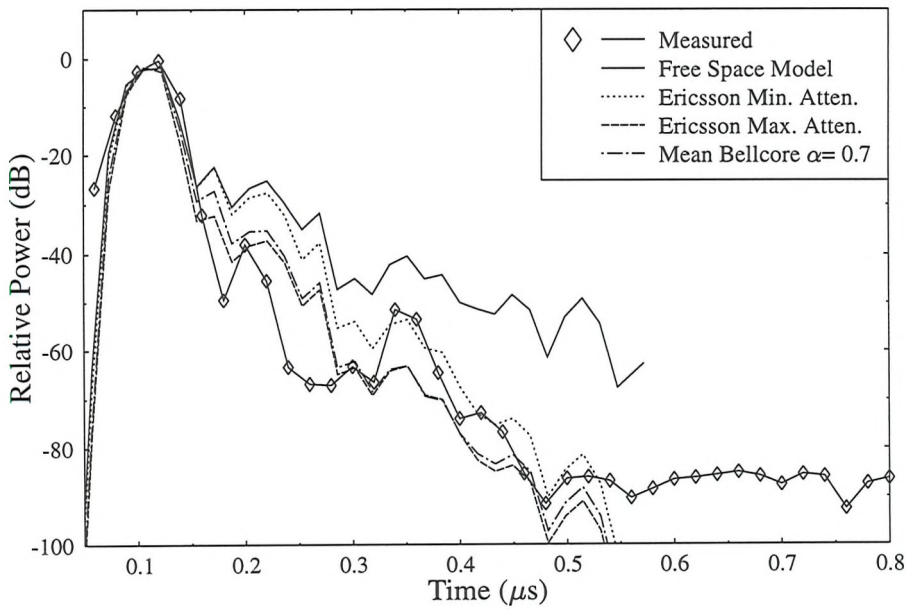

Figure 2.19: Measured and simulated impulse responses at position (25,3)

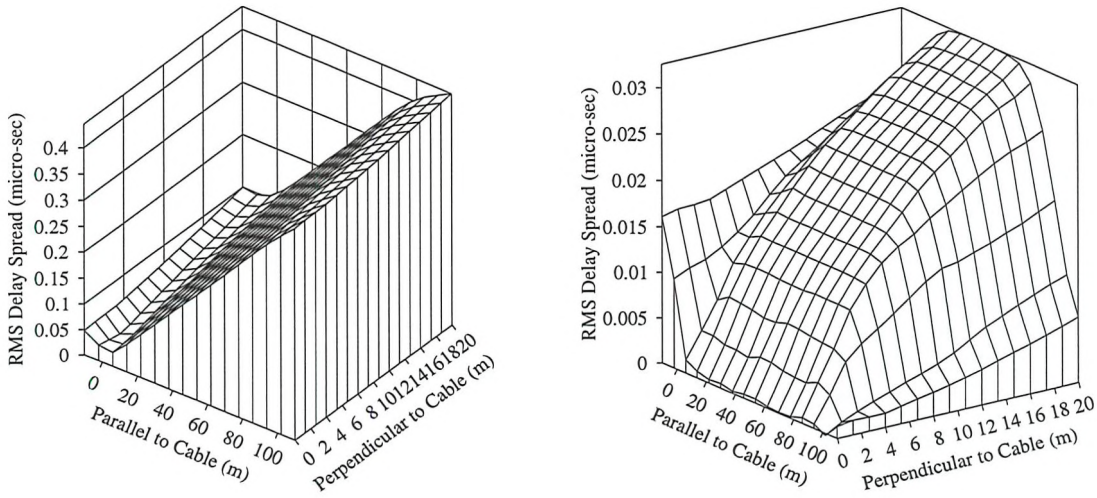

(a) Mean delay, D.

(b) RMS delay spread, Δ.

Figure 2.20: Simulated results with 100m leaky feeder using mean of Bellcore model with $\alpha = 0.7$

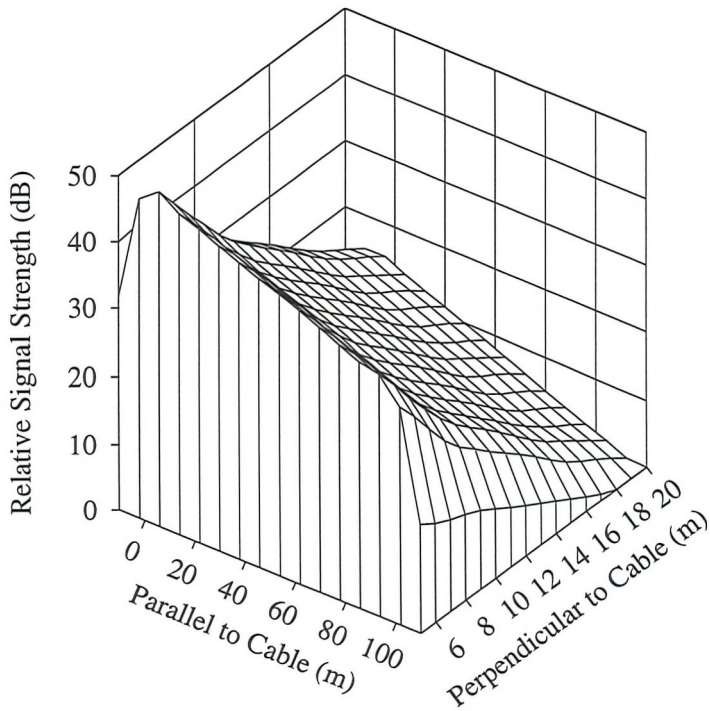

Figure 2.21: Relative strength of maximum peak with 100m leaky feeder using mean of Bellcore model with $\alpha = 0.7$

2.6.2.2 Calculation of Mean delay, D and RMS delay spread, Δ

Using Equations 2.40 and 2.41 the mean delay D, and the RMS delay spread Δ, can be calculated for the simulated impulse response given in Equation 2.46. Figure 2.20 shows these values for $-10\text{m} < x < 110\text{m}$ and $0\text{m} < y < 20\text{m}$. From Figure 2.20:a it is apparent that most of the mean delay to the signal results from the relative phase velocity, β, of the leaky feeder. This is because the gradient along the parallel axis, for $0\text{m} < x < 100\text{m}$, is much greater than that along the perpendicular axis or other points along the parallel axis. The minimum delay corresponds to the point closest to the input of the leaky feeder. However, even the greatest mean delay is unlikely to hinder either typical Time Division Duplex (TDD) or Time Division Multiple Access (TDMA) systems. Figure 2.20:b illustrates the delay spread which is a better statistic in determining the maximum symbol rate that can be sustained by the channel without wide-band conditions prevailing. There is a general trend to increased delay spread as the Y coordinate increases. This is particularly true in the central region of the cable where the most sources make the largest contribution towards the received signal. Towards the ends of the cable the delay increases; beyond the end of the cable, at $X < 0$, the delay becomes large. The problems caused by this can be minimised by ensuring that the cable runs from wall to wall with the building. Considering a DECT type system, from Lopes [65], it can be seen that if 30dB of SNR is achieved at the receiver, the maximum acceptable RMS dispersion is $\Delta \approx 0.025\mu s$. Figure 2.21 plots the relative signal strength of the largest peak in the impulse. There is about 45dB difference between the signal at (0,5)m and (110,20)m. If the mean of the Bellcore model were assumed with $\alpha = 0.7$ and a single omni-directional antenna were used this figure would be 102dB.

2.7 Conclusions

Jakes' and QNS methods for the simulation of Rayleigh fading channels were considered. Both methods gave good results when comparing the simulated channel with the theoretical statistics for amplitude and phase PDF, LCR and MFD. However, better results were registered, for both methods when a greater number of fades are considered. Very low statistical significance was observed when using the χ^2 test to obtain a quality measure of the PDFs for the channels. It was proposed to use the mean absolute error between the theoretical and experimental PDF bins.

Jakes' method required less simulation time, however, it was less accurate than the QNS method. At lower normalised Doppler frequencies its performance relative to the QNS method

was improved. This was as a result of the improved frequency resolution in the Doppler passband.

A simple model for the simulation of leaky feeders was presented and compared with measurements that were taken using a STDCC. The model proved powerful and when used in conjunction with a post-processing technique predicted impulse responses similar to those that were measured. The model was used to predict mean delay, RMS delay spread and relative received power for a set of points around the leaky feeder.

Chapter 3

Coherent and Non-coherent Modulation

3.1 Introduction

Early multi-level modulation schemes that employed more than a single signaling dimension include those proposed by Lucky et al [66] or Smith [67]. Origninally it was proposed to use multi-level modulation for transmission over non-fading channels. However, Sundberg et al [68] and Steele et al [69] proposed using it for transmission of speech over fading channels.

Unlike non-coherent modulation, coherent modulation requires absolute phase alignment between the transmitter and receiver. This means that the receiver must recover the absolute phase of the transmitted signal and therefore less complexity is involved in non-coherent detection. Non-coherent detection utilises the phase of the previous symbol (or symbols) as a reference. When transmission takes place over mobile radio channels, the difference between coherent and non-coherent carrier recovery complexity is greater than when the transmission is over a Gaussian channel. Moreover, modulation schemes that transmit more Bits Per Symbol (BPS) require a more accurate and hence more complex carrier recovery scheme.

The drawbacks of non-coherent recovery of symbols are typically two-fold. The first is that for successful non-coherent modulation differential encoding has to be deployed, this inherently leads to reduction in Bit Error Rate (BER) performance. The second is that, in order to construct a QAM constellation that is suitable for differential encoding, the mean Euclidean distance between constellation points is no longer optimum in terms of SNR protection.

This chapter considers the performance of one, two, four and six BPS modulation schemes.

The performance of coherent and non-coherent detection is considered. This is investigated for both Gaussian and Rayleigh channels. A scheme that permits coherent, non-differential detection of multi-level modulation called, Pilot Symbol Assisted Modulation (PSAM) [6, 70], is discussed.

3.1.1 Square Constellations

Square Quadrature Amplitude Modulation (QAM) phasor constellations offer the maximum protection from AWGN, if all symbols are equally likely to be transmitted. This is the case because a square constellation has the greatest minimum distance between the constellation points for a given average power. Gray coding can be implemented so that the minimum number of bits are affected by a phasor being erroneously decoded as its neighbour. This results in the formation of sub-channels, where some bits have a greater level of protection than others. The number of sub-channels depends upon the size of the constellation. Square 16 point QAM has 2 sub-channels, a more protected C1 and a less protected C2. Square 64 point QAM has 3 sub-channels, C1, C2 and C3, where C1 is the most protected and C3 the least. Figure 3.1 shows square constellations for one, two, four and six BPS.

3.1.2 Star Constellations and Differential Encoding

Differential coding in the case of one and two BPS involves differentially encoding the phase. For four and six BPS differential coding is more complex, because a square constellation only posses rotational symmetry of order four. However, for modulation schemes with more than two BPS the order of symmetry can be increased by configuring the constellation as a ring. Having increased the order of symmetry, differential coding is more straightforward, although the noise tolerance will be reduced when compared with a similar square constellation. Concentric rings can offer more noise protection than a single ring with many points and such constellations are called star constellations. These, too, are less tolerant to AWGN than the equivalent square constellations.

For differential star 16 point QAM three bits are differentially encoded in the phase and the fourth bit is differentially encoded in the amplitude, as proposed by Webb et al [71]. Differential encoding of this nature results in a BER performance penalty when compared to the same non-differentially encoded constellation. Figure 3.2 shows star QAM constellations for one, two and four BPS. The Differential BPSK (DBPSK) and Differential QPSK (DQPSK) constellations are exactly equivalent to the BPSK and QPSK schemes in Figure 3.1 and are shown here for completeness. Figures 3.1 and 3.2 also highlight how BPSK can

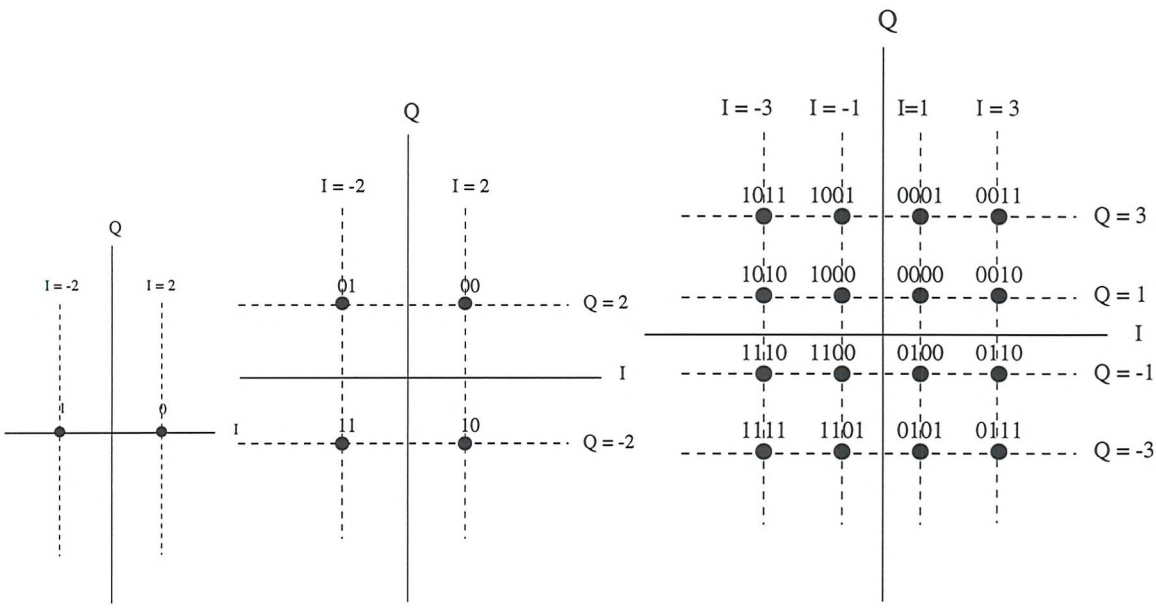

(a) BPSK (b) QPSK (c) Square 16 point QAM

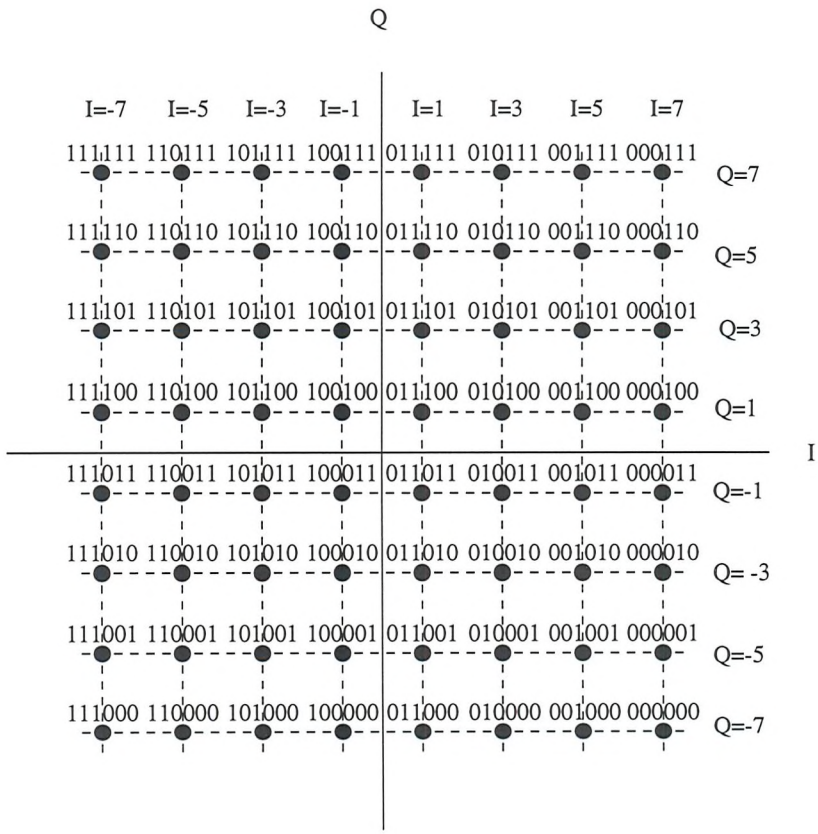

(d) Square 64 point QAM

Figure 3.1: Modulation constellations

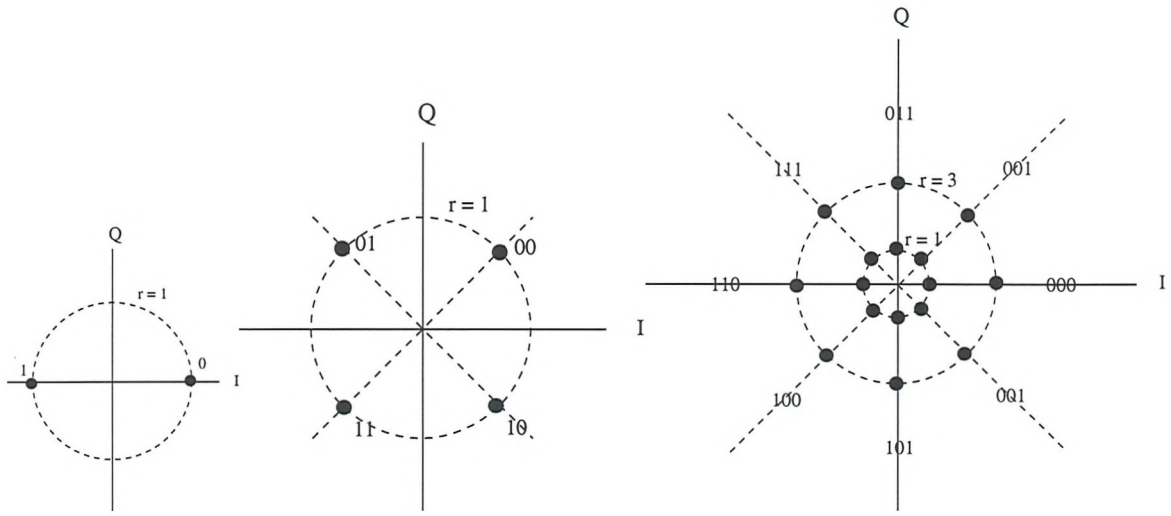

(a) DBPSK (b) DQPSK (c) Differential star 16 point QAM

Figure 3.2: Modulation constellations

equally well be considered as Amplitude Modulation (AM), Frequency Modulation (FM) or Phase Modulation (PM) and that QPSK may be considered as QAM or PM.

3.2 Modulation Performance in Gaussian Channels

Gaussian channels were described in chapter 2 and in this section the BER performance of both differential and non-differential modulation schemes in these channels is considered. When the receiver hardware supports coherent detection, Square QAM constellations are favoured. As with all BER results that are presented, it will be assumed that there is perfect matched filtering and clock recovery.

3.2.1 Coherent Detection

Closed solutions for BPSK and QPSK BERs have been published by, among others, Proakis [25]. They are stated below to allow for comparison with simulated results. The BER for BPSK, P_b, is

$$P_b(\gamma) = Q\left(\sqrt{2\gamma}\right), \tag{3.1}$$

and the BER for QPSK, P_q, is

$$P_q(\gamma) = Q\left(\sqrt{\gamma}\right), \tag{3.2}$$

where γ is the channel SNR as given by Equation 2.2 and the function $Q()$ is defined by

$$Q(y) = \frac{1}{\sqrt{2\pi}} \int_y^\infty e^{-x^2/2} dx = \frac{1}{2} \text{erfc}\left(\frac{x}{\sqrt{2}}\right). \tag{3.3}$$

The performance of both square 16 and 64 point QAM in Gaussian channels has been presented by Fortune et al [72]. The BER for the sub-channels C1 and C2 for square 16 point QAM is given by

$$P_{16_1}(\gamma) = \frac{1}{2}\left[Q\left(\sqrt{\frac{\gamma}{5}}\right) + 3Q\left(\sqrt{\frac{\gamma}{5}}\right)\right], \tag{3.4}$$

and

$$P_{16_2}(\gamma) = Q\left(\sqrt{\frac{\gamma}{5}}\right), \tag{3.5}$$

respectively. For square 64 point QAM the BER for C1, C2 and C3 are given by

$$P_{64_1}(\gamma) = \frac{1}{4}\left[Q\left(\sqrt{\frac{\gamma}{21}}\right) + Q\left(3 \cdot \sqrt{\frac{\gamma}{21}}\right) + Q\left(5 \cdot \sqrt{\frac{\gamma}{21}}\right) + Q\left(7 \cdot \sqrt{\frac{\gamma}{21}}\right)\right], \tag{3.6}$$

$$P_{64_2}(\gamma) = \frac{1}{2}Q\left(\sqrt{\frac{\gamma}{21}}\right) + \frac{1}{2}Q\left(3 \cdot \sqrt{\frac{\gamma}{21}}\right) + \frac{1}{4}Q\left(5 \cdot \sqrt{\frac{\gamma}{21}}\right) + \frac{1}{4}Q\left(7 \cdot \sqrt{\frac{\gamma}{21}}\right) \tag{3.7}$$

and

$$\begin{aligned} P_{64_3}(\gamma) &= Q\left(\sqrt{\frac{\gamma}{21}}\right) + \frac{3}{4}Q\left(3 \cdot \sqrt{\frac{\gamma}{21}}\right) - \frac{3}{4}Q\left(5 \cdot \sqrt{\frac{\gamma}{21}}\right) - \frac{1}{2}Q\left(7 \cdot \sqrt{\frac{\gamma}{21}}\right) \\ &+ \frac{1}{2}Q\left(9 \cdot \sqrt{\frac{\gamma}{21}}\right) + \frac{1}{4}Q\left(11 \cdot \sqrt{\frac{\gamma}{21}}\right) - \frac{1}{4}Q\left(13 \cdot \sqrt{\frac{\gamma}{21}}\right), \end{aligned} \tag{3.8}$$

respectively. Figure 3.3 shows close correspondence between the theoretical results that are presented above and the experimental simulations. The mean BER performance of square 16 point QAM, $P_{16}(\gamma)$, and square 64 point QAM, $P_{64}(\gamma)$, is given by

$$P_{16}(\gamma) = \frac{P_{16_1}(\gamma) + P_{16_2}(\gamma)}{2} \tag{3.9}$$

and

$$P_{64}(\gamma) = \frac{P_{64_1}(\gamma) + P_{64_2}(\gamma) + P_{64_3}(\gamma)}{3}, \tag{3.10}$$

assuming transmission through any of the sub-channels are equally likely.

3.2.2 Non-coherent Detection

The performance of differentially encoded modulation schemes in a Gaussian channel is inferior to non-differential encoding. An error condition in the reception of one symbol is likely to result in erroneous detections of the next symbol. This is particularly likely for BER below about 0.1; for higher BER erroneous detection of two consecutive symbols becomes more likely and consequently the possibility of these errors cancelling effects the overall BER

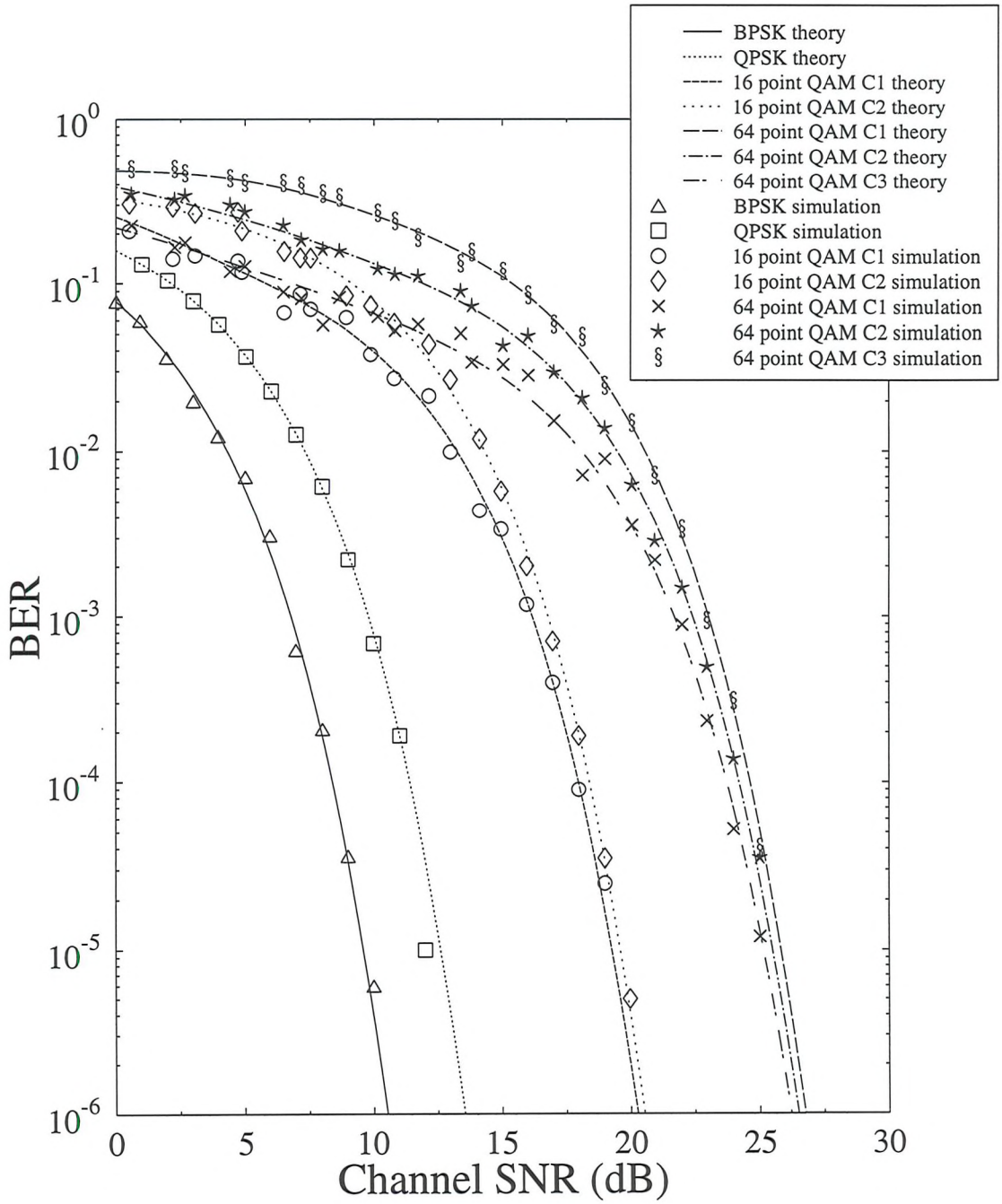

Figure 3.3: BER performance of BPSK, QPSK, square 16 point and square 64 point QAM through a Gaussian channel, showing both theoretical and simulated results

in a positive manner. Twice the BER is likely to be encountered with differential schemes compared with non-differential schemes. Although the BER may be twice that of the non-differential scheme, there may only be a very small difference in SNR for a given BER. Figure 3.4 compares the differential and non-differential modulation schemes over Gaussian channels. The difference in BER between the differential and non-differential schemes is greater than the expected factor of two and this is addressed below.

3.2.2.1 Decision Directed

In a non-fading channel, where the only corruption introduced to received symbols is noise, the corruption experienced by one symbol and the next are uncorrelated. The differential encoding at the transmitter is differential with respect to the transmitted symbol. It is therefore advantageous to differentially decode the current received symbol with respect to what is assumed to be the previous transmitted symbol, rather than the previously received symbol. This can be achieved by differentially decoding a received symbol with respect to the modulation constellation point closest to the previous received symbol. This is referred to as Decision Directed (DD) reception. The results of DD are plotted in Figure 3.4 and for one and two BPS, the two-fold increase in BER between differential and non-differential schemes can be observed. When it cannot be assumed that the difference between the received and the transmitted signal will be uncorrelated from symbol to symbol, DD gives sub-optimum results and non-DD is favoured.

3.2.2.2 Reduced Minimum Distance Constellation

The difference between differential and non-differential schemes for one and two BPS has been explained in Figure 3.4. However, the difference between differential and non-differential schemes is much larger for 16 point QAM and even with the aid of DD, and hence coherent detection, there are several orders of magnitude difference in BER. This difference amounts to about five dB of SNR between differential star 16 point QAM and non-differential square 16 point QAM. The difference is a result of both the reduced minimum distance modulation constellation shape as well as the differential encoding penalty.

3.3 Block Codes

By introducing some redundancy to a the stream of bits before transmission it is possible to achieve some error correction at the receiver. In this section the performance of systematic

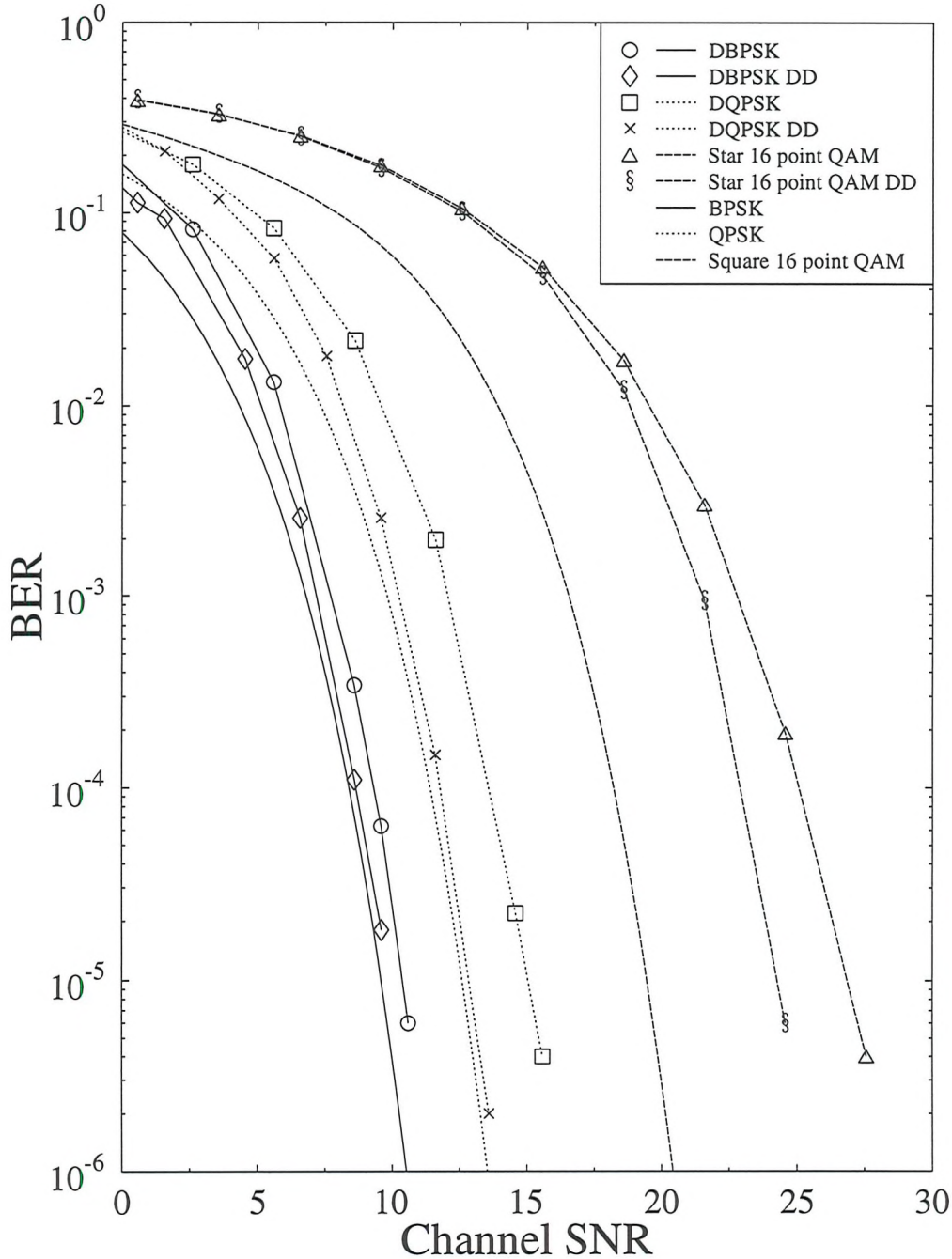

Figure 3.4: Simulated BER performance of DBPSK, DQPSK and differential star 16 point QAM with and without DD, compared with the theoretical performance BPSK, QPSK and the mean of square 16 point QAM through a Gaussian channel

block codes [1] are considered. A code is called systematic if the information bits are part of the codeword. The codes are referred to as n, k, t codes where n is the total number bits in the codeword, k is the number of information bits and t is the number of bits that may be corrected. A table of permissible n, k, t codes may be found in reference [73] and the probability of the code being successfully received in a Gaussian channel is given by,

$$y = \sum_{e=0}^{t} \left(\begin{array}{c} n \\ e \end{array} \right) \cdot p^e \cdot (1-p)^{(n-e)} \tag{3.11}$$

where p is the BER which may be derived for BPSK, QPSK, Square 16 and 64 QAM, at given SNR values using Equations 3.1-3.10

It is assumed [1] that the code offers sufficient protection that, even if error correction is not alway possible, error detection is always achieved. Therefore, when the number of errors in the received bits exceed t the systematic nature of the code may be exploited. This means that the parity bits are neglected and the information bits are assumed to be what was detected. The BER of the information bits is not statistically independent of the code being overloaded and therefore must be written as

$$q = \frac{1}{n} \sum_{e=t+1}^{n} \left(\begin{array}{c} n \\ e \end{array} \right) \cdot p^e \cdot (1-p)^{(n-e)}. \tag{3.12}$$

The overall probability of error for a transmission of block codes through a Gaussian channel is given as $y \cdot 0 + q = q$. Both y and q are given in Figure 3.5 for various codes from the $n = 127$ and $n = 255$ family and over a range of channel SNRs assuming perfect coherent detection of BPSK. Simulations were conducted, given the error detection assumption above, to compare with the analysis, and close correspondence is registered under all conditions.

Figure 3.5(b) and 3.5(d) show how the integrity of data increases as the number of redundant bits increase. This is what would be expected and often the SNR axis is modified to show energy per information bit as a ratio of the noise, E_b/N_0. This allows a comparison between increasing the received power or increasing the redundant bits in a signal.

3.4 Coherent Modulation in Rayleigh Channels

The performance of the non-differentially encoded modulation schemes in Rayleigh channels is intrinsically very poor. The phase corruption introduced by the channel can corrupt a symbol so much that a residual BER would be experienced in very high SNR scenarios. For

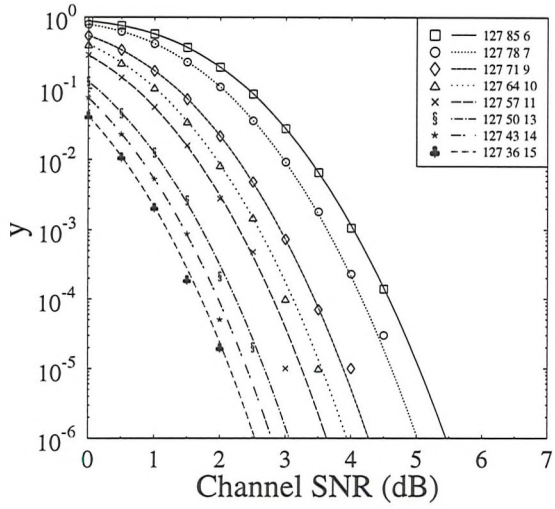

(a) Over-load probability for 127 bit family

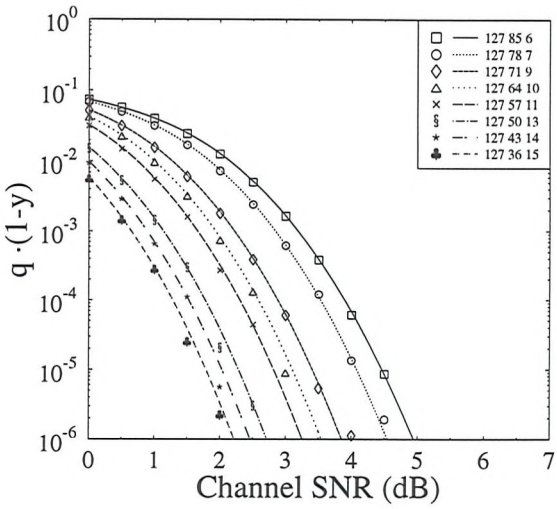

(b) BER for 127 bit family

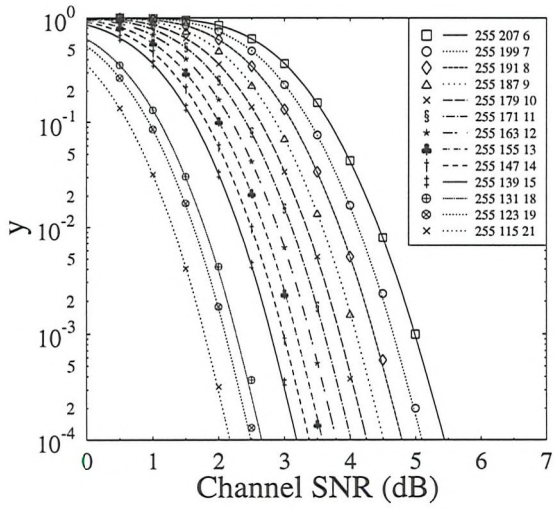

(c) Over-load probability for 255 bit family

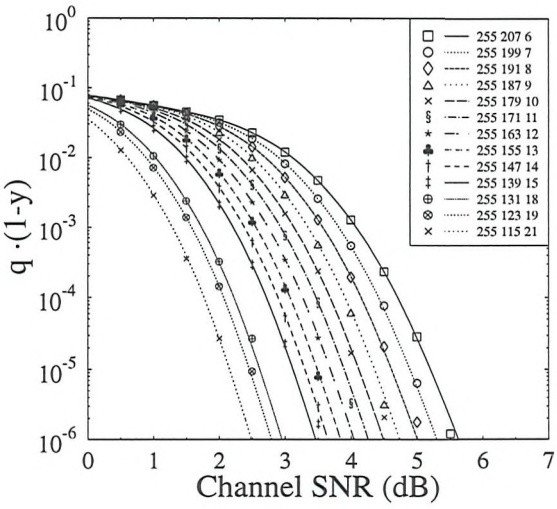

(d) BER for 255 bit family

Figure 3.5: Simulated (markers) and analytical (lines) performance of block coding over Gaussian channel employing BPSK

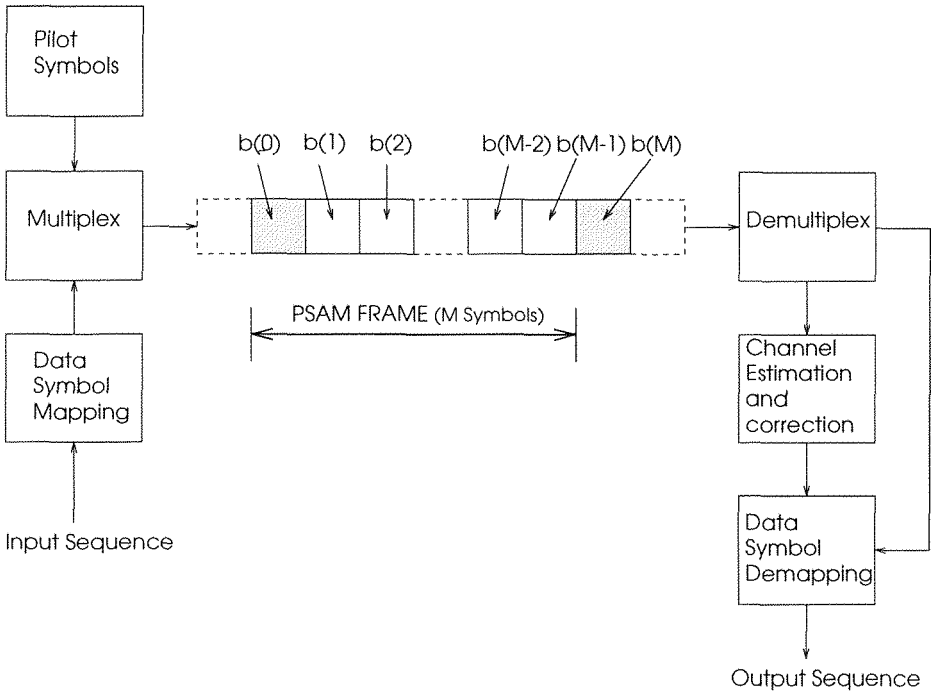

Figure 3.6: Schematic of a PSAM System showing the PSAM Frame

modulation schemes that exploit the amplitude of the transmitted symbol to carry information, channel induced amplitude corruption can also induce residual BERs. Exploiting the correlative characteristics of the channel fading and transmitting some redundant information through the channel with the data, it is possible for the receiver to estimate and hence compensate for the phase corruption and amplitude fading induced by narrow-band multi-path effects. One such method is referred to as Pilot Symbol Assisted Modulation (PSAM) and is described below.

3.4.1 PSAM Overview

The block diagram of a general PSAM scheme is depicted in Figure 3.6. Pilot symbols are cyclically inserted into the sequence of data symbols prior to pulse shaping. For this investigation a frame of data is constructed from a total of M symbols of which one is a pilot. The first symbol in every frame is assumed to be the pilot symbol $b(0)$, followed by $(M-1)$ useful data symbols $b(1), b(2) \ldots b(M-1)$. For simulation purposes, one of the symbols from the set of legitimate symbols shown in the constellation diagram was used as a pilot. The pilot symbol was always one of the largest amplitude symbols in the constellation. A pseudo random pattern of these legitimate symbols known to both the transmitter and receiver would be used in a practical implementation. This removes the periodicity of the

pilots and hence reduces the spectral occupancy.

The detection is performed by matched filtering and then the output of the filter is split in data and pilot paths, as seen in Figure 3.6. The set of pilot symbols is extracted by decimating the matched filter's sampled output sequence, using a decimation factor of M. The extracted sequence of pilot symbols is then interpolated in order to derive a channel estimate $v(k)$ for every useful received information symbol, $r(k)$. Finally, decision is carried out against a decision level reference grid which has been scaled and rotated according to the instantaneous channel estimate $v(k)$.

3.4.2 Comparison of PSAM Techniques [74]

In this section the performance of interpolation performed by simple linear, low-pass, polynomial and optimum linear interpolaters is compared. The optimum linear interpolator was originally proposed in [70] and is referred to as Cavers interpolation.

The received data symbols must be delayed according to the interpolation and prediction delay incurred. Increasing the number of pilots that are buffered before the interpolation is performed can improve the channel estimate at the cost of greater system latency. Latency is also increased by increasing the length of the PSAM frame, however, this results in more sparse pilots and reduced redundancy in the transmission sequence. Consequently, there is a trade-off between processing, redundancy, latency and accuracy.

Let the complex envelope of the modulated signal be

$$m(t) = \sum_{k=-\infty}^{\infty} b(k)p(t - kT), \tag{3.13}$$

where $b(k)$ represents the complex symbols to be transmitted, T is the symbol duration and $p(t)$ is a band-limited unit-energy signalling pulse for which

$$\int_{-\infty}^{\infty} |p(t)|^2 dt = 1. \tag{3.14}$$

For a narrow-band Rayleigh channel the received signal, $s(t)$, is

$$s(t) = f(t) \cdot m(t) + n(t), \tag{3.15}$$

where $n(t)$ is the AWGN and $f(t)$ is the channel's complex gain. Assuming a Rayleigh fading envelope $\alpha(t)$ and uniformly distributed phase $\phi(t)$ as described in chapter 2, then

$$f(t) = \alpha(t)e^{j\phi(t)}. \tag{3.16}$$

The matched filter's output symbols at the sampling instant kT are then

$$r(kT) = b(k) \cdot f(kT) + n(kT). \tag{3.17}$$

and the estimation of the fading is given by

$$\hat{f}(kT) = \frac{r(kT)}{b(kT)} \tag{3.18}$$

It is convenient to assume that in every PSAM frame $b(0)$ is the pilot symbol and to consider that the useful information symbols are in the range

$$\lfloor -M/2 \rfloor \leq k \leq \lfloor (M-1)/2 \rfloor, \tag{3.19}$$

where $\lfloor \bullet \rfloor$ is the integer part of $\bullet$. The interpolated estimate corresponding to the received symbol $r(k)$ in the range given by Equation 3.19, is the channel gain estimate, $v(k)$. It can be derived as a function of the surrounding K buffered pilot symbols $r(iM)$ for $\lfloor -K/2 \rfloor \leq i \leq \lfloor K/2 \rfloor$.

Different techniques can be deployed to estimate $v(k)$. Linear interpolation of the pilots offers computational simplicity and reduced latency. Lau et al [75] proposed linear extrapolation of pilot information that allows fading correction and de-mapping for symbols as they arrive rather than correcting for the fading on a frame by frame basis. This results in very low latency while sacrificing BER performance. Low-pass interpolation of the pilots [76] has been implemented by Moher et al [77], with a raised cosine window [78, 79] and other windows [80]. This method requires moderate computational complexity.

Gaussian interpolation is proposed by Sampei et al [81]. It has been implemented in hardware [82] and has been used for other Rayleigh fading compensation experiments [83, 84], including the trellis coded approach [85]. Gaussian interpolation is a form of polynomial interpolation but is only derived for the quadratic case. The computational complexity is the same as that with low-pass interpolation. Tsie et al [86] uses a similar approach but uses three previous and one future pilot in an attempt to reduce latency. Optimum interpolation [87] has been proposed for estimating the fading between pilots in narrow-band [70] and wide-band [88] [89] channels. More recently Tsie et al [90] has used optimum interpolation of pilots in conjunction with trellis coding and frequency hopping. While other techniques of interpolation exist [91, 92] and [93] this comparison is resticted to Linear, Low-pass, Polynomial and Cavers interpolation.

3.4.2.1 Linear Interpolation

The linear interpolated estimate of the fading is defined as

$$v(k) = \hat{f}(0) + k \cdot \left[\frac{\hat{f}(M) - \hat{f}(0)}{M} \right]. \tag{3.20}$$

Comparisons between interpolating the magnitude and the phase independently, compared with conducting the interpolation on the orthogonal complex axes independently showed, that the latter approach was favourable.

3.4.2.2 Low-pass Interpolation

Low-pass interpolation can be achieved by convolving a windowed impulse response with the received pilots, hence,

$$v(k) = \sum_{i=-K}^{K} h(k-i) \cdot \hat{f}(iM), \tag{3.21}$$

where

$$h(n) = \frac{\sin\left(\frac{n\pi}{M}\right)}{\frac{n\pi}{M}} \cdot W(n), \tag{3.22}$$

and $W(n)$ is the window function that is selected. The Hamming, Hanning and Blackman window functions were compared to determine which gave the best interpolation performance. When using a buffering of 5 PSAM frames with a pilot separation of 40 data symbols and evaluating the mean absolute error, the mean squared error and the maximum error between the real fading file and the interpolated file, the Hamming window was found to be marginally superior. The Hamming window was therefore used for all low-pass interpolation simulations.

3.4.2.3 Polynomial Interpolation

Polynomial interpolation is an extension of linear interpolation. It is possible to utilise pilot symbols to sample the fading an arbitrary number of times at arbitrary positions. A polynomial may then be fitted to these samples and an estimate of the fading at any other position may then be achieved. The P_n coefficients of such a polynomial are given by,

$$\begin{bmatrix} \lfloor -\frac{K}{2} \rfloor^{n-1} & \lfloor -\frac{K}{2} \rfloor^{n-2} & \cdots & \lfloor -\frac{K}{2} \rfloor^{1} & \lfloor -\frac{K}{2} \rfloor^{0} \\ \left(1 + \lfloor -\frac{K}{2} \rfloor\right)^{n-1} & \left(1 + \lfloor -\frac{K}{2} \rfloor\right)^{n-2} & \cdots & \left(1 + \lfloor -\frac{K}{2} \rfloor\right)^{1} & \left(1 + \lfloor -\frac{K}{2} \rfloor\right)^{0} \\ \vdots & \vdots & \cdots & \vdots & \vdots \\ \lfloor \frac{K}{2} \rfloor^{n-1} & \lfloor \frac{K}{2} \rfloor^{n-2} & \cdots & \lfloor \frac{K}{2} \rfloor^{1} & \lfloor \frac{K}{2} \rfloor^{0} \end{bmatrix}$$

$$\cdot \begin{bmatrix} P_1 \\ P_2 \\ \vdots \\ P_n \end{bmatrix} = \begin{bmatrix} r\left(\lfloor -\frac{K}{2} \rfloor\right) \\ r\left(\lfloor -\frac{K}{2}+1 \rfloor\right) \\ \vdots \\ r\left(\lfloor \frac{K}{2} \rfloor\right) \end{bmatrix}, \tag{3.23}$$

and then the channel estimate is given by,

$$v(k) = \frac{k}{M} P_1^{n-1} + \frac{k}{M} P_2^{n-2} + \ldots + P_n. \tag{3.24}$$

It is justifiable to assume that the relative spacing of the pilots will be constant. This implies that the matrix in Equation 3.23 need only be inverted once and from then on can be stored in memory. This means that for each channel estimate, $v(k)$, there need only be one multiplication and addition for each buffered pilot in both the in-phase and quadrature interpolaters.

3.4.2.4 Cavers Interpolation

This assumes that a linear model $v(k)$ can be derived as a linear sum,

$$v(k) = \sum_{i=\lfloor -K/2 \rfloor}^{\lfloor K/2 \rfloor} h(i,k) \cdot \hat{f}(iM), \tag{3.25}$$

and that the weighting coefficients $h(i,k)$ explicitly depend on the symbol position k within the frame of M symbols.

The estimation error $e(k)$ associated with the gain estimate $v(k)$ is computed as

$$e(k) = f(k) - v(k). \tag{3.26}$$

Cavers interpolation employs an optimum Wiener filter in order to minimise the channel estimation error variance, $\sigma^2{}_e(k) = E\{e^2(k)\}$, where $E\{\ \}$ represents the expectation. This well-known estimation error variance minimisation problem can be formulated as follows:

$$\begin{aligned} \sigma_e^2(k) &= E\{e^2(k)\} = E\{[c(k) - v(k)]^2\} \\ &= E\left\{\left[f(k) - \textstyle\sum_{i=\lfloor -K/2 \rfloor}^{\lfloor K/2 \rfloor} h(i,k) \cdot \hat{f}(iM)\right]^2\right\}. \end{aligned} \tag{3.27}$$

In order to find the optimum interpolater coefficients $h(i,k)$, minimising the estimation error variance $\sigma^2{}_e(k)$, the k^{th} sample and set are estimated:

$$\frac{\partial \sigma_e^2(k)}{\partial h(i,k)} = 0 \quad \text{for} \quad \lfloor -K/2 \rfloor \leq i \leq \lfloor K/2 \rfloor. \tag{3.28}$$

Then using Equation 3.27

$$\frac{\partial \sigma^2{}_e(k)}{\partial h(i,k)} = 0$$
$$= E\left\{ 2\left[f(k) - \sum_{i=\lfloor -K/2 \rfloor}^{\lfloor K/2 \rfloor} h(i,k) \cdot r(iM) \right] \cdot \hat{f}(jM) \right\}.$$

After multiplying both square bracketed terms with $\hat{f}(jM)$ and computing the expected value of both terms separately,

$$E\{f(k) \cdot \hat{f}(jM)\} = E\{ \sum_{i=\lfloor -K/2 \rfloor}^{\lfloor K/2 \rfloor} h(i,k) \cdot \hat{f}(iM) \cdot \hat{f}(jM)\}. \tag{3.29}$$

Observe that

$$\Phi(j) = E\{f(k) \cdot \hat{f}(jM)\} \tag{3.30}$$

is the cross-correlation of the received pilot symbols and complex channel gain values, while

$$R(i,j) = E\{r(iM) \cdot \hat{f}(jM)\} \tag{3.31}$$

represents the pilot symbol autocorrelations, hence Equation 3.29 yields:

$$\sum_{i=\lfloor -K/2 \rfloor}^{\lfloor K/2 \rfloor} h(i,k) \cdot R(i,j) = \Phi(j), \quad j = \lfloor -\frac{K}{2} \rfloor \ldots \lfloor \frac{K}{2} \rfloor. \tag{3.32}$$

If the fading statistics can be considered stationary, the pilot autocorrelations $R(i,j)$ will only depend on the difference $|i-j|$, giving $R(i,j) = R(|i-j|)$. Therefore, Equation 3.32 can be written as:

$$\sum_{i=\lfloor -K/2 \rfloor}^{\lfloor K/2 \rfloor} h(i,k) \cdot R(|i-j|) = \Phi(j), \quad j = \lfloor -\frac{K}{2} \rfloor \ldots \lfloor \frac{K}{2} \rfloor, \tag{3.33}$$

which is a form of the well-known Wiener-Hopf equations, often used in estimation and prediction theory.

This set of K equations contains K unknown prediction coefficients $h(i,k)$, where $i = \lfloor -K/2 \rfloor \ldots \lfloor K/2 \rfloor$, which must be determined in order to arrive at a minimum error variance estimate of $f(k)$ by $v(k)$.

First the correlation terms $\Phi(j)$ and $R(|i-j|)$ must be computed and hence the expectation value computations in Equations 3.30 and 3.31 need to be restricted to a finite duration window. The pilot autocorrelation, $R(i,j)$, may then be calculated from the fading estimates at the pilot positions within this window. Calculation of the received pilots' and the complex channel gains' cross correlation is less straightforward, because in order to calculate the cross-correlation the complex channel gains have to be known at the position of the data symbols

as well as at the pilot symbols. However, the channel gains are only known at the pilot positions, while for the data symbol positions they must be derived by interpolation. Hence, a polynomial was fitted to the known samples of $R(|i-j|)$ and then the values of $\Phi(j)$ for the unknown positions were estimated.

The set of Equations 3.33 can also be expressed in a convenient matrix form as:

$$\mathbf{R} = \begin{bmatrix} R(0) & R(1) & R(2) & \dots & R(K) \\ R(1) & R(0) & R(1) & \dots & R(K-1) \\ R(2) & R(1) & R(0) & \dots & R(K-2) \\ \vdots & \vdots & \vdots & \dots & \vdots \\ R(K) & R(K-1) & R(K-2) & \dots & R(0) \end{bmatrix}$$

$$\cdot \begin{bmatrix} h\left(\lfloor -\frac{K}{2} \rfloor, k\right) \\ h\left(\lfloor -\frac{K}{2}+1 \rfloor, k\right) \\ h\left(\lfloor -\frac{K}{2}+2 \rfloor, k\right) \\ \vdots \\ h\left(\lfloor \frac{K}{2} \rfloor, k\right) \end{bmatrix} = \begin{bmatrix} \Phi\left(\lfloor -\frac{K}{2} \rfloor\right) \\ \Phi\left(\lfloor -\frac{K}{2}+1 \rfloor\right) \\ \Phi\left(\lfloor -\frac{K}{2}+2 \rfloor\right) \\ \vdots \\ \Phi\left(\lfloor \frac{K}{2} \rfloor\right) \end{bmatrix},$$

which can be solved for the optimum predictor coefficients $h(i,k)$ by matrix inversion using Gauss-Jordan elimination or any appropriate recursive algorithm. Once the optimum predictor coefficients $h(i,k)$ are known, the minimum error variance channel estimate $v(k)$ can be derived from the received pilot symbols using Equation 3.25. This is reevaluated frame by frame.

3.4.3 Simulation Lengths

If an insufficient number of symbols is simulated in Gaussian channel modulation simulation, then the SNR/BER curve is inaccurate. Generally, when insufficient symbols are simulated, the curve does not appear smooth. This is especially true at high SNRs because the significance of a BER result in a Gaussian channel, is a function of the number of error events [94] and there are less errors at higher SNRs. Therefore, the smoothness of the SNR/BER curve gives an indication as to whether the simulation length was long enough for significant measure of BER performance. For Gaussian channels, it is possible to run a simulation at a given SNR until the number of errors exceeds a threshold, that is shorter simulations for lower SNR.

For a Rayleigh channel, applying this criteria for the simulation length, would result in the

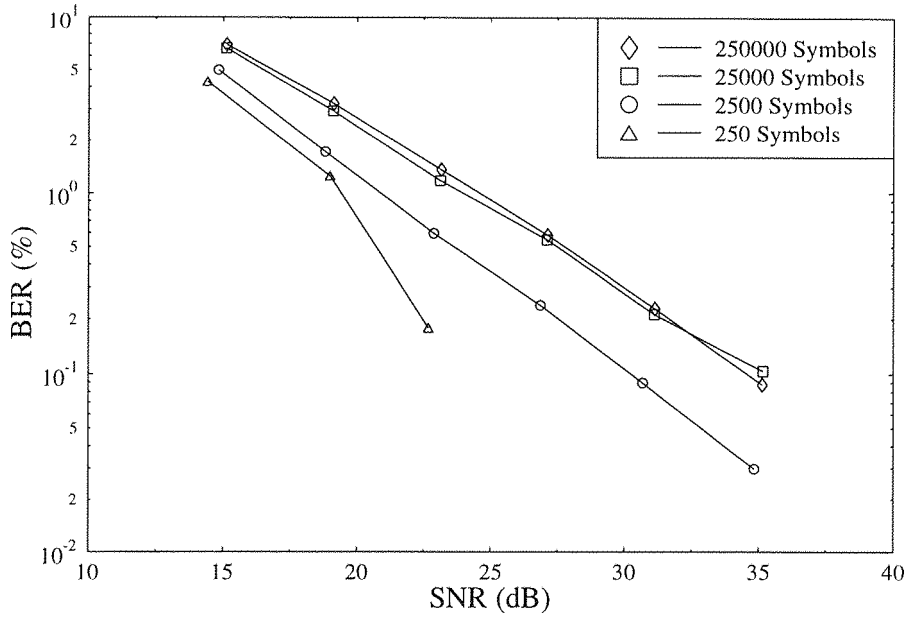

Figure 3.7: BER for square 16 point QAM, polynomial interpolation with 5 buffered pilots and $M = 30$ through a Rayleigh channel with a normalised Doppler frequency of 4.16955×10^{-3} for various run lengths.

simulations at different SNRs experiencing a different length segment of the Rayleigh channel. Therefore, the PDF of the fading experienced in the shorter length simulations, would not necessarily be significantly Rayleigh distributed, consequently, an unfair comparison of the performance, at different SNRs, would occur. When performing Rayleigh channel simulations, the simulation length must be the same for all values of SNR. Rayleigh channel simulations must have a significant number of errors, as with Gaussian simulations, moreover, the segment of channel used in the simulation must be long enough to significantly represent Rayleigh channel. Ideally, for each Rayleigh channel simulation, the whole file of fading that was generated in chapter 2 should be used to evaluate the performance at every SNR because, comprehensive tests were conducted to insure that this fading was significantly representative of Rayleigh fading. However, this is often prohibitive in terms of simulation run time. Figure 3.7 shows the SNR/BER curve for simulations where the run length was fixed at 250, 2500, 25000 and 250000 symbols for each of the SNR values. It can be seen that for simulations

conducted with 250 symbols, at above 20 dB, the number of errors registered was not significant for an accurate estimation of the BER. For the simulation with 2500 symbols the number of errors become significant for an accurate BER estimation, however, insufficient channel samples were considered, so the BER performance was significant for a channel that could not be considered to be Rayleigh. When the simulation length reached 25000 the performance was approximately the same as with 250000 symbols and from this it is concluded that a minimum of 25000 symbols had to be simulated at all SNRs.

The figure of 25000 symbols only applies to a Rayleigh channel with a normalised Doppler frequency of 4.16955×10^{-3}. However, a reasonable assumption would be calculate the number of fades in 25000 samples in a Rayleigh channel with a normalised Doppler frequency of 4.16955×10^{-3}, and ensure that all Rayleigh simulations are for channels with a length of that many fades. The equation,

$$D_s = \frac{1}{2 \cdot f_d T} \tag{3.34}$$

where D_s and f_d are the mean number of symbols per fade and $f_d T$ is the normalised Doppler frequency, can be used to show that the 25000 symbols, above, correspond to two hundred fades. Therefore, for all Rayleigh channel simulations, the performance of a modem must be evaluated over a minimum of 200 fades.

3.4.4 Simulation Parameters

The PSAM investigations were restricted to continuous rather than packetised transmission. The effects of TDMA framing restrict the number of pilots that may be buffered to assist the channel estimation. However, in TDMA systems it is possible to for the handset receiver not to power down during transmissions slots from the base-station to other users. Provided the handset is aware of the transmitted power of these slots, the pilots could be used to make extra estimates of the channel and aid the performance of the interpolation.

At the relatively low signalling rate, 20kBd, used by the Pan-American IS-54 system, the fading channel that characterises such a system is quite hostile to PSAM schemes and is used for these simulations. The propagation frequency was increased from 900 MHz to 1.8 GHz and the vehicular speed was fixed at 50 km/h. The corresponding Doppler frequency is 83.3 Hz, giving a normalised Doppler frequency of 0.0042. In comparison, the GSM-like DCS1800 system under identical propagation conditions results in a normalised Doppler frequency of 0.0003, which is associated with less dramatic fading of the signal envelope and hence better fade tracking properties. The corresponding Doppler filter emulated a vertical loop antenna in a plane perpendicular to the vehicle's motion and, apart from the channel's phase rotations,

perfect carrier and clock recovery were assumed.

The four previously mentioned interpolation methods were simulated and compared for BPSK, QPSK and square 16 point QAM. The performance was evaluated at channel signal to noise ratios (SNR) of 20, 30 and 40 dB, which yielded $3 \cdot 4 \cdot 3 = 36$ sets of results. In each set of results the buffering was 3, 5, 7, 9, 11 PSAM frames and the pilot separation was 10, 20, 40, 60, 80, 100, 116 data symbols. This lead to a plethora of performance curves, which allowed the generation of a corresponding set of 3-dimensional (3D) graphs of BER versus the number of buffered PSAM frames, labelled Buffer, and the gap between pilot symbols, labelled Gap.

3.4.5 Results and Discussion

Results are shown for BPSK, QPSK and square 16 point QAM in Figures 3.8-3.10, respectively. For all modulation schemes and interpolation techniques, as well as at all Buffer and Gap values, the BER reduces with increasing channel SNR. Furthermore, increasing the Buffer and reducing the Gap will typically reduce the BER but all scenarios exhibited a BER floor. Furthermore, the Residual BER (RBER) did not depend significantly on the interpolation scheme used.

For each of the modulation schemes, interpolation techniques and SNRs the RBER was inferred from Figures 3.8-3.10. The RBER values can be portrayed more conveniently in terms of bit energy per noise spectral density (E_b/N_0), and are summarised in Table 3.1 and shown in Figure 3.11. Note that the Buffer and Gap values required to achieve the RBER are dependent upon the type of interpolation technique used. System latency and complexity also depend on the choice of interpolation scheme. The BPSK and the QPSK are very similar, since QPSK constitutes two orthogonal BPSK systems and perfect clock and carrier recovery are assumed, except for the corruption that is induced by the channel. Square 16 Point QAM requires approximately 3.5 dB more E_b/N_0 and a further 6 dB more channel SNR than QPSK.

Figure 3.11 also shows what can be achieved with perfect coherent detection. This was simulated assuming perfect fading estimates by correcting for the channel fading at the receiver with the reciprocal of the actual fading rather than the interpolated estimation derived from the pilot samples. This limit is not achieved with PSAM because the channel noise corrupts the pilots and consequently impairs the quality of the channel estimate. It can be seen that if it were possible to correct for the fading perfectly, only another 2dB of performance could be gained. Sending bursts of pilots was considered, so that the noise on one pilot burst could be

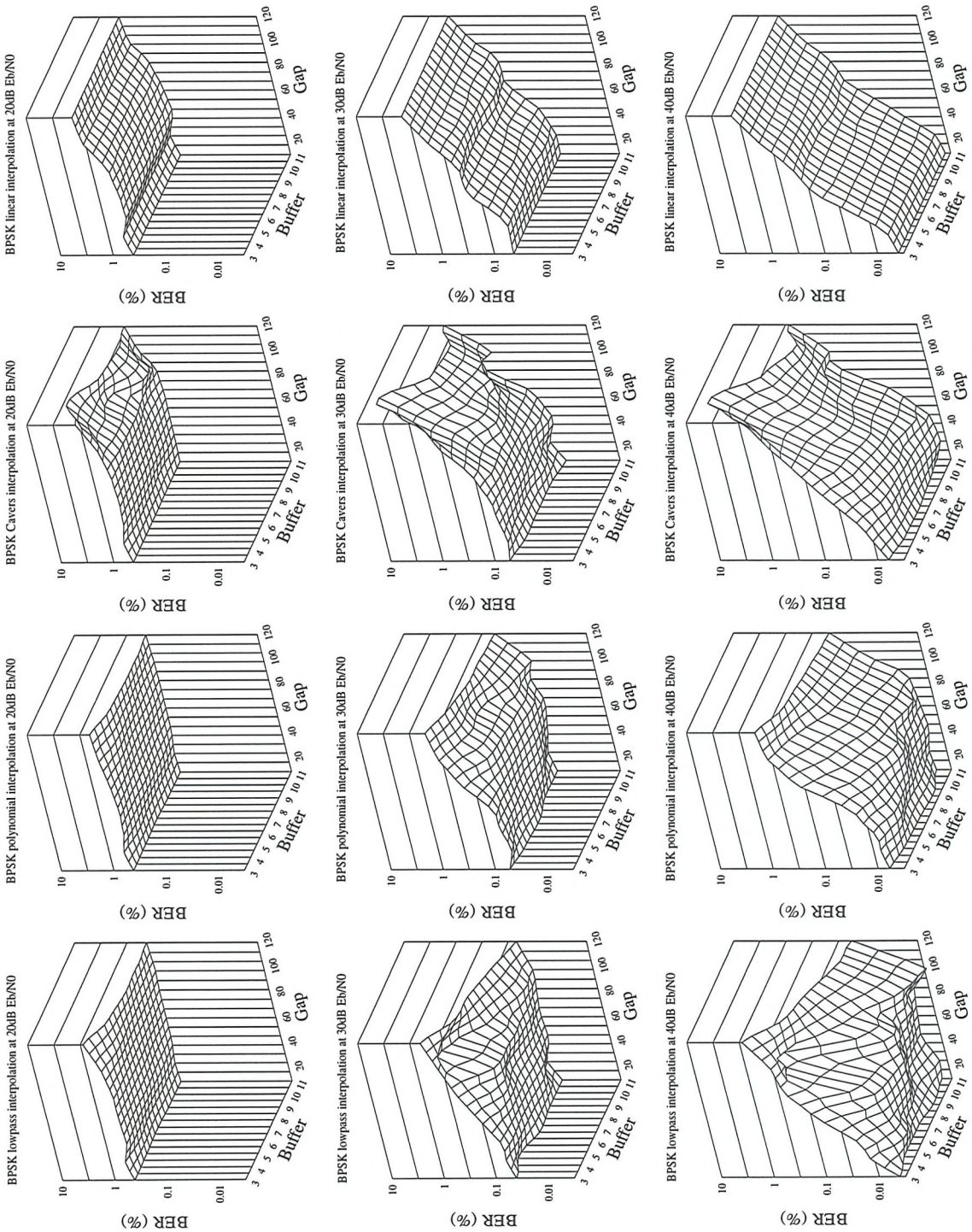

Figure 3.8: BER performance versus Buffer and Gap of pilot symbol assisted BPSK over Rayleigh channels at 20 kBd, 50 km/h, 1.8 GHz

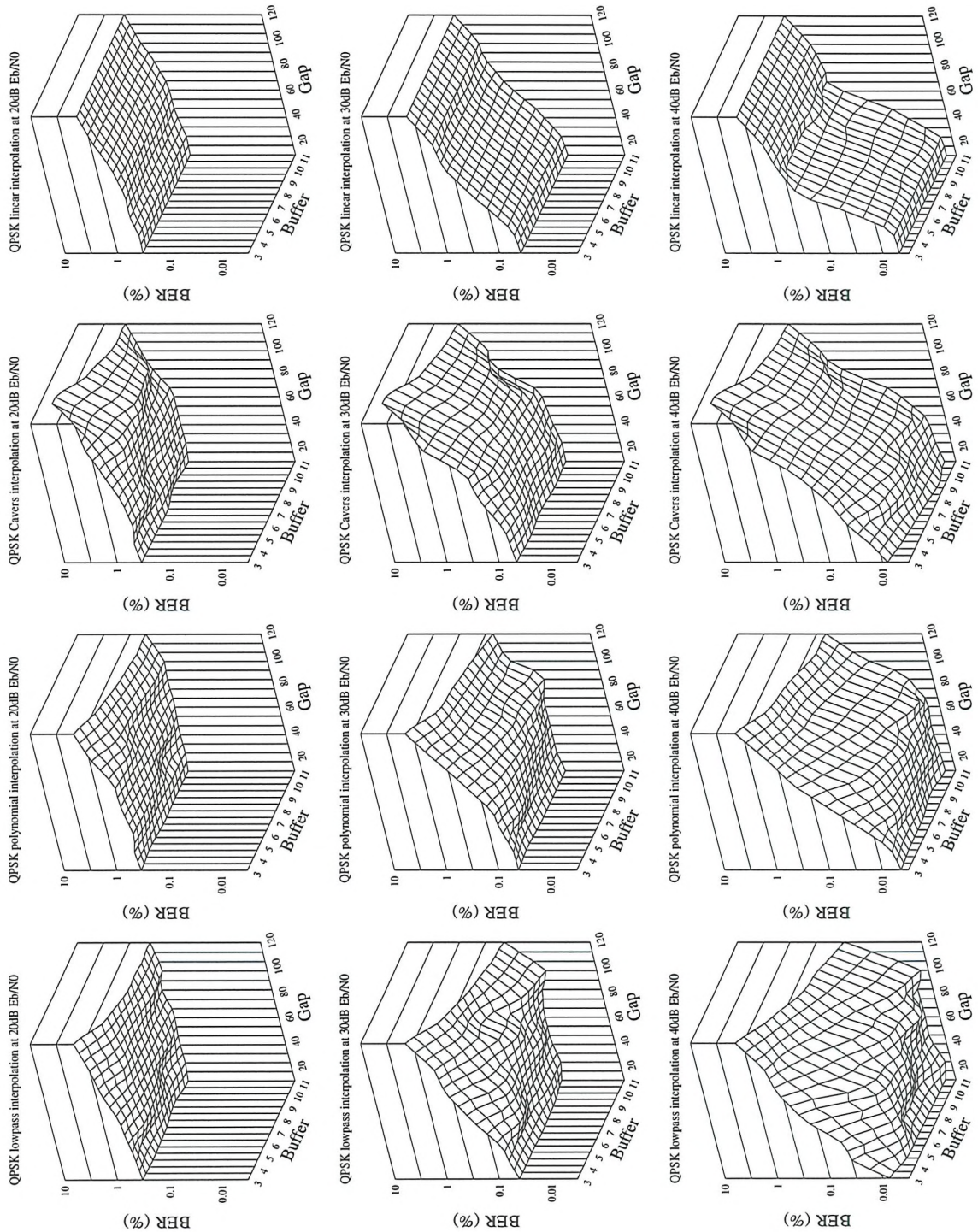

Figure 3.9: BER performance versus Buffer and Gap of pilot symbol assisted QPSK over Rayleigh channels at 20 kBd, 50 km/h, 1.8 GHz

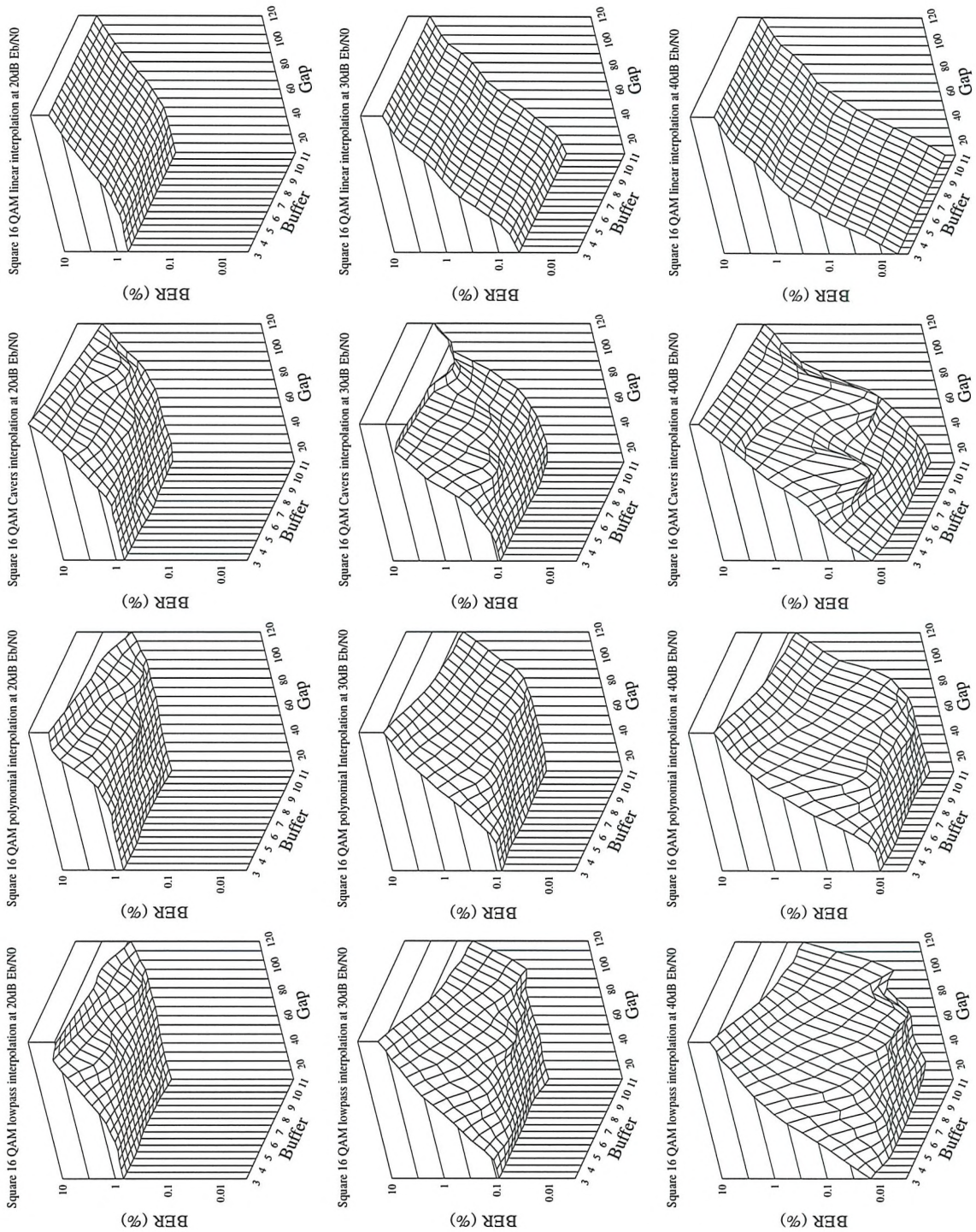

Figure 3.10: BER performance versus Buffer and Gap of pilot symbol assisted square 16 point QAM over Rayleigh channels at 20 kBd, 50 km/h, 1.8 GHz

Interpolation technique	BPSK $\frac{E_b}{N_0}$[dB]			QPSK $\frac{E_b}{N_0}$[dB]			QAM $\frac{E_b}{N_0}$[dB]		
	20	30	40	20	30	40	20	30	40
Linear	0.41	0.042	0.0040	0.32	0.039	0.0049	0.62	0.041	0.006
Polynomial	0.43	0.040	0.0045	0.35	0.040	0.0050	0.68	0.090	0.009
Low-pass	0.43	0.040	0.0045	0.35	0.040	0.0050	0.68	0.080	0.009
Optimum	0.43	0.040	0.0045	0.35	0.040	0.0050	0.68	0.080	0.009

Table 3.1: RBER (%) of PSAM BPSK, QPSK and square 16 point QAM over narrow-band Rayleigh fading channel using Linear, Polynomial, Low-pass and Optimum Linear Interpolation at 20 kBd, 50 km/h, 1.8 GHz

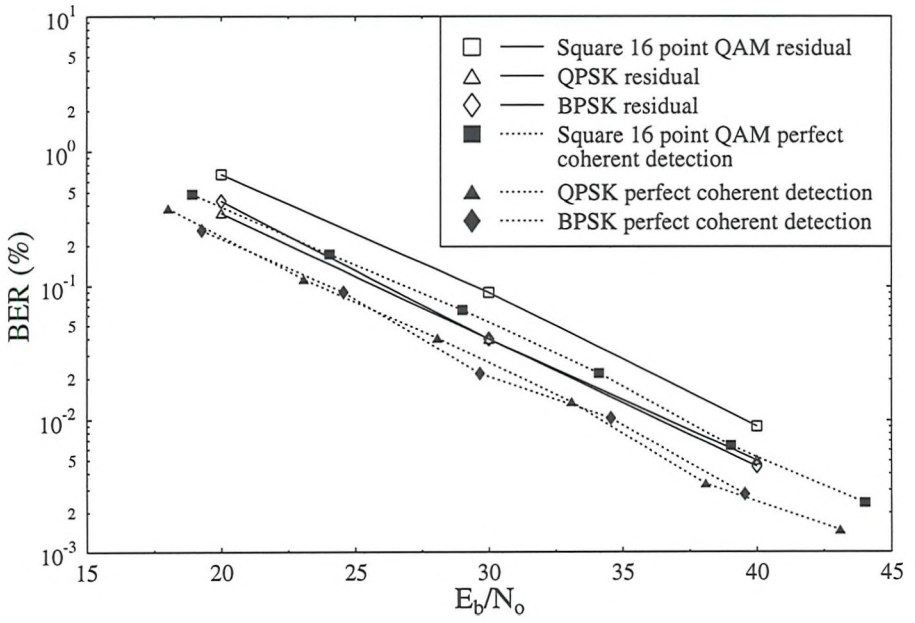

Figure 3.11: RBER (%) of PSAM BPSK, QPSK and square 16 point QAM compared with perfect coherent detection of BPSK, QPSK and square 16 point QAM over narrow-band Rayleigh fading channel using Linear, Polynomial, Low-pass and Optimum Linear Interpolation at 20 kBd, 50 km/h, 1.8 GHz

averaged. It was decided that this trade off would give a disproportionate increase in signal redundancy for the gain in SNR/BER performance.

Comparing either the residual or the perfect coherent detection graphs in Figure 3.11 with the performance of differential or non-differential modulation schemes in a Gaussian channel in Figures 3.3 and 3.4, two observations can be made. The first is that the performance in Rayleigh channels is very much worse than in a Gaussian channel. At a BER of 0.01 the performance is at least 30 dB less favourable in the Rayleigh channel. The second observation is that the difference between the Rayleigh and the Gaussian channel becomes greater as the SNR increases. From this it can be concluded that the phase distortion introduced by the channel can relatively easily be corrected through the use of PSAM. However, the amplitude fading of the transmitted signal still results in a large number of errors with respect to the Gaussian channel of the same average SNR. This is because, despite PSAM compensating for the amplitude of the fading, the noise corruption is additive to the faded signal and any correction will not be able to separate the noise from the signal. Consequently when the symbol rate is high enough and the phase correction good enough, a Rayleigh channel can be considered as a Gaussian channel with many segments of different average SNRs. The short-term SNR of these segments is likely to be correlated with its adjacent segments.

Referring again to Figures 3.8-3.10, it can be observed that in case of small Buffer the polynomial interpolater gave the best BER performance. With the polynomial interpolation RBER performance was achieved, for all modulation schemes and at all SNRs, with the lowest cost in terms of redundancy, i.e., with the largest Gap. This is because in case of short Buffer, that is, when few pilots are buffered and correspondingly few channel estimates are known, the non-linear nature of the polynomial model will out-perform both the linear interpolation and low-pass interpolation performed with a severely truncated impulse response. As Buffer is increased, the high-order coefficients of the polynomial interpolator diminish and hence increasing Buffer becomes less beneficial. As Buffer increases, the impulse response of the low-pass interpolater becomes more like that of an ideal Sinc function and therefore its performance improves.

When comparing the three interpolation techniques, the linear interpolation requires the least complexity and the latency is low because only two pilots need to be buffered. The latency is related to the product of the number of buffered pilots and Gap. For linear interpolation the latency is reduced further as a result of the need to maintain a small Gap; linear interpolation had poor performance over large Gaps. It is generally true, that to increase Gap, there will be a two-fold negative effect on the latency. The first is the need to buffer more pilots in order to make the channel estimation acceptable. The second is because of the increased number

of data symbols between pilots space between the pilots. The investment of increased Gap is less signal redundancy.

It can be seen from Figures 3.8-3.10 that the benefit of increased complexity interpolation is less worthwhile in a noisy channel. That is the RBER is achieved for less computation, latency and redundancy in channels with a lower SNR.

The experiments discussed have been conducted with a normalised Doppler frequency of 4.16955×10^{-3}. It is reasonable to assume that results for simulations conducted at other normalised Doppler frequencies can be extrapolated from these results by modifying the Gap measurement by an equivalent amount, for example, the BER performance at a gap of 40 with the normalised Doppler frequency of 4.16955×10^{-3} would correspond to a gap of 20 with the normalised Doppler frequency of 8.3391×10^{-3}.

Generally the polynomial or linear interpolation appear to offer the best performance. Particularly in a TDMA/TDD environment where buffering many pilots may not be possible. Cavers and low-pass interpolation, however, offer an interesting performance benchmark.

3.4.6 Transparent Tone In Band

An alternative to PSAM is Transparent Tone In Band (TTIB)[1]. TTIB separates the spectrum of transmitted signal and inserts a reference tone into the gap in the spectrum. At the receiver, compensation for the channel can be evaluated from the attenuation and phase rotation experienced by the tone. Having evaluated the distortion and assuming that narrowband conditions prevail, the channel effects can be compensated for, the pilot tone can be removed and the separation in the spectrum closed. Martin et al [95] presents such a technique for the use of square 16 point QAM. They conclude that there is only a small signalling redundancy in Gaussian channels and a residual BER of 0.0001 in a Rayleigh fading channel with a normalised Doppler frequency of 0.0625. Cavers et al [96] conducted a comparison between PSAM and TTIB. They evaluated average power ratio, ease of linearisation, spectral occupancy, delay and complexity and concluded that for most applications PSAM is superior to TTIB.

[1]TTIB is mentioned here for completeness although all the work presented is the result of other authors' endeavours

	Differential			PSAM		
$\frac{E_b}{N_0}$[dB]	DBPSK	DQPSK	16 Star	BPSK	QPSK	16 Square
20	0.38	0.42	1.2	0.43	0.35	0.68
30	0.05	0.058	0.18	0.04	0.04	0.09
40	0.011	0.012	0.03	0.0045	0.005	0.009

Table 3.2: RBER (%) for PSAM Schemes and Differential Schemes, of various modulation constellations and at various SNRs over a narrow-band Rayleigh fading channel at 20 kBd, 50 km/h, 1.8 GHz

3.5 Non-coherent Modulation in Rayleigh Channels

As a comparison with the results from Section 3.4, a series of differential modulation experiments were conducted. These used the star constellations and differential encoding discussed in Section 3.1.2. PSAM was not used, so buffer length and pilot separation are not an issue. For the three modulation schemes, DBPSK, DQPSK and differential star 16 point QAM, BERs were evaluated at values of E_b/N_0 equal to 20, 30 and 40 dB for the same channel conditions that were experienced in the PSAM simulations. The results are shown in Table 3.2 and Figure 3.12.

It can be observed that as the modulation constellation becomes less complex, that is, the number of BPS is reduced, the benefits of coherent modulation are reduced, although this is also a function of the channel SNR. For BPSK at an SNR of 20 dB, the differential scheme actually has a marginally better BER performance than the corresponding PSAM scheme, even when disregarding the proportion of power allocated to the pilots. In contrast, for higher order constellations, such as QPSK and square 16 point QAM , PSAM does reduce the RBER and has a better performance than differential star 16 point QAM , while having a somewhat higher latency and similar complexity, when using linear interpolation. This is entirely consistent with the observations of Section 3.2.2 where it was observed that the difference between differential and non-differential schemes was greater for more complex constellations.

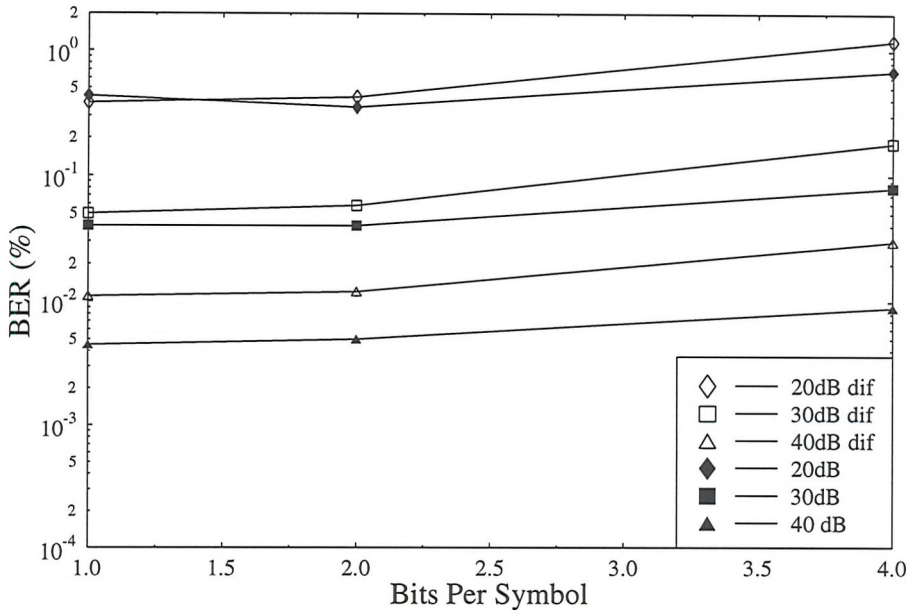

Figure 3.12: RBER (%) for one, two and four BPS PSAM modulation compared with equivalent differential schemes.

3.6 Conclusions

The BER performance, through a Rayleigh channel, of PSAM with non-differential, coherent modulation schemes was very much better than what was be achieved without PSAM. It was also better than differential, non-coherent modulation for 2 and 4 BPS; the difference in performance being greater at 4 BPS than 2 BPS. However, the performance of the non-differential, coherent modulation schemes with PSAM was still very much worse than the performance of the modulation schemes over Gaussian channels with the same mean SNR.

In terms of E_b/N_0, PSAM can mitigate the effects of the amplitude and phase distortion inflicted upon the transmitted symbols within 2dB of an upper bound. This suggests that PSAM performs well in terms of achieving coherent demodulation and normalisation of amplitude for QAM schemes. PSAM, however, can do nothing about the noise corruption experienced during fading. This explains why PSAM non-differential, coherent modulation through Rayleigh channels still has a much worse BER performance in Gaussian channels.

The shortest system latency and lowest complexity amongst the PSAM schemes was associated with the one employing the first-order linear interpolater. For higher-order phasor constellations, such as that of QPSK and square 16 point QAM the linearly interpolated PSAM arrangement outperformed the corresponding non-coherent scheme, while exhibiting similar complexity.

The preferred PSAM scheme employed polynomial interpolation when few pilots had to be buffered. This would typically be the case in a cellular system. However, in a broadcasting application, where latency is likely to be less important than redundancy and continuous transmission is employed, low-pass interpolation may be favoured.

Chapter 4

A Numerical Investigation into Narrow-band Adaptive Modulation

4.1 Introduction

Mobile radio channels exhibit fluctuations in received signal power and phase. These channels were discussed in chapter 2. Chapter 3 introduced PSAM and it was observed that such a technique could mitigate the effect of the phase distortion introduced by the channel to within 2dB of the case when assuming perfect channel estimates. However, pilot-based compensation for the received power fluctuations results in amplification of the corrupting noise at the receiver, as well as amplification of the signal. PSAM can do nothing to combat the fluctuating short term SNR that is experienced in a fading channel.

There are two distinct approaches towards combating short term fluctuations of the SNR, such as that experienced in a fading channel. One approach is stochastic and the other deterministic. Stochastic techniques involve adding redundancy to the signal so that the information successfully received during periods of higher short term SNR, can be used to reconstruct the information lost during the fades. Such techniques employ either Forward Error Correction (FEC), such as block or convolutional codes [1], or modulation constellation expansion and Trellis Coded Modulation (TCM) [97].

An ideal deterministic approach could vary the transmitter power on the basis of the fading induced by the channel. If this could be done successfully the multi-path channel would be rendered a Gaussian channel and would have the BER performance of the latter. This idea is tempting because the extra transmitter energy needed to compensate for deep fades could be saved by reducing the transmitter power during periods of constructive superposition of

radio waves. However, apart from complicated hardware ramifications, the result of short term fluctuations in transmitter power from -60 dB to $+10$ dB would result in considerable peak co-channel interference problems in a cellular system. However, optimum power control could reduce overall co-channel interference.

An alternative deterministic approach to mitigating the effects of fading would be to vary the modulation scheme on the basis of the expected received signal level. For example, when a low short term SNR is expected at the receiver, a more robust modulation scheme should be employed. When the short term SNR increased again a less rugged scheme with greater throughput should be employed. Such schemes have been proposed to mitigate the effects of the path loss described in Section 2.3; these include proposals by Sampei et al [98] and the European RACE project regarding Advanced Time Division Multiple Access (ATDMA) [99, 100, 101, 102, 103]. Investigations have begun into deploying adaptive modulation schemes to mitigate the effects of fast fading. These were initiated by Steele and Webb and presented in a keynote paper [104] which discussed adaptive differential modulation and considered the effect of SNR and Co-channel interference. This work was based around star modulation constellations. Otsuki et al [105] worked using square constellations and have considered using Walsh functions to inform the receiver of which modulation scheme was used for the transmitted symbols, Morinaga [106] considers the position of adaptive modulation in terms of its future within mobile multimedia apparatus. Other authors have investigated the performance of various parameters of adaptive modulation schemes that include varying the symbol and coding rates [107, 108, 109, 110, 111, 112]. Alouini et al [113] have considered continiously varying the modulation scheme and power level on a symbol by symbol basis. The work in this thesis takes a different approach, by exploiting a numerical relationship between the channel conditions and the performance of square adaptive modulation. This is exploited in the optimisation of parameters associated with adaptive modulation. In later chapters interference cancellation as a complimentary technique to adaptive modulation is discussed. This is followed by an investigation of the network and control issuses that are neglected in this chapter.

4.2 System Overview

It has already been noted that the phase rotation introduced by the mobile channel can be largely mitigated using PSAM. However, the resulting channel still has a fluctuating short term SNR. If the fade duration is significantly longer than the duration of a slot within a TDMA frame, then the short term SNR will be approximately constant for the duration of

the slot and the characteristics of the channel for that slot will be approximately Gaussian. An instantaneous SNR, γ', for a TDMA slot can be derived from Equation 2.2, where the averaging operation, $\langle\rangle$, is performed over the length of the slot within the TDMA frame. The power of the noise is independent of the received signal and therefore the mobile channel can be considered as a Gaussian channel with SNR γ', where γ' varies from frame to frame. For successful adaptive modulation the transmitter needs to estimate the value of γ' at the receiver and transmit using a suitable modulation scheme. The estimation of γ' can be achieved in a TDD scenario by exploiting the reciprocity between the up and down link. The autocorrelation of the fading can be exploited, too. Therefore, the signal energy that will be received at one end of the TDD link may be estimated on the basis of what energy was received at the other end of the link in previous TDMA/TDD frames. Both the Gaussian channel nature of each slot and the correlation between slots from adjacent TDD frames can be seen in Figure 4.1.

In adaptive modulation with a TDD scenario the transmitting end of the link estimates what the instantaneous received power, s, will be for each slot on the basis of received frames. This estimation is compared against a set of n switching levels, l_n, and the appropriate modulation scheme is selected accordingly. Following Kamio et al [112] the modulation schemes that are used are selected as follows;

$$\text{modulation scheme} = \begin{cases} \text{No Transmission} & \text{if} \quad s < l_1 \\ \text{BPSK} & \text{if} \quad l_1 \leq s < l_2 \\ \text{QPSK} & \text{if} \quad l_2 \leq s < l_3 \\ \text{Square 16 Point QAM} & \text{if} \quad l_3 \leq s < l_4 \\ \text{Square 64 Point QAM} & \text{if} \quad s \geq l_4 \end{cases} \tag{4.1}$$

where the values of l_n will be discussed later. This principle is illustrated in Figure 4.2.

At the receiver the modulation scheme that was used by the transmitter must be determined. The easiest way for the receiver to determine this is for the transmitter to include some control information that will allow the receiver to identify the modulation scheme used. Figure 4.3 shows a general frame and slot structure that could be used. The pilot symbols are for the use of the PSAM scheme and the control symbols allow the receiver to determine the modulation scheme that was used at the transmitter. In this example, the control symbols have a maximum average separation and therefore their independence is marginally improved.

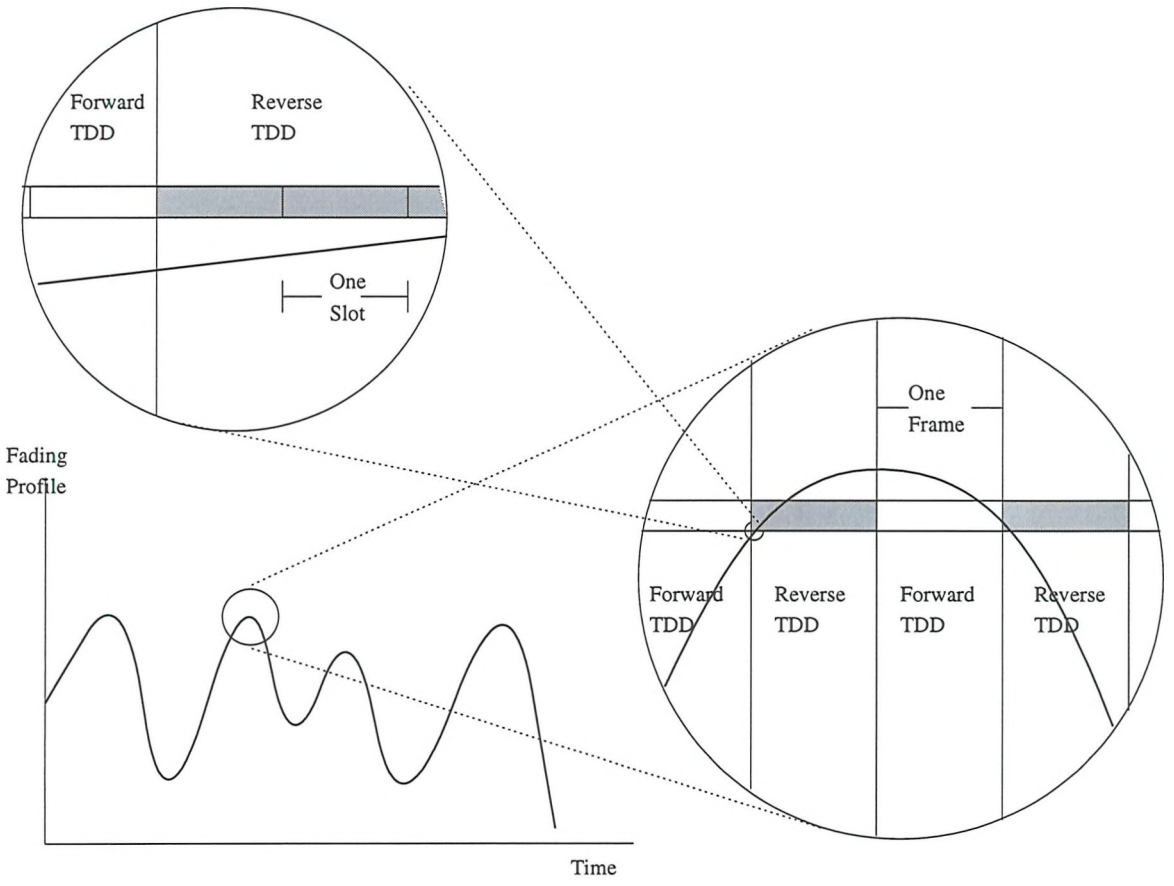

Figure 4.1: A small variation in average received power, over the length of one slot, when compared with the deviation over the whole channel results in a single slot tending to Gaussian channel characteristics. The correlation between corresponding slots in adjacent TDD frames may be exploited

4.2.1 Transmission Integrity versus Capacity

The values of the switching levels, l_1, l_2, l_3 and l_4 define the performance of an adaptive modulation scheme in a set of given channel conditions. The lower the values are, the greater the throughput because on average more symbols will be transmitted using a higher number of Bits Per Symbol (BPS). Conversely, the higher the values of l_1, l_2, l_3 and l_4, the lower the mean BER of the overall adaptive modulation scheme for given channel conditions. BER can be traded for BPS and vice versa. The optimum trade-off will depend upon the type of information being transmitted and the source and channel coder that is used to encode it.

The trade-off is dependent upon the type of information that is to be transmitted because of the different network characteristics required by, for example, video, voice and computer

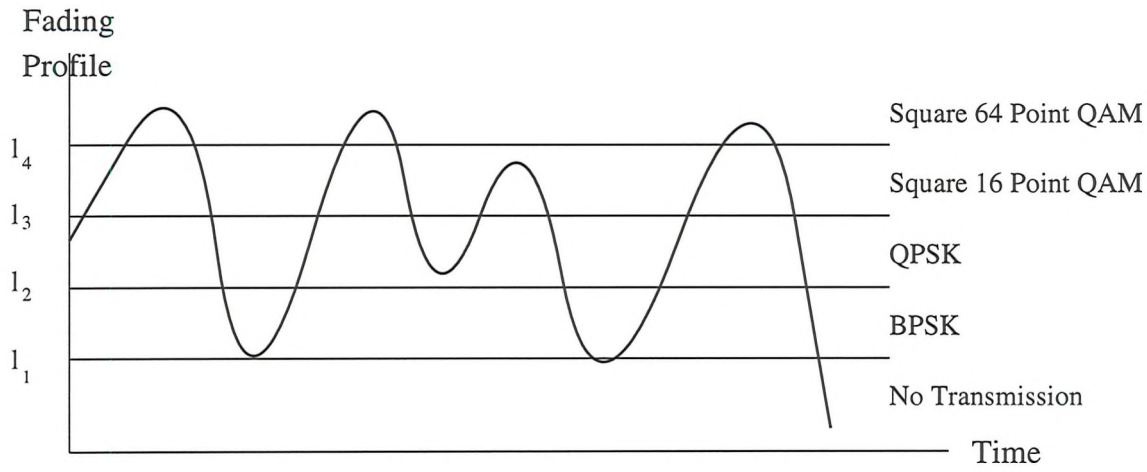

Figure 4.2: The modulation scheme used for transmission is based upon estimation by the transmitter of what the instantaneous signal power will be at the receiver

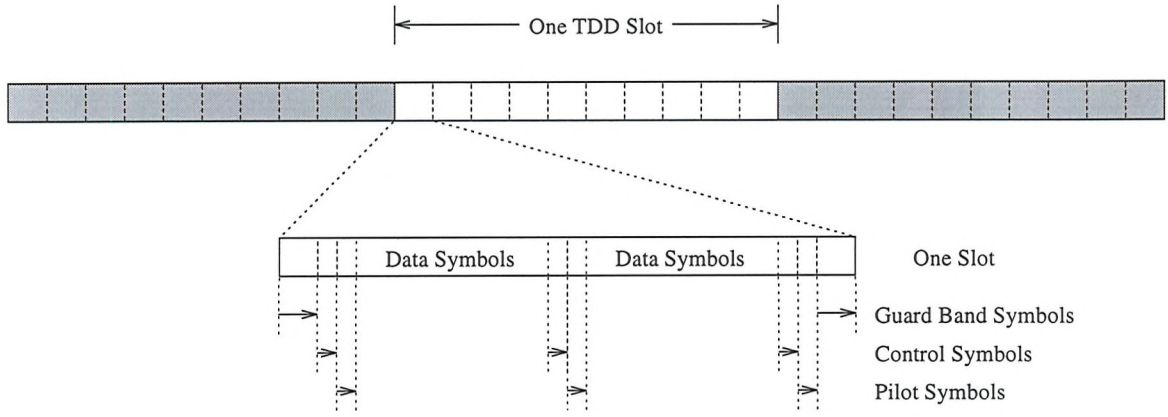

Figure 4.3: Frame and slot construction for a general TDD/TDMA adaptive modulation scheme

data. Generally, interactive video and voice information cannot sustain as much latency across the link as computer data information. However, computer data information is less robust to channel errors. The mean BER performance of the adaptive modulation identifies how robust the information transmitted over the link needs to be. The latency introduced depends upon whether the information is buffered at the transmitter when the instantaneous channel SNR is low. As the instantaneous channel SNR increases, the buffer may be emptied but latency has been incurred. The latency is therefore dependent upon the mean BPS.

The source coder and adaptive modulation scheme should be selected for optimum compatibility. Several examples of both voice and video source coders [114, 115, 116] illustrate how the overall quality of the transmission can be improved in poor channel conditions by reducing

the bit rate and consequently reducing the mean BER. Moreover, in good channel conditions, the overall quality can be increased by increasing the bit rate although the mean BER will typically be increased.

In section 4.2 'No Transmission' was considered as a modulation scheme. From Equation 2.3 it can be seen that the highest BER that can be experienced for a real system is 50 % and occurs when the information rate is 0 Bits/Hz, which corresponds to $-\infty$ dB SNR. Consequently, in poor channel conditions some information will be conveyed from the transmitter to the receiver. This seems to question the wisdom of ever having l_1 higher than 0 (i.e. $-\infty$ dB) as proposed in Section 4.2. However, for the reasons stated above, reduction of the equivocation of information is often worth the cost of reduced throughput.

4.3 Upper-bound Performance [117]

In this Section a numerical average upper-bound for performance of fixed and adaptive modulation schemes, in Rayleigh and Rician fading channels is developed. This is compared with simulated results and then the numerical model is used to optimise the switching levels to obtain the desired trade-offs in throughput and equivocation.

4.3.1 Assumptions

In order to develop an average upper-bound estimation of the performance of adaptive modulation in a Gaussian channel, several assumptions are made. These are discussed and justified below and experimental results addressing these assumptions are given in Chapter 7.

- In Section 4.2 it was assumed that PSAM could approximately render each slot of a TDMA/TDD frame transmitted through a fading channel equivalent to a slot transmitted through a Gaussian channel, where the specific SNR is constant over a frame but varies from frame to frame. This assumption is maintained throughout the development of this theoretical upper-bound but would only be the case when using perfect channel estimates to compensate for the fading. However, practical PSAM fails to achieve this by a margin of approximately 3dB. The same discrepancy applies to the fixed modulation schemes as well as the adaptive schemes. Therefore, a correction factor could be added to both the fixed and adaptive graphs to compensate for the difference between using perfect channel estimates to compensate for the fading and the best that can be achieved by PSAM. This correction factor is not included in any of the following Figures.

- A narrow-band channel is considered, as expected in an indoors environment with a symbol rate of 900 kBd. Dossi et al [118] report typical indoors dispersion representing an RMS delay spread of approximately 100 ns and therefore, considering the condition for narrow-band propagation discussed in Section 2.5.2 in excess of 100 % margin is offered for the narrow band condition. Santella [119] further supports the narrow-band approximation by showing that at 1 and 5.5 GHz, with various antenna heights and omni-directional radiation patterns that the probability of experiencing a 50 ns RMS delay spread is approximately zero.

- Assuming a Gaussian channel for the duration of the slot implies that the effect of the fading on the power of the received symbols is constant along the length of the frame. To justify this assumption a system with mobile speed of 2.5 ms^{-1}, slot duration of approximately 70 μs and 2 GHz carrier is considered. Under these circumstances one data frame is less than 0.25 % the length of an average fade.

- It is assumed that when the frame is synthesised for transmission, a perfect estimation of the received power will be made. This cannot be achieved perfectly in a causal system in the presence of fading, but the quality of the estimation is dependent on the normalised Doppler frequency. By assuming that the channel's behaviour is Gaussian over the length of a TDD/TDMA slot, it is already assumed that the fading is slow relative to the symbol rate. This means that there will be close correlation between adjacent frames, which should aid the transmitter's estimation of the received signal power for each frame it transmits. However, perfect estimation is hindered, particularly during fades. The estimation of what power will be received is based on measurements of what power was received in other slots. This is achieved by finding the ratio of received power in the pilot and control symbols, to the known noise power in the receiver. However, the pilot and control symbols have also been corrupted with noise and, therefore, any SNR measurement will be based on the ratio of Signal + Noise to Noise.

- Finally, it is assumed for each received frame that the receiver will always make the correct decision about which modulation scheme was used at the transmitter. Figure 4.3 shows how control symbols can be used to convey this information from the receiver to the transmitter. This is not the only technique for the modulation scheme that is used for a particular frame to be transmitted. However, by considering the effect of corruption upon the control symbols it is possible for the receiver to erroneously determine the modulation scheme used at the transmitter for a particular frame. The

result of such an event would be system dependent depending upon how synchronisation was achieved at network and data-link layers.

4.3.2 Development of Theory

The distribution of the instantaneous SNR for such slots, after PSAM correction, is dependent on the distribution of the fading. Generally, for a Rician fading channel the PDF of the fading amplitude is given by Equation 2.25 and more specifically for a Rayleigh channel it is given by Equation 2.14. The PDF for the Rician and Rayleigh channels may be written in terms of instantaneous received power, s, and average received power S, as,

$$F(s,S) = \frac{s(2+2K)}{S} \cdot e^{-\frac{s^2(2+2K)}{2S}} \cdot e^{-K} \cdot \frac{s\sqrt{4(K+1)}}{\sqrt{S}} \tag{4.2}$$

and

$$F(s,S) = \frac{2s}{S} \cdot e^{-s^2/S} \tag{4.3}$$

respectively.

For BPSK, QPSK, square 16 and 64 point QAM, if $X_g(\gamma)$ is the Gaussian BER performance, as given in Equations 3.1, 3.2, 3.9 or 3.10, then $X_r(S/N)$ given below will be the upper-bound for the mean BER performance in a fading channel [120],

$$X_r(S/N) = \int_0^\infty X_g(s/N) \cdot F(s,S)\, ds. \tag{4.4}$$

Therefore, the narrow-band upper-bound mean BER performance of an adaptive modulation scheme described in Section 4.2, may be computed from,

$$P_a(S/N) = B^{-1} \cdot \begin{bmatrix} 1 & \cdot \int_{l_1}^{l_2} P_b(s/N) \cdot F(s,S) & ds \\ + \ 2 & \cdot \int_{l_2}^{l_3} P_q(s/N) \cdot F(s,S) & ds \\ + \ 4 & \cdot \int_{l_3}^{l_4} P_{16}(s/N) \cdot F(s,S) & ds \\ + \ 6 & \cdot \int_{l_4}^{\infty} P_{64}(s/N) \cdot F(s,S) & ds \end{bmatrix}, \tag{4.5}$$

where B is the mean number of BPS and is given by

$$\begin{aligned} B &= 1 \cdot \int_{l_1}^{l_2} F(s,S)\, ds + 2 \cdot \int_{l_2}^{l_3} F(s,S)\, ds \\ &+ 4 \cdot \int_{l_3}^{l_4} F(s,S)\, ds + 6 \cdot \int_{l_4}^{\infty} F(s,S)\, ds. \end{aligned} \tag{4.6}$$

4.3.2.1 Solution of BER integrals

Analytical solution of Equations 4.4 and 4.5 is not simple. Hence a numerical solution was opted for. The limits of 0 and ∞ for the integral were replaced by -80 dB and $+20$ dB

relative to the average signal power, S. The integration was approximated by the trapezoidal rule [121] with 0.001 dB steps in s, where the dBs are again relative to S. The infinite series, in the calculation of the Rician CDF, was truncated so that the last term of the summation had less than 0.1% contribution. This is the same procedure that was adopted in Section 2.4.1.2.

4.3.3 Average upper-bound performance in Rayleigh fading

Equation 4.5 was solved by numerical integration with l_1=0 and l_2=l_3=l_4=∞, l_1=l_2=0 and l_3=l_4=∞, l_1=l_2=l_3=0 and l_4=∞, and l_1=l_2=l_3=l_4=0 and $F(s, S)$ defined for a Rayleigh channel as in Equation 4.2. This is a very accurate approximation of the upper-bound of BPSK, QPSK, 16 Point QAM and 64 Point Square QAM respectively, in a Rayleigh fading channel. The performance of the same PSAM schemes was then determined by simulation in a Rayleigh channel with perfect channel estimates to compensate for the fading and the other assumptions introduced in Section 4.3.1.

Two arbitrary adaptive modulation schemes were considered. The switching levels are expressed in terms of estimated instantaneous SNR and for the first adaptive scheme they were l_1=$-\infty$dB, l_2 =8dB, l_3 = 14dB and l_4=20dB. For the second scheme the values were l_1=5dB, l_2 =8dB, l_3 = 14dB and l_4=20dB. The first scheme, referred to as ($-\infty$,8,14,20) always transmitted data compared with the second scheme, referred to as (5,8,14,20), which would actually not transmit when the fades were too deep. The switching levels were decided upon because 5dB, 8dB, 14dB and 20dB are the SNR values at which the BERs of BPSK, QPSK, 16 and 64 level QAM are approximately 1% in a Gaussian channel.

The mean BER versus average channel SNR simulation results for the fixed modulation schemes show a close agreement with the numerical results as seen in Figure 4.4. From Figure 4.4 it can also be seen that there is very good correspondence between the simulated and numerical solutions for the mean number of BPS and mean BER versus average channel SNR. This is the case for both adaptive schemes.

The upper-bound mean BER performance of the ($-\infty$,8,14,20) adaptive modulation scheme is better than that of QPSK for all average channel SNRs in the range 0dB to 45dB and is better than BPSK between 0 and 20 dB. A better mean BER performance than BPSK may at not appear feasible at first. However, in the average channel SNR range from 0 to 20 dB, with the switching regime that has been implemented, the result of instantaneous SNR increase and consequential increase in mean BPS, is an average reduction in mean BER when compared with BPSK. This can be explained by reference to Figure 4.5. Figure 4.5(a)

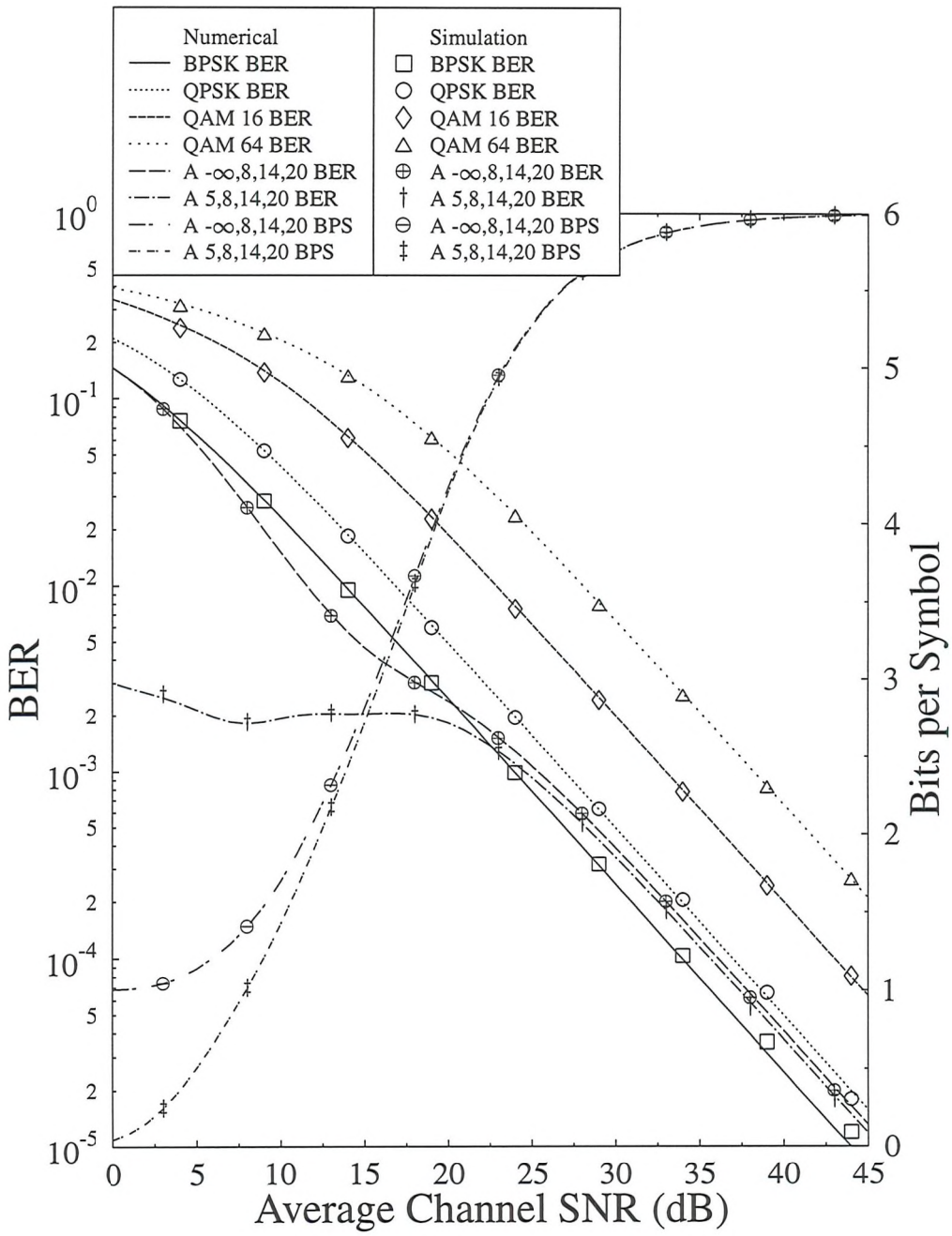

Figure 4.4: Upper-bound average mean BER performance of BPSK, QPSK, square 16 and 64 point QAM in Rayleigh channel by simulation and numerical solution. Adaptive QAM (A) upper-bound mean BER and mean BPS performances in Rayleigh channel with switching levels of $l_1 = -\infty$dB, $l_2 = 8$dB, $l_3 = 14$dB and $l_4 = 20$dB ($-\infty$,8,14,20) and $l_1 = 5$dB, $l_2 = 8$dB, $l_3 = 14$dB and $l_4 = 20$dB (5,8,14,20) by simulation and numerical solution

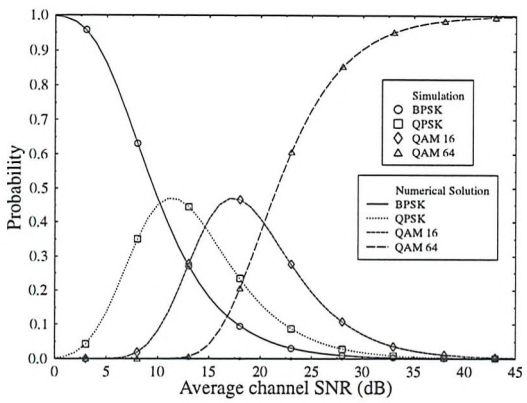

(a) Probability of each modulation scheme

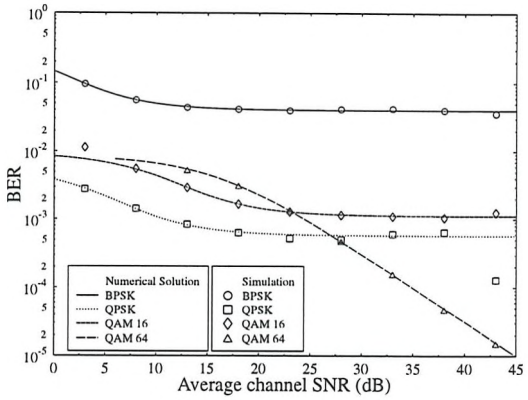

(b) BER of each modulation scheme

Figure 4.5: Simulated and numerical solution for the mean BER and probability of the individual modulation schemes within the $(-\infty,8,14,20)$ adaptive scheme plotted against average channel SNR in Rayleigh channel

displays the probability at a given average channel SNR of a BPSK, QPSK or square 16 or 64 QAM symbol being transmitted. At any given average channel SNR the total probability must be one. Figure 4.5(a) also displays that at low average channel SNR, BPSK is the dominant modulation scheme and as the average channel SNR increases QPSK, square 16 and 64 point QAM become more influential in turn. Figure 4.5(b) shows each schemes contribution to the overall mean BER at various average channel SNRs. The mean BER for BPSK is greater than that for QPSK. This unusual ordering of BER performance is a result of each modulation scheme being deployed on the basis of instantaneous SNR.

The results in Figure 4.4 can be derived from the results in Figure 4.5. Figure 4.4 represents the individual mean BERs in Figure 4.5(b) weighted by, from Figure 4.5(a), the probability that each of the individual schemes will be employed. The correspondence between simulated and numerical mean BER results appears poorer in Figure 4.5(b) than in Figure 4.4. Particular discrepancies are apparent in the QPSK mean BER curve at higher average channel SNRs and in the square 16 point QAM mean BER curve at lower average channels SNRs. Figure 4.5(a) reveals that at the average channel SNRs where the discrepancies occur and for the type of symbol for which the discrepancy was registered the probability of that symbol being transmitted is very low. These discrepancies are therefore insignificant in terms of the overall mean BER performance of the adaptive schemes. The explanation for the deviations is that during the simulation, an insufficient number of symbols of the type that are least

likely to be transmitted were evaluated. Therefore, having established that the numerical solution corresponds very well with the simulated results, for the remainder of this section on upper-bound performance, only numerical results will be presented.

Figure 4.4 also shows that, in terms of mean BPS, both of the adaptive modulation schemes offers a benefit of almost a factor of 6 in throughput at high average channel SNRs when compared with BPSK. How this figure would be eroded in a practical system by the overhead control information, sub-optimum phase and signal level estimation will be discussed later. This numerical evidence identifies benefits in adaptive level modulation compared with fixed level modulation schemes.

The adaptive modulation schemes do not converge with the 64 point square QAM in the average channel SNR range plotted because even at 45 dB average channel SNR, 0.4 % of the symbols are being transmitted as 16 point square QAM symbols, and a total of 0.1 % of the symbols are being transmitted as BPSK and QPSK symbols.

The mean BER performances of the $(-\infty,8,14,20)$ and $(5,8,14,20)$ schemes converge at higher average channel SNRs. This is because the probability of having an instantaneous SNR below 5dB reduces as the average channel SNR increases and the schemes become more similar in terms of their mean BER and mean BPS performance. At lower average channel SNRs there is a significant difference between the two schemes in terms of both mean BER and mean BPS.

4.3.4 Upper-bound Performance in Rician Fading

Equation 4.5 was solved by numerical integration with $l_1{=}0$ and $l_2{=}l_3{=}l_4{=}\infty$, $l_1{=}l_2{=}0$ and $l_3{=}l_4{=}\infty$, $l_1{=}l_2{=}l_3{=}0$ and $l_4{=}\infty$, and $l_1{=}l_2{=}l_3{=}l_4{=}0$ and $F(s,S)$ defined for a Rician channel as in Equation 4.3. K values of 16 and 4 were evaluated and therefore upper-bound performance curves were defined for fixed modulation schemes over Rician channels. The results are shown in Figure 4.6 and may be compared with the results for fixed modulation schemes through a Rayleigh channel ($K = 0$) as shown in Figure 4.4. It can be seen that as the K factor is increased the mean BER performance of the fixed schemes tends towards the BER performance in a Gaussian channel as given in Section 3.2.

The same adaptive schemes that were evaluated for the Rayleigh channel were considered under Rician conditions. The $(-\infty,8,14,20)$ and the $(5,8,14,20)$ schemes were evaluated for Rician channels with K factors of 4 and 16. The results are plotted in Figures 4.7 - 4.8 and also include a comparison with the performance in a Rayleigh channel. For both schemes, as the K factor becomes larger, both the mean BER and the mean BPS curves become

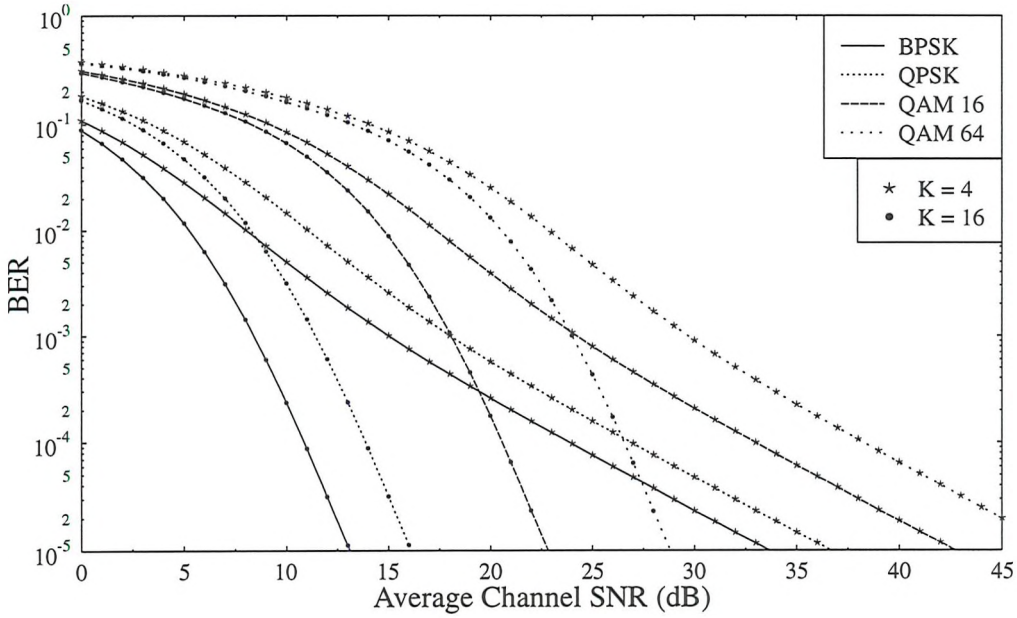

Figure 4.6: Upper-bound mean BER performance of BPSK, QPSK, square 16 and 64 point QAM in Rician channel by numerical solution

less smooth. This is because as K becomes larger the PDF of the fading has less statistical deviation from the mean values, as seen Figure 2.3. Consequently for a given average channel SNR the distribution of 1, 2, 4 and 6 BPS will have less statistical deviation. Therefore, the number of BPS becomes more dependent upon the average channel SNR than upon the fading. What is seen with $K = 16$ in Figures 4.7 and 4.8 is reasonably abrupt changes in the most likely modulation scheme as the average channel SNR is increased. This explains why variations in the gradient of the mean BPS graph and variations in the gradient of the mean BER coincide at the same average channel SNR for the $K = 16$ plots.

The correspondence at high average channel SNR between both the $(-\infty,8,14,20)$ and (5,8,14,20) schemes, with the performance of square 16 point QAM, given the same K factor, increases as K increases. From Figure 4.4 it can be seen that, at a mean BER of 1.0×10^{-4} the adaptive and square 16 point QAM modulation schemes in a Rayleigh channel require respective average channel SNRs of about 35 dB and 47 dB which has a difference of 12 dB. From Figure 4.6 and Figure 4.7 or Figure 4.8, it can be seen when K is 4 that this difference is 7 dB and when K is 16 the difference is 0 dB. At the higher end of the average channel SNR range, but before the adaptive schemes converge upon the square 16 point QAM modulation scheme performance, they converge upon one another. The value of average channel SNR

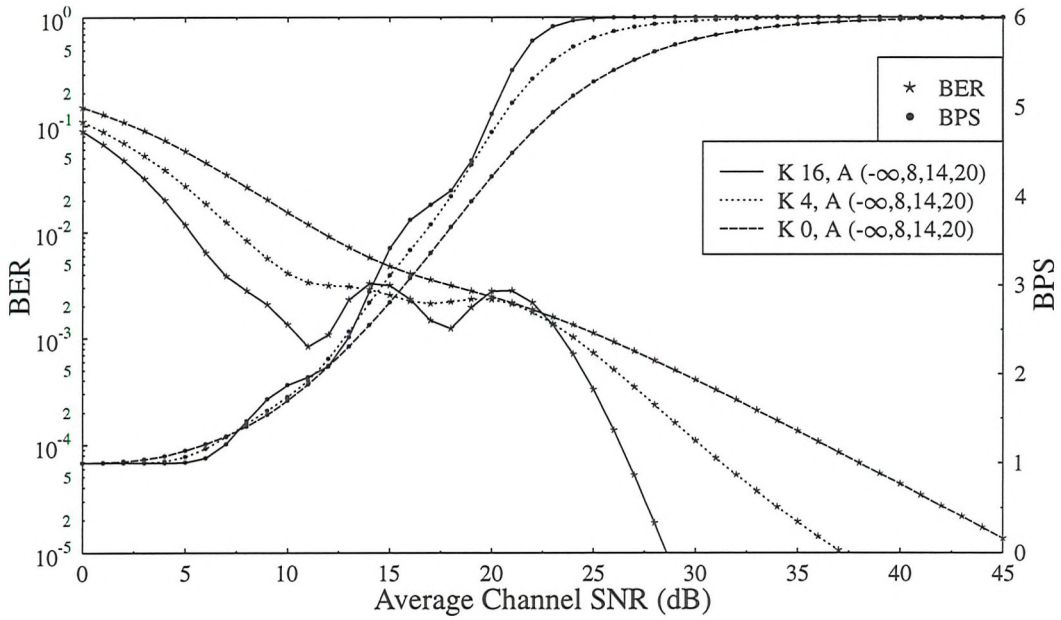

Figure 4.7: Upper-bound mean BER and mean BPS performance of adaptive QAM in Rician channel $K = 16, 4$ and 0, with switching levels of $l_1 = -\infty$dB, $l_2 = 8$dB, $l_3 = 14$dB and $l_4 = 20$dB by numerical solution

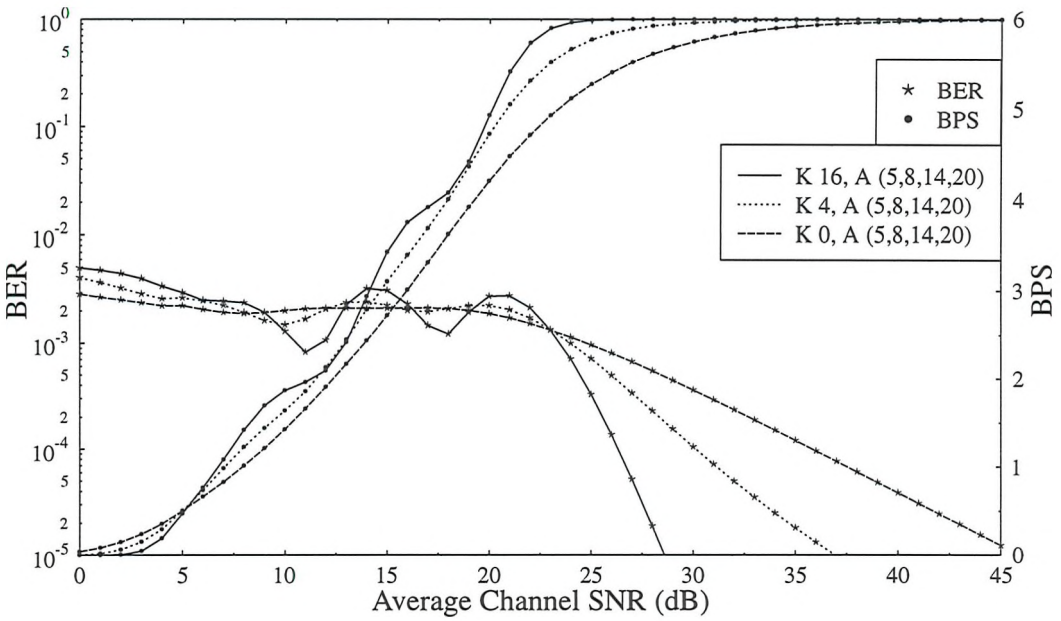

Figure 4.8: Upper-bound mean BER and mean BPS performance of adaptive QAM in Rician channel $K = 16, 4$ and 0, with switching levels of $l_1 = 5$dB, $l_2 = 8$dB, $l_3 = 14$dB and $l_4 = 20$dB by numerical solution

at which this happens depends upon the K factor. As the K factor increases the average channel SNR at which the adaptive schemes converge upon one another reduces. For $K = 0$ they converge at about 25 dB average channel SNR, while at $K = 16$ they converge at about 8dB. This is again explained by higher K values representing less variation in channel fading levels. Therefore, the influence of not transmitting below 5dB instantaneous SNR is present over a smaller range of average channel SNRs when K is higher.

For average channel SNRs below 15 dB, there is more performance variation between $K = 0$ and $K = 16$ with the ($-\infty$,8,14,20) scheme than in the case of the (5,8,14,20) arrangement. This is due to the asymmetry of the fading PDF. Considering Figure 2.3(a) it may be observed that as K is increased, the probability of the larger constructive superpositions is eroded to values considerably less than the probability of the larger destructive superpositions. Consequently as the K factor is increased the probability of experiencing a deep fade is reduced more than the probability of the channel exhibiting positive effects upon the received signal. With the (5,8,14,20) scheme the tail of the distribution which represents the fades, and varies most as a function of K, has less effect at lower average channel SNRs than with the ($-\infty$,8,14,20) scheme. This is because in the case of the (5,8,14,20) arrangement there is no transmission when the instantaneous SNR is less than 5dB.

The mean BER performance of the ($-\infty$,8,14,20) scheme of Figure 4.7 improves as the K factor increases, except at a very few values of average channel SNR. These exceptions correspond to average channel SNR values where the number of mean BPS for the channels with higher K factors is greater than those with lower K factor. Therefore, the higher mean BER can be attributed to higher mean BPS and, therefore, to greater use of less robust modulation schemes.

Both the ($-\infty$,8,14,20) and (5,8,14,20) schemes, but particularly the latter, exhibit less performance variation in the range of average channel SNR from 0dB to 25dB, as a result of variations in the K factor, when compared with the very significant variation observed with fixed modulation schemes in Figures 4.4 - 4.6. As the K factor increases, there is less variation in the fading envelope and therefore, for a given average channel SNR there is less variation in the type of symbols that are transmitted. This can be seen by comparing the distribution of individual modulation schemes within the ($-\infty$,8,14,20) adaptive scheme, at $K = 4$ and $K = 16$, in Figures 4.9(a) and 4.9(c), with the same graph for $K = 0$ in Figure 4.5(a). As the K factor increases, for a given average channel SNR, the diversity of individual modulation schemes that are employed is reduced. It is this diversity of different symbols varying with the fast fading that gives adaptive modulation its advantages over fixed modulation schemes. Therefore, the benefits of adaptive modulation are eroded as K increases.

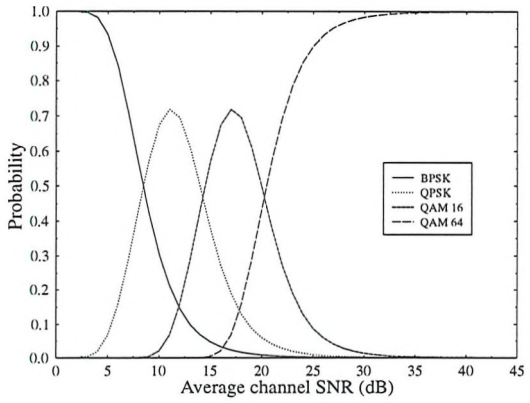

(a) Probability of each modulation scheme, $K = 4$

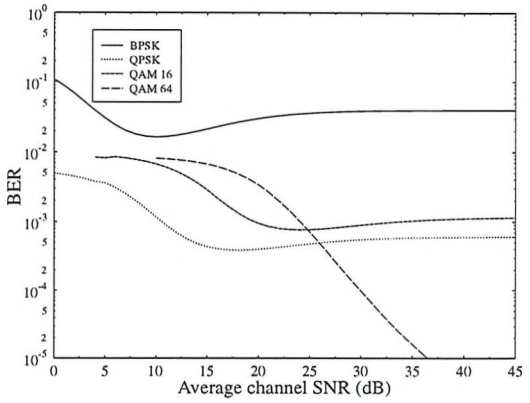

(b) BER of each modulation scheme, $K = 4$

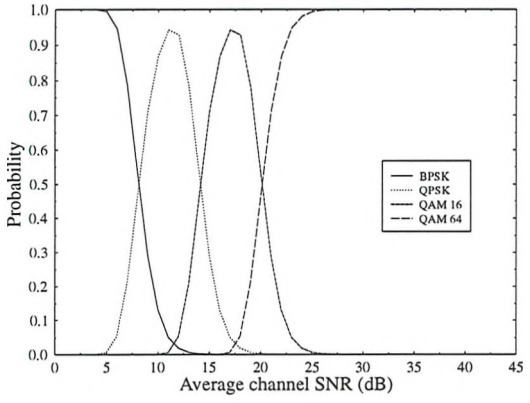

(c) Probability of each modulation scheme, $K = 16$

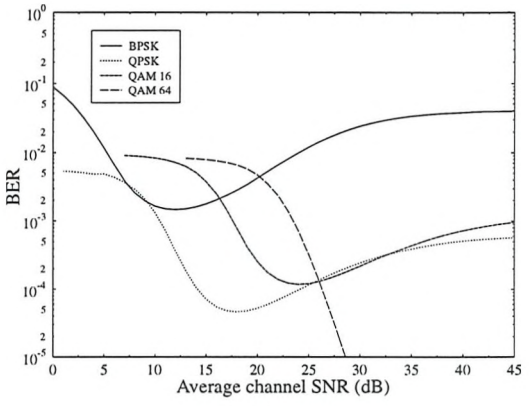

(d) BER of each modulation scheme, $K = 16$

Figure 4.9: Probability and mean BER of the individual modulation schemes within the $(-\infty,8,14,20)$ adaptive scheme plotted against average channel SNR for Rician channel with $K = 4$ (a and b) and $K = 16$ (c and d)

In what follows the individual BER contributions for each of the modulation schemes in Rician channels for the $(-\infty,8,14,20)$ adaptive modulation scheme are considered. They are shown in Figures 4.9(b) and 4.9(d) and compared with the results for the Rayleigh channel that were portrayed in Figure 4.5(b). Under all channel conditions, and for all modulation schemes, the mean BER is at its highest when the average channel SNR is at its lowest. As the average channel SNR increases from 0 dB, the mean BER reduces. In the case of square 64 point QAM, under all channel conditions there appears to be no residual BER. This is

because as the average channel SNR increases, in all but the case of the very deepest fades, a square 64 point QAM symbol is transmitted. As the average channel SNR increases further, the probability of these symbols being erroneously decoded decreases. In the case of the other modulation schemes an increase in average channel SNR results in a reduction of mean BER until a threshold is reached. Once this threshold is reached, in the case of Rayleigh channels the mean BER remains approximately constant. In the case of the Rician channels the mean BER increases again as the average channel SNR increases. This is because the PDF of the fading experienced with higher K values has a lower variance. Consequently, at a given average channel SNR the probability that one individual modulation scheme being used most of the time is higher than with higher K values. As the average channel SNR increases, the mean BER of that particular modulation scheme reduces because most of the symbols are still transmitted with the same modulation scheme but now on average the instantaneous SNR is greater. In the case of BPSK, QPSK and square 16 point QAM, as the average channel SNR increases further, the next individual modulation scheme will start to dominate, as discussed previously. At this increased average channel SNR, the only symbols that will be transmitted at the lower modulation level are the ones transmitted during the deepest fades. The positive effect upon the mean BER, for the individual lower modulation scheme, concerning the bulk of the symbols transmitted will not take place, as this majority of symbols will now be transmitted in the next modulation scheme up. However, this increase in mean BER of the individual schemes has little effect upon the overall mean BER of the adaptive scheme. This is because of the low overall probability of these deep fades and corresponding low probability of an individual scheme being selected when the average channel SNR results in an mean BER increase for that particular scheme.

At very high average channel SNRs the mean BER for each of the individual modulation schemes in both of the Rician channels appear to converge on the corresponding mean BERs for the Rayleigh channel. This is because when the average channel SNR is very high, compared with the instantaneous SNR range where the individual modulation scheme of interest will be employed, the fading PDF this SNR range is very flat irrespective of the K factor. Therefore, the mean BER for the individual modulation schemes will converge for all K factors.

4.3.5 Upper-bound Performance in a Gaussian channel

The performance of the $(-\infty,8,14,20)$ adaptive modulation scheme in a non-fading channel is shown in Figure 4.10. This is the mean BER and PBS performance when the K factor is very large and is included to clarify the trends that were identified in Section 4.3.4. Under Gaussian

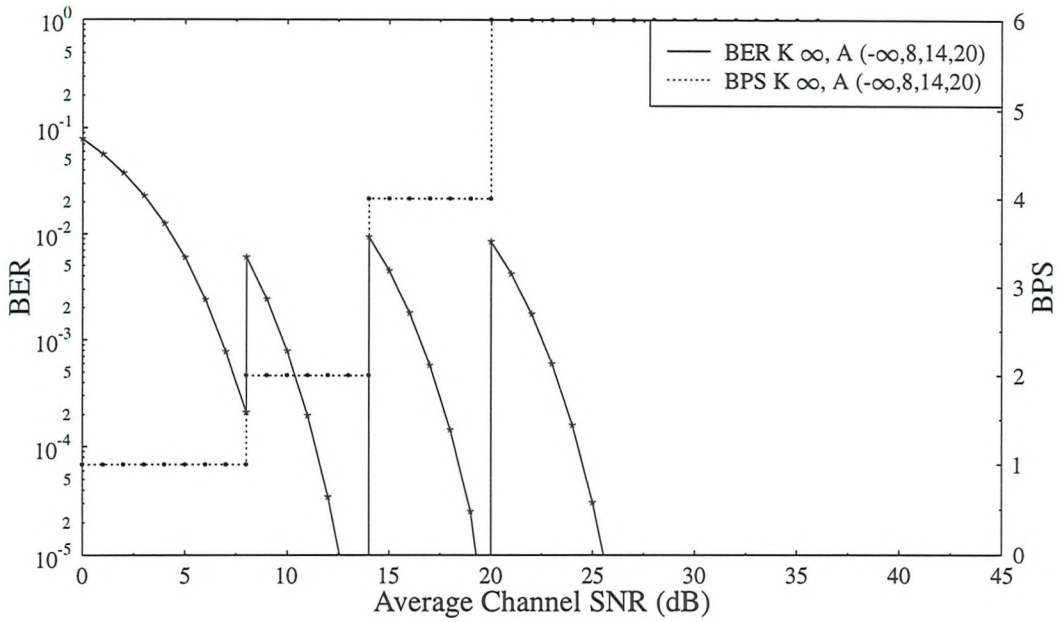

Figure 4.10: Upper-bound mean BER and PBS performance of adaptive QAM in Gaussian channel with switching levels of $l_1 = -\infty$dB, $l_2 = 8$dB, $l_3 = 14$dB and $l_4 = 20$dB by numerical solution

channel conditions the instantaneous SNR is the same as the average channel SNR. The figure shows BPSK performance up to 8dB followed by a discrete transition to QPSK performance until 14dB average channel SNR. Square 16 point QAM performance then prevails until another discrete transition, at 20dB, takes place, yielding square 64 point QAM performance. Employment of such a scheme in a Gaussian channel may have applications to exploit long term increases in channel SNR. However, it should not be confused with the deployment of adaptive modulation to attempt to mitigate some of the effects of fast fading.

4.3.6 Level Switching

Numerical evaluation of the mean BER and mean BPS performance is significantly quicker than simulation. This is particularly true when considering the performance of adaptive modulation, because adaptive modulation is inherently only worth employing when there is a very low normalised Doppler frequency. This results in very long fades and consequently, to achieve statistically significant results, the simulation lengths must be very long. Reduction in the time required to evaluate the upper-bound mean BER and mean BPS performance makes it practical to iteratively optimise the switching levels. In Section 4.2.1 the trade-off between

mean BER and mean BPS was discussed. Here, Powell's [15] method of optimisation in multi-dimensions is employed to optimise the switching levels for a certain target performance. By selecting a desired profile of mean BER and mean BPS over an range of average channel SNRs the optimisation algorithm can iteratively update the switching levels. This will yield a mean BER and mean BPS performance closest to the desired performance.

Initially $l_1 = 5\text{dB}$, $l_2 = 8\text{dB}$, $l_3 = 14\text{dB}$ and $l_4 = 20\text{dB}$ and these values can be considered as a vector $\mathbf{P}$ in 4 dimensional space. The vector can be linearly combined with another vector $\mathbf{n}$ so that a cost function of $\mathbf{P}$, $f(\mathbf{P})$ can be minimised along the line $\mathbf{n}$ by some one dimensional minimisation method. The precise nature of $f(\mathbf{P})$ is discussed below but it will be defined by the desired mean BER and mean BPS performance. The proposed linear minimisation seeks a scalar of λ, which minimises $f(\mathbf{P} + \lambda\mathbf{n})$ and then replaces $\mathbf{P}$ with $\mathbf{P} + \lambda\mathbf{n}$.

The mean BER and mean BPS performances were evaluated for average channel SNRs in the range from $\gamma_{\text{min}} = 0$ dB to $\gamma_{\text{max}} = 50$ dB in 1dB intervals. The cost function was defined as

$$\text{Total Cost} = \sum_{i=\gamma_{\text{min}}}^{\gamma_{\text{max}}} \text{BER Cost}(i) + \text{BPS Cost}(i) \tag{4.7}$$

where

$$\text{BER Cost}(i) = \begin{cases} 10 \cdot \left[log_{10} \left(\dfrac{\text{BER}_m(i)}{\text{BER}_d(i)} \right) \right] & \text{if BER}_m(i) > \text{BER}_d(i) \\ 0 & \text{otherwise} \end{cases}, \tag{4.8}$$

$$\text{BPS Cost}(i) = \begin{cases} \text{BPS}_d(i) - \text{BPS}_m(i) & \text{if BPS}_d(i) > \text{BPS}_m(i) \\ 0 & \text{otherwise} \end{cases} \tag{4.9}$$

and $\text{BER}_m(i)$, $\text{BER}_d(i)$, $\text{BPS}_m(i)$ and $\text{BPS}_d(i)$ are, respectively, the measured and desired mean BER and mean BPS at an average channel SNR of i. It can be seen from Equations 4.7, 4.8 and 4.9 that the cost function can only be positive and increases when either the mean BER or the mean BPS performance become inferior to their desired performance at an average channel SNR of i. The cost function cannot be negative, therefore at high average channel SNRs, where both the mean BER and the mean BPS outperform their respective desired performance targets, the combined performance will be sacrificed. The advantage of this approach is that it reduces the minimum average channel SNR above which both desired mean BER and mean BPS performance criteria is achieved. However, the performance does improve at higher average SNRs because of the favourable prevailing channel conditions. Equation 4.8 utilises the logarithm function to increase the significance of small mean BERs. A weighting factor of 10 is employed to bias the optimisation towards achieving the desired mean BER performance in preference to the mean BPS performance.

Scheme	l_1	l_2	l_3	l_4
Speech	3.31	6.48	11.61	17.64
Computer Data	7.98	10.42	16.76	26.33

Table 4.1: Optimised switching levels for speech and computer data systems through a Rayleigh channel, shown in dB instantaneous channel SNR

Two desired system performance profiles were considered, one which was optimised for a speech codec with a target mean BER and mean BPS of 1×10^{-2} and 4.5 respectively, and the second intended for computer data transfer with target mean BER and mean BPS of 1×10^{-4} and 3 respectively. The optimisation was performed for Rayleigh channel conditions and the initial condition for both minimisations was $l_1 = 5$dB, $l_2 = 8$dB, $l_3 = 14$dB and $l_4 = 20$dB. After optimisation the values given in table 4.1 were registered [122].

The performance of adaptive modulation schemes with these switching levels were determined and the results are shown in Figure 4.11. The switching levels had been optimised for a Rayleigh channel and it has already been stated that a perfect Rayleigh channel is unlikely to occur in a practical mobile radio environment. Therefore, there was a concern that the switching levels would have been optimised to a specific channel and very poor results would be registered in non-Rayleigh channels. For this reason the Rayleigh optimised switching levels for both the speech and computer data requirements were evaluated over Rician channels with $K = 4$ and $K = 16$ and shown in Figure 4.12. The break-down of the performance of the individual modulation schemes under all three channel conditions is given in Figures 4.13, 4.14 and 4.15.

Considering Figure 4.11 the desired mean BER is achieved between 0 and 50 dB for both the speech and computer data switching levels schemes. The mean BPS performance is achieved at approximately 18 dB and 19 dB average channels SNR for the speech and computer data schemes respectively. The mean BER performances for both schemes, at average channel SNRs greater than these values, start to reduce. The performance of the same schemes through Rician channels, Figure 4.12, is quite similar for average channel SNRs below about 20 dB. The mean BER never exceeds twice the desired mean BER and it is often below the desired mean BER. Above 20dB the mean BER performance over Rician channels is much better than over Rayleigh channels. The mean BPS for the Rician channels is greater than for the Rayleigh except at very low average channel SNR. Above about 20dB the difference becomes more significant as K increases. In the both $K = 4$ and $K = 16$ the average channel SNR at which the mean BPS reaches the desired level is at about 17 dB for both the speech and the computer data schemes. Both the mean BER and mean BPS performance over Rician

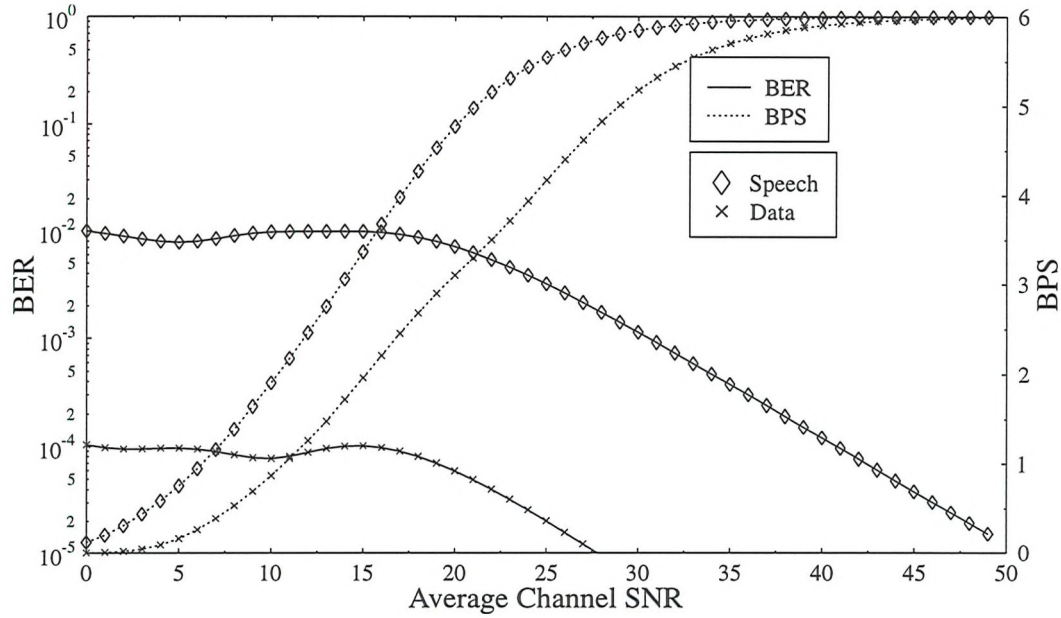

Figure 4.11: Upper-bound mean BER and mean BPS performance of adaptive QAM in Rayleigh Channel optimised separately for Speech and Data transfer and found by numerical solution

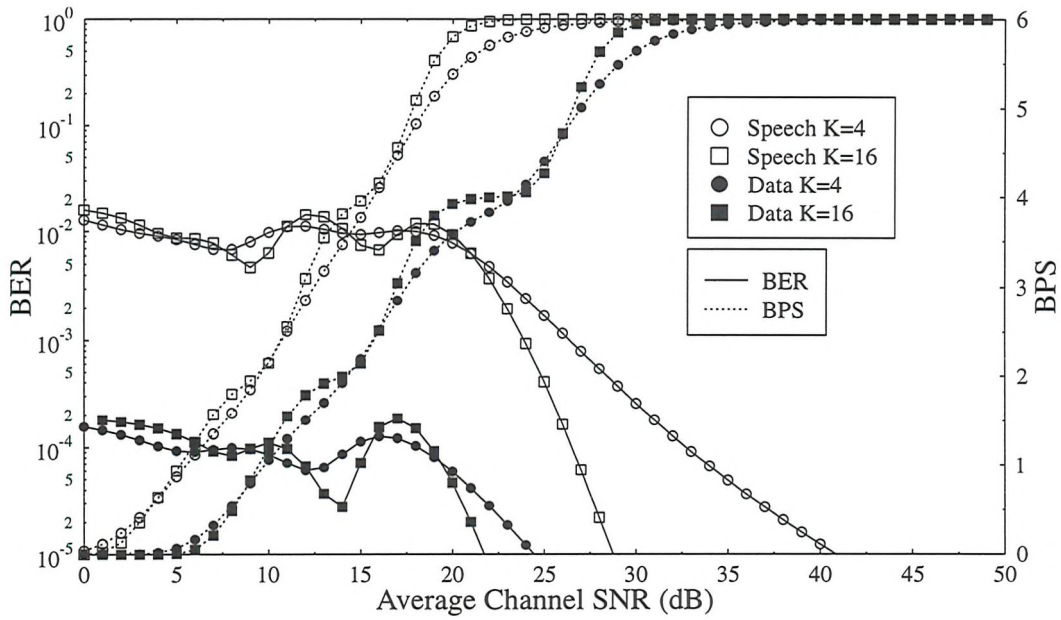

Figure 4.12: Upper-bound mean BER and mean BPS performance of adaptive QAM in Rician Channels having been optimised separately for Speech and Data transfer and found by numerical solution

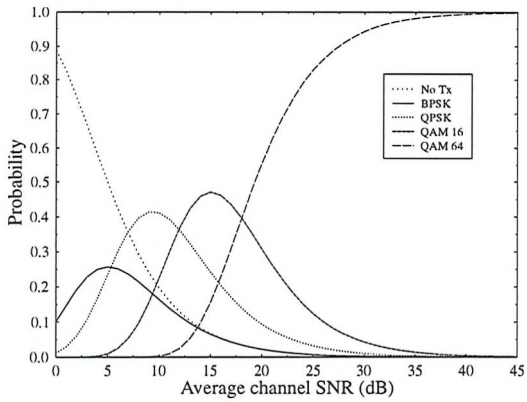

(a) Probability of each modulation scheme, Speech

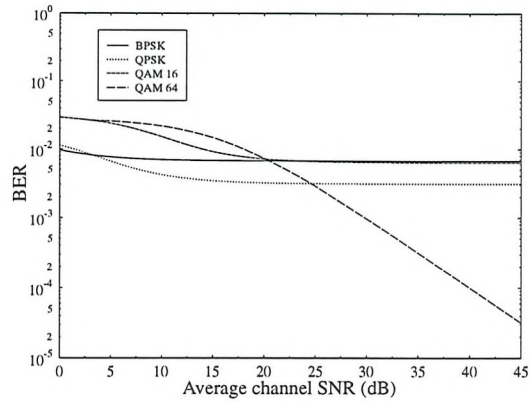

(b) BER of each modulation scheme, Speech

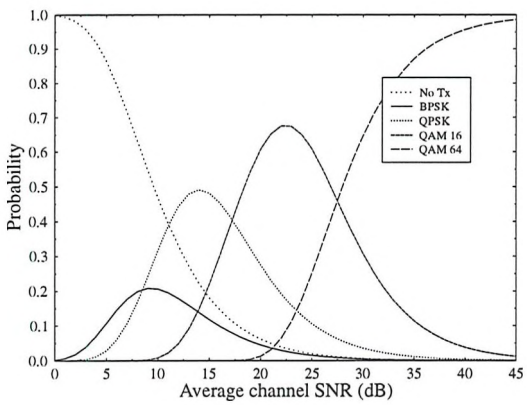

(c) Probability of each modulation scheme, Data Transfer

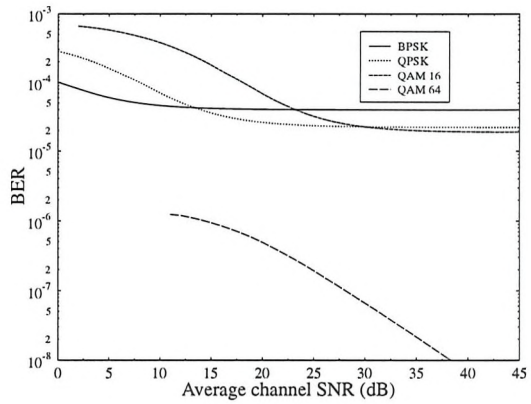

(d) BER of each modulation scheme, Data Transfer

Figure 4.13: Upper-bound probability and mean BER of the individual modulation schemes for adaptive modulation optimised separately for Speech (a and b) and Data transfer (c and d) scheme plotted against average channel SNR for a Rayleigh channel

channels of a scheme optimised for Rayleigh channels is similar up to 20dB average channel SNR. Above this level the performance in the Rician channel is always better and this is because the probability of deep fades is very much reduced.

The switching levels optimised for a Rayleigh channel are suitable for Rician channel with K values up to 16. However, optimum switching levels could be determined for different K

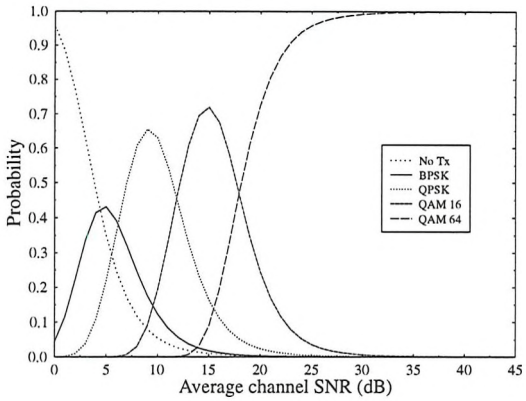

(a) Probability of each modulation scheme, Speech

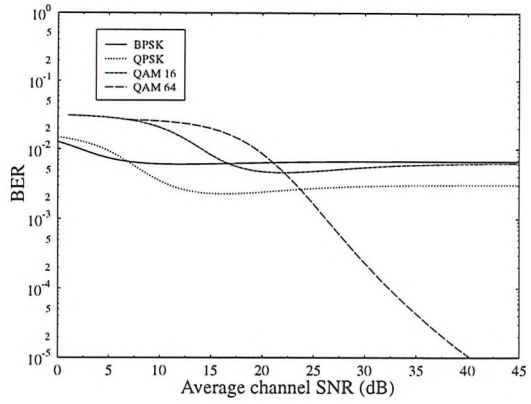

(b) BER of each modulation scheme, Speech

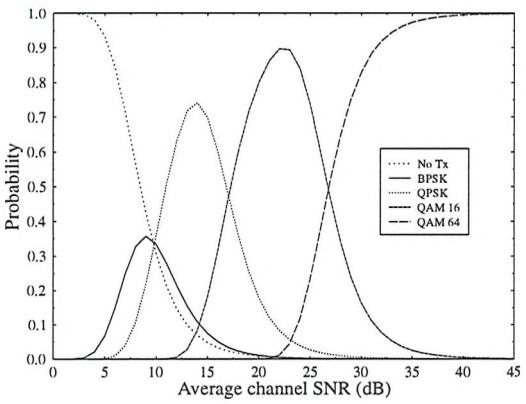

(c) Probability of each modulation scheme, Data transfer

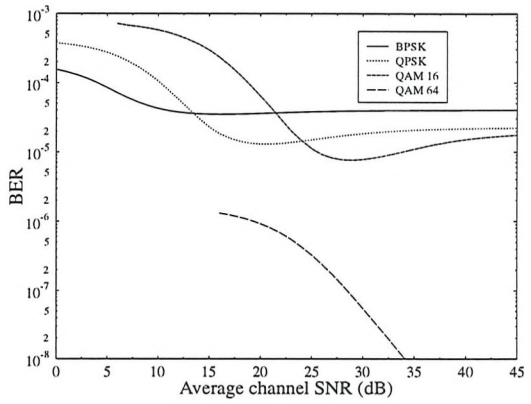

(d) BER of each modulation scheme, Data transfer

Figure 4.14: Upper-bound probability and mean BER, for the individual modulation schemes of adaptive modulation optimised for Rayleigh channel conditions, separately for Speech (a and b) and Data transfer (c and d), plotted against average channel SNR for a Rician channel with $K = 4$

values and the switching levels could be adaptive depending upon the expected fading conditions. This would require the estimation of the fading statistics. However, the complexity required and the relatively small difference between the curves in Figure 4.11 and Figure 4.12 means that the employment of such a technique is not considered.

Sub-figures a and c of Figures 4.13, 4.14 and 4.15 are summarised in Tables 4.2 and 4.3. The

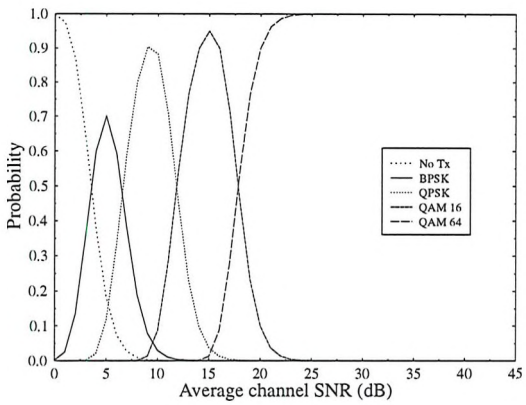

(a) Probability of each modulation scheme, Speech

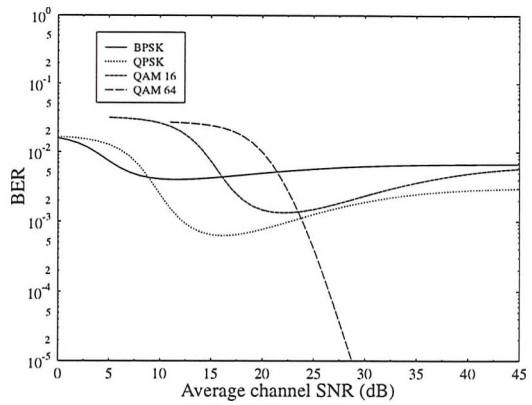

(b) BER of each modulation scheme, Speech

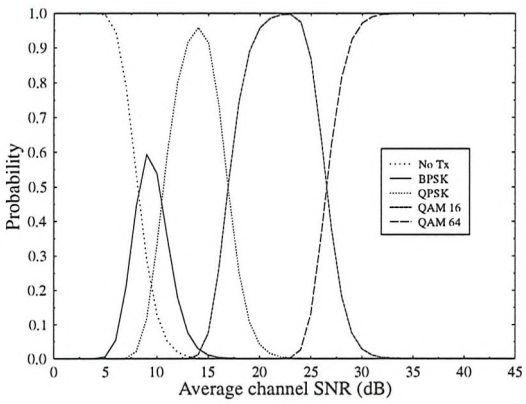

(c) Probability of each modulation scheme, Data transfer

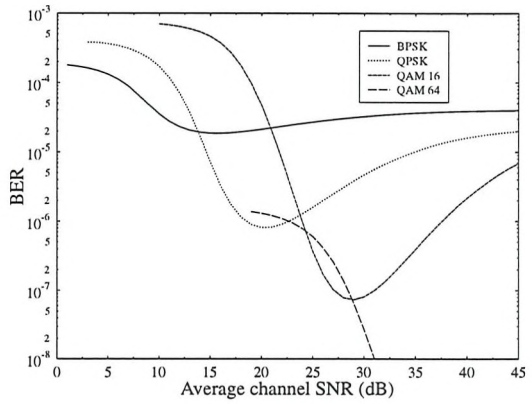

(d) BER of each modulation scheme, Data transfer

Figure 4.15: Upper-bound probability and mean BER, for the individual modulation schemes of adaptive modulation optimised for Rayleigh channel conditions, separately for Speech (a and b) and Data transfer (c and d), plotted against average channel SNR for a Rician channel with $K = 16$

Tables show explicitly the maximum probability that a particular modulation scheme will be employed for K factors of 0, 4 and 16, which were inferred from the above Figures. The average channel SNR at which this maximum occurs is also given. Large K values result in larger probability values, for the same reasons as explained in Section 4.3.3. When the switching levels are optimised for computer data, the average channel SNR at which the peak in the probability of an individual modulation scheme being employed is greater than with

the switching levels optimised for speech data. This is a consequence of the lower mean BER requirement associated with typically higher average channel SNR. With both optimisation criteria the average channel SNR, where the peak in probability occurs is only marginally dependent upon the K factor for BPSK, QPSK and square 16 point QAM. However, the average channel SNR, where square 64 point QAM is likely to be employed is significantly dependent upon the K factor. Square 64 point QAM is mainly employed at high average channel SNRs and its employment is dependent upon K. This explains the difference in throughput for average channel SNRs above 20 dB between the Rayleigh and Rician channels, which can be seen by comparing Figure 4.12 and Figure 4.11. Tables 4.2 and 4.3 show that for both speech and computer data and for K equals 0, 4 and 16, the maximum probability for a modulation scheme being employed increases as the number of mean BPS increases. This is because after optimisation, for both systems, the gap between switching levels is greater for the higher levels. When more regular differences between switching levels were utilised, before the optimisation, the characteristics of the probability of each of the individual modulation schemes were more similar. Comparison of parts a and c of Figures 4.13, 4.14 and 4.15 with Figures 4.9(a), 4.9(c) and 4.5(a) illustrates this.

Parts b and d of Figures 4.13, 4.14 and 4.15 show very much the same trends as Figures 4.5(b), 4.9(b) and 4.9(d). The interpretation of the latter, given in Sections 4.3.3 and 4.3.4 is also pertinent to the former graphs. However, the individual mean BER performances after either optimisation are closer together than they were when the switching levels were chosen arbitrarily.

4.4 Comparison with Fixed Schemes

Evaluating the efficiency of adaptive schemes compared with fixed modulation schemes is dependent upon how the efficiency is defined. An incomplete, yet still interesting, approach to evaluate the efficiency of a transmission scheme is to consider the number of bits that can be transmitted every second for every Hertz of bandwidth, given a particular E_b/N_0 and a acceptable BER. Shannon's [14] relationship, Equation 2.3, may be exploited to derive an upper-bound for a Gaussian channel in terms of the capacity in Bits/Second/Hz and E_b/N_0 and this is the solid, un-marked, line Figure 4.16. The BER performance on the Shannon limit is defined as arbitrarily low and the arbitrary BER, in the context of this comparison, is either 1×10^{-2} or 1×10^{-4}. This upper-bound performance is intended for a Gaussian channel. Lee [123] gives a more pertinant upper bound performance, by considering the upper

	$K=0$		$K=4$		$K=16$	
Scheme	Prob	SNR	Prob	SNR	Prob	SNR
No Tx	0.87	0	0.95	0	0.99	0
BPSK	0.26	5	0.43	5	0.70	5
QPSK	0.41	9	0.65	9	0.90	9
QAM 16	0.47	15	0.71	15	0.95	15
QAM 64	1.00	45	1.00	36	1.00	25

Table 4.2: Summary of the individual modulation scheme's maximum probability of being employed in Rician channels with $K = 0, 4$ and 16. Results generated using upper-bound performance and switching levels optimised for speech transfer through Rayleigh channels

	$K=0$		$K=4$		$K=16$	
Scheme	Prob	SNR	Prob	SNR	Prob	SNR
No Tx	1.00	0	1.00	2	1.00	4
BPSK	0.20	9	0.35	9	0.60	9
QPSK	0.49	14	0.74	14	0.95	14
QAM 16	0.68	22	0.89	22	0.99	23
QAM 64	0.98	45	1.00	45	1.00	32

Table 4.3: Summary of the individual modulation scheme's maximum probability of being employed in Rician channels with $K = 0, 4$ and 16. Results generated using upper-bound performance and switching levels optimised for computer data transfer through Rayleigh channels

bound approximation in a Rayleigh fading channel as

$$C \approx \log_2 e \cdot e^{-1/\gamma}(-E + \ln\gamma + \frac{1}{\gamma}), \tag{4.10}$$

where $E \approx 0.577$ is the Euler constant.

There a many issues in comparing adaptive modulation with fixed modulation and these will be considered in depth throughout the remainder of this thesis. In this Chapter the optimised mean BER performance has been obtained and it is important to note that the fluctuating nature of the channel will result in bursts where the BER is above the mean; there are other positions where the BER is below the mean. The increases and reductions in BER are respectively coincident with the signal level being marginally above and below any of the modulation switching levels l_1, l_2, l_3 or l_4.

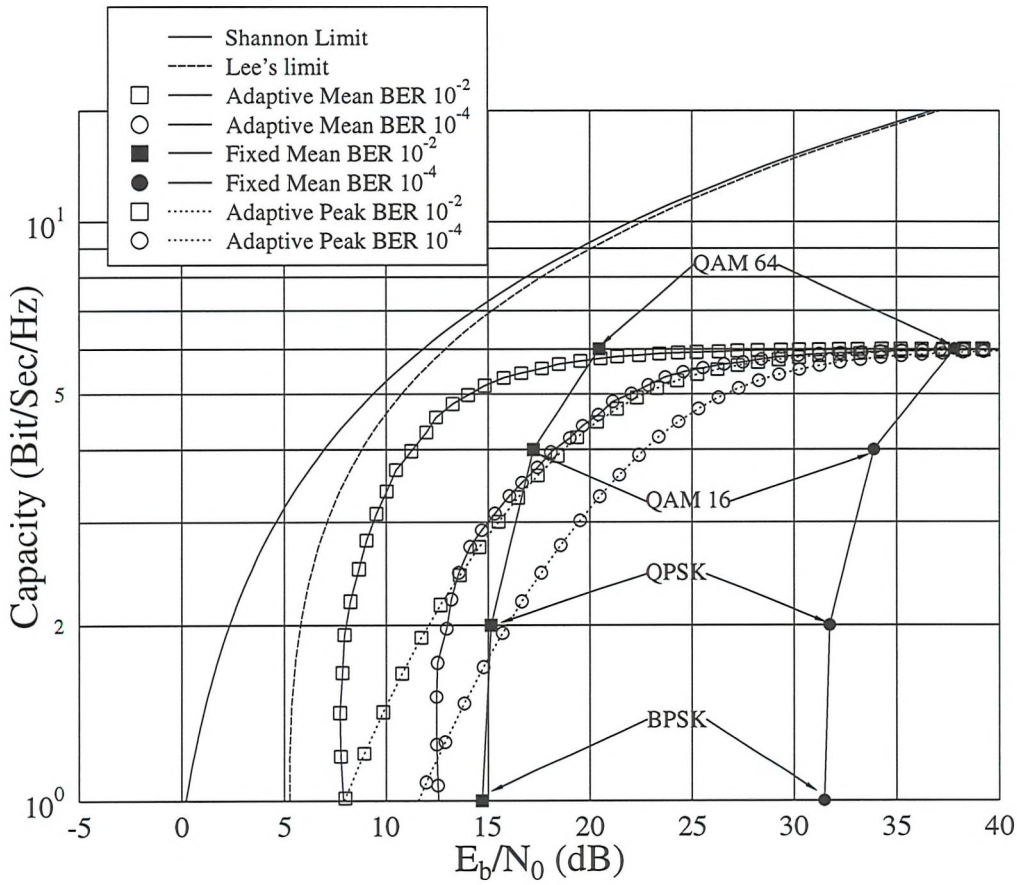

Figure 4.16: Capacity limit and upper-bound performance of fixed and adaptive (peak and mean BER) modulation schemes in Rayleigh fading channels with arbitrary BERs of 1×10^{-2} and 1×10^{-4}. Signalling and pilot over-head neglected, assuming perfect filtering and single sided bandwidth.

Under the slow fading conditions the error burst duration would be worse for fixed modulation schemes than adaptive schemes. This because the proposed adaptive modulation schemes can disable transmission or switch to an modulation scheme less sensitive to error, in a potential burst condition. Further, compensation for the transmission capacity lost during poor channel conditions is achieved by employing high level modulation scheme during good channel conditions. Interleaving and coding may be included in both the fixed [1] and adaptive [124] modulation schemes to mitigate some of the bursts and improve the overall modulation efficiency. However, the ramifications of coding and interleaving are complex and to permit a clear comparison of fixed and adaptive schemes they are not considered.

Scheme	l_1	l_2	l_3	l_4
Speech	4.3	7.3	13.9	19.4
Computer Data	8.3	11.3	18.2	24.2

Table 4.4: Switching levels for speech and computer data systems through a Rayleigh channel, shown in dB instantaneous channel SNR to achieve peak BERs of 1×10^{-2} and 1×10^{-4}

4.4.0.1 Fixed Modulation

Assuming perfect clock and carrier recovery the performance of fixed BPSK, QPSK and Square 16 and 64 QAM through a Rayleigh channel were evaluated. This yields the results shown in Figure 4.4. The (E_b/N_0) required to achieve a mean BER of 1×10^{-2} and 1×10^{-4} was evaluated. The resulting values are plotted in Figure 4.16, vs the capacity in Bits Per Second Per Hertz. This was based on the assumption of a single sided bandwidth with perfect filtering. As expected, the energy required to achieve the lower BER is higher than that for the higher BER, given the same capacity. Shannon's limit could be violated if the BER were allowed to become very large. However, in terms of this work, the limit is merely a reference and the comparisons of interest are different transmission schemes under the two BER constraints.

The mean BER performance of fixed modulation will be unaffected by the correlation of the faded received power. However, a completely uncorrelated channel would result in all frames of data received by the source decoded having the same average BER and the is the best case scenario for fixed modulation. As the channel becomes more correlated E_b/N_0 would have to be increased because, although the mean BER would be the same, bursts of low power symbols will be received in some particular frames. Therefore, under the assumptions given fixed modulation will deteriorate with increased channel correlation.

4.4.0.2 Adaptive modulation

The performance of adaptive modulation was evaluated for speech and computer data switching levels under the same set of assumptions as used in the fixed modulation performance evaluation. The results are shown in Figure 4.16 labelled as adaptive mean BER. With the capacity between one and five Bits/Second/Hz the energy reduction with adaptive modulation is approximately 7 to 5 dB per bit. As the capacity of the channel increases the channel conditions result in square 64 QAM being the predominant mode of the adaptive scheme. The differential between the adaptive and the fixed schemes consequently erodes. Similar observations may be made about fixed and adaptive schemes with the mean BER constrained to

1×10^{-4}. However, the margin of energy reduction is much greater, explicitly: 18 to 10 dB per bit between 1 and 5 Bits/Second/Hz. Unlike the fixed schemes the mean BER performance never coincides with the BER experienced by the all frames received by the source coder. This is because in order to exploit adaptive modulation the channel must be correlated and, therefore, unless the source coder's frames are impractically long the BER of each of these frames must fluctuate above and below the mean. To overcome this difficulty the switching levels in Table 4.4 may be used. These switching levels were obtained by identifying the exact SNR in a Gaussian channel that is required to achieve the respective target BER. These switching levels are higher than the equivalent switching levels required to achieve the desired mean BER. As a consequence they reduce the mean BER below the original target and reduce the throughput of the adaptive transmission. Importantly, however, they constrain the BER for any arbitrarily short source coded frames to below the target BER. The performance of such schemes, again on the basis of the same assumptions, are also included in Figure 4.16.

The most crucial comparison to be made from Figure 4.16 is between the peak BER adaptive performance and the mean BER fixed performance. This represents the comparison between fixed and adaptive modulation where both schemes, in channels that are favourable to them, obtain the target BER of all source coded frames. This comparison at 1×10^{-4} BER shows that the modulation efficiency of the adaptive scheme outperforms a fixed modulation scheme at all interesting values. However, when the BER is 1×10^{-2} square 16 and 64 QAM are more, and BPSK and QPSK are less, efficient than the adaptive scheme.

4.4.0.3 Dual mode air interface

It has been shown that if adaptive modulation is used in slowly fading channels, at 1 % BER is performs about as efficiently, and at 0.01 % it is more efficient, than fixed modulation in fast fading. It can be seen that adaptive modulation will become less efficient as the fading becomes less correlated and the fixed modulation will also become less efficient but as the fading becomes more correlated. It is, therefore, proposed to develop a dual-mode air interface [125] that would switch from adaptive modulation to a fixed modulation scheme depending upon the normalised Doppler frequency. Such a scheme is illustrated by Figure 4.17 and it should be noted that the maximum adaptive performance is greater than the maximum fixed modulation performance.

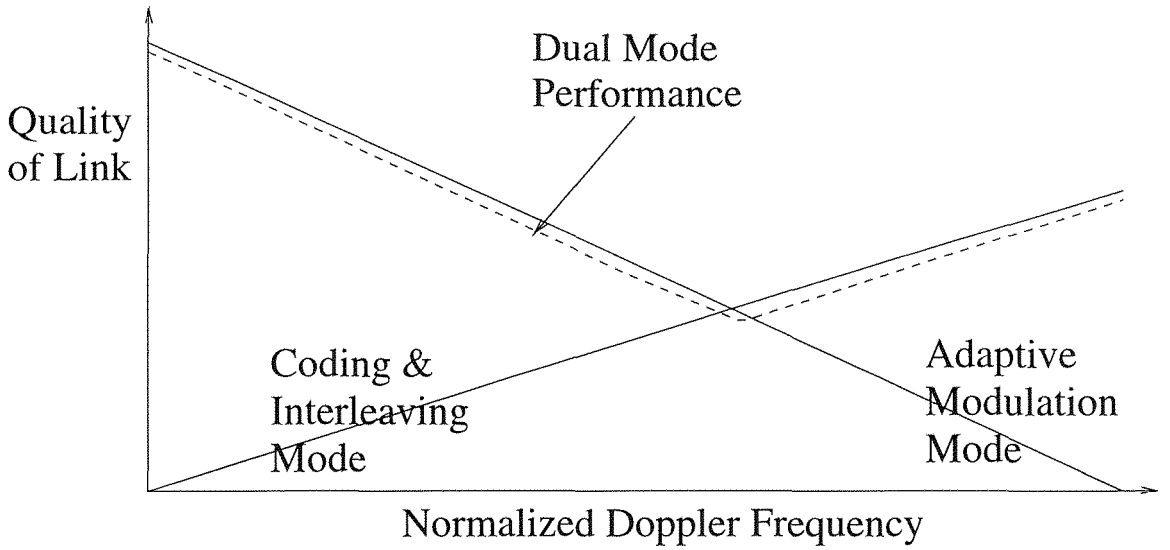

Figure 4.17: Stylised performance characteristics of, single mode adaptive modulation system, single mode fixed modulation system and a dual mode adaptive modulation and fixed modulation system, relative to normalised Doppler frequency.

4.5 Conclusions

Adaptive modulation has been introduced as a deterministic technique to mitigate the effects of the fast fading experienced in a mobile radio channel. The adaptive schemes indicate that practical performance improvements may be achieved by changing the modulation scheme depending upon the prevailing channel conditions. The modulation schemes considered were BPSK, QPSK, square 16 point QAM and square 64 QAM. The possibility of not transmitting was also considered, when channel conditions were particularly poor.

A series of assumptions were made and a numeric upper-bound solution was proposed. A simulation based upon the same criteria was conducted. This illustrated the high level of correspondence between the numeric and simulated performances for both fixed and adaptive schemes. The numerical solution was used to determine the performance of both fixed and adaptive modulation schemes in Rayleigh ($K = 0$) and Rician channels with K factors of 4 and 16. Fixed modulation schemes in channels with larger K factors had BER performance more similar to Gaussian performance than channels with smaller K factors. Consequently, adaptive modulation offers greater benefit, when the K factor is low.

Powell optimisation in conjunction with the numerical solution was used to optimise the switching levels for two particular scenarios through a Rayleigh channel. The first was a speech system, where the mean BER had to be below 1×10^{-2} and the second was a computer

data system, where the mean BER had to be below 1×10^{-4}. The optimised switching levels were 3.31 dB, 6.48 dB, 11.61 dB and 17.64 dB for the speech system and 7.98 dB, 10.42 dB, 16.76 dB and 26.33 dB for the computer data system.

Apart from adapting the modulation scheme on the basis of the instantaneous SNR, the value of the switching levels could be adapted depending on the PDF of the fading (the K factor). However, the performance of the optimised adaptive schemes through a Rician channel of $K = 4$ and $K = 16$ was investigated. This suggested that the complexity of adaptive switching on the basis of the K factor was not worth while.

A dual mode air interface is proposed that would employ adaptive modulation when the fading was slow and fixed modulation when it was fast. The efficiency of adaptive modulation in slow fading, was superior to, fixed modulation in fast fading, when the mean BER performance was considered for both. However, fast fading results in the mean BER being equivalent to the BER experienced by source coder frames, where as slow fading results in the mean BER being higher than the BER experienced by source coder frames. Therefore, the adaptive modulation switching levels were recalculated to insure that the peak BER did not exceed the target BERs. Comparing the peak BER performance adaptive modulation in slow fading, with the, mean BER performance fixed modulation in fast fading, at 1×10^{-4} BER, the adaptive modulation is more efficient. However, the aggregate performance of both fixed and adaptive modems, in the respective desired channel conditions, will be about the same for desired BERs of 1×10^{-2}.

Chapter 5

Interference

5.1 Introduction

In the previous Chapter the performance of adaptive modulation in noise limited conditions was considered. It was shown that such a scheme could offer significant improvements in channel capacity and BER. However, the effects of interference, which often dominate in wireless communications, were not considered. Initially, this Chapter considers some of the practicalities of pulse shaping. The length of impulse response that must be used in future mobile communications standards to prevent inter-symbol interference resulting from pulse shaping is discussed. This is evaluated within the frame-work of Advanced Time Division Multiple Access (ATDMA)[126] for which the cell types and modulation schemes are summarised in Table 5.1. Then, co-channel interference is discussed and numerical results are given for the performance of multi-level cellular and indoors schemes in Gaussian and Rayleigh channels. These results are verified by simulation. Adjacent channel interference is discussed and the ATDMA frame-work is used to exemplify, how the level of adjacent channel interference varies with symbol-rate, filter shape and carrier separation.

Having obtained the performance of fixed modulation schemes in fading and interference channels, adaptive schemes are considered. The effects of the interference upon both the channel estimate and the overall BER are considered. This is followed by a re-optimisation of the switching levels for the adaptive schemes in order to compensate for the interference.

As the adaptive schemes considered in this thesis are based around coherent detection and maximum minimum distance constellations, there is considerable scope to employ interference cancellation, an issue to be detailed at a later stage. A limited numerical solution is derived for fixed modulation schemes employing interference cancellation and this is followed by full

Cell type	Long-macro	Short-macro	Micro	Pico
Modulation	GMSK	Offset 4/16QAM		
Baud-rate (kBaud)	360	450	1800	
Carrier spacing (kHz)	276.92		$1107.69 = 4 \times 276.92$	
Bit-rate (kbps)	360	450/900	1800/3600	
Frame duration (ms)	5			
Slots per frame	15	18	72	
Guard time (symbol)	13	12		8

Table 5.1: ATDMA cell types and modulation schemes, note that symbol rates refer to offset rates which are twice as high as the equivalent non-offset modem discussed in this thesis.

simulation results for fixed and adaptive modulation schemes with interference cancellation. The interference cancellation is used in conjunction with further adjusted switching levels to achieve results similar to those presented in Figure 4.16.

5.2 Band-limited Signalling

The results that have been presented so far have not considered the spectrum of the signalling waveforms. Reducing the spectral occupancy of a modulated signal is desirable, if it is not at the cost of substantially increased BER. Nyquist's fundamental work [127] implies that pulse shaping of the signal waveform must be employed to minimise the bandwidth which the signal occupies. Full response modulation, in the absence of equalisation, requires the pulse shaping to be performed without the introduction of Inter-Symbol Interference (ISI). Kingsbury [128] proposed pulse shaping techniques to minimise ISI by employing trigonometric functions in the time domain. Nyquist's work showed that an odd-symmetric amplitude frequency response leads to an impulse response, which introduces no ISI. An example of such an amplitude frequency response is the raised cosine function [14]. It is also known from matched filter theory, which is treated by for example Sklar [14], that for optimum noise performance the transmitter and receiver impulse responses should be identical, with one of them reversed in time.

Webb [6] defines the raised cosine amplitude frequency response as:

$$|H(f)| = \begin{cases} T & |f| \leq a \\ \frac{T}{2}\left(1 - \sin\left(\frac{\pi T}{\alpha}\left(f - \frac{1}{2T}\right)\right)\right) & a \leq |f| \leq b \\ 0 & |f| \geq b. \end{cases} \tag{5.1}$$

where α is the so called roll-off factor, T is the symbol period, $|H(f)|$ is the overall amplitude frequency response of the receiver,

$$a = \frac{1-\alpha}{2T} \tag{5.2}$$

and

$$b = \frac{1+\alpha}{2T}. \tag{5.3}$$

The values a and b, respectively, represent the frequency at which the raised cosine function begins and ends. Therefore, the implementation of perfect Nyquist filtering and perfectly linear amplification results in the whole signal being contained within a bandwidth of $2b$. Matched filter theory and the direct relationship between time domain convolution and frequency domain multiplication permits both the transmitter and receiver filters to have a frequency response, given by the square-root of Equation 5.1. That is, $|H_t(f)|^2 = |H_r(f)|^2 = |H(f)|$, where $|H_t(f)|$ and $|H_r(f)|$ are the amplitude frequency response of the transmitter and receiver filters, respectively.

The amplitude frequency response of the square-root raised cosine filters given by[129] is,

$$|H_t(f)| = |H_r(f)| = |H(f)| = \begin{cases} T^{\frac{1}{2}} & |f| \leq a \\ T^{\frac{1}{2}} \sin\left[\frac{\pi}{4\alpha}\left(1 + \alpha - 2T|f|\right)\right] & a \leq |f| \leq b \\ 0 & |f| \geq b. \end{cases} \tag{5.4}$$

The impulse response of the square-root Nyquist filter is given by [129, 130] as,

$$h(t) = \frac{4\alpha}{\pi\sqrt{T}} \cdot \frac{\cos((1+\alpha)\pi t/T) + \frac{T\sin((1-\alpha)\pi t/T)}{4\alpha t}}{1 - (4\alpha t/T)^2}. \tag{5.5}$$

A linear phase response is achieved, because the impulse response is symmetric. However, this impulse response is defined for $-\infty < t < \infty$ and therefore cannot be implemented, as it is currently defined. Moreover, to allow the filter to be implemented in a causal fashion a delay must be incurred. To overcome these problems, the impulse response defined in Equation 5.5 must be windowed. Rectangular and Hanning windows [131] were considered for truncating the impulse response. The Hanning window is advantageous in terms of controlling the spectrum of the signalling waveform, however, this was at the expense of introducing ISI. In the absence of any equalisation technique to remove ISI at the receiver, the effects of the extra spectral spillage were considered less significant than the ISI. If the

filtering was performed only at the transmitter (or the receiver), then the impulse response could be truncated without the introduction of ISI. This would, however, result in inferior noise performance [14].

The BER for digital modulation schemes is dependent upon both α and the length of the impulse response employed at the transmitter and receiver. The upper-bound scenario is achieved under the theoretical conditions of infinite length impulse responses at both the transmitter and the receiver. In this case the PSD of the noise entering the receiver filter,

$$|N(f)|^2 = N_0 \quad \text{for} - f_s < f < f_s \tag{5.6}$$

and the PSD of the signal before entering the transmitter filter

$$|S(f)|^2 = S \quad \text{for} - f_s < f < f_s \tag{5.7}$$

where,

$$f_s = \frac{\Upsilon}{T}, \tag{5.8}$$

Υ is the over sampling ratio, N_0 is the noise power, S is the signal power and T is the symbol separation. Therefore, exploiting Parseval's theorem [15] the total signal power after the receiver filter is

$$S_r = \int_{-f_s}^{f_s} S \cdot |H(f)|^2 df, \tag{5.9}$$

and the total noise power after the receiver filter is

$$N_r = \int_{-f_s}^{f_s} N_0 \cdot |H(f)| df. \tag{5.10}$$

Therefore, when square-root raised cosine filters are implemented with infinite length, the received SNR becomes:

$$\gamma_\alpha = \gamma \cdot \frac{\int_{-f_s}^{f_s} |H(f)|^2}{\int_{-f_s}^{f_s} |H(f)|} \tag{5.11}$$

where γ is the received SNR with $\alpha = 0.0$. Solving the integral in Equations 5.4,

$$\gamma_\alpha = \gamma \cdot \left(1 + \frac{4}{T\alpha}\right) \tag{5.12}$$

The BER for BPSK, QPSK and Square 16 and 64 QAM may be calculated using Equations 3.1, 3.2, 3.9 and 3.10 by letting $\gamma = \gamma_\alpha$. Figure 5.1 shows the upper-bound BER versus channel SNR performance of BPSK over Gaussian channels assuming an infinite impulse response length. Identical variations in performance, with respect to α, are observed for QPSK and 16 and 64 Square QAM, that is SNR reductions of 0.4, 0.58 and 1.25 dB for α of 0.35, 0.5 and 1.0, for all BER, when comparing against $\alpha = 0$. These benefits are solely

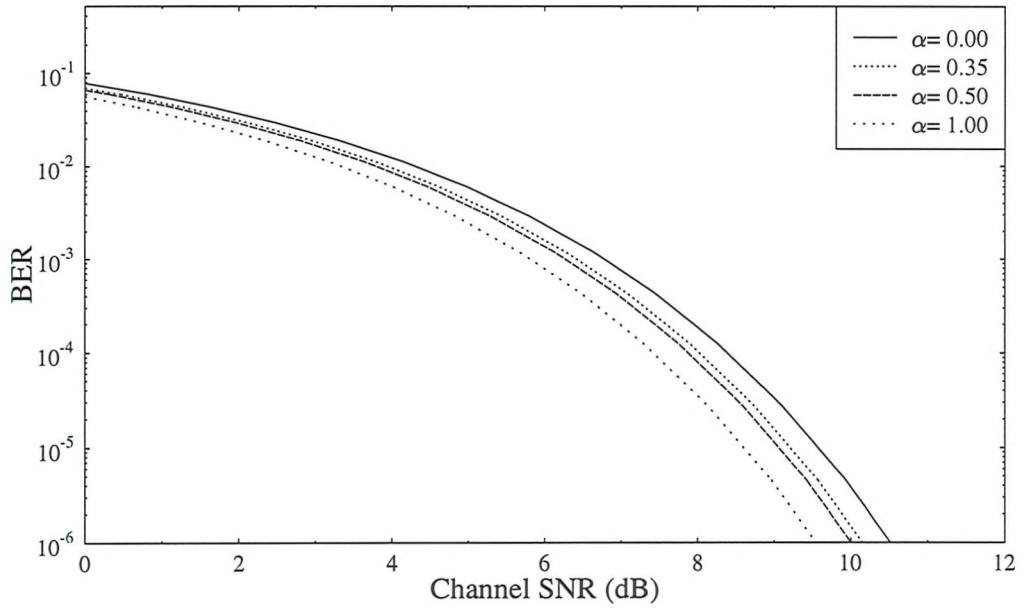

Figure 5.1: Theoretical upper bound BER performance of BPSK in a Gaussian channel, for $\alpha = 0.0$, 0.35, 0.5 and 1.0, assuming infinitely long impulse response and perfect clock and carrier recovery. The simulations were conducted with $\Upsilon = 8$.

a result of different pulse shaping. As α increases, the impulse response decays quicker and the transmitted energy at positions other than the sample points is reduced. In a real system, with non-ideal clock and carrier recovery systems having a large α would perform better than equivalent small-α systems.

5.2.1 Impulse Response Truncation

In a practical system an infinite impulse response is not practical, therefore, evaluation of the effect of truncating the impulse response was conducted by simulation. The four fixed schemes modulation schemes, mentioned above, were evaluated in Gaussian channels, with α values of $0.2, 0.35, 0.5$ and 0.65, and impulse response lengths of $5, 7$ and 9 symbols duration. For the purpose of these simulations signal and noise were filtered separately at the receiver and the average ratio of the powers passed by these filters was used as the SNR measure. The BER was calculated from the filtered signal plus the filtered noise, that is, from the linear sum of the amplitude of both filters' output. The experiments were performed with oversampling ratios of $\Upsilon = 8$ and $\Upsilon = 4$ and only marginal differences were registered. All results are shown for $\Upsilon = 8$.

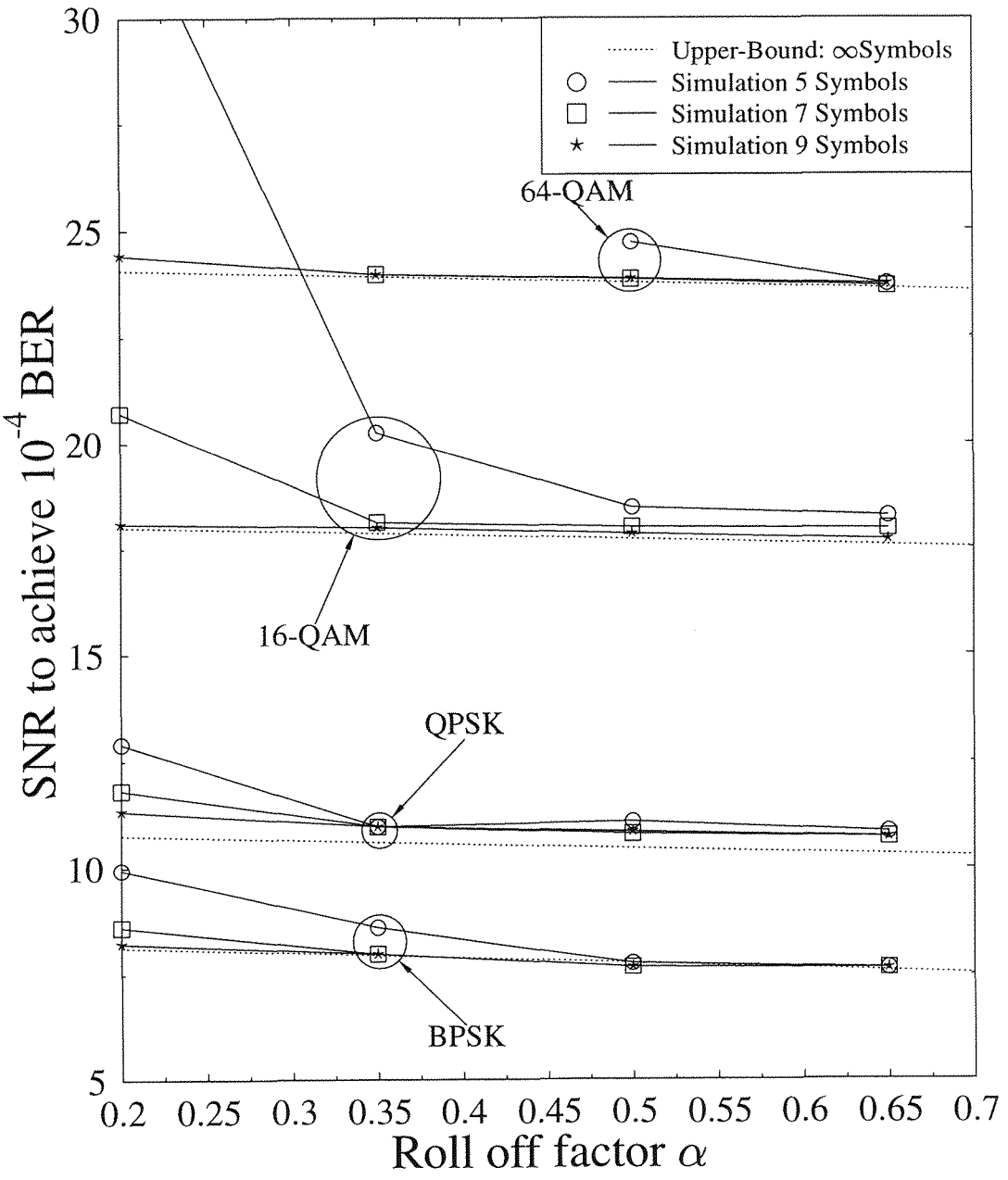

Figure 5.2: SNR value required to achieve 10^{-4} BER in a Gaussian channel for BPSK, QPSK, square 16 and 64 QAM with impulse response lengths of $5, 7$ and 9 symbol and ∞ (upper-bound) duration

Figure 5.2 shows the SNR value required to achieve 10^{-4} BER for the impulse response durations of $5, 7$ and 9 symbols and the infinite-length upper-bound value. The ISI that results from the shortening of the square-root raised cosine filters' impulse response manifests a residual BER in excess of 10^{-4} for Square 64 QAM, when the impulse response is 5 symbols long and $\alpha < 0.5$; consequently these points are omitted in Figure 5.2. For the smaller α values the BER is more dependent upon the length of the impulse response and, as expected, longer impulse responses improve the BER performance. As α becomes larger than 0.35, the BER performances with impulse response lengths of either 7 or 9 symbols converge for each of the modulation schemes. Further, the BER performance with both 7 or 9 symbols long impulse response correspond closely to the upper-bound performance. This convergence in performance of the different length impulse responses, as α increases, is because as α becomes larger, the impulse response has less frequency constraint and can decay more quickly. Therefore, regions of the impulse response which are set to zero by the truncation are already approximately zero, consequently, the truncation introduces less ISI. Figure 5.2 also shows that for all modulation schemes, including the most sensitive square 64 QAM, an impulse response of length of 7 symbols is sufficient to achieve an irreducible level of ISI, provided that $\alpha \geq 0.35$. ATDMA [101], as seen in Table 5.1 is proposed with 8 tail symbols per slot in a micro-cell environment and it is assumed that these symbols can be used to initialising the Nyquist filters. However, these are offset QAM symbols and correspond to 4 non-offset symbols. Therefore, in order to implement optimised adaptive modulation as proposed in [132], within an ATDMA micro-cell framework, the redundancy due to tail symbols would have to be increased. In a pico-cell the redundancy due to tail symbols would also have to be increased. A total of 6 non-offset symbols or 12 offset symbols, would be required in order to realise a filter that would not introduce errors caused by ISI from impulse response truncation.

Therefore, considering only the effects of ISI upon BER that are introduced by truncation of the impulse response of square-root raised cosine filters, it has been shown that if adaptive modulation is to be exploited within an micro-cell ATDMA system, where no ISI combating technique is to be employed, redundancy due to tail symbols must be increased from 4.8 % to 9.6%. However, previous work [132] has suggested that for a BER of 1×10^{-4} adaptive modulation may achieve 4-5 times the through-put of fixed schemes in slow Rayleigh fading channels and this is shown in Figure 4.11.

5.3 Multi-user Interference - Fixed Modulation Schemes

Lee [133] investigated the spectrum efficiency of cellular systems. He defines the signal to interference ratio as

$$SIR = \frac{S}{\sum_{k=1}^{6} I_k} + n \tag{5.13}$$

where there are six, so-called first-tier, interferers, S is the Signal Power, I_k is the power from the k^{th} interferer and n is the noise power. He also defines a measure of radio capacity as m expressed in terms of the traffic channels per hexagonal cell, assuming the inverse fourth-power law, as follows:

$$m = \frac{B_t}{B_c\sqrt{\frac{2}{3}SIR}} \tag{5.14}$$

where B_t, B_c and SIR are the total system bandwidth, channel bandwidth, and minimum signal to interference ratio that the modulation scheme can operate at for a given BER, respectively. This expression was derived on the assumption that, interference is the limiting factor in a cellular system. Another measure of radio capacity based upon Equation 5.14, assuming the Erlang B tele-traffic model [1] and the knowledge of the cell area is also defined. Lee refers to this measure of radio capacity as m_2 with units of Erlang/km^2, where one Erlang is defined as 3600 call-seconds per hour. The quantity m_2 is calculated by evaluating m from Equation 5.14 and then exploiting the acceptable blocking probability, P_B, the Erlang B model can be invoked in order to evaluate the maximum offered traffic A. The Erlang B model [1] is defined as:

$$P_B = \frac{A^m/m!}{\sum_{k=0}^{m} \frac{A^k}{k!}}. \tag{5.15}$$

The value of m_2 is then simply given by the quotient of A and A_1, where A_1 is the area of a cell. Lee acknowledges that his model is simple and it only considers co-channel interference, neglecting both adjacent channel interference and noise. Webb [134] refined Lee's approach for evaluating spectral efficiency by using a micro-cellular propagation design system. This is a more applicable approach for the work included in this thesis and therefore, had a micro-cellar design system been available, it would have been used. In the following section the effect of interference upon fixed modulation is investigated with a view to making comparisons with adaptive modulation.

5.3.1 Co-Channel Interference

Co-Channel Interference (CCI) results from the frequency reuse [1] that is fundamental to cellular radio systems. The interference is the energy that leaves one cell operating at a

particular frequency and is received by equipment in another cell operating at the same frequency, resulting in distortion of the desired signal. The problem is alleviated by increasing the number of frequencies available and reusing each frequency more sparsely. However, this has the very undesirable effect of reducing the overall spectrum efficiency [135].

C-C Lee and Steele [136] investigated CCI for a GSM type system employing frequency hopping and power control; the same definition of CCI is used here. That is, CCI is the ratio of the average power received from the desired transmitter, S, to the power, I, received from other transmitters on the same channel. The effect of an interferer upon a communications channel is dependent upon the modulation scheme under investigation, it is also dependent upon the modulation scheme of the interfering signal.

Modelling of the interference is not simple and various authors make different decisions about the trade-off between accuracy and implementational practicalities. Malkamaki [137] asymptotes that the carrier and interferer are temporally synchronous, that is, the start and finish of the desired symbol and the interfering symbol coincide at the receiver. He also assumed that a constant frequency offset of 1kHz between the carrier and interference will render the two signals non-coherent in terms of phase. Webb [134] considers differential modulation schemes and also assumes temporal synchronisation, however, he assumes that the independent fading nature of the channels will result in the signal and interference being phase non-coherent. Burr [138] considers time-synchronous interference but introduces a random uncorrelated phase difference between the signal and the interference. Beaulieu et al [139] and Chiani [140] consider phase non-coherent and time-asynchronous interference. This is a more complete representation, however, the results become dependent upon α and the filter impulse response length. Moreover, when considering multi-level modulation, the simulation complexities of time-asynchronous interference become practically prohibitive. It is assumed that time-synchronous interference represents a worse case scenario and this assumption is adopted throughout this work. Furthermore, both the signal and the co-channel interference are considered at their optimum sampling positions both in terms of the distortion caused and the SIR measurement. The phase non-coherence is introduced by corrupting the interference with an uncorrelated random phase which is independent burst by burst. Figure 5.3 portrays a square 16 QAM phasor corrupted by a time-synchronous, phase non-coherent QPSK interferer.

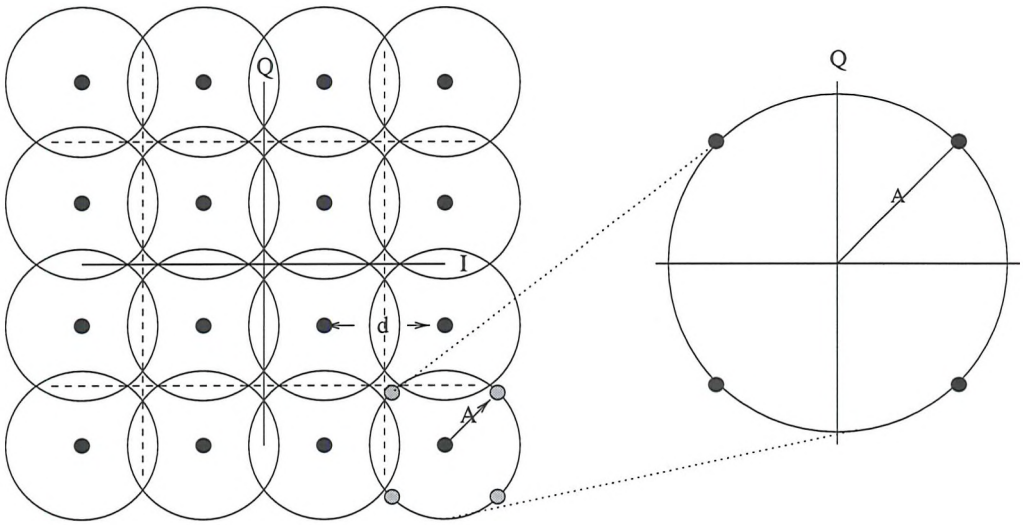

Figure 5.3: A Square 16 QAM symbol experiencing QPSK co-channel interference. The SIR is $10d^2/A^2$

5.3.1.1 Gaussian Channel

The performance of BPSK, QPSK and square 16 and 64 QAM in the presence of noise and CCI are now considered. The performance with both the desired signal and interfering signal transmitted through Gaussian channels is initially considered. The distribution of the in-phase components of noise and an interfering signal are derived.

The distribution of a zero mean Gaussian noise source has an amplitude PDF given by:

$$P(v) = \frac{1}{\sqrt{2\pi}\sigma} e^{-\frac{v^2}{2\sigma^2}} \tag{5.16}$$

where σ^2 is the variance. The amplitude of interference depends upon what symbol is transmitted on the interfering channel and this depends upon the modulation scheme employed on that channel. Modulation schemes considered as potential interferers are BPSK, QPSK and square 16 and 64 QAM. When the interfering symbol is BPSK or QPSK, the magnitude of the corruption in one dimension is only dependent upon the relative phase difference between the desired signal and the interfering signal. This is, because both BPSK and QPSK symbols are of fixed amplitude. However, when the interfering symbol is square 16 or 64 QAM, the magnitude of the interference is dependent upon the actual symbol. The maximum interfering amplitudes occur, when the phase difference between the desired signal and the interferer is least favourable. For each interfering modulation scheme vectors **A** and **B** are defined as the interfering symbols' maximum amplitude and probability of occurrence, respectively.

Assuming that I is the average interfering power, $\mathbf{A}$ and $\mathbf{B}$ are given by

$$\mathbf{A} = \left(\sqrt{I}\right), \quad \mathbf{B} = (1) \quad \text{for BPSK,} \tag{5.17}$$

$$\mathbf{A} = \left(\sqrt{I}\right), \quad \mathbf{B} = (1) \quad \text{for QPSK,} \tag{5.18}$$

$$\mathbf{A} = \begin{pmatrix} \sqrt{I/5} \\ \sqrt{I} \\ \sqrt{9I/5} \end{pmatrix}, \quad \mathbf{B} = \begin{pmatrix} \frac{1}{4} \\ \frac{1}{2} \\ \frac{1}{4} \end{pmatrix} \text{for Square 16 QAM} \tag{5.19}$$

and

$$\mathbf{A} = \begin{pmatrix} \sqrt{I/21} \\ \sqrt{5I/21} \\ \sqrt{3I/7} \\ \sqrt{13I/21} \\ \sqrt{17I/21} \\ \sqrt{25I/21} \\ \sqrt{29I/21} \\ \sqrt{37I/21} \\ \sqrt{7I/3} \end{pmatrix} \text{ and } \mathbf{B} = \begin{pmatrix} \frac{1}{16} \\ \frac{1}{8} \\ \frac{1}{16} \\ \frac{1}{8} \\ \frac{1}{8} \\ \frac{3}{16} \\ \frac{1}{8} \\ \frac{1}{8} \\ \frac{1}{16} \end{pmatrix} \text{ for Square 64 QAM.} \tag{5.20}$$

It is assumed that the distribution of the relative phase difference between the desired signal and the interferer is uniform and therefore the interference amplitude PDF in either the real or imaginary axis, represented by the variable x is given by

$$P(x) = \begin{cases} \sum_{m=1}^{N} \frac{|\mathbf{B}_{m1}|}{\pi\sqrt{|\mathbf{A}_{m1}|^2 - x^2}} & \text{if } |x| \leq |\mathbf{A}_{m1}| \\ 0 & \text{otherwise,} \end{cases} \tag{5.21}$$

where $\mathbf{A}$ and $\mathbf{B}$ are selected for the relevant interferer N is the order of the appropriate column vector from those given in Equations 5.17- 5.20, and x is the variable that defined the amplitude of the interference. The PDF in Equation 5.21 is plotted in Figure 5.4, for BPSK, QPSK, and Square 16 and 64 QAM.

If z is defined as the real component of the interference, described by the vectors $\mathbf{A}$ and $\mathbf{B}$, plus the noise, with variance σ, its PDF may be determined by combining Equations 5.16 and 5.21, using the technique given in Papoulis [141]. This new PDF is called $P_\sigma()$ and may be written:

$$P_\sigma(z) = \int_{-\infty}^{\infty} P(z+w) \cdot \frac{1}{\sqrt{2\pi}\sigma} e^{-\frac{z-w}{2\sigma^2}} dw \tag{5.22}$$

where w is the integration variable that insures the total length of the real component of interference plus the noise is z. However, it is known that $P()$ is zero outside the range

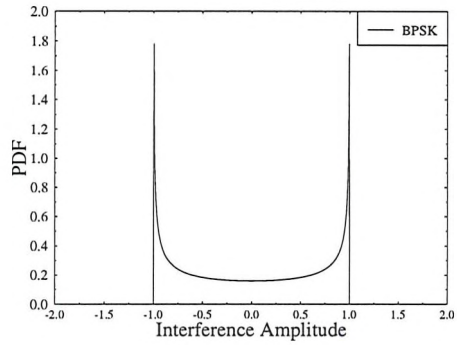

(a) BPSK

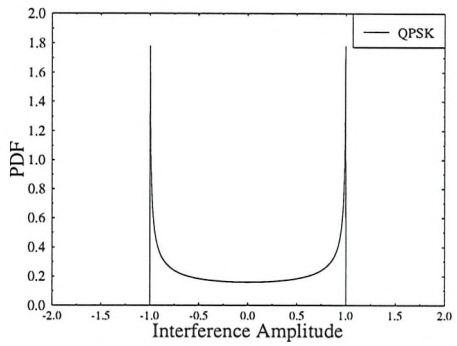

(b) QPSK

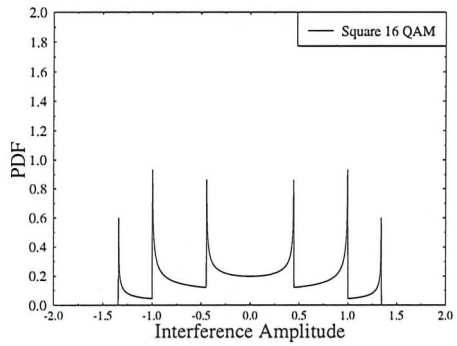

(c) Square 16 QAM

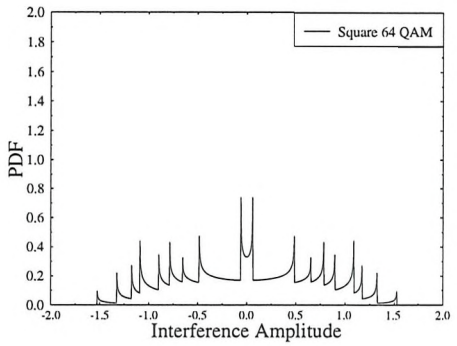

(d) Square 64 QAM

Figure 5.4: PDF of interference amplitudes inflicted by BPSK, QPSK, Square 16 and 64 QAM, where the average power for each constellation is unity and the relative phase difference between the useful signal and the interferer is uniformly distributed.

$\pm|\mathbf{A}_{m1}|$ and therefore

$$P_\sigma(z) = \sum_{m=1}^{N} \frac{\mathbf{B}_{m1}}{\pi^{\frac{3}{2}}\sigma\sqrt{2}} \int_{(z+w)^2=-|\mathbf{A}_{m1}|}^{(z+w)^2=|\mathbf{A}_{m1}|} \frac{e^{-\frac{(z-w)^2}{2\sigma^2}}}{\sqrt{|\mathbf{A}_{m1}|^2-(z+w)^2}} dw. \tag{5.23}$$

The limits of the integration may be simplified by solving the quadratic equation $(z+w)^2 = |\mathbf{A}_{m1}|$ for w, hence,

$$P_\sigma(z) = \sum_{m=1}^{N} \frac{\mathbf{B}_{m1}}{\pi^{\frac{3}{2}}\sigma\sqrt{2}} \int_{w=-z-|\mathbf{A}_{m1}|}^{w=-z+|\mathbf{A}_{m1}|} \frac{e^{-\frac{(z-w)^2}{2\sigma^2}}}{\sqrt{|\mathbf{A}_{m1}|^2-(z+w)^2}} dw. \tag{5.24}$$

The CDF of z is the CDF of an orthogonal projection of interference plus noise. It can be

used to extend the results in Section 3.2.1, where the Q() function was introduced, to characterise the performance of modulation schemes in the presence of both noise and interference. Therefore, similar nomenclature is used and the CDF is defined as

$$Q'_\sigma(y) = \int_y^\infty P_\sigma(z)dz, \tag{5.25}$$

where the prime represents the inclusion of interference to the distribution.

The SIR may be defined as

$$\text{SIR} = P_s/I, \tag{5.26}$$

where P_s is the power received from the desired signal. Therefore, the BER of BPSK and QPSK can be computed as,

$$P'_b(P_s, \sigma) = Q'_\sigma(\sqrt{P_s}) \tag{5.27}$$

and

$$P'_q(P_s, \sigma) = Q'_\sigma(0.5 \cdot \sqrt{P_s}), \tag{5.28}$$

respectively, when neither the signal nor the interference experience fading. This is a similar result to that quoted in Section 3.2.1, where interference was not considered, with the exception that the corruption PDF includes the interference as well as the Gaussian noise.

Square 16 and 64 QAM were also considered in Section 3.2.1, however, certain, low-probability, terms could be neglected there, since the corruption was due to noise only. When interference is considered in addition to noise, these terms may no longer be neglected and the exact BER performance of sub-channels 1 and 2 of Square 16 QAM and sub-channels 1, 2 and 3 of Square 64 QAM are given by,

$$P'_{16_1}(P_s, \sigma) = 0.5 \cdot \left\{ Q'_\sigma\left(\sqrt{\frac{P_s}{10}}\right) + Q'_\sigma\left(3\sqrt{\frac{P_s}{10}}\right) \right\}, \tag{5.29}$$

$$P'_{16_2}(P_s, \sigma) = Q'_\sigma\left(\sqrt{\frac{P_s}{10}}\right) + 0.5 \cdot \left\{ Q'_\sigma\left(3\sqrt{\frac{P_s}{10}}\right) - Q'_\sigma\left(5\sqrt{\frac{P_s}{10}}\right) \right\}, \tag{5.30}$$

$$P'_{64_1}(P_s, \sigma) = 0.25 \cdot \left\{ Q'_\sigma\left(\sqrt{\frac{P_s}{21}}\right) + Q'_\sigma\left(3\sqrt{\frac{P_s}{21}}\right) + Q'_\sigma\left(5\sqrt{\frac{P_s}{21}}\right) + Q'_\sigma\left(7\sqrt{\frac{P_s}{21}}\right) \right\}, \tag{5.31}$$

$$P'_{64_2}(P_s, \sigma) = 0.25 \cdot \left\{ Q'_\sigma\left(3\sqrt{\frac{P_s}{21}}\right) + Q'_\sigma\left(5\sqrt{\frac{P_s}{21}}\right) + Q'_\sigma\left(\sqrt{\frac{P_s}{21}}\right) + Q'_\sigma\left(7\sqrt{\frac{P_s}{21}}\right) \right.$$

$$+ \quad 1 - \left[Q'_\sigma \left(\sqrt{\frac{P_s}{21}} \right) - Q'_\sigma \left(9\sqrt{\frac{P_s}{21}} \right) + Q'_\sigma \left(3\sqrt{\frac{P_s}{21}} \right) - Q'_\sigma \left(11\sqrt{\frac{P_s}{21}} \right) \right] \Bigg\} \tag{5.32}$$

and

$$\begin{aligned} P'_{64_3}(P_s, \sigma) &= 0.25 \cdot \left\{ Q'_\sigma \left(3\sqrt{\frac{P_s}{21}} \right) - Q'_\sigma \left(7\sqrt{\frac{P_s}{21}} \right) + Q'_\sigma \left(\sqrt{\frac{P_s}{21}} \right) - Q'_\sigma \left(5\sqrt{\frac{P_s}{21}} \right) \right. \\ &+ 1 - \left[Q'_\sigma \left(9\sqrt{\frac{P_s}{21}} \right) + Q'_\sigma \left(1\sqrt{\frac{P_s}{21}} \right) - Q'_\sigma \left(5\sqrt{\frac{P_s}{21}} \right) + Q'_\sigma \left(3\sqrt{\frac{P_s}{21}} \right) \right] \\ &+ 1 - \left[Q'_\sigma \left(11\sqrt{\frac{P_s}{21}} \right) + Q'_\sigma \left(3\sqrt{\frac{P_s}{21}} \right) - Q'_\sigma \left(7\sqrt{\frac{P_s}{21}} \right) + Q'_\sigma \left(1\sqrt{\frac{P_s}{21}} \right) \right] \\ &\left. Q'_\sigma \left(3\sqrt{\frac{P_s}{21}} \right) - Q'_\sigma \left(7\sqrt{\frac{P_s}{21}} \right) + Q'_\sigma \left(9\sqrt{\frac{P_s}{21}} \right) - Q'_\sigma \left(13\sqrt{\frac{P_s}{21}} \right) \right\}. \end{aligned} \tag{5.33}$$

Equations 5.29 - 5.33 are not presented in their most simplified manner thus allowing straightforward verification of their validity. A rigorous step-by-step verification with reference to the phasor constellations would be verbose and since verification by simulation follows, it is also unnecessary.

Averaging the performance of the sub-channels gives the average performance of square 16 and 64 QAM schemes as

$$P'_{16}(P_s, \sigma) = \frac{P'_{16_1}(\sigma, P_s) + P'_{16_2}(\sigma, P_s)}{2} \tag{5.34}$$

and

$$P'_{64}(P_s, \sigma) = \frac{P'_{64_1}(\sigma, P_s) + P'_{64_2}(\sigma, P_s) + P'_{64_3}(\sigma, P_s)}{3} \tag{5.35}$$

respectively.

The BER performance of BPSK, QPSK and Square 16 and 64 QAM may now be computed in the presence of noise plus BPSK, QPSK and Square 16 or 64 QAM interference. This is achieved by numerical solution of the equations above and verified by simulation. Figure 5.5 illustrates the BER versus channel SNR performance of BPSK in the presence of a single BPSK interferer, QPSK in the presence of a single QPSK interferer, Square 16 QAM in the presence of a single Square 16 QAM interferer and Square 64 QAM in the presence of a single Square 64 QAM interferer. In all cases both the signal and the interferer are transmitted through Gaussian channels. The Figure shows that for all schemes there is very

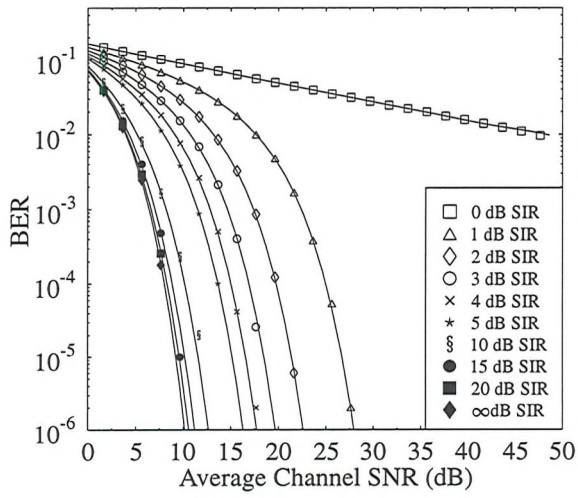

(a) BPSK

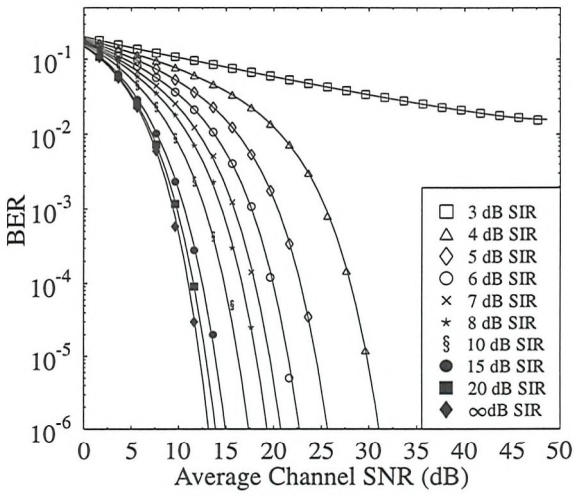

(b) QPSK

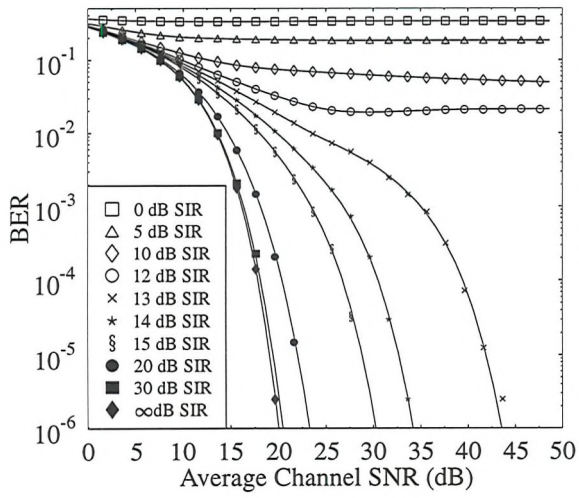

(c) Square 16 QAM

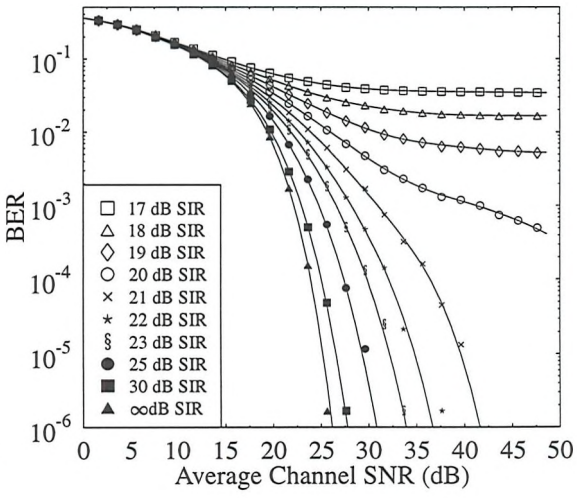

(d) Square 64 QAM

Figure 5.5: Numerical and simulated performance of fixed modulation schemes in Gaussian channels with the same modulation scheme interfering at various SIR values, when $\alpha = 0.35$ and no interference cancellation.

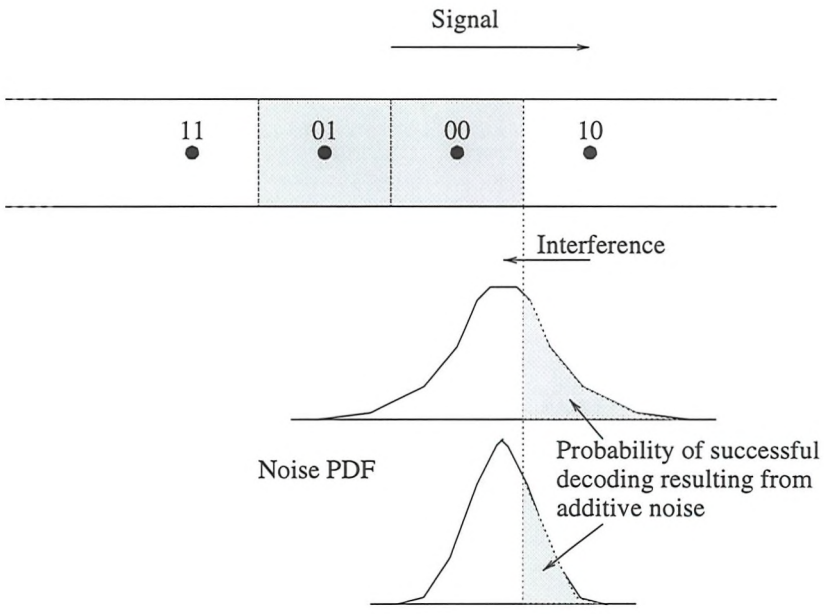

Figure 5.6: Sketch of a section of a Square 16 QAM constellation showing how under specific conditions increased noise can actually reduce the BER.

close correspondence between the numerical and simulated results. It is shown that at 50 dB average channel SNR and low SIR there is a significant residual BER for all of the schemes. Residual BERs exist for BPSK, QPSK, and square 16 and 64 QAM when the SIR is below 1, 4, 13 and 21 dB respectively.

Generally, as expected, an increase in average channel SNR results in a reduction in BER or at the very least a constant BER. However, in Figure 5.5(c), it can be seen that between average channel SNRs of approximately 27 dB and 37 dB, the BER increases when the SIR is 12 dB. The BER is dependent upon a complex interaction of the desired signal and interfering symbols. It is the dominance of one specific interaction that results in the BER increasing with SNR. In the absence of noise the interference corrupting the desired signal may result in the received symbol being the wrong side of a constellation decision boundary. However, as shown in Figure 5.6 the noise can add further corruption which may result in the received symbol being correctly decoded.

A further informative figure can be produced from the results of Figure 5.5 which is shown in Figure 5.7. Here, the minimum SNR required to achieve the desired BER performances of 1×10^{-2} and 1×10^{-4} is plotted against varying values of SIR. As expected, for a BER of 1×10^{-4} the SNR and SIR must be greater than for a BER of 1×10^{-2}. For each modulation scheme and at both BERs the plotted line appears to converge to both a vertical and a horizontal asymptote. The approximate values of these asymptotes are given in Table 5.2.

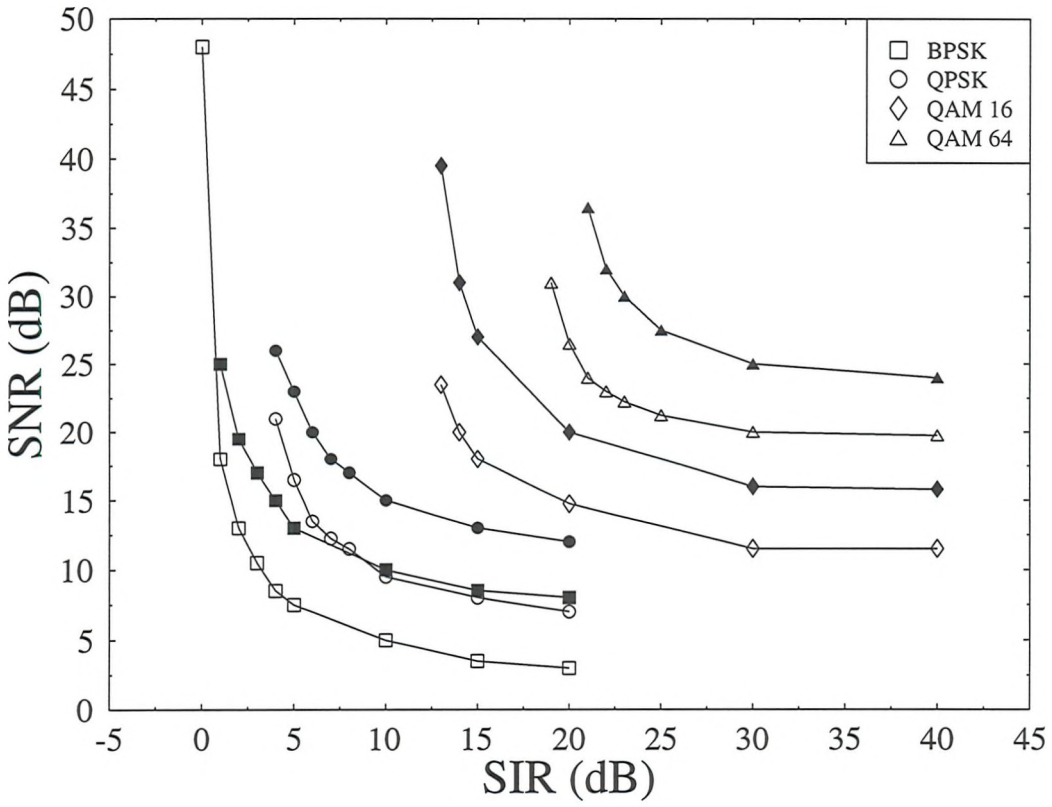

Figure 5.7: Minimum SIR and SNR required to achieve 1×10^{-2} BER (white markers) and 1×10^{-4} BER (black markers) for BPSK, QPSK, Square 16 and 64 QAM in a Gaussian channel with a single Gaussian channel interferer of the same modulation scheme as the desired signal, when using no interference cancellation.

The vertical asymptote represents the minimum SIR that is required to achieve the desired BER performance, if the SNR is infinite. Equivalently, the horizontal asymptote represents the minimum SNR required to achieve the desired BER performance, when the SIR is infinite.

Considering Table 5.2 it can be noted that the difference between the horizontal asymptote, for the two desired BER performances, is approximately constant for all of the modulation schemes and is approximately 4 dB SIR. However, the difference between the vertical asymptotes, for the two desired BER performances, varies for each modulation scheme and becomes larger as the constellation order increases. This is a manifestation of the different shape of the PDFs of noise and interference. The well known PDF of the noise, given by Equation 5.16, reduces gradually for the outlying values. However, the PDF of the interference, given in Equation 5.21 and plotted in Figure 5.4 varies, depending on which modulation scheme is

	BPSK	QPSK	QAM 16	QAM 64
Vertical SIR(dB)				
1×10^{-2}	-0.5	2	11	17.5
1×10^{-4}	0	3	12.5	20
Horizontal SNR(dB)				
1×10^{-2}	2.5	7	11.25	19.5
1×10^{-4}	6.5	11.25	15.5	23.5

Table 5.2: Approximate Vertical and Horizontal asymptotes for the curves in Figure 5.7

producing the interference. For BPSK and QPSK the PDF of the interference amplitude is very different from that of noise, it increases to a peak for extreme interference values and then drops to zero. Consequently, for small variations in SIR, dramatic changes in BER can be experienced. This is especially the case when the amplitude corresponding to the interference PDF peak, seen in Figure 5.4, results in the received symbol being close to a decision threshold. As the constellation order increases, the interference amplitude PDF decreases more smoothly at extreme values of interference amplitude and therefore the potential for dramatic changes in BER resulting from small variations in SIR is reduced.

5.3.1.2 Fading Signal and Fading Interference

In order to derive the analytical BER performance of the interference contaminated scenario, Equations 5.27, 5.28, 5.34 and 5.35 may be used instead of the Gaussian channel BER relationships (Equations 3.1, 3.2 3.9 and 3.10) in Equation 4.5. Therefore, the BER performance of both fixed and adaptive modulation schemes can be evaluated in a fading channel with a non-fading interferer. To obtain the performance of a slow fading signal and slow fading interferer Equation 5.25 may be modified to:

$$Q''_{\sigma}(y) = \int_{y}^{\infty} P'_{\sigma}(z)dz \tag{5.36}$$

where $P'_{\sigma}()$ is the PDF of the Cartesian orthogonal decomposition of Rayleigh faded interference plus noise. This could be computed by combining the PDF of Rayleigh fading, Equation 2.14, with the PDF of the interference, Equation 5.21, and the PDF of Gaussian noise. However, the PDF of Cartesian orthogonal decomposition of noise and Rayleigh faded interference, $P'_{\sigma}(z)$, appears complicated. However, it was observed that the PDF of the Cartesian orthogonal decomposition of Rayleigh faded interference was a Gaussian distribution for each of the N components. This observation drastically reduces the complexity as it is well known [25] that the result of the superposition of more than one Gaussian random

variable results in another Gaussian random variable. Consequently, given that the noise is also Gaussian,

$$P'_{\sigma}(z) = \sum_{m=1}^{N} \frac{|\mathbf{B}_{m1}|}{\sqrt{2\pi}\zeta_m} e^{-\frac{z^2}{2\cdot\zeta_m^2}}, \tag{5.37}$$

where

$$\zeta_m^2 = \frac{|\mathbf{A}_{m1}|^2}{4} + \sigma^2 \tag{5.38}$$

and, therefore, Equation 5.36 becomes simply

$$Q'_{\sigma}(y) = \frac{1}{2} \sum_{m=1}^{N} |\mathbf{B}_{m1}| \cdot \text{erfc}\left(\frac{y}{\sqrt{2}\cdot\zeta_m}\right). \tag{5.39}$$

Exploiting this simple relationship, the performance of fixed and adaptive modulation schemes transmitted through a Rayleigh fading channel, with Rayleigh fading interferers may be easily computed. Figure 5.8 shows both the numerical and simulated performance results.

5.3.2 Adjacent Channel interference

Adjacent Channel Interference (ACI) results from energy spilling from one frequency band to another as shown in Figure 5.9. The signal to adjacent channel interference, (S/I_a), is given by [142] as:

$$S/I_a(\Delta f) = \frac{|A|^2 \int_{-\infty}^{+\infty} |H_t(f)|^2 \cdot |H_r(f)|^2 df}{|B|^2 \int_{-\infty}^{+\infty} |H_r(f)|^2 \cdot |H_t(f \pm \Delta f)|^2 df}. \tag{5.40}$$

The powers of the signal and the interferer at their centre frequencies are given by A and B respectively. The numerator of Equation 5.40 is the power received of the desired signal after transmitter and receiver Nyquist filters. The denominator is the received power from the interferers after being filtered by the receiver's Nyquist filter and interferer's Nyquist transmitter filter, which has its centre frequency offset of Δf from the desired signal's Nyquist transmitter filter. Equation 5.4 may be substituted into Equation 5.40 and by simple integration the numerator becomes:

$$\begin{aligned} |A|^2 \int_{-\infty}^{+\infty} |H_t(f)|^2 \cdot |H_r(f)|^2 df &= |A|^2 \cdot \int_{-\infty}^{+\infty} |H(f)|^2 \cdot |H(f)|^2 df & (5.41) \\ &= |A|^2 \cdot T\,(1-\alpha) & (5.42) \\ &+ |A|^2 \cdot \frac{T\alpha}{\pi} \left[\frac{3\theta}{4} + \cos(\theta) - \frac{\cos(\theta)\sin(\theta)}{4}\right]_{\theta=-\pi T}^{\theta=\pi T} \end{aligned}$$

where

$$\theta = \frac{\pi \cdot T}{\alpha}\left(f - \frac{1}{2T}\right). \tag{5.43}$$

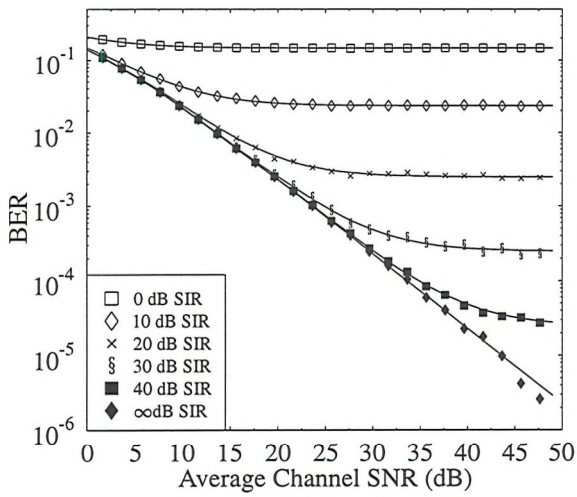

(a) BPSK

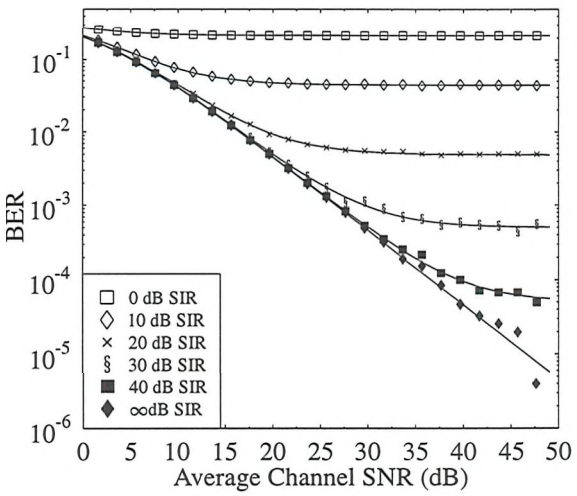

(b) QPSK

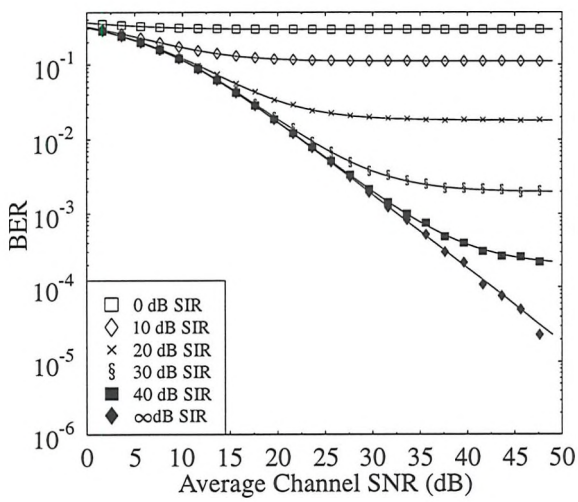

(c) Square 16 QAM

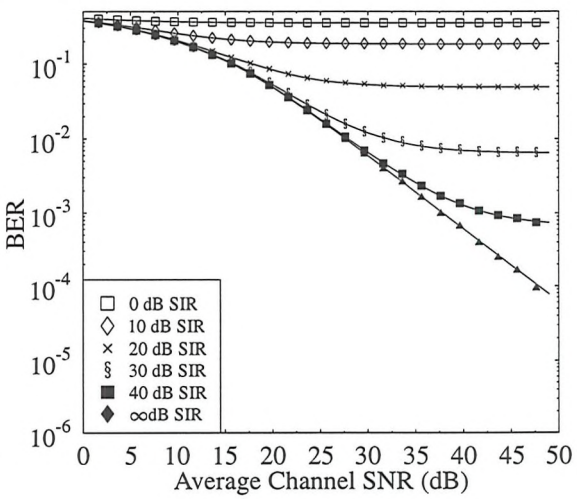

(d) Square 64 QAM

Figure 5.8: Simulated performance of fixed modulation schemes in Rayleigh channels without interference cancellation at various SIR values, where the interfering modulation scheme was the same as the useful signal and received over an independent Rayleigh channel. $\alpha = 0.35$ was used.

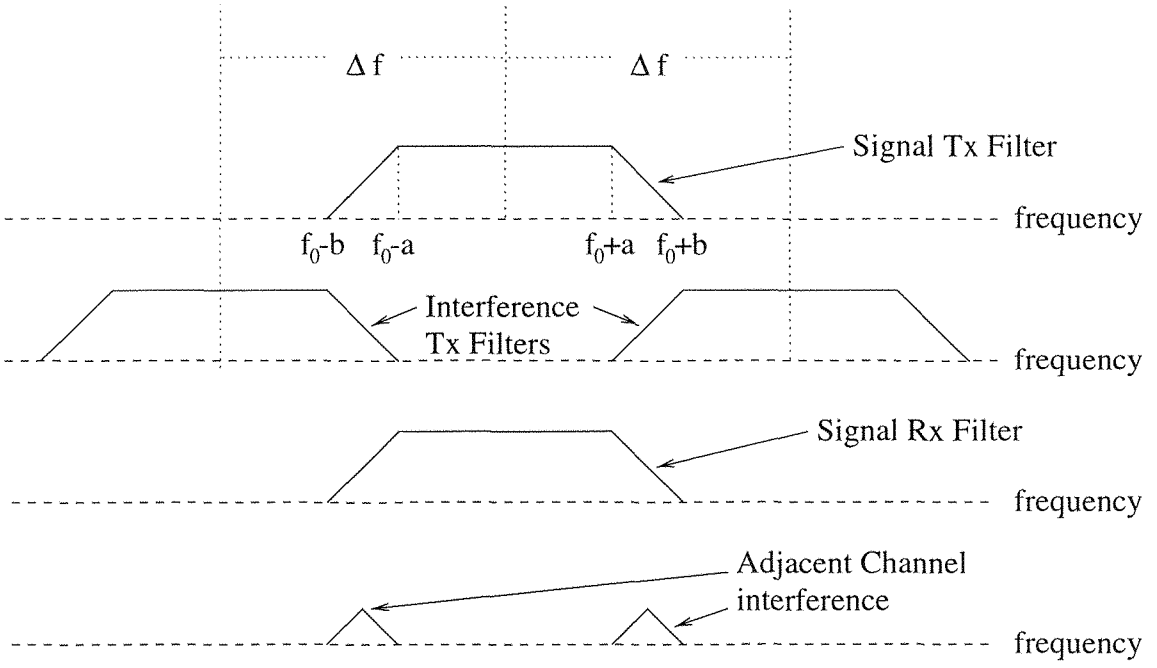

Figure 5.9: Schematic representing the Nyquist filters of transmitters at f_0, $f_0 + \Delta f$ and $f_0 - \Delta f$, and the receiver filter for the central carrier. The adjacent interference experience by the central carrier is shown as are the start and finish of the the roll-off section of the Nyquist filter, represented by $f_0 \pm a$ and $f_0 \pm b$, respectively.

Assuming that the carrier separation and roll-off factors of the higher and the lower frequency adjacent channel interferers are the same, only the integration for one of these interferers needs to be calculated. The integral forming the denominator of Equation 5.40 must be calculated separately for different α and carrier separation scenarios. There are six different solutions depending upon the value of Δf and the roll-off factor and they are all shown in Figure 5.10. For each of these six cases the denominator of Equation 5.40 may be evaluated by a piece-wise analytical solution and a complete solution is given below:

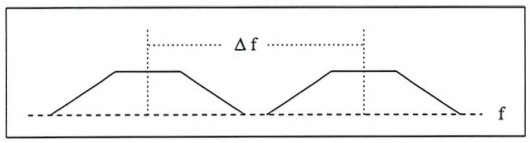

(a) if $\Delta f \geq 2b$

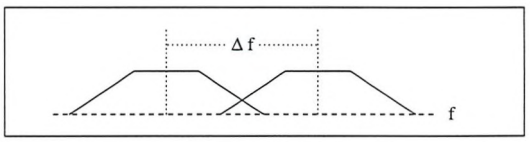

(b) if $(a+b) \leq \Delta f$ and $\Delta f < 2b$

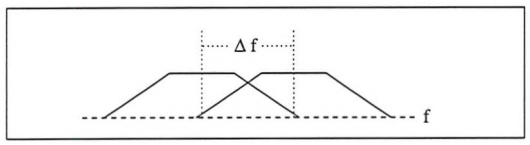

(c) if $(b-a) \leq \Delta f, \Delta f \leq (a+b)$ and $2a < \Delta f$

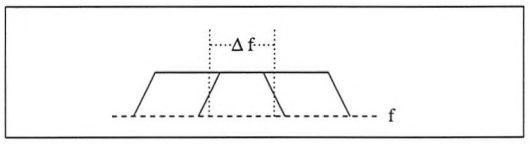

(d) if $(b-a) \leq \Delta f$ and $2a > \Delta f$

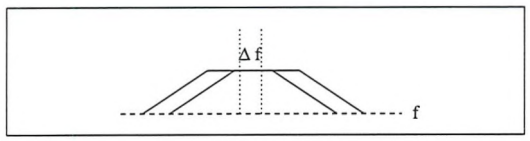

(e) if $0 \leq \Delta f, \Delta f < 2a$ and $\Delta f < (b-a)$

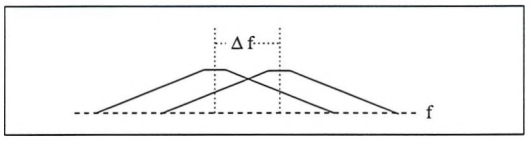

(f) if $2a \leq \Delta f$ and $\Delta f < (b-a)$

Figure 5.10: Representation of receiver Nyquist filter and adjacent interfer's transmitter for all the cases in Equation 5.44.

$$\int_{-\infty}^{+\infty} |H_r(f)|^2 \cdot |H_t(f+\Delta f)|^2 df = \begin{cases} 0 \ \} & \text{if } \Delta f \geq 2b \\ I_1(\Delta f - b, b) \ \} & \text{if } (a+b) \leq \Delta f \text{ and } \Delta f < 2b \\ \left.\begin{array}{l} I_2(\Delta f - b, a) \\ +I_1(a, \Delta f - a) \\ +I_3(\Delta f - a, b) \end{array}\right\} & \text{if } (b-a) \leq \Delta f, \ \Delta f \leq (a+b) \text{ and } 2a < \Delta f \\ \left.\begin{array}{l} I_2(\Delta f - b, \Delta f - a) \\ +I_4(\Delta f - a, a) \\ +I_3(a, b) \end{array}\right\} & \text{if } (b-a) \leq \Delta f \text{ and } 2a > \Delta f \\ \left.\begin{array}{l} I_5(\Delta f - b, -a) \\ +I_2(-a, \Delta f - a) \\ +I_4(\Delta f - a, a) \\ +I_3(a, \Delta f + a) \\ +I_6(\Delta f + a, b) \end{array}\right\} & \text{if } 0 \leq \Delta f, \ \Delta f < 2a \text{ and } \Delta f < (b-a) \\ \left.\begin{array}{l} I_5(\Delta f - b, -a) \\ +I_2(-a, a) \\ +I_1(a, \Delta f - a) \\ +I_3(\Delta f - a, \Delta f + a) \\ +I_6(\Delta f + a, b) \end{array}\right\} & \text{if } 2a \leq \Delta f \text{ and } \Delta f < (b-a) \end{cases} \tag{5.44}$$

where,

$$I_1(l_1,l_2) = \frac{-T}{16\pi}\left[-4\pi fT + 4\alpha\cos(\frac{\pi}{2\alpha}(2fT - 2\Delta fT + 1)) - 4\alpha\cos(\frac{\pi}{2\alpha}(2fT - 1)) \right.$$
$$\left. -\alpha\sin(\frac{\pi T(2f - \Delta f)}{\alpha}) + 2f\pi T\cos(\frac{\pi(-1 + \Delta fT)}{\alpha})\right]_{f=l_1}^{f=l_2}, \quad (5.45)$$

$$I_2(l_1,l_2) = \frac{T}{2\pi}\left[\pi fT - \alpha\cos(\frac{\pi}{2\alpha}(2fT - 2\Delta fT + 1))\right]_{f=l_1}^{f=l_2}, \quad (5.46)$$

$$I_3(l_1,l_2) = \frac{T}{2\pi}\left[\pi fT + \alpha\cos(\frac{\pi}{2\alpha}(2fT - 1))\right]_{f=l_1}^{f=l_2}, \quad (5.47)$$

$$I_4(l_1,l_2) = T^2(l_2 - l_1), \quad (5.48)$$

$$I_5(l_1,l_2) = \frac{T}{16\pi}\left[4\pi fT - 4\alpha\cos(\frac{\pi}{2\alpha}(2fT - 2\Delta fT + 1)) - 4\alpha\cos(\frac{\pi}{2\alpha}(2fT + 1)) \right.$$
$$\left. +2f\pi T\cos(\frac{\pi\Delta fT}{\alpha}) - \alpha\sin(\frac{\pi(2fT + 1 - \Delta fT)}{\alpha})\right]_{f=l_1}^{f=l_2}, \quad (5.49)$$

and

$$I_6(l_1,l_2) = \frac{T}{16\pi}\left[4\pi fT + 4\alpha\cos(\frac{\pi}{2\alpha}(2fT - 2\Delta fT - 1)) + 4\alpha\cos(\frac{\pi}{2\alpha}(2fT - 1)) \right.$$
$$\left. +2f\pi T\cos(\frac{\pi\Delta T}{\alpha}) - \alpha\sin(\frac{\pi(2fT - 1 - \Delta fT)}{\alpha})\right]_{f=l_1}^{f=l_2}. \quad (5.50)$$

Equations 5.44-5.50 may be used to investigate, how the ACI varies with carrier separation and excess bandwidth. If

$$\text{Normalised Carrier Separation} \triangleq \Delta f \cdot T \equiv \frac{\text{Carrier Separation}}{\text{Symbol Rate}}, \quad (5.51)$$

then a graph of how S/I_a varies with α and $\Delta f \cdot T$ may be drawn. Such a graph is shown in Figure 5.11(a) for $\alpha = 0 \ldots 0.9$ and $\Delta f \cdot T = 0.1 \ldots 0.9$. Note that here, the minimum achievable S/I_a is -3 dB; this is the case when both upper and lower interferers are at coincident frequency with the desired signal. When $\Delta f \cdot T \geq (1.0 + \alpha)$, S/I_a will be infinite. Figure 5.11(b) shows S/I_a for $\alpha = 0.35$. ATDMA has been proposed with $\Delta f \cdot T = 0.23$ and from Figure 5.11(b) it can be seen that the average S/I_a in a Gaussian channel is approximately 31 dB.

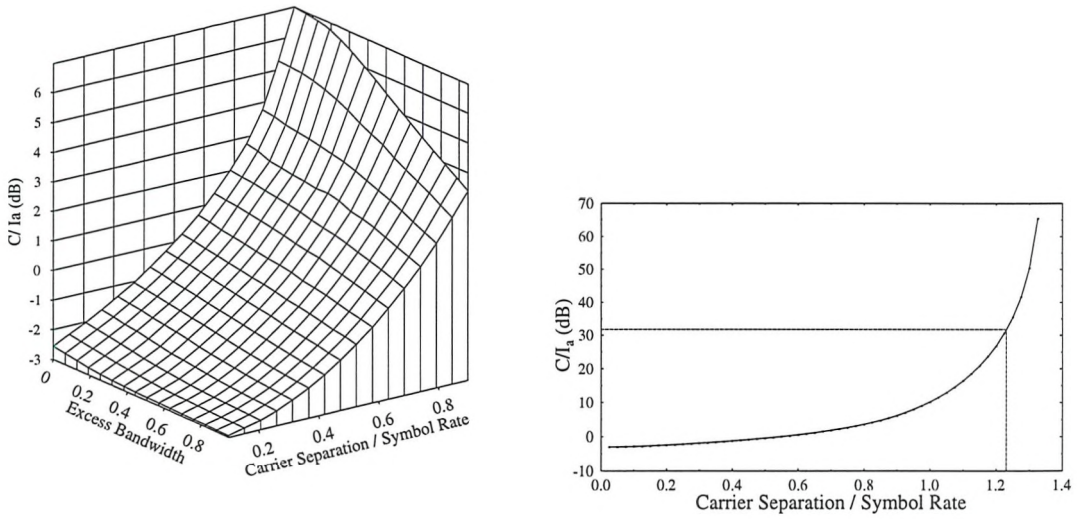

(a) Variation of ACI

(b) ATDMA Specific ACI identifying Carrier Separation / Symbol Rate of 1.23

Figure 5.11: Carrier to adjacent channel interference ratios, with one upper and one lower interferer, calculated using Equations 5.44-5.50, assuming perfect linear amplification, perfect filter transfer function and identical power for the signal and the upper and lower interferers

5.3.3 Comparison of ACI and CCI in Fixed Modulation Schemes

The effect of ACI, CCI and SNR, upon the BER, was investigated by simulation for BPSK, QPSK, Square 16 and 64 QAM over Gaussian and Rayleigh channels. The ACI was generated by a fixed QPSK transmission scheme where the frequency separation was $\Delta f \cdot T = 0.23$ and $\alpha = 0.35$ was used for the signal and the interferer. Only the upper adjacent channel interferer was simulated. PSAM was not used, as the simulation was over a Gaussian channel, employing $\Upsilon = 8$. The CCI was from a single QPSK transmission having random phase with respect to the carrier.

5.3.3.1 Gaussian Channel

Figure 5.12 shows the results for QPSK. All ACI results were evaluated with no CCI and the CCI results are also in the absence of ACI.

From Figure 5.12 it can be seen that when the S/I_a is less than 10 dB, there is a residual BER. However, CCI appears to result in no residual BER even when S/I_c is as low as 4 dB. The residual BERs for S/I_a at 4 and 10 dB are approximately 9×10^{-2} and 1×10^{-3}, respectively.

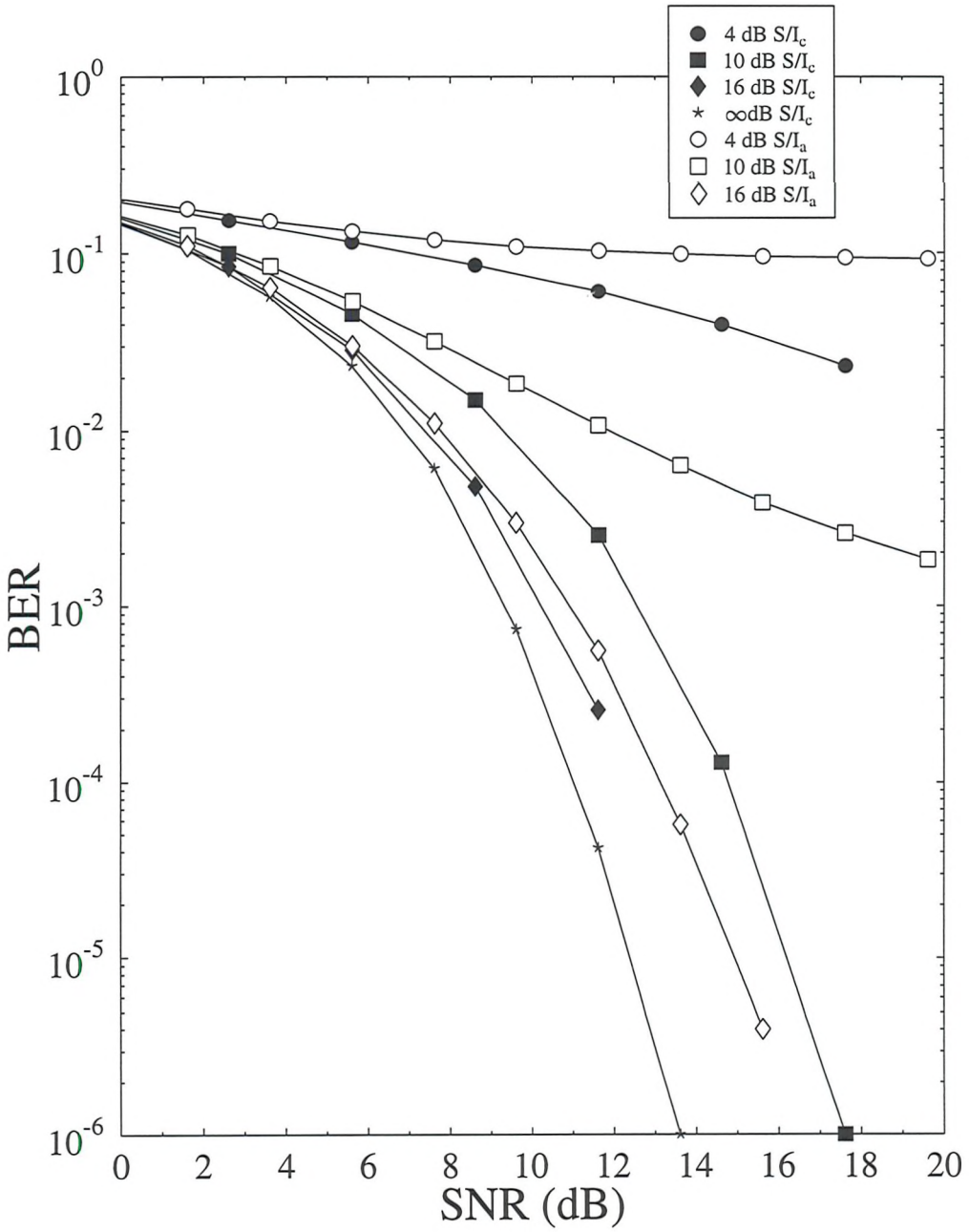

Figure 5.12: BER for QPSK with adjacent QPSK carrier, $\Delta f \cdot T = 0.23$, $\alpha = 0.35$, no PSAM and each simulated symbol represented by $\Upsilon = 8$ samples and a single non-coherent co-channel interferer

S/I_a	BPSK	QPSK	QAM 16	QAM 64
4	12 dB,2%	7 dB,9%	6 dB,30%	7 dB,30%
10	×	>20dB,≈0.1%	15 dB,9%	12 dB,20%
16	×	×	>30dB,≈ 0.2%	20 dB,7%
22	×	×	×	>30 dB,≈ 0.3%

Table 5.3: SNR and residual BER values for various modulation schemes in a Gaussian channel. Interference simulated using QPSK, $\Delta f \cdot T = 0.23$, $\alpha = 0.35$. The × reflects no residual registered.

A comparison can be made with the case of infinite S/I_a but SNR values of 4 and 10 dB; here the BERs are approximately 3×10^{-2} and 6×10^{-4} respectively. Therefore, over the values of SNR and S/I_a in the range of these experiments, it appears that for the same average power corrupting the signal after the receiver matched filter, a single interfering adjacent channel has a detrimental impact on the overall BER, which is by a factor of approximately 3 worse than in an AWGN channel.

From Figure 5.12 it can be seen that for all SNRs and SIRs ACI registers a higher BER than CCI. Experiments for BPSK and Square 16 and 64 QAM reflect the same results. ACI is more detrimental to BER than CCI and noise, since in the case of CCI the error energy is spread over all received frequencies. However, the adjacent channel interference has much greater peak energy and this is concentrated in one frequency region of the signal. This is analogous to a single co-channel interferer having a more detrimental effect than many co-channel interferers with the same total power. This could be attributed to the central limit theroem.

Table 5.3 shows the residual BERs and the SNRs at which they occur for various modulation schemes with various levels of ACI in an ATDMA system considering a Gaussian channel. This identifies the relative susceptibilities of the modulation schemes to adjacent channel interference.

5.3.3.2 Rayleigh Channel

As discussed in Chapter 2, Gaussian and Rayleigh channels represent the best and worse case in terms of the distribution of received energy for narrow-band radio channels. Therefore, in a system subject to interference, not only is the Rayleigh channel the worse case between transmitter and receiver, but also between receiver and interferer. There is no evidence to support any significant correlation between the Doppler frequency of the channel between the

transmitter and receiver, and the channel between the interferer and the receiver. The only exception to this is during the down-link, where the correlation bandwidth is wide enough, and hence two channels adjacent in frequency and in the equivalent time slots could have fading with the same Doppler frequencies. This would result in the generally favourable situation where, high interference levels are temporally correlated with high received signal levels. This situation is not representative and therefore no general correlation is expected between the interference and signal levels.

In order to evaluate the performance of BPSK, QPSK and Square 16 and 64 QAM in Rayleigh channels with single Rayleigh interferers a series of simulations was conducted. These were performed using the ATDMA frames as described in Reference [126]. In order to ensure that the interference levels were uncorrelated with the signal levels, channels exhibiting different Doppler frequencies were used for the signal and interferer. However, using a channel with the same Doppler frequency for the signal and the interference, gave comparable results to using different Doppler frequencies, if there was sufficient temporal decoupling between the fading of the signal and that of the interference. The experiments were conducted for SNR values between 0 and 50 dB, and a range of SIR values of 9, 19 and 29 dBs for BPSK, 9, 19, 29, 39 and 49 dBs for QPSK, 19, 29 and 39 dBs for Square 16 QAM and 29, 39 and 49 dBs for Square 64 QAM. Adjacent and co-channel interference were investigated in isolation and in every case the signal was transmitted through a 10 ms^{-1} vehicular speed Rayleigh channel and the interference was faded through a 1 ms^{-1} channel. An example of the results are shown in Figure 5.13.

Figure 5.13:a shows the performance of QPSK through a Rayleigh channel with Rayleigh fading ACI. The results for CCI were indistinguishable from these results and this is different from the comparison between ACI and CCI in the Gaussian channel, with Gaussian interference. The BER performance is independent of the type of interference in the Rayleigh case, because the fluctuation in signal and interference is so large that the fine structure of the interference becomes insignificant. It can be seen from Figure 5.13:a that for all S/I_a (and S/I_c) there is some observable residual BER. Figure 5.13:b shows the performance for all the schemes at 29 dB S/I_a, which also identifies the residual BER. Table 5.4 shows the residual BERs, and the SNRs at which they occur for various modulation schemes with various levels of ACI and CCI.

Table 5.4 may be compared with Table 5.3. In the case of the Gaussian channel, with Gaussian channel interference, the residual BER is lower and the SNR required to achieve it is also lower than in the Rayleigh case. These experiments have been based on either one co-channel interferer or one adjacent-channel interferer. In a real system there will be combinations of

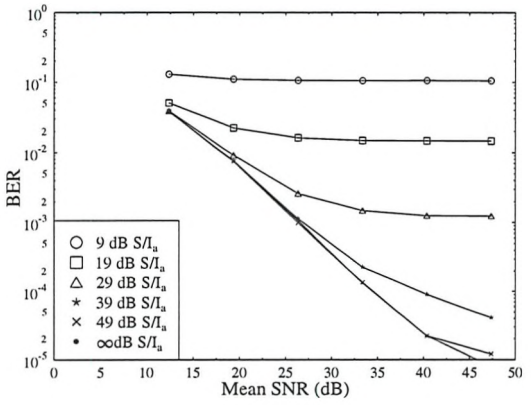

(a) QPSK at a range of SNRs and SIRs

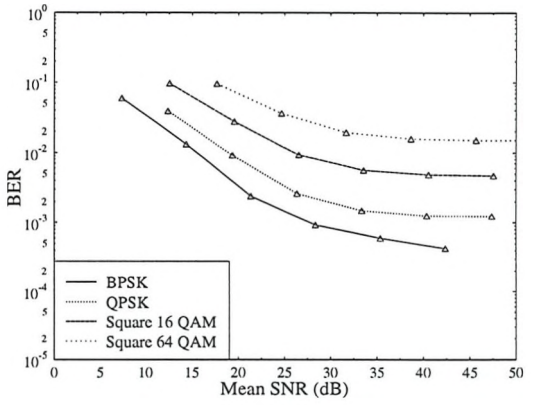

(b) BPSK, QPSK, 16 and 64 Square QAM at 29dB S/I_a

Figure 5.13: BER performance of various modulation schemes through a Rayleigh channel with Rayleigh ACI.

co- and/or adjacent-channel interferers. Multiple interferers will result in both the ACI and CCI becoming more noise like, and the central limit theorem would suggest that the resultant PDF of interference would become Gaussian. Therefore, for a given SIR with six interferers as proposed by Lee [133], defined by Equation 5.13, the corruption caused is likely to be less than introduced by a single interferer with the same SIR. Hence the experimental results documented here represent the worst case interference scenario.

S/I_a	BPSK	QPSK	QAM 16	QAM 64
9	27dB,7%	27dB,10%	-	-
19	37dB,0.8%	34dB,1.5%	34dB,4%	-
29	>50dB,≈0.02%	41dB,0.12%	42dB,0.45%	47dB,1.3%
39	-	>50dB,≈0.003%	>50dB,≈0.025%	>50dB,≈0.15%
49	-	×	×	×

Table 5.4: SNR and BER values of residual BER for various modulation schemes in a Rayleigh channel. Interference simulated using QPSK, $\Delta f \cdot T = 0.23$, $\alpha = 0.35$. The × reflects that 50dB was an insufficient SNR to identify a residual BER, and the - reflects that no experiment was conducted.

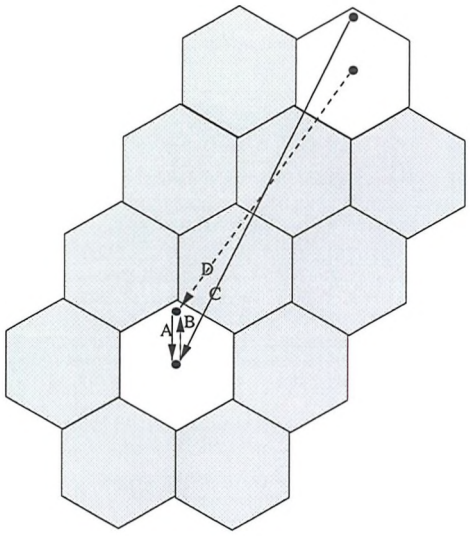

Figure 5.14: The path A is equivalent to B, however, the interference D combined with the signal B and the interference A combined with the signal C reduce this equivalence.

5.4 Multi-user Interference - Adaptive Modulation Schemes

The effect of CCI upon an adaptive modulation scheme is potentially more detrimental than for a fixed modulation scheme. The reason for this is that the interference at the base-station and mobile-station is uncorrelated. Therefore, interference does not only corrupt the received symbols, as discussed above, but also adversely affects the TDD-based estimation of the channel. These problems are initially considered separately.

5.4.1 Impact of interference upon channel estimate

The lack of correlation between up- and down-link interference is illustrated in Figure 5.14. Here, it can be seen that although the path A (mobile-station to base-station) will approximate path B (base-station to mobile-station), the interference from the paths C (interfering mobile-station to base-station) and D (interfering base-station to mobile station) could be very different. This is because the average signal strength received from the interfering base-station and interfering mobile-station may vary considerably. Furthermore, even if transmission along each path resulted in the same received average signal strength, both paths will be fading independently.

It is assumed that the characteristics of the interference upon the up-link signal are the same as those on the down-link. This permits the analysis of only the down-link BER without loss of generality. Therefore, the effects of Frequency Hopping (FH), Voice Activity Detection

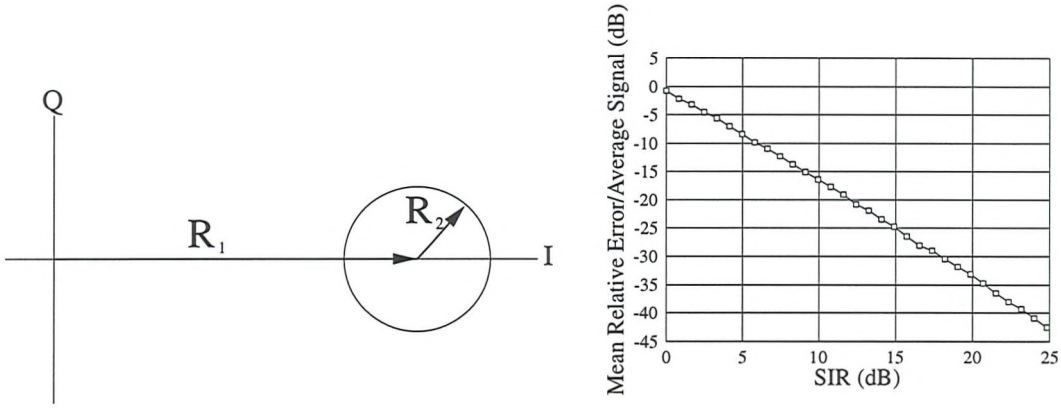

(a) R_1 represents the desired signal vector, R_2 represents the interfering vector, therefore, $|R_1|$ is the true channel amplitude estimate and $|R_1 + R_2| - |R_1|$ is the error introduced by the interference.

(b) Mean relative error in estimation of Rayleigh fading channel introduced by Rayleigh fading interferer in the range of 0 dB to 25 dB SIR, evaluated by simulation of 100000 independent points.

Figure 5.15: Model and results of impact of interference upon channel estimate.

(VAD), directional antennae and power control upon the impact of interference corrupted channel estimates are left for further study.

Figure 5.15(a) shows how the interference effects upon the estimation of the channel may be modelled. The vector R_1 represents the received signal vector, which in the absence of noise would result in $|R_1|$ being a perfect estimation of the channel's amplitude gain. However, the signal is corrupted by interference and the channel amplitude gain is estimated as $|R_1 + R_2|$ and, therefore, the error in the channel estimation is given by $|R_1 + R_2| - |R_1|$. The error is most critical, when $|R_1|$ is small, hence the relative error is defined as $(|R_1 + R_2| - |R_1|)/|R_1|$. Mathematical analysis of the relative error is complex, given that $|R_1|$ and $|R_2|$ are Rayleigh distributed and $|R_2|$ has random uniform phase. A simplification can be achieved by assuming that $|R_1| >> |R_2|$, where upon the error becomes Gaussian distributed, however, analysis is unnecessary, as it will be shown later. Furthermore, simulation of the relative error versus SIR performance is trivial, which is shown in Figure 5.15(b).

Figure 5.15(b) shows that although large relative errors in the channel gain estimation will result from 0 dB SIR Rayleigh fading interference, increased SIR results in considerable improvements in the relative error. This is prima facie evidence that the down-link[1] BER

[1]Equally, this is true for the down-link BER, if interference at the mobile-station were considered instead of the base-station.

will be relatively unaffected by interference at the base-station, given that the interference is below a certain threshold value. Considering this hypothesis, experiments were conducted, which considered the down-link BER over a Rayleigh fading channel with ∞dB SIR at the mobile-station. The channel was assumed to fade slowly and the estimates of the channel gain made at the base-station were performed in the presence of an independent Rayleigh fading interferer. The experiments were conducted with SIRs of 0, 10, 20, 30, and ∞dB for both the speech optimised switching levels and the computer data optimised switching levels.

The results are shown in Figures 5.16 and 5.17 and from these it can be seen that as the up-link SIR increases, the BER reduces at all SNRs. It can be seen that the computer data system is most sensitive to up-link interference with several orders of magnitude BER performance degradation, for all SNRs of interest, at 0 dB SIR and at least one order of magnitude BER performance degradation, for all SNRs of interest, at 10dB SIR. The maximum BER performance degradation with the speech system is one order of magnitude at 0 dB SIR and at lower SNRs the degradation is less than a factor of two.

The consequence of up-link interference on the BPS performance is less dramatic than on the BER performance. However, for both systems at low SIR and SNR, the average throughput is mistakenly increased due to the interference boosted received signal levels and, therefore, less robust modulation schemes are employed more often than expected with the given (optimised) switching levels, if the up-link SIR was infinite. This is an explanation for the increased BER, when both the SIR and SNR are low for the speech and computer data schemes.

At low SIRs and high SNRs, the average BPS performance is reduced and, therefore, more robust modulation schemes are employed more often in comparison to when the up-link SIR is infinite. At first sight, this reduction in BPS performance is not consistent with the reduced BER performance observed under such conditions. However, although the average throughput is reduced, and on average more robust modulation schemes are employed, the interference results in the base-station failing to identify the depth of some fades and hence employing a higher-order modulation-scheme with insufficient protection. This generates small bursts of errors that increase the average BER. These bursts have less significance, when the average BER is relatively high. Therefore, at the SNRs shown in the Figures, the effect of up-link SIR in the computer data system is more noticeable than in the speech system.

The discussions above can be summarised by stating that the adaptive modulation's down-link performance is degraded, even in the absence of interference at the mobile, by interference at the base-station, because the up-link interference results in the channel estimation being corrupted and a sub-optimum modulation scheme being employed.

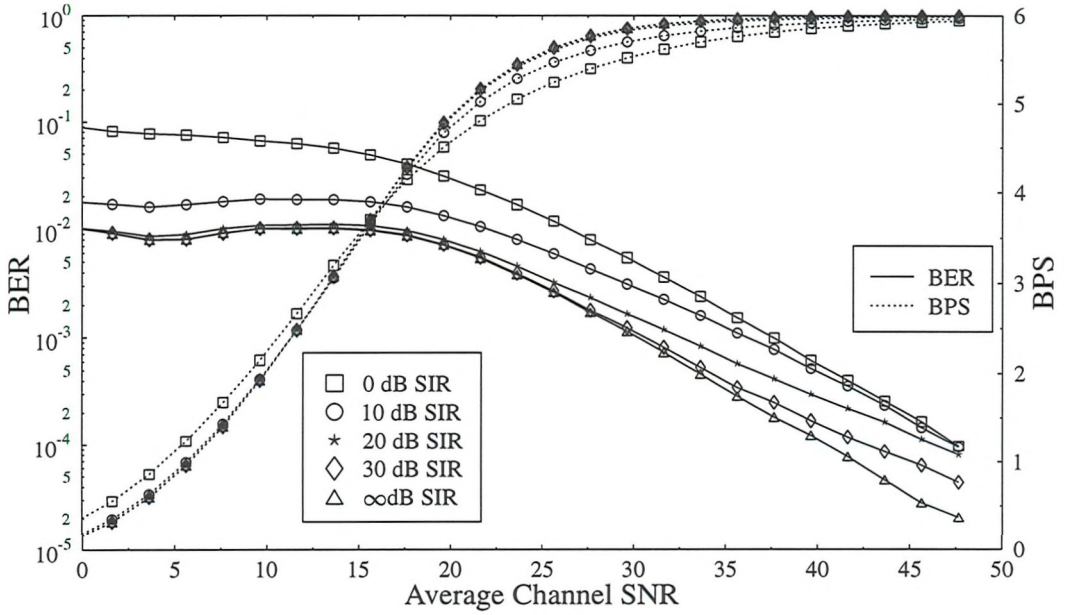

Figure 5.16: Down-link BER over a slow Rayleigh fading channel with ∞dB SIR at the MS and independent Rayleigh fading interference at the BS with SIRs of 0, 10, 20, 30, and ∞dB with adaptive speech system mean BER switching levels. The interference at the BS affects only the channel-quality estimates.

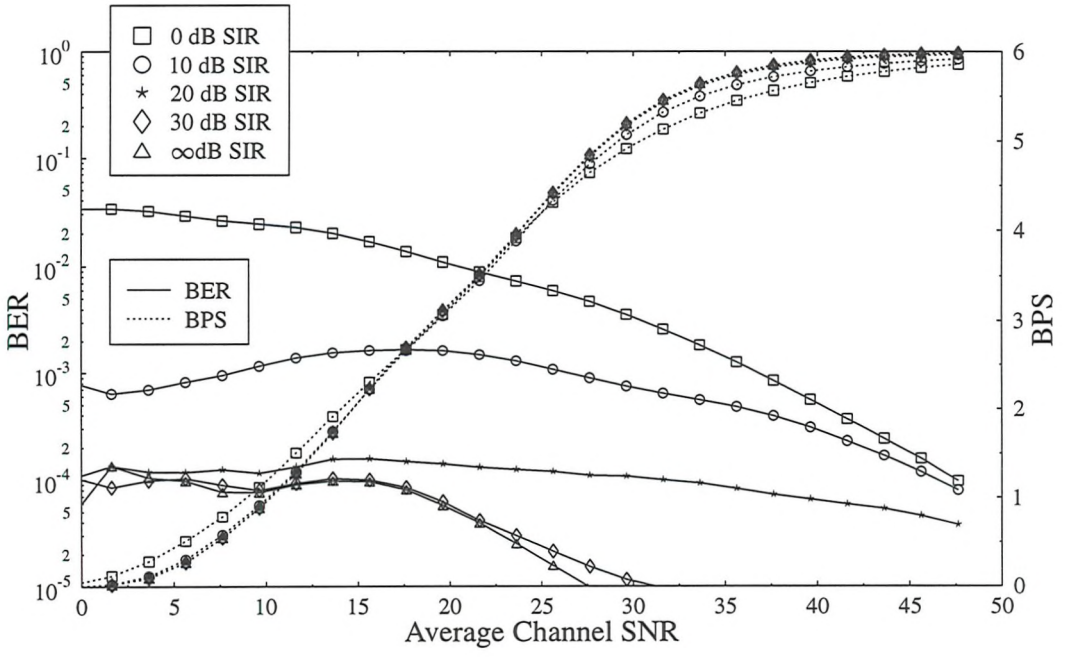

Figure 5.17: Down-link BER over a slow Rayleigh fading channel with ∞dB SIR at the MS and independent Rayleigh fading interference at the BS with SIRs of 0, 10, 20, 30, and ∞dB with adaptive computer-data system mean BER switching levels. The interference at the BS affects only the channel-quality estimates.

	0 dB SIR	10 dB SIR	20 dB SIR	30 dB SIR
-0.36 dB SNR	0.324	0.153	0.131	0.129
1.64 dB SNR	0.561	0.354	0.323	0.320
3.64 dB SNR	0.866	0.640	0.606	0.603
5.64 dB SNR	1.243	1.000	0.967	0.963
7.64 dB SNR	1.676	1.439	1.412	1.408

Table 5.5: BPS performance versus SNR and SIR extracted from Figure 5.16.

	0 dB SIR	10 dB SIR	20 dB SIR	30 dB SIR
-0.36 dB SNR	0.033	0.003	0.002	0.002
1.64 dB SNR	0.120	0.028	0.021	0.020
3.64 dB SNR	0.284	0.116	0.097	0.095
5.64 dB SNR	0.512	0.304	0.272	0.270
7.64 dB SNR	0.787	0.583	0.550	0.546

Table 5.6: BPS performance versus SNR and SIR extracted from Figure 5.17.

There are two modes of this mis-estimation of the channel amplitude gain discussed here. Considering the model of the interference presented in Figure 5.15(a) the two modes correspond to the case when the condition $|R_1| >> |R_2|$, is met and when it is not. In the former case, the Rayleigh faded up-link interference results in an approximately equal probability of over- and under-estimation of the channel amplitude gain. This is because the component of $|R_2|$ perpendicular to $|R_1|$ becomes negligible. Figures 5.16 and 5.17 reveal that the 0dB SIR BPS curve behaves differently from the 10, 20, 30 and infinity dB SIR curves by not converging with the others at low SNRs. Therefore, it is concluded that the condition $|R_1| >> |R_2|$ is not true for 0dB SIR, but it is true for 10dB SIR.

Considering SIRs of 10 dB or higher and the PDFs of the individual modulation schemes employed for the speech and computer data systems, which were plotted in Figures 4.13(a) and 4.13(c) respectively, it can be seen at low SNRs that mis-estimation of the channel amplitude gain results in an increase in the average BPS and at high average SNRs the reverse is true. This is consistent with the evidence in Figures 5.16 and 5.17 for high average channel SNRs. For low average channel SNRs the Figures do not show the effect well, however, a tabulation of the average BPS results is shown for the lower SNR values in Tables 5.5 and 5.6, which show the expected increase in average BPS at low SNR, as the SIR reduces.

The effect of 0 dB SIR on the channel amplitude gain is more complex than at higher SIRs. Moreover, it is relatively unimportant, because the following work will not propose adaptive

modulation at such low SIRs.

The effects of up-link interference on the performance of adaptive modulation has been discussed to some length. However, in terms of the design of two adaptive modulation schemes with BERs of 1×10^{-2} and 1×10^{-4} it may be concluded that the average up-link SIR must be 10 and 20 dB, or above, for the respective systems. Furthermore, it transpires from the previous discussion that the adaptive switching levels optimised for non-interfered channels have to be reconsidered in order to account for the effects of interference.

5.4.2 Re-optimisation

As in the previous section, only the performance of the down-link is considered. However, it is assumed that the performance of the up-link would be identical, provided that the assumptions made about down-link interference applied to the up-link and vice versa. The effect of only down-link interference, that is interference only at the mobile, is shown in Figures 5.18 and 5.19 for the speech and computer data systems, respectively. In these experiments the effect of the interference upon the channel estimate is neglected. The results were obtained by employing the relationships, for the interference and noise corruption, from Section 5.3.1.2 into Equation 4.5. The results were verified by simulation, however, only the numerical results are shown for clarity. For both the speech and computer data systems the through-put is unaffected by the interference inflicted at the MS, since the channel-quality estimates are unaffected. This is as expected because the decision upon which modulation scheme should be employed is made at the base-station, which is unaffected by the interference experienced by the mobile-station.

However, the BER is increased considerably for both the speech and computer data systems as the SIR reduces since the MS's effective channel quality is reduced. In all cases except the speech system at 30 and 40 dB SIR, the introduction of co-channel interference results in the BER increasing, as the average channel SNR increases. The explanation for this is that at higher average channel SNRs the probability of an higher order modulation scheme being employed increases, as was the case in the absence of interference. However, these schemes are more susceptible to interference as well as to noise, as seen in Sections 5.3.3.1 and 5.3.1.2. Therefore, bearing in mind that the switching levels were optimised in the absence of interference, the BER should increase.

A logical approach to overcoming the interference would be to back-off the switching levels at which the higher order modulation scheme should be employed. Such a technique would require an outer loop to identify the level of average interference and select a different set of

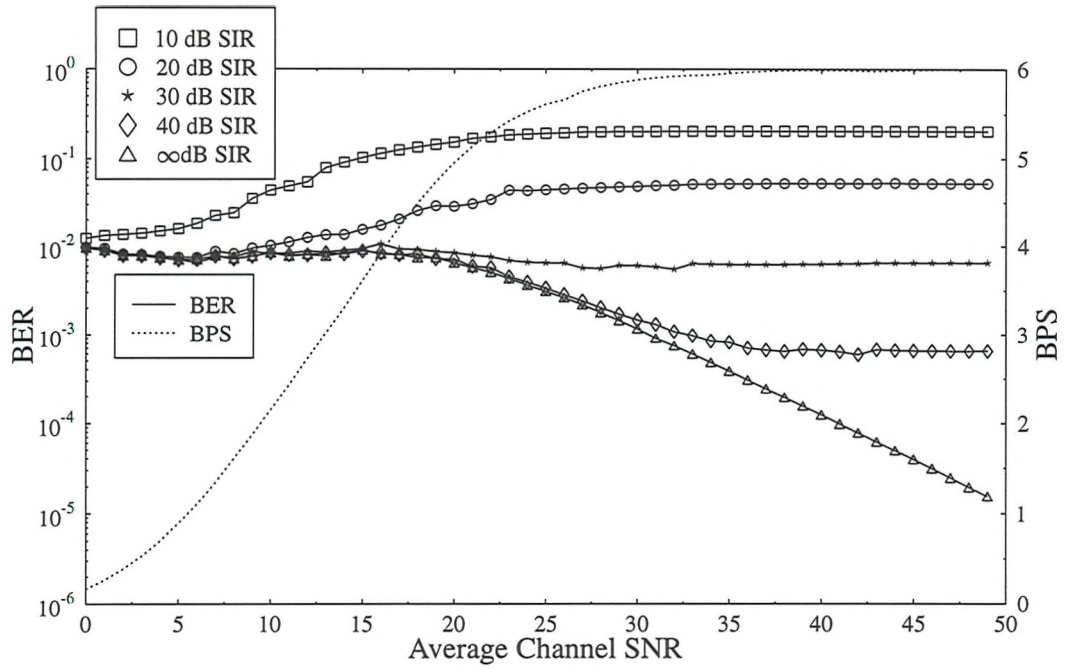

Figure 5.18: Down-link BER over a slow Rayleigh fading channel with 10, 20, 30, 40 and ∞dB SIR at the MS and no interference at the BS with the adaptive speech system mean BER switching levels, $\alpha = 0.35$ and no interference cancellation.

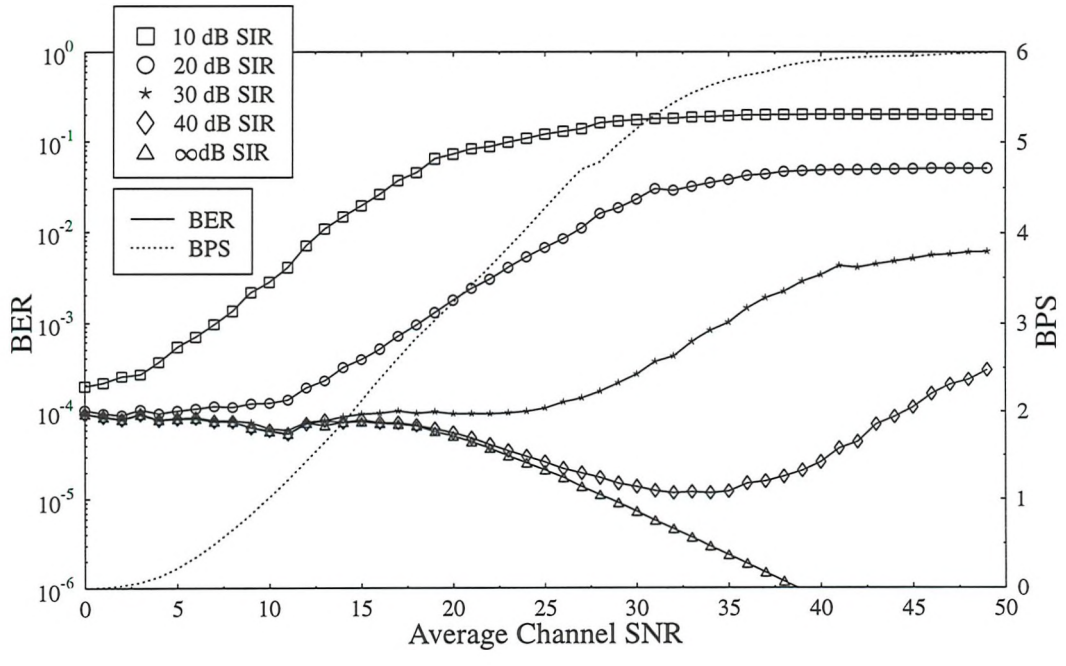

Figure 5.19: Down-link BER over a slow Rayleigh fading channel with 10, 20, 30, 40 and ∞dB SIR at the MS and no interference at the BS with adaptive computer data system mean BER switching levels, $\alpha = 0.35$ and no interference cancellation.

switching levels accordingly. This could be achieved by considering the average received signal strength and comparing it with some information about the quality of the reception. This quality measure could be obtained from either FEC overload rate or soft-decision information about the distance between received symbols and the ideal modulation constellation points. It is proposed that different switching levels would be engaged when the average interference varied by 10 dB. It is accepted that this is assumes the SIR varies slowly when compared with the instantaneous SNR.

To obtain the switching levels in the presence of interference the optimisation algorithm described in Section 4.3.6 was employed again. This time the Q' functions were used for the combined signal and interference PDFs. Also, the cost function was slightly modified with Equation 4.9 becoming,

$$\text{BPS Cost}(i) = \begin{cases} 5 \cdot (\text{BPS}_d(i) - \text{BPS}_m(i)) & \text{if BPS}_d(i) > \text{BPS}_m(i) \\ 0 & \text{otherwise.} \end{cases} \tag{5.52}$$

This increased the weighting towards achieving the desired BPS performance at the cost of the desired BER performance. It was necessary, because in the presence of interference the optimisation total cost, given by Equation 4.7 was minimised, when the no-transmit mode was employed for all signal levels.

Re-optimised switching levels were derived for both the speech and computer data systems, where the desired performances were the same as those in Section 4.3.6, that is, a speech system with BER and BPS of 1×10^{-2} and 4.5, respectively, and a computer data system with BER and BPS of 1×10^{-4} and 3, also respectively. For the speech system the switching levels were re-optimised for 10, 20, 30 and 40 dBs SIR and for the computer data system they were optimised for 20, 30 and 40 dBs SIR. No levels were derived for the computer data system at 10 dB down-link SIR, because channel estimation for the reverse link channel estimation has already been shown unacceptable, in Figure 5.17, at this level of interference, when the desired BER is 1×10^{-4}. The initial switching levels that were used to start the re-optimisation algorithm were switching levels derived in the original optimisation, at ∞ dB SIR; the levels that are shown in Table 4.1.

The re-optimised switching levels for the speech and computer data systems are shown in Tables 5.7 and 5.8, respectively. The BER and BPS performance of both schemes with the re-optimised switching levels are shown in Figures 5.20 and 5.21, where the original optimised schemes performance at ∞ dB are also included for comparison.

The re-optimised switching levels for the speech system are generally similar to the switching

Scheme	l_1	l_2	l_3	l_4
10 dB SIR	4.06	9.37	14.05	18.38
20 dB SIR	3.02	7.07	11.59	44.38
30 dB SIR	2.98	6.48	11.60	17.64
40 dB SIR	2.33	6.55	11.33	17.36

Table 5.7: Re-optimised switching levels for speech system through a Rayleigh channel with independent Rayleigh interference at different average SIRs; switching levels shown in dB SNR.

levels that were obtained with the original optimisation at ∞ dB SIR. The exceptions are the switching levels obtained with the re-optimisation at 10 dB SIR, where all levels are generally 1-3 dB SNR higher than the original corresponding optimal levels, and l_4 for the re-optimisation at 20 dB SIR, which is approximately 27 dB higher that the original optimal level. This value of l_4 appears inconsistent compared with the l_4 values at other SIRs. However, at 10 dB SIR $l_4 > 18.38$ would have had produced a greater increase in total cost, in terms of the cost increase associated with reducing the throughput, compared with cost reduction registered from reducing the BER. This is because the Square 64 and 16 QAM BER performance is very similar at 10 dB SIR and consequently reducing l_4 will result in Square 16 QAM being employed rather than Square 64 QAM. Therefore it can be observed, compared with the 20 dB SIR case, the 10 dB SIR case benefits less from the reduction of the BER cost associated with reducing l_4 but is penalised equally in terms of the increases in BPS cost associated with the same reduction of l_4. At 30 dB SIR there is no need to reduce l_4 because the target BER is achieved.

The effect of the significant changes in switching levels, and the more subtle changes can be identified in the performance curves. Inspection of the BPS performance curves shown in Figure 5.20 reveals that the throughput for the re-optimised speech schemes at 20, 30 and 40 dB SIR closely coincided with the originally optimised scheme between 0 and 12.5 dB average channel SNR. Above 12.5 dB average channel SNR the 20 dB SIR re-optimised throughput is lower than observed with the other schemes. This is the effect of the large value of l_4 in the 20 dB re-optimised scheme. Further, the throughput of the 10 dB SIR re-optimised scheme is below the originally optimised scheme's throughput and again this is an expected consequence of the increased value of the switching levels for the re-optimised scheme at 10 dB SIR.

Considering the BER performance curves in Figure 5.20 it may be observed that only the 30, 40 and ∞ dB SIR re-optimised switching levels result in the target BER being achieved

Scheme	l_1	l_2	l_3	l_4
20 dB SIR	30.13	40.37	42.92	72.99
30 dB SIR	7.93	11.22	32.14	102.81
40 dB SIR	7.88	10.42	17.44	53.41

Table 5.8: Re-optimised switching levels for computer data system through a Rayleigh channel with independent Rayleigh interference at different average SIRs; switching levels shown in dB SNR.

for all average channel SNRs, at the respective interference levels. The 10 and 20 dB SIR re-optimised switching levels do not result in the target BER being achieved for all average channel SNRs. However, the same observation may be made about the originally optimised switching levels and their BER performance which is shown in Figure 5.18. It is not surprising that the 30 and 40 dB SIR re-optimised switching levels result in similar BER performance to the original optimised switching levels with 30 and 40 dB SIR, because the switching levels are so similar. Further, the re-optimisation at these interference levels was unlikely to result in the switching levels being altered significantly, since the original switching levels already met the BER performance criteria. Re-optimising the switching levels for 10 and 20 dB SIR resulted in significant changes in the switching levels, when compared with the original optimised levels. This change in switching levels reflects in the change in BER performance that can be observed by comparing Figures 5.18 and 5.20. This comparison reveals that the re-optimisation improved the BER performance at 10 dB SIR below an average channel SNR of 15 dB and at 20 dB SIR from 10 - 50 dB average channel SNRs. In the latter case the effect was approximately a reduction in BER of 5 times.

The re-optimised switching levels for the computer data system at 20, 30 and 40 dB SIR differ considerably more from the original ∞ dB SIR levels, than the speech switching levels at 20, 30 and 40 dB SIR do from their original ∞ dB SIR optimised switching levels. This is because the originally optimised switching levels for the computer data system, when the SIR was 40 dB or less, resulted in a lower BER performance than that desired. Therefore, re-optimisation resulted in the switching levels being modified. Employing the original computer data system switching levels, that were optimised for ∞ dB SIR, in interfered channels revealed that SIRs greater than 40 dB would be required to achieve the desired BER for average channel SNRs from 0 to 50 dB. The re-optimised switching levels result in the desired BER being achieved for 20[2] and 40 dB SIR. Moreover, re-optimisation at a specific SIR results in the performance

[2]The 20 dB SIR re-optimised switching levels result in an extremely low BER with maximum value of 5.78×10^{-10} at 50 dB average channel SNR and the corresponding curve is therefore not plotted in Figure 5.21

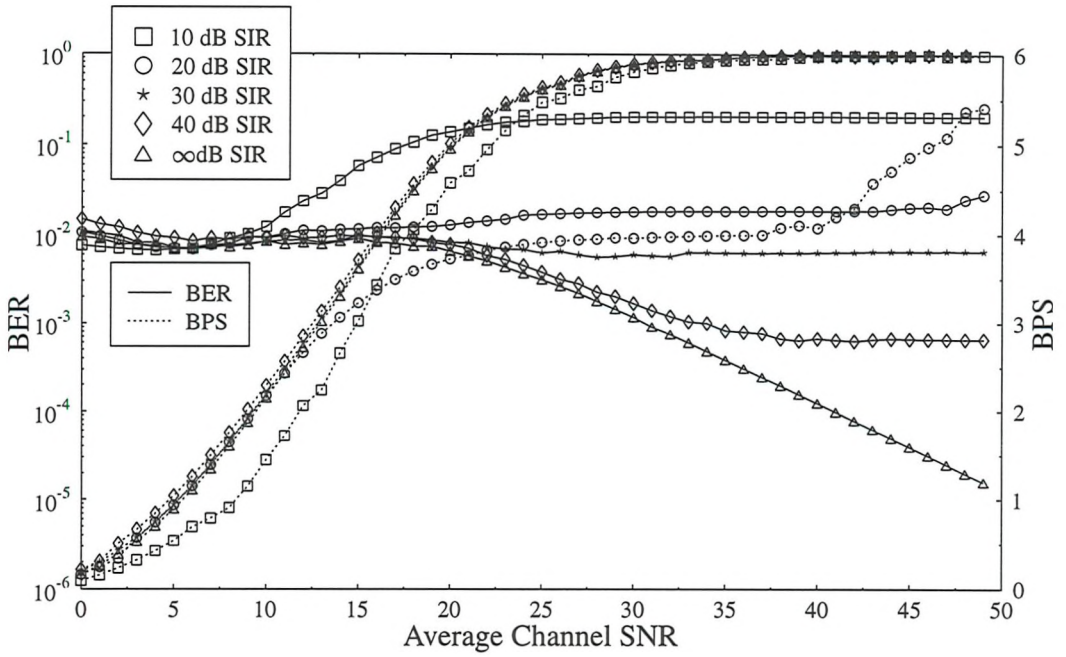

Figure 5.20: Down-link BER over a slow Rayleigh fading channel with 10, 20, 30, 40 and ∞dB SIR at the MS and no interference at the BS and adaptive modulation with switching levels re-optimised for each SIR. The desired performance was BER 1×10^{-2} and 4.5 BPS, $\alpha = 0.35$ and no interference cancellation.

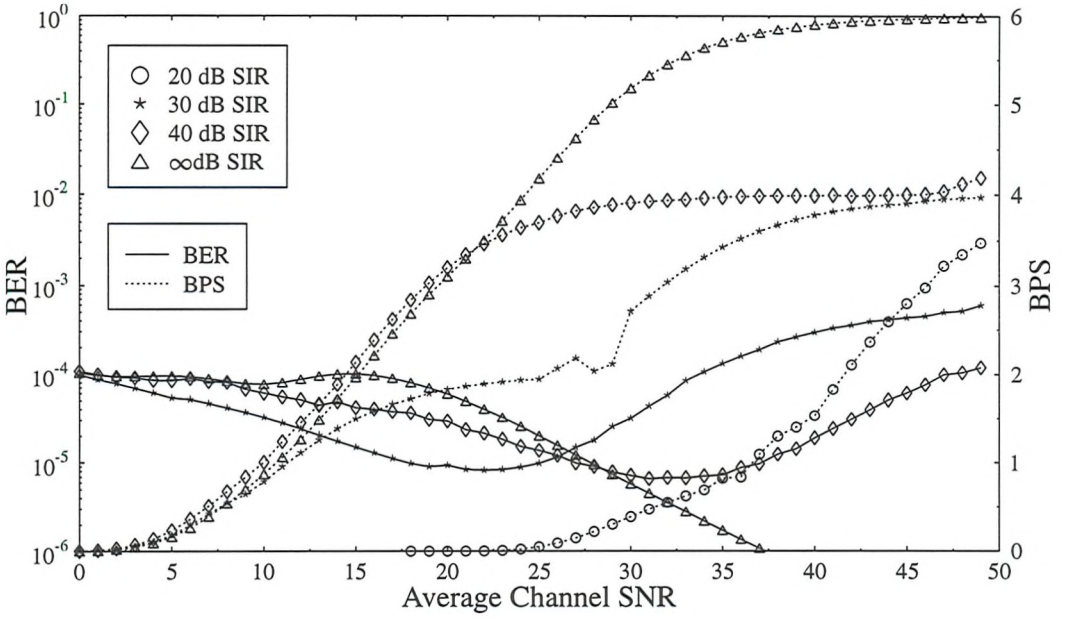

Figure 5.21: Down-link BER over a slow Rayleigh fading channel with 20, 30, 40 and ∞dB SIR at the MS and no interference at the BS and adaptive modulation with switching levels re-optimised for each SIR. The desired performance was BER 1×10^{-4} and 3 BPS, $\alpha = 0.35$ and no interference cancellation.

Scheme	$l_1(dB)$	l_2 (dB)	l_3 (dB)	l_4 (dB)
Manual 1	4.06	9.37	14.05	18.38
Manual 2	4.06	9.37	14.05	45.00
Manual 3	4.06	9.37	25.00	45.00
Manual 4	4.06	1000	1000	1000

Table 5.9: Manually selected switching levels expressed in SNR dB for performance curves in Figure 5.22.

of the re-optimised switching levels at 30 dB SIR approaching the desired BER performance.

The penalty of employing re-optimised switching levels is, as expected, a reduction in throughput. In the case of the BPS performance of the switching levels re-optimised for 20 dB SIR there is no throughput for average channel SNRs below 17 dB and, therefore, the BER performance below this level is uninteresting and the corresponding BER curve was omitted. The average throughput performance of the re-optimised switching levels at 20 dB SIR is approximately equivalent to BPSK at 40 dB average channel SNR. The BER at this average SNR is less than 1×10^{-6}, which compares favourably with the fixed BPSK BER performance at the same average channel SNR of 2.3×10^{-3}. The BPSK performance was determined from Figure 5.5(a).

5.4.2.1 Intuitive Threshold Adjustment

The re-optimised switching levels for the speech system in the presence of CCI are considered again. Since the target BER performance was not achieved for the 10 and 20 dB down-link SIR, there is some doubt over the suitability of the optimisation algorithm or the definition of the cost function. Therefore, in an attempt to achieve the desired BER performance the re-optimised switching levels at 10 dB SIR were manually adjusted. Figure 5.22 is a plot of the performance of the manually adjusted switching levels and Table 5.9 shows a summary of the manually selected levels.

The set of switching levels 'Manual 1' are the values from the re-optimisation that were given in Table 5.7 at 10 dB SIR and are included for comparison. The set of 'Manual 2' values reduces the employment of Square 64 QAM. This also reduces the average throughput for average channel SNRs higher than approximately 12 dB. Square 64 QAM is the most corruption sensitive modulation scheme and reducing its employment reduced the average BER. However, the performance at 10 dB SIR is still worse than the target BER, of 1%, across the range of average channel SNRs. The 'Manual 3' set of switching levels reduces the

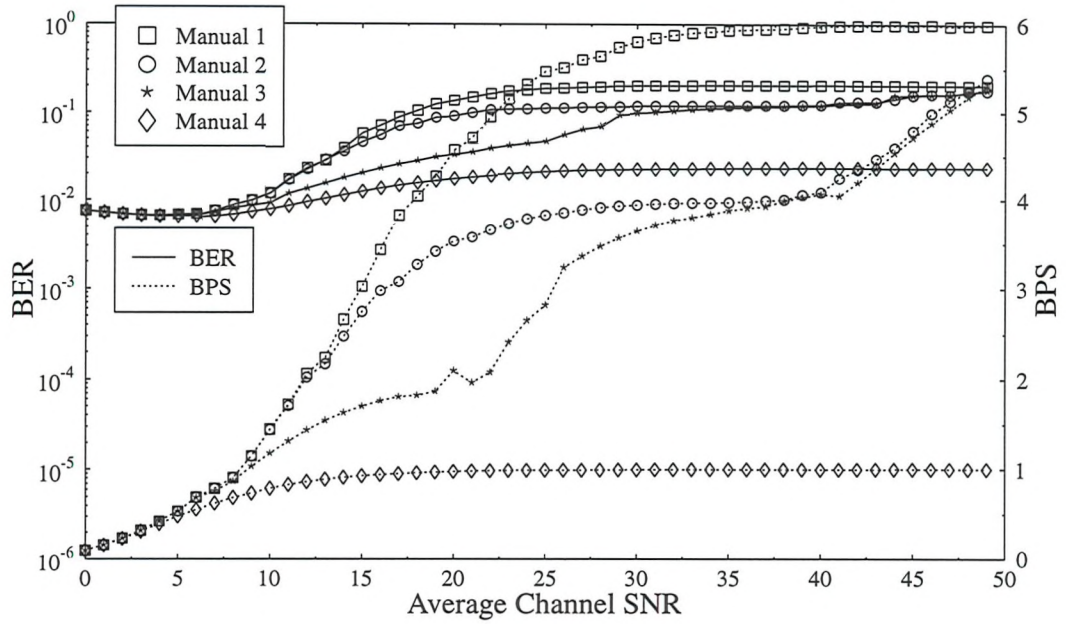

Figure 5.22: Down-link BER over a slow Rayleigh fading channel with ∞dB SIR at the base-station and 10dB SIR independent Rayleigh fading interference at the mobile-station using manually selected switching levels shown in Table 5.9 and $\alpha = 0.35$.

throughput further by reducing the employment of Square 16 QAM. This again reduces the throughput, but does improve the BER mainly in the range of average channel SNRs from 10 to 30 dB. However, the target BER performance is not achieved, especially at higher average channel SNRs.

In an extreme attempt to achieve the target BER at high average channel SNRs the switching levels 'Manual 4' were evaluated. These essentially eliminated the employment of QPSK, and Square 16 and 64 QAM. The resulting performance at high average channel SNRs is unsurprising. The average BPS performance converges with fixed BPSK performance, that is one BPS, and the BER performance converges with the fixed BPSK residual BER performance at 10 dB SIR, which was shown in Figure 5.8(a) to be 2.5×10^{-2}. Therefore, in order to reduce the BER below the BPSK residual, l_1 must be increased. This is undesirable, because at low average channel SNR the target BER is obtained with l_1 at its current value. Therefore, increasing l_1 will result in excessively low BER and a state of permanent non-transmission at low average channel SNRs. This is similar to what was experienced, when l_1 became large in the 20 dB SIR re-optimisation for the computer data target system.

It can be concluded that re-optimisation, as described above, may be employed to reduce the

margin between the desired BER and that achieved in the presence of interference. However, as a mechanism to overcome the effects of interference and achieve an arbitrary BER further techniques will be considered in the next Section.

5.5 Interference Cancellation

5.5.1 Introduction

Equalisation is a well established technique in cellular systems for reducing the effects of ISI. GSM [30], for example, incorporates a training sequence into a data burst. This provides information about the impulse response of the channel and, therefore, at to the inter-symbol interference. This knowledge can be exploited to remove the inter-symbol interference from the received sequence. The reduction of CCI may be incorporated into this equalisation process, for example as proposed by Reference [143]. Wales [144] recognised that if the interference came from a single interferer [145], then the joint equalisation and co-channel interference cancellation could be improved by acquiring information about the phase and amplitude of the co-channel interference propagation channel. He proposed obtaining information about the co-channel interference propagation channel by exploiting the orthogonality of the different training sequences. Murata et al [146] considered exploiting the additional redundancy in both the signal and co-channel interferer, introduced by trellis coding, in order to improve performance in an interference cancellation algorithm. However, they achieved this without an exponential growth in complexity that would typically be expected in such a system. Berangi et al [147] show a up to a factor of 30 improvement in BER for narrow-band constant amplitude modulation schemes through Rayleigh fading channels.

Adaptive modulation, as discussed in Chapter 4, is useful in combating the variation in received signal strength, and the consequential variation in SNR, which are encountered in mobile radio channel. However, Section 5.4.2.1 revealed that adaptive modulation is vulnerable to CCI. Therefore, it is proposed to invoke some of the interference cancellation techniques that have recently been suggested, in combination with adaptive modulation, and therefore propose an overall adaptive transmission scheme that is resistant to noise and interference.

5.5.2 Principle of Operation

The implementation of interference cancellation is explained for a BPSK signal experiencing CCI from a single BPSK interferer. The principle is easily extended for other scenarios.

Consider the transmission of binary bits, at a rate of T^{-1}, where $b_s(nT)$ is the n^{th} bit. This may be modulated as a stream of BPSK symbols. It will be assumed, as in Section 5.3.1, that the interference is phase non-coherent and time synchronous with the signal. Therefore, the transmitted symbols may be represented in the baseband by their value at the perfect sample position, namely by:

$$X_s(nT) = \begin{cases} +1 + j0 & \text{if } b_s(nT) = 0 \\ -1 + j0 & \text{if } b_s(nT) = 1, \end{cases} \tag{5.53}$$

assuming that the clock recovery will be perfect at the receiver. A single BPSK interferer's transmission may be represented by:

$$X_i(nT) = \begin{cases} +1 + j0 & \text{if } b_i(nT) = 0 \\ -1 + j0 & \text{if } b_i(nT) = 1. \end{cases} \tag{5.54}$$

The channel distortion introduced to $X_s(nT)$ and $X_i(nT)$ are respectively given by the complex variables $R_s(nT)$ and $R_i(nT)$. Therefore, the received signal is given by

$$Y(nT) = R_s(nT) \cdot X_s(nT) + R_i(nT) \cdot X_i(nT) + N(t), \tag{5.55}$$

where $N(t)$ is the complex Gaussian noise.

Restricting the investigation to narrow-band channels, and initially assuming perfect knowledge of $R_s(nT)$ and $R_i(nT)$, the receiver can determine, which $X_s(nT)$ and $X_i(nT)$ symbols are most likely to have been transmitted on the basis of the received signal $Y(nT)$. This is simply achieved by determining the possible values of $R_s(nT) \cdot X_s(nT) + R_i(nT) \cdot X_i(nT)$, and finding the value with the minimum Euclidean distance from $Y(nT)$. In the case of a BPSK signal and BPSK interference $R_s(nT) \cdot X_s(nT) + R_i(nT) \cdot X_i(nT)$ has four possible values, assuming fixed values of $X_s(nT)$ and $X_i(nT)$. Without loss of generality, it is assumed $R_s(nT) = 1 + j0$ for all n. Figure 5.23 shows the four possible received points for arbitrary and equi-probable phase values of $\theta = \pi/3, \pi/2, 5\pi/6$ or π where, θ is the phase of $R_i(nT)$. This Figure will be discussed in more detail in Section 5.5.3, however, it shows how the decision boundaries vary with θ.

5.5.3 Fixed Schemes

As stated above, the key motivation behind investigating interference cancellation is that it would appear to be an ideal technique to support adaptive modulation in a fading multi-user environment. However, in order to characterise the interference cancellation techniques and

understand how they perform, they are initially considered in non-fading environments in conjunction with fixed modulation schemes.

The performance of interference cancellation is relatively easily determined by simulation. However, analytical performance studies become increasingly difficult, as the constellation size increases. The analysis is particularly difficult because, unlike the performance of square constellations in the presence of noise (Section 3.2.1) or noise and interference (Section 5.3.1.1), the acceptable corruption in the in-phase and quadrature components in not independent. The analytical performance is given below for BPSK and QPSK. The results are confirmed by simulation and simulation results are also provided for Square 16 and 64 QAM.

5.5.3.1 Theoretical performance of BPSK with interference cancellation

It is assumed that the interfering signal can have any relative phase with respect to the desired signal. The effective angle between the two constellations in the base-band is denoted by θ, where all values of θ are equally likely. The amplitude of the signal is given by A_s and the amplitude of the interferer is given by A_i. The effect of corrupting the BPSK signal with a BPSK interferer generates a four position constellation as shown in Figure 5.23. The Figure includes the conventional decision boundaries for BPSK as would be used in the absence of interference and used when evaluating the performance of the scheme shown in Figure 3.1(a). Interference cancellation allows the decision boundaries to be modified to improve the BER performance on the basis of knowledge of the interfering modulation scheme and the interfering channel characteristics. The decision boundaries with interference cancellation are a locus of points equi-distant from two, of the four, constellation points of the combined BPSK signal with a BPSK interferer. The two points are always chosen so both of the possible data symbols are represented, in addition they are selected such that the equi-distant criteria is met, but with the minimum Euclidean distance between the two selected points. In Figures 5.23(b) and 5.23(d) the decision boundaries with cancellation are the same as those without. However, with Figure 5.23(a) and 5.23(c) they are different and it can be seen that they are in three regions. The interface between the regions exists at the point where three constellation points are equi-distant from the decision boundary. By simple geometry it can be shown the coordinates for the two interface points are $(A_s - A_i\cos(\theta), (A_s - A_i\cos(\theta)) \cdot A_i\cos(\theta))$ and $(A_s + A_i\cos(\theta), (A_i\cos(\theta) - A_s) \cdot A_i\cos(\theta))$. The decision boundary for a BPSK signal with a BPSK interferer will be a straight line from one of these two points to the other. At all other places it will be a vertical line with the same x coordinate as the nearer of these two points. Therefore, considering this in conjunction with Figure 5.23(a) and Figure 5.23(c),

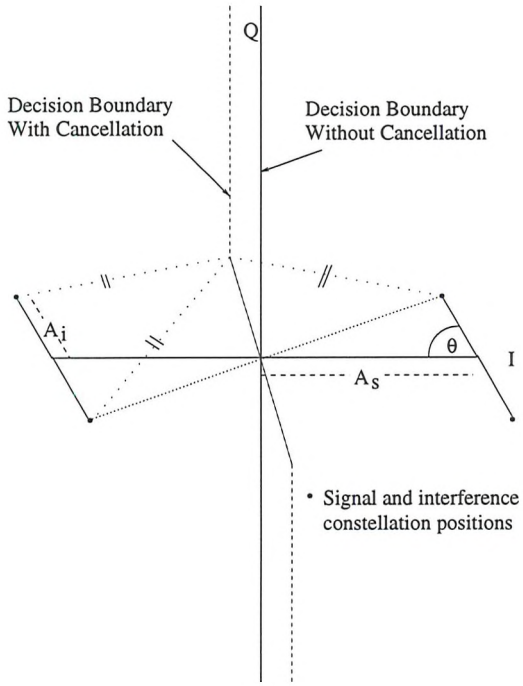

(a) $\theta = \pi/3$

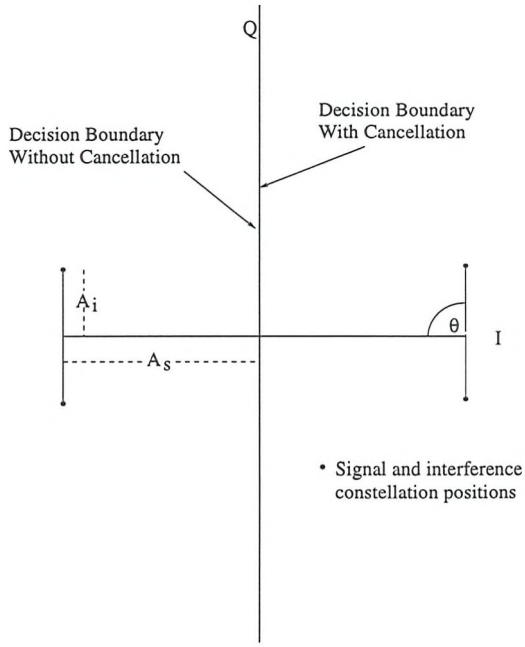

(b) $\theta = \pi/2$

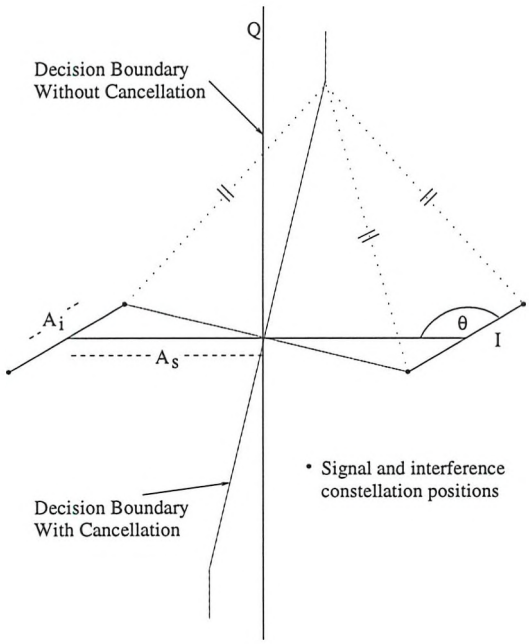

(c) $\theta = 5\pi/6$

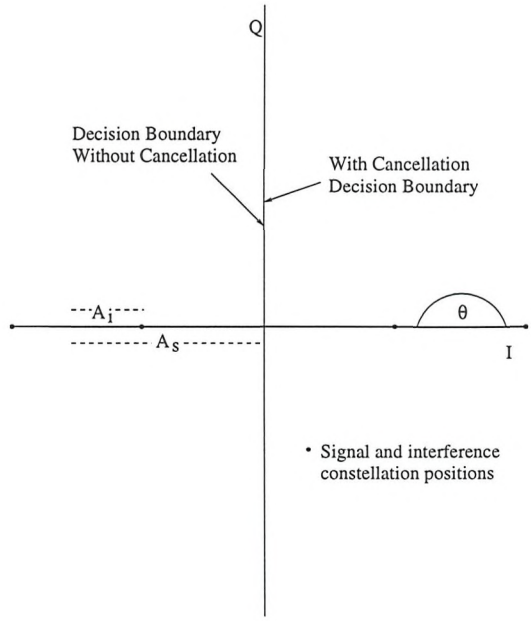

(d) $\theta = \pi$ or 0

Figure 5.23: Constellation diagrams of BPSK signal, with a phase non-coherent BPSK co-channel interferer at 8dB SIR, before the addition of AWGN for various θ values showing the decision boundary with and without interference cancellation

it can be seen for a large positive or negative component to the noise results in a vertical decision boundary, when interference cancellation is employed. However, in the region that includes the origin, the decision boundary is oblique. These three cases are evaluated for all θ, where y is the quadrature component of the noise, to yield the BER performance of BPSK, with a single BPSK interferer as

$$P_b''(A_s, A_i) = \int_{\theta=0}^{\pi} \int_{y=-\infty}^{\infty} P_e(y) \cdot \frac{1}{\sqrt{2\pi}\sigma} \exp\left(-y^2/2\sigma^2\right) dy d\theta \tag{5.56}$$

where,

$$P_e(y) = \begin{cases} Q(A_s^2/N) & \text{if } y > (A_s - A_i\cos(\theta)) \cdot A_i\cos(\theta) \\ Q\left((A_s - 2A_i\cos(\theta))^2/N\right) & \text{if } y < (A_i\cos(\theta) - A_s) \cdot A_i\cos(\theta) \\ Q\left(\frac{\left(A_s - A_i\cos(\theta) - \left(\frac{(y + A_i\sin(\theta)) \cdot A_i\sin(\theta)}{W \cdot (A_s - A_i\cos(\theta))}\right)\right)^2}{N}\right) & \text{otherwise} \end{cases} \tag{5.57}$$

and $W = -1$ if $\theta < \pi/2$ or $W = +1$ if $\theta > \pi/2$. The parameters for the $Q()$ function are based upon the distance of the constellation point, with y added to the quadrature component, from the decision boundary. The solution to these equations was evaluated numerically, where N was the noise power such that

$$N = 2\sigma^2 \tag{5.58}$$

and the limits of the integration with respect to y were approximated by $\mp 6\sigma$. The translated decision boundaries take into account the effect of the possible interferes and therefore attempt to compensate for the interference. The corresponding BER performance curves will be compared to simulated results in Figures 5.24(a)

5.5.3.2 Theoretical performance of QPSK with interference cancellation

Expressing the performance of QPSK with a single QPSK interferer and interference cancellation is considerably more complex than with BPSK and a single BPSK interferer. In the case of BPSK the decision boundary with cancellation was defined over three regions and the symbol error rate was equal to the BER. However, with QPSK the decision boundary with cancellation is defined for 28 regions in order to determine the BER. Therefore, a technique to determine the theoretical performance was exploited that did not require explicit evaluation of the decision boundaries. This was achieved by considering the QPSK phasor constellation, with a QPSK interferer similarly to Figure 5.23, which results in a 16-point constellation. The positions of all 16 points could be computed for all θ angles given the received signal

and interference amplitudes, determined by the corresponding propagation channels. The decision boundaries were calculated by considering the half-way point along the shortest line between each of the constellation points and then bi-secting that point with a perpendicular. This yielded $12 \times 16/2 = 384$ decision boundaries. The integral in Equation 5.56 was then solved numerically, however, for QPSK this Equation had to be solved in both the x and y directions order to compute the BER. The function $P_e(y)$ was evaluated on the basis of which boundary offered the least one dimensional protection for a given y.

5.5.3.3 Simulated Performance with channel estimation

Having derived the theoretical performance of the interference cancellation algorithm for BPSK and QPSK, their performance may be compared with the simulated performance. When the simulation was conducted with perfect estimation of both the useful and interfering channel, there was extremely good correspondence between the simulated and numerical results. However, the more realistic simulation, where the a perfect estimation of the interfering channel's magnitude and phase was not assumed was also considered by simulation. The channel was estimated by employing two orthogonal sequences, 24 symbols long in the centre of the TDD/TDMA burst, referred to as the mid-amble.

Figure 5.24(a) shows the numerical performance of BPSK with a single BPSK interferer, on the basis of perfect signal and interfering channel estimation. For comparison it shows the simulated performance of BPSK with a single BPSK interferer, using the mid-amble for estimation of the interfering channel's magnitude and phase. Figure 5.24(b) shows the same comparison for QPSK with a single QPSK interferer. In both cases it can be seen that there is little deterioration in performance resulting from using the mid-amble for estimating the interfering channel's magnitude and phase. Figure 5.25 shows a the simulated performance of square 16 and 64 QAM with perfect channel estimation for the signal and interference channel. In these figures the markers represent the simulated performance using the mid-amble to estimate the interfering channel, however the signal channel is known perfectly. Again, it can be observed that the deterioration in performance resulting from using the mid-amble to estimate the interfering channel is negligible.

Figure 5.24(a) shows the BPSK performance for SIRs greater than 0dB, and Figure 5.24(b) portrays the QPSK performance for SIRs greater than 3dB, since the theory presented above is only valid for these respective ranges. For SIRs below these values there would be a residual BER even with infinite SNR. In Figures 5.25(a) and 5.25(b) the same SIR values are used as in Figure 5.5 because the results were generated by simulation and therefore

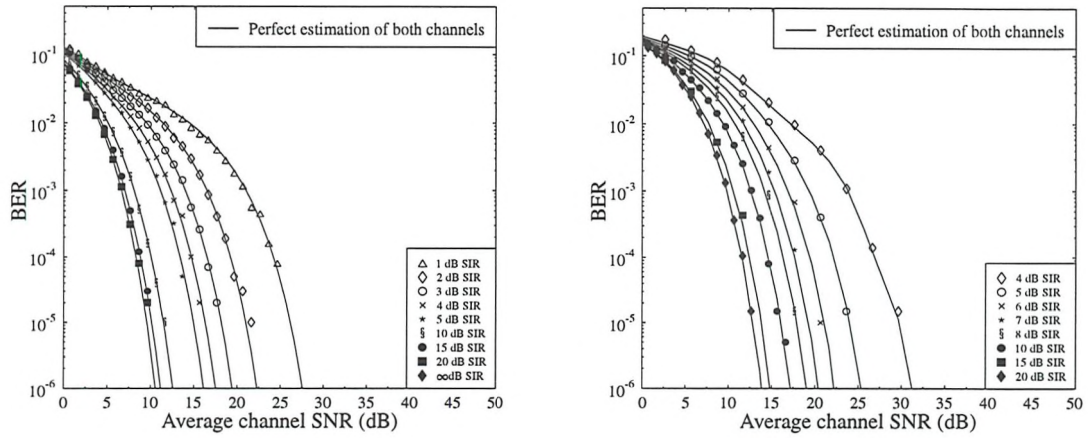

(a) BPSK (b) QPSK

Figure 5.24: Theoretical performance, with perfect magnitude and phase channel estimation and simulated performance with mid-amble based estimation, for BPSK and QPSK schemes over Gaussian channels with a single BPSK and QPSK interferer, at various SIR values, also received over a Gaussian channel using interference cancellation and $\alpha = 0.35$.

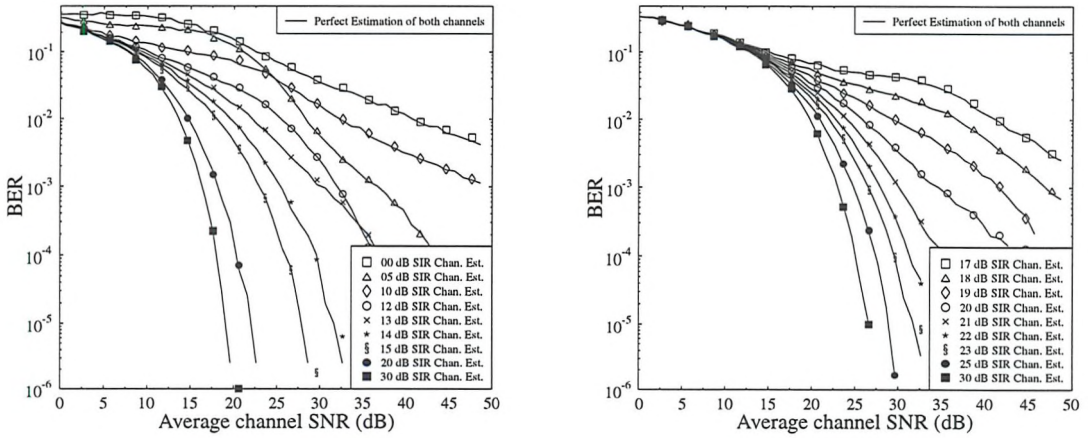

(a) Square 16 QAM (b) Square 64 QAM

Figure 5.25: Simulated performance, with perfect magnitude and phase channel estimation for the signal channel and mid-amble based estimation for the interfering channel, for Square 16 and 64 QAM schemes over Gaussian channels with a single Square 16 and 64 QAM interferer, at various SIR values, also received over a Gaussian channel using interference cancellation and $\alpha = 0.35$.

there was no restriction upon the SIR that could be evaluated. It should be noted that in Figure 5.25(a), the performance at 5 and 12 dB SIR, respectively, is better than at 10 and 13 dB SIR in the high average channel SNR range. This results from the complicated interaction of the $16^2 = 256$ combined signal and interference constellation points. When the maximum interference amplitude is higher than the distance between the Square 16 QAM signal constellation points, the combined constellation points overlap for different θ values.

Having verified the model for interference cancellation with BPSK and QPSK, and shown that employing a mid-amble to estimate the phase and amplitude of the interfering channel, the performance of the fixed modulation schemes over Gaussian channels is compared with and without interference cancellation. This is achieved by comparing Figure 5.24 and Figure 5.25 with Figure 5.5. The effect of the interference cancellation upon the BPSK and QPSK modulation schemes is most significant at low SIRs and low SNRs. Figure 5.24(a) compared with Figure 5.5(a) reveals that at 1,2,3,4, and 5 dB SIR, the SNR required for BERs in the region of 2 - 5 % is reduced by as much as 3 dB by employing interference cancellation within BPSK modulation. Similar gains are recorded for QPSK by comparing Figure 5.24(b) with Figure 5.5(b). What is not shown is how the BERs are reduced, at SIRs below 3dB since, as stated above, the theoretical approach for evaluating the BER performance is not applicable at low SIRs.

However, for Square 16 and 64 QAM the performance gains achieved using interference cancellation are more striking. This is because the performance with interference cancellation was evaluated at SIR values, where a residual BER existed without the cancellation. Consider Figure 5.25(a) in comparison with Figure 5.5(c), from which it can be identified that at 0 or 5 dB SIR, and at 30 dB SNR, the interference cancellation reduces the BER by an order of magnitude. At higher SNRs the improvement becomes as large as four orders of magnitude. In a realistic communications system the channel and network conditions are unlikely to result in a Gaussian line of sight scenario where the, signal and interferer, produce, 0 or 5 dB SIR and 30 dB SNR, as implied by these Gaussian channel experiments. However, in the fading channels of the type described in Chapter 2, with independent signal and interfering paths such SNR and SIR values could occur instantaneously. Therefore, the performance is now evaluated assuming that both the signal and interferer are Rayleigh fading independently.

5.5.3.4 Rayleigh Channel Performance using channel estimation

The performance of each of the fixed modulation schemes is evaluated with either a single BPSK or single square 64 QAM interferer by simulation. This will reveal the performance

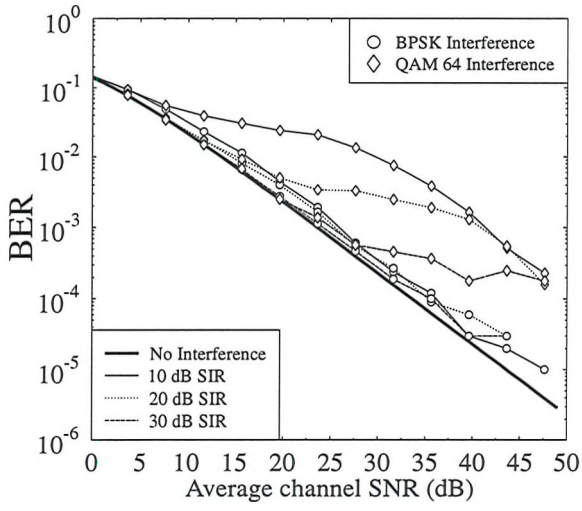

(a) BPSK

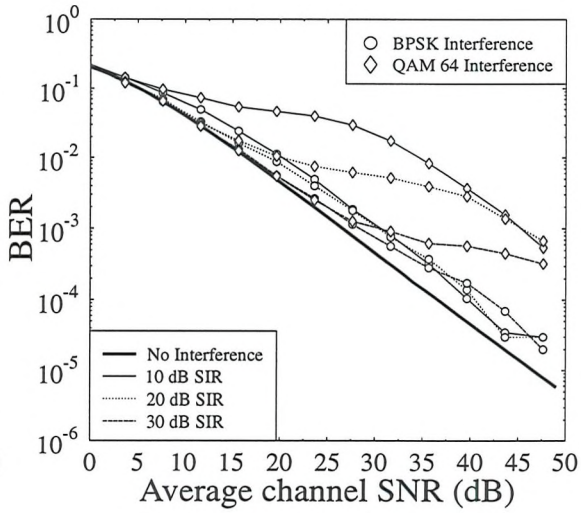

(b) QPSK

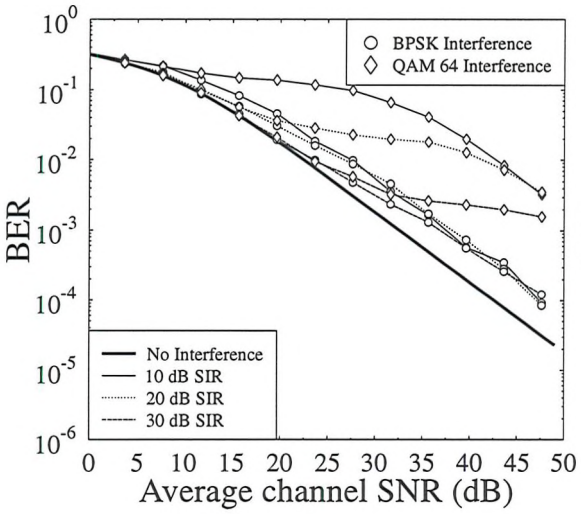

(c) Square 16 QAM

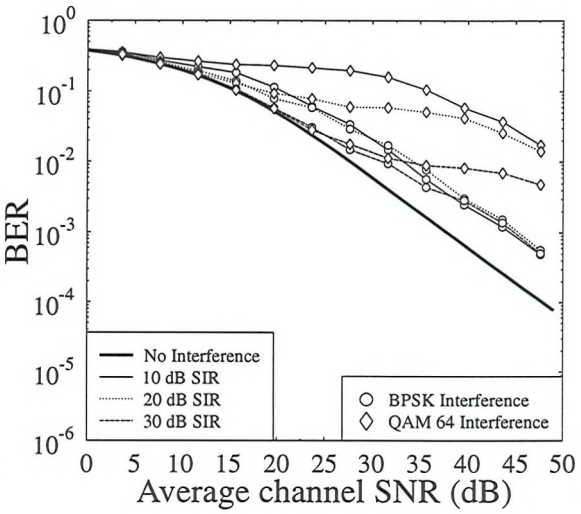

(d) Square 64 QAM

Figure 5.26: Simulated performance of fixed modulation schemes in slow Rayleigh channels with single interfering transmission at various SIR values also received via a Rayleigh channel using interference cancellation, estimated channel characteristics and $\alpha = 0.35$.

of interference cancellation for each scheme in a Rayleigh fading channel and show, how it is affected by the least and most complex phase non-coherent time-synchronous interferer. The performance was evaluated by simulation and using the mid-amble to estimate the interfering channel's magnitude and phase. Both the signal and interferer were assumed to be constant over a time slot and 1×10^5 symbols were simulated for every SNR and SIR value. The results are shown in Figure 5.26 which reveals:

- Logically, the use of interference cancellation never results in the BER being lower than it would have been, had there been no interference.
- At high SNR there is a margin between the performance obtained when there is no interference and the performance achieved when a single interferer is cancelled. This gap increases as the useful signal scheme increases with complexity.
- At low SNRs the BER performance is limited by the noise irrespective of the SIR. As the SNR increases, it becomes constrained by the level of SIR and the interfering modulation scheme, where Square 64 QAM is more detrimental. Lastly, at high SNRs the BER performance limited only by the interfering modulation scheme.

The first of these observations is what would be expected. The second can be explained by considering the constellation that the interference cancellation algorithm uses to determine the transmitted symbol, that is the joint constellation combined from the estimation of the service and interfering channels and knowledge of the modulation scheme transmitted over both. Consider Figure 5.23, which shows the constellation of possible received positions if a single BPSK interferer is superimposed upon a BPSK transmission. Generally, the cancellation decision boundary results in superior BER performance in comparison to the original decision boundary without cancellation. However, as discussed before, the boundary translation does not fully mitigate the effects of interference. It is this reduction in mitigation as the signalling constellation becomes more complex that must be explained. The explanation is that as the signalling constellation increases in complexity, and both itself and the interferer are fading, the noise tolerance of the combined constellation reduces more rapidly than the constellation without the presence of an interferer.

The final observation made above is best explained by comparing the sub-figures in Figure 5.26 with the corresponding results in Figure 5.8. It is the case for all signalling schemes with both of the interfering schemes, but more clearly seen with the square 64 QAM interferer, shown in Figure 5.26 that the BER curves with interference and cancellation initially decay with increased SNR, then experience a range of SNRs where the BER performance

	SNR	BPSK Interferer			QAM64 Interferer		
	(dB)	10 dB SIR	20 dB SIR	30 dB SIR	10 dB SIR	20 dB SIR	30 dB SIR
BPSK	20	1.8×10^{-2}	1.0×10^{0}	1.0×10^{0}	1.0×10^{0}	1.0×10^{0}	1.0×10^{0}
QPSK	20	2.5×10^{-2}	1.0×10^{0}	1.0×10^{0}	1.0×10^{0}	1.0×10^{0}	1.0×10^{0}
QAM16	20	2.8×10^{-2}	1.0×10^{0}	1.0×10^{0}	1.0×10^{0}	1.0×10^{0}	1.0×10^{0}
QAM64	20	5.5×10^{-1}	1.0×10^{0}	1.0×10^{0}	1.0×10^{0}	1.0×10^{0}	1.0×10^{0}
BPSK	30	1.5×10^{-3}	1.3×10^{-1}	1.0×10^{0}	4.1×10^{-1}	1.0×10^{0}	1.0×10^{0}
QPSK	30	2.5×10^{-3}	3.8×10^{-1}	1.0×10^{0}	5.0×10^{-1}	1.0×10^{0}	1.0×10^{0}
QAM16	30	2.7×10^{-2}	3.4×10^{-1}	1.0×10^{0}	5.5×10^{-1}	1.0×10^{0}	1.0×10^{0}
QAM64	30	1.8×10^{-1}	4.0×10^{-1}	1.0×10^{0}	9.0×10^{-1}	1.0×10^{0}	1.0×10^{0}
BPSK	40	1.4×10^{-4}	2.5×10^{-2}	1.3×10^{-1}	6.8×10^{-2}	4.6×10^{-2}	7.8×10^{-1}
QPSK	40	6.8×10^{-4}	4.0×10^{-2}	3.4×10^{-1}	7.8×10^{-2}	5.1×10^{-1}	1.0×10^{0}
QAM16	40	3.6×10^{-3}	3.9×10^{-2}	3.0×10^{-1}	1.7×10^{-1}	6.5×10^{-1}	1.0×10^{0}
QAM64	40	1.1×10^{-2}	4.6×10^{-2}	3.5×10^{-1}	2.5×10^{-1}	8.0×10^{-1}	1.0×10^{0}

Table 5.10: BER reduction due to interference cancellation with fixed modulation schemes transmitted through a slow Rayleigh fading channel with a single independent slow Rayleigh fading interferer, using the mid-amble to estimate the interfering channel and perfect estimates for the wanted channel.

levels out, and then the BER reduces again with SNR. However, by considering Figure 5.8 it can be observed that the SNR regions, where the BER performance levels out in Figure 5.26 correspond to the corner SNRs, where the BER residual was experienced without interference cancellation for the given SIRs. In this flat region the interference cancellation is unable to function, because the noise is corrupting the combined constellation of signal and interferer. At SNRs beyond the flat region the interference cancellation begins to have a significant positive effect. The difference between the length of the flat BER region with a BPSK compared to a Square 64 QAM interferer is due to the reduced noise tolerance of the combined signal and interference constellation, resulting from any of the signalling schemes with a single BPSK interferer compared with single Square 64 QAM interferer.

Table 5.10 summarises the advantage of employing interference cancellation, when comparing Figure 5.26 with Figure 5.8. The interference cancellation achieves the maximum performance, when the signal and interference constellations are least complicated. That is, interference cancellation is most useful, when employed in conjunction with low order modulation schemes. The BER is reduced by interference cancellation the most, when the average SIR is low, but the average channel SNR is high.

5.5.4 Adaptive Schemes

Having studied fixed modulation schemes assisted by interference cancellation, employing interference cancellation in conjunction with adaptive modulation is considered. These experiments are based upon the assumptions used for the fixed experiments, however, it is additionally assumed that there is an equal probability of a 'No Transmission', BPSK, QPSK, Square 16 or 64 QAM symbol interfering with the data transmission and that the modulation schemes used in both the signal and interfering channels are known at the receiver. The transmission of this control information is discussed in Section 7.3.

Figures 5.27 and 5.28 show the BER and BPS performance of the optimised mean BER, speech and computer data scheme with switching levels given in Table 4.1 ie with switching levels ignoring the effects of interference, over slow Rayleigh fading channels with various levels of CCI from a single interferer, when interference cancellation is employed. The results were generated with perfect estimation of the wanted channel and exploitation of the mid-amble to estimate the interfering channel. These results may be compared with the same performance in the absence of interference cancellation shown in Figures 5.18 and 5.19. For both the speech and computer data schemes at 10, 20, 30 and 40 dB SIR interference cancellation improves the BER performance. The performance improves most at high average channel SNR values, and this is what would be expected, bearing in mind the results from Section 5.5.3. However, the speech system still fails to achieve the BER target of 1×10^{-2} for some average channel SNRs at 10 and 20 dB SIR. As seen in the Figure, in the case of the computer data system the BER performance curve also fails to achieve the target BER of 1×10^{-4}, when interference cancellation is employed if the SIR is lower than 40 dB.

As seen in the captions, the down-link results shown in Figures 5.27 and 5.28 are based upon an interference-free up-link. That is, as the up-link transmission is used for the channel estimation and thus for the choice of modulation scheme to be employed for the down-link transmission, the optimum modulation scheme will be chosen for the given switching levels. Although this is an unlikely scenario in a cellular environment, here this assumption is used to allow comparison with the earlier Figures. Furthermore, when interference cancellation is employed this situation is much more realistic. This is because both the signal and interferer channels are estimated by separate orthogonal mid-ambles, as explained in Section 5.5.1. This means, within the resolution of the mid-amble to estimate the signal channel, which is shown to be excellent for a FRAMES type system in Section 7.2.2, the interference can be neglected. Therefore, if Figures 5.16 and 5.17 were reproduced considering the effects of interference cancellation, the performance at finite interference would be similar to that at

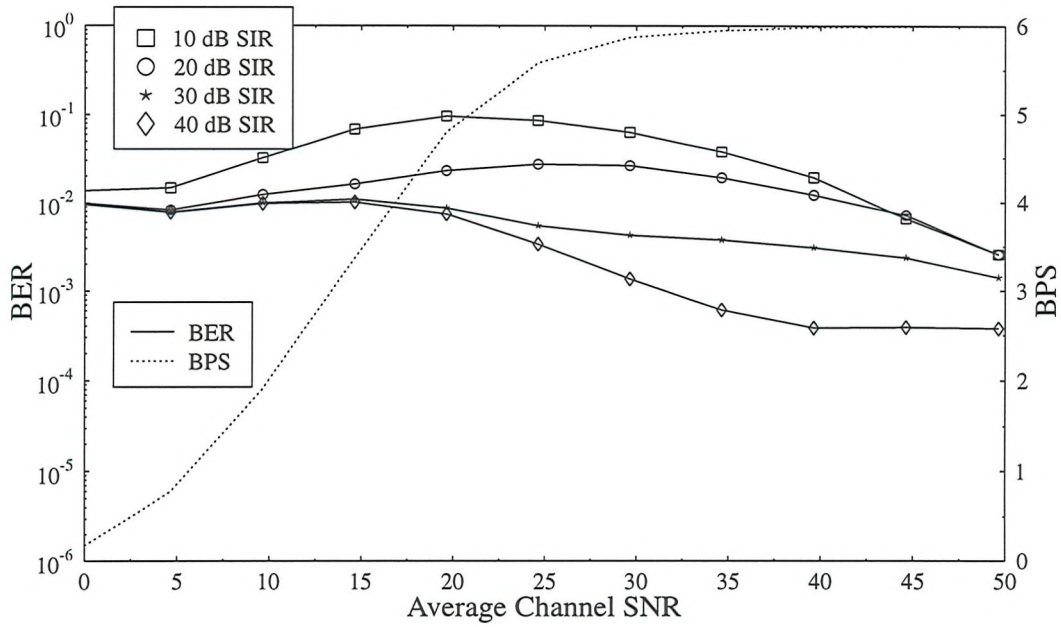

Figure 5.27: Down-link BER over a slow Rayleigh fading channel with various SIR levels at the MS and no interference at the BS, the original optimised adaptive speech switching levels and interference cancellation with perfect estimation and mid-amble estimation of the signal and interference channels, respectively. $\alpha = 0.35$

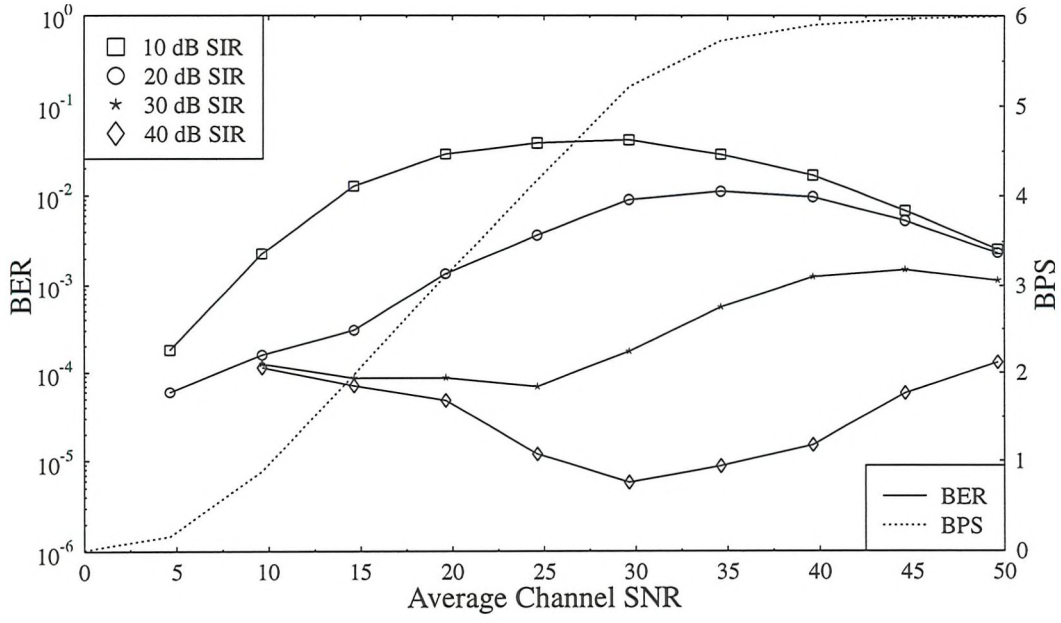

Figure 5.28: Down-link BER over a slow Rayleigh fading channel with various SIR levels at the MS and no interference at the BS, the original optimised adaptive computer data switching levels and interference cancellation with perfect estimation and mid-amble estimation of the signal and interference channels, respectively. $\alpha = 0.35$

	Speech				Computer Data			
SIR (dB)	l_1	l_2	l_3	l_4	l_1	l_2	l_3	l_4
10	4	10	27	35	Unused			
20	3	6	12	30	14	30	38	60
30	3	6	12	18	8	11	17	60
40	3	6	12	18	8	11	17	25

Table 5.11: Manually determined switching levels, in dB, for adaptive schemes over Rayleigh fading channels experiencing co-channel interference and employing interference cancellation, where the performance is shown in Figures 5.29 and 5.30

zero interference.

In order to achieve the target BERs of 1×10^{-2} and 1×10^{-4} in the presence of interference, simply using the switching levels from Table 4.1 and employing interference cancellation is not sufficient. A feasible approach that could be used to achieve the target BERs for both schemes across the desired range of average channel SNRs would be to segment the switching levels for different average channel SNRs. This would mean that the switching levels would be varied depending upon the prevailing average channel SNR conditions. This could be a successful approach because, assuming a constant SIR, when the average channel SNR is low, the noise is the dominant corrupting influence upon the received signal, and when the SNR is high, the noise becomes negligible and it is principally the interference that causes the corruption. Therefore, increasing the switching levels, at low average channel SNRs, essentially protects the transmitted symbols against noise, and at higher average channel SNRs the switching levels protect the symbols against Rayleigh-faded interference. However, the draw-back with such an approach is that it would involve accurate estimation of the average signal and interference levels. Therefore, it was decided that the same switching levels must be used for all average channel SNRs, and the switching levels would only be varied on the basis of the average interference level.

In order to obtain optimum switching levels for Rayleigh fading channels in the absence of noise and with CCI, without employing interference cancellation, Powell optimisation has been used, as in Section 5.4.2. This has been possible, because a numerical solution to the performance of adaptive modulation was derived for these cases and therefore iterative optimisation has been feasible. However, a full numerical solution for adaptive modulation, with an independent co-channel interferer and cancellation, has not been found. Therefore, the switching levels are derived by an iterative manual technique.

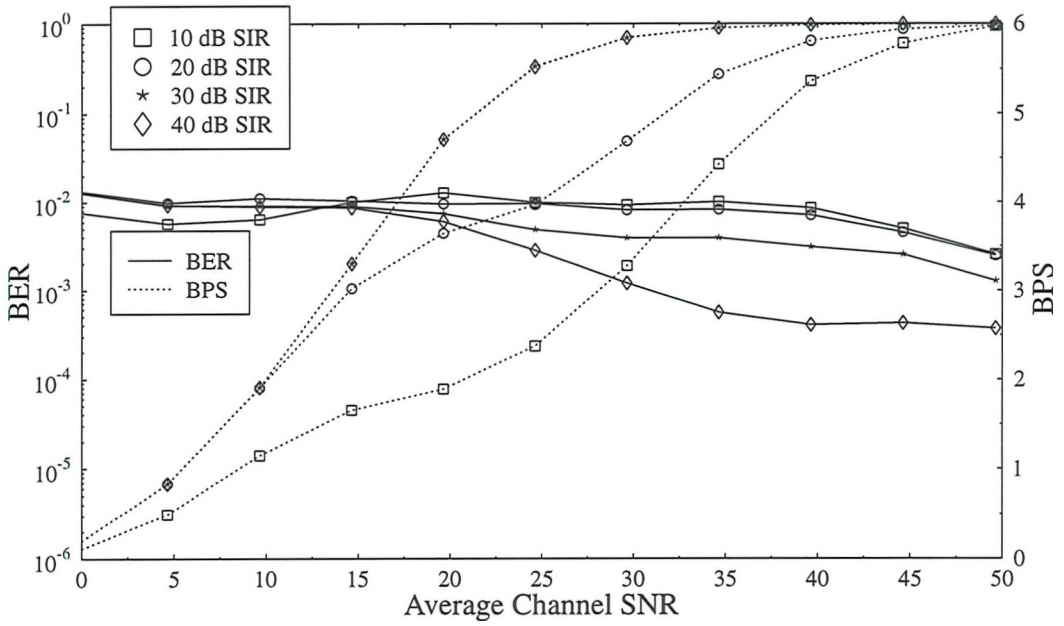

Figure 5.29: Down-link BER over a slow Rayleigh fading channel with various SIR levels at the MS and no interference at the BS, the manually adjusted for interference cancellation adaptive speech switching levels and interference cancellation with perfect estimation and mid-amble estimation of the signal and interference channels, respectively. $\alpha = 0.35$

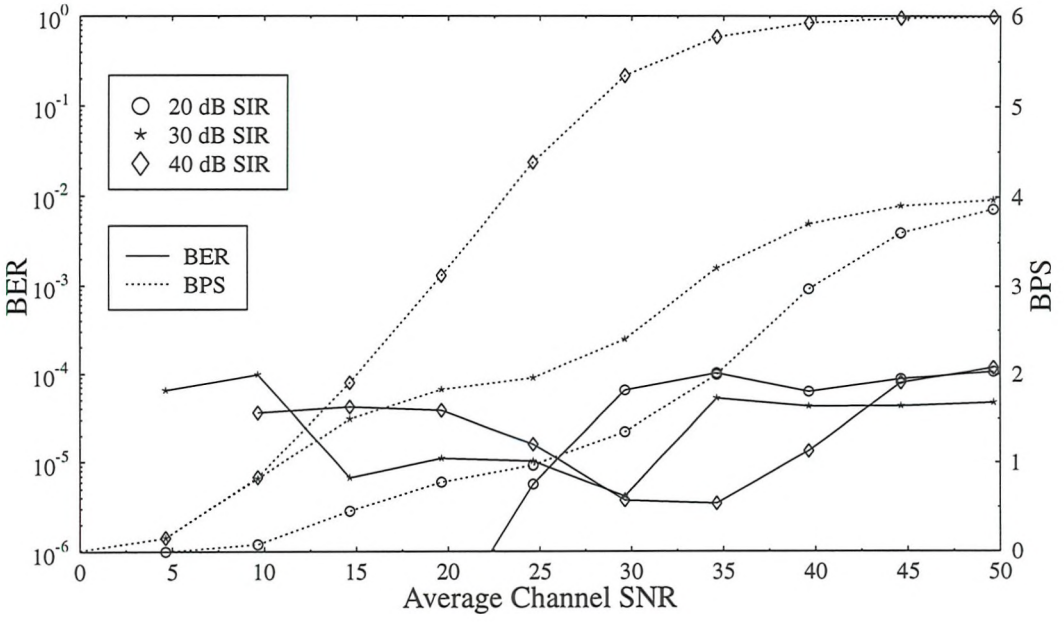

Figure 5.30: Down-link BER over a slow Rayleigh fading channel with various SIR levels at the MS and no interference at the BS, the manually adjusted for interference cancellation adaptive computer data switching levels and interference cancellation with perfect estimation and mid-amble estimation of the signal and interference channels, respectively. $\alpha = 0.35$

The interference cancellation was simulated with the perfect magnitude and phase estimations of the signal channel and mid-amble based results for the the interfering channel. The proposed switching levels are given in Table 5.11 and the performance curves are shown in Figures 5.29 and 5.30. The results in Table 5.11 may be compared with the re-optimised switching levels in the presence of interference, but without interference cancellation that are shown in Tables 5.7 and 5.8. This comparison, for the speech system, shows that only the l_4 values are changed significantly. In the case of 10 dB SIR, l_4 is increased to 35 dB and at 20 dB SIR it is reduced to 30 dB. These changes in switching levels, for the speech system, used in conjunction with interference cancellation allow the target BER of 1×10^{-2} to be maintained over the range of average channel SNRs from 0 to 50 dB and SIRs of 10, 20, 30 or 40 dB, which is shown in Figure 5.29. This was not the case, when the switching levels from Table 5.7 were used, without interference cancellation, in the presence of a single phase-non-coherent time-synchronous Rayleigh fading interferer at SIRs of 10 or 20 dB, as was shown in Figure 5.20. Therefore, making the modifications to l_4 mentioned above, with respect to the re-optimised switching levels and invoking interference cancellation means that adaptive modulation may be used for transmission with an average BER below 1×10^{-2} over a Rayleigh fading channel with average channel SNRs from 0 to 50 dB and SIRs of 10 dB or greater from a single adaptive modem.

Now the computer data system with a target BER of 1×10^{-4} is considered. Firstly, when comparing Table 5.11 with Table 5.8 it can be observed that the values of most of the switching levels are reduced, except at the combination of low SNRs and high SIRs, where the noise is dominant and the interference cancellation yields no significant benefits. However, Figure 5.30 shows that despite this, the BER performance compared with Figure 5.21 is improved, in terms of the range of SNR and SIR, for which the target BER can be achieved. The benefits associated with the switching levels being varied depending upon the average channel SNR conditions can be seen in Figure 5.30 and Figure 5.21, when the SIR is low. It can be seen, for example, in Figure 5.30 that with 20 dB SIR and 22 dB average channel SNR, the BER performance is very much below the target BER of 1×10^{-4}. Under these channel conditions lower switching levels would be desirable, since then additional BPS capacity would be yielded. However, the BER is considerably closer to the target level, as the SNR increases, and because the same switching levels are used for all average channel SNRs, the switching levels cannot be reduced. For this reason, switching the modulation scheme on the basis of the corrupted bits detected in the FEC [148, 6, 104] may be preferable, however other issues that are discussed in Section 7.2.2 must be considered, when this principle. In summary, it should be noted that the target BER is achieved for all average channel SNRs and SIRs

that are shown in Figure 5.30. Furthermore, that the proposed manual switching levels, with interference cancellation, for high SIRs correspond closely to the Powell-optimised switching levels given in Table 4.1, for both speech and computer data systems.

5.6 Channel Capacity

The above discussion has focused upon the BER performance, but if it is accepted that for both the speech and computer data schemes the target BER is achieved, a similar comparison to that which was conducted in Section 4.4 may be performed to compare the relative efficiency of the fixed and adaptive schemes. However, this time by also considering the effects of interference and interference cancellation. As stated before, this type of comparison is not as pertinent, as the spectral efficiency [134] technique used by Webb, although it dispenses with the need for a micro-cellular design propagation system. Figures 5.31 and 5.32 show the capacity that may be achieved for a given E_b/N_0, using fixed and adaptive modulation schemes with target BERs of 1×10^{-2} and 1×10^{-4}, over a slow Rayleigh fading channel, assuming a single interferer at various SIRs and the use of interference cancellation. The fixed scheme's performance was derived from Figure 5.26. The roll-off factor, α, is set to zero for normalisation purposes, the 'small bold' markers represent the performance of fixed schemes, when the interfering signal is square 64 QAM, the 'large hollow' markers represent the performance for fixed schemes, when the interfering symbol is BPSK. The adaptive results are derived from Figures 5.29 and 5.30. Considering Figure 5.31, it can be seen than the adaptive performance at 10 dB SIR is closer to the Shannon (or Lee) limit that the fixed 1, 2 and 4 BPS schemes with the same level of interference, when they are corrupted by square 64 QAM and interference cancellation is invoked. This is also the case, when comparing the adaptive scheme with the fixed 1 BPS scheme and a single BPSK interferer. However, the other fixed schemes out-perform the adaptive modem at 10 dB SIR. At 30 dB SIR, however, only the 6 BPS fixed scheme, can outperform the adaptive scheme irrespective of the type of interferer. Considering Figure 5.32, which shows the performance at 1×10^{-4} BER, it can be seen that the 10 dB SIR adaptive scheme is not represented, and neither are the fixed schemes with 64 QAM interferers. This is, because the maximum average channel SNRs of Figures 5.26, 5.29 and 5.30 are insufficient to determine the E_b/N_0, at which a BER of 1×10^{-4} is achieved. In some cases the required E_b/N_0 could be very high, however, Figure 5.32 shows that at 30 dB SIR and above the adaptive scheme is generally more efficient than the fixed schemes with any interferer and at 20 dB it is more efficient than the fixed schemes with square 64 QAM interferes.

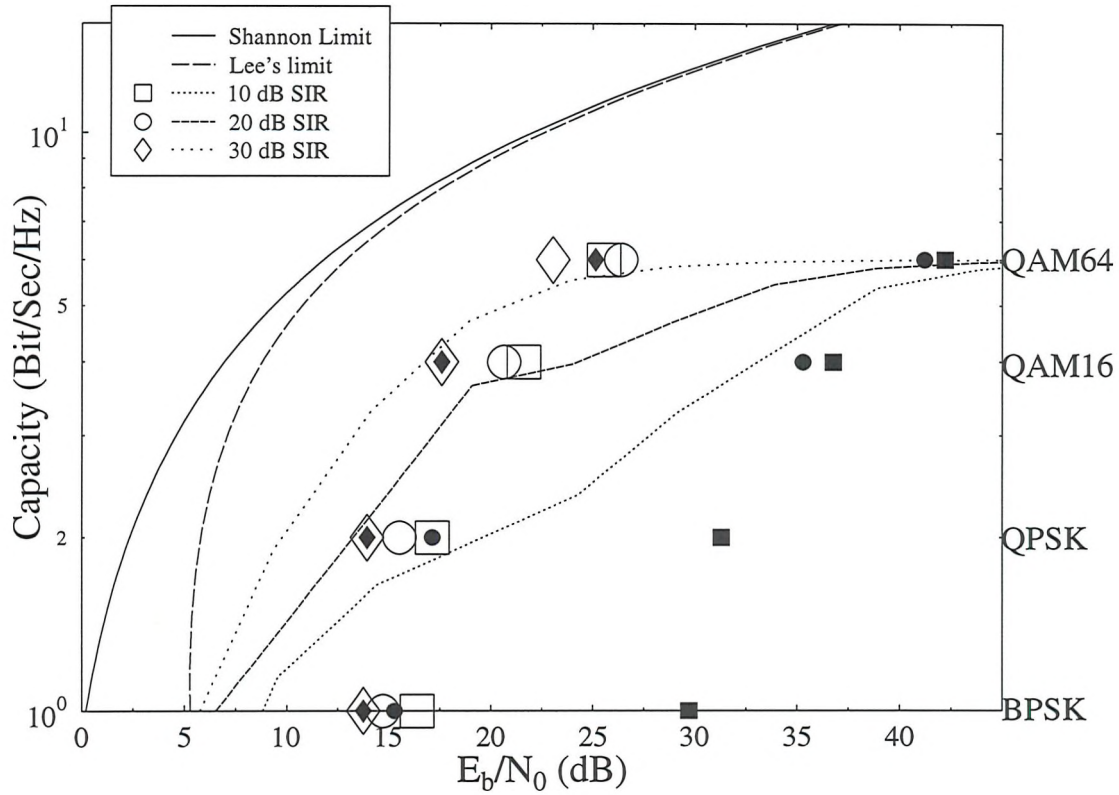

Figure 5.31: Capacity limit and upper-bound performance of fixed and adaptive modulation schemes in Rayleigh fading channels for specific BER of 1×10^{-2}. Signalling and pilot overheads were neglected, assuming perfect filtering and single-sided bandwidth with $\alpha = 0$. A single Rayleigh fading co-channel interferer at 10, 20 and 30 dB SIR was used for adaptive schemes, shown with lines, and 10, 20 and 30 dB SIRs were employed for the fixed schemes shown with markers. Interference cancellation was invoked, where **'large hollow' markers represent BPSK interference and 'small bold' markers correspond to Square 64 QAM interference.**

Figures 5.31 and 5.32 give a summary of the performance of the fixed and adaptive schemes, with interference and interference cancellation. However, it is important to note that they neglect the exact BERs encountered other than stating that a specific target has been achieved.

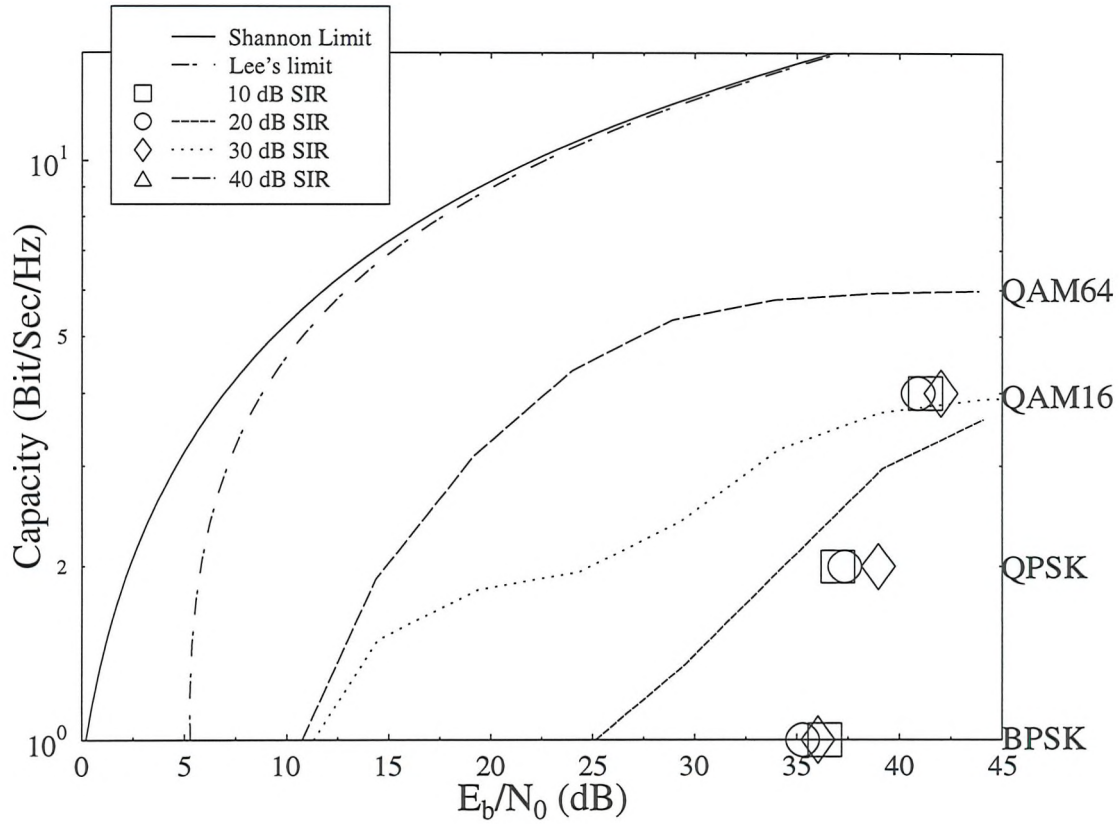

Figure 5.32: Capacity limit and upper-bound performance of fixed and adaptive modulation schemes in Rayleigh fading channels for specific BER of 1×10^{-4}. Signalling and pilot over-heads were neglected, assuming perfect filtering and single-sided bandwidth with $\alpha = 0$. A single Rayleigh fading co-channel interferer at 10, 20 and 30 dB SIR was used for adaptive schemes, shown with lines, and 10, 20 and 30 dB SIRs were employed for the fixed schemes shown with markers. Interference cancellation was invoked, where **'large hollow' markers represent BPSK interference**. There are no 'small bold' markers in this Figure to represent Square 64 QAM interference, since these values fell outside the plotted range.

5.7 Conclusion

It was shown in Figure 5.2, that a roll-off factor of $\alpha = 0.35$, may be used to achieve BERs of 1×10^{-4} with a 7 symbol impulse response employing Square 64 QAM and this can be incorporated within an ATDMA type system. The effects of co-channel interference for fixed modulation schemes in Gaussian channels were given by numerical integration and simulation in Figure 5.5 and over slow Rayleigh channel in Figure 5.8. In Figure 5.11(b) it was shown that the adjacent channel interference experienced from both upper and lower interferers

in an ATDMA scheme is approximately 31 dB over a Gaussian channel. It was shown in Figure 5.13 that Adjacent and Co-channel interference have approximately the same effects upon BER, for a given SIR, over Rayleigh fading channels.

Co-channel interference potentially has a doubly negative effect upon adaptive modulation. Figures 5.16 and 5.17 showed the effect of interference upon the BER of adaptive modems, in the artificial scenario of when the interference only corrupts the channel estimate. This problem was addressed as a bi-product of interference cancellation and can be neglected in a system that invokes interference cancellation. The effect of the interference upon the received symbols was shown in Figures 5.18 and 5.19, where there was a significant degradation of BER performance. However, this problem was addressed to a certain extent with re-optimised switching levels, given in Tables 5.7 and 5.8, yielding BER performance curves shown in Figures 5.20 and 5.21.

Interference cancellation offered a more complete solution, especially when combined with manual adjustment of the adaptive switching levels. Initially, however, the effect of interference cancellation was characterised for fixed modulation, yielding the gains given in Table 5.10. The manual adjustment and interference cancellation results for adaptive modulation yielded a guaranteed BER of 1×10^{-2} and 1×10^{-4} for the speech and computer data schemes for a range of values, shown in Figures 5.29 and 5.30.

In conclusion adaptive modulation is best suited to indoor environments. This is because TDD is the most appropriate vehicle to estimate the channel conditions, and un-equalised indoors TDD requires sufficiently low propagation delays. Adaptive modulation is also most suitable for low mobile velocities, this will be discussed in more depth in Section 7.2.1, and low mobile velocities are expected in an indoors environment. In such an indoors environment, co-channel interference would be mitigated by walls and doors in the building. However, there is scope for interference to be produced on a short term basis, when a combination of doors are opened, internal partitions are moved inside the building or a vehicle passes the building reflecting some potentially interfering signal back into the property. Such examples of interference are likely to result in single interferer, a scenario which is amiable to interference cancellation. The results shown in Figures 5.31 and 5.32 portray how adaptive modulation can result in significant capacity gains compared with fixed modulation schemes in such situations. The benefits of adaptive modulation are greater than shown in Figures 5.31 and 5.32 because the BER of the adaptive scheme is often significantly lower than the target. Furthermore, as also mentioned in Section 6.9.3.1, the comparison with the fixed modulation schemes is conducted assuming that the most appropriate fixed scheme for the prevalent average channel conditions is employed. By definition, the mobile will move from one position

to another, this will have an effect upon the average channel conditions. Therefore, some dynamic change in the fixed modulation scheme is implicitly assumed during the comparison between fixed and adaptive schemes.

Finally, it should be clarified that these results are based upon a single interferer and the effects of further interferers that are not cancelled are not considered.

Chapter 6

Network Layer Considerations

6.1 Introduction

In the preceding analysis of adaptive modulation it has been assumed that the phase distortion and amplitude attenuation of the channel is constant over the duration of a TDD slot. However, adaptive modulation exploits the varying channel conditions from one TDD/TDMA frame to the next. The changing nature of the channel results in two serious problems for adaptive modulation. Firstly the channel estimation will be sub-optimum and, therefore, a modulation scheme other than the most appropriate could be employed. This is addressed in Section 7.2.1 and Reference [149]. The second effect, that is investigated here, is the variable throughput resulting from the time-variant modulation scheme.

In this Chapter two techniques for modelling the variation of the modulation scheme are compared. The latency resulting from the variable throughput is then characterised. This is followed by a discussion upon mitigating the latency and the Chapter is concluded with a case study comparing adaptive modulation with a fixed modulation scheme.

6.2 Buffering

An appropriate technique to manage the variable throughput intrinsic to adaptive modulation is to implement a buffer between the channel codec and the modulator. The buffer holds data when the channel conditions result in a low throughput, low order modulation scheme being employed. When the channel conditions improve and the high order modulation schemes are employed, the buffer would be emptied. As an example, the instantaneous 'fullness' of the buffer and the instantaneous throughput are shown in Figure 6.1(a) as a function of the

transmission frame index. The buffer length has ramifications as to system latency.

Lower normalised Doppler frequencies result in higher temporal channel correlation, which is exploited in order to estimate the channel quality and, therefore, to employ the most appropriate modulation scheme. Ironically, very low-Doppler channels result in prolonged fades that contribute to the adaptive modulation's latency. But these fades would result in long error bursts with a fixed scheme.

For given average channel conditions the average BPS performance of an adaptive modulation scheme in a Rayleigh fading channel is characterised by Equation 4.6. This upper bound average throughput is denoted B. In practice, if a buffer is to be employed, the average throughput must be less than this performance limit, in order to prevent the buffer becoming too long. Therefore, it is assumed that the average number of transmitted bits per symbol period is given by $\bar{B}$. The variable Ξ may be defined as the ratio of B and $\bar{B}$:

$$\Xi = \frac{\bar{B}}{B}. \tag{6.1}$$

In order to prevent a buffer overflow, the average number of bits transmitted per symbol is kept below B, therefore, $\Xi < 1$. The buffer will introduce a latency to the transmission and this latency will depend upon the fading frequency, the modulation switching levels, the average channel SNR and Ξ. The average BPS performance of an adaptive, 1% mean BER speech, and, a 0.01 % mean BER computer data scheme for Ξ values of 0.6, 0.7 and 0.8 is shown for a range of average channel SNRs in Figure 6.1(b).

6.3 Simulation Model

A convenient approach to understanding how the above parameters will affect the latency of an adaptive modulation scheme is to model the transmission scheme with a Markov model [141]. This approach is appropriate for modelling the throughput of adaptive modulation because the modulation scheme that is employed is only dependent upon which of the switching levels the instantaneous SNR falls between. By contrast the BER depends upon the actual value of the instantaneous SNR.

Wang and Moayeri [150] proposed a Markov model of the Rayleigh channel. This can be applied to modelling the instantaneous throughput of adaptive modulation in a Rayleigh fading channel. Assuming that the Doppler frequency is f_d, a state transition can take place every T seconds, the noise power is N, the mean signal power is P and l_1, l_2, l_3 and l_4 are the previously defined switching levels, the average probability of each modulation scheme

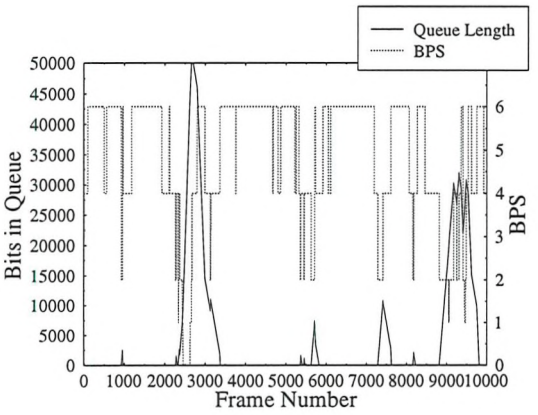

(a) Instantaneous length of the buffer and the instantaneous throughput

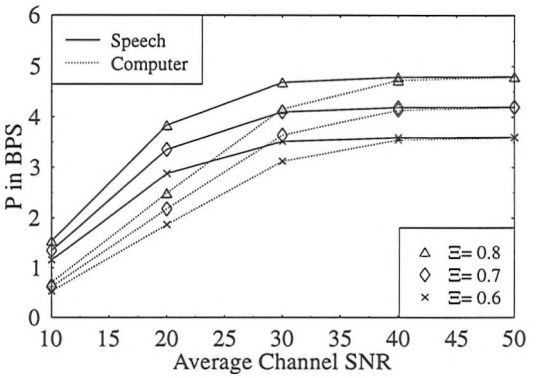

(b) BPS performance in terms of P for adaptive speech and computer data schemes, Ξ values of 0.6, 0.7 and 0.8 and for a range of average channel SNRs.

Figure 6.1: Queue length and Throughput for a typical adaptive modem

being employed in a Rayleigh fading channel is given by

$$p_{\text{no tx}} = 1 - \exp\left\{-\frac{N \cdot 10^{(l_1/10)}}{P}\right\}, \tag{6.2}$$

$$p_{\text{BPSK}} = \exp\left\{-\frac{N \cdot 10^{(l_1/10)}}{P}\right\} - \exp\left\{-\frac{N \cdot 10^{(l_2/10)}}{P}\right\}, \tag{6.3}$$

$$p_{\text{QPSK}} = \exp\left\{-\frac{N \cdot 10^{(l_2/10)}}{P}\right\} - \exp\left\{-\frac{N \cdot 10^{(l_3/10)}}{P}\right\}, \tag{6.4}$$

$$p_{\text{QAM 16}} = \exp\left\{-\frac{N \cdot 10^{(l_3/10)}}{P}\right\} - \exp\left\{-\frac{N \cdot 10^{(l_4/10)}}{P}\right\} \tag{6.5}$$

and

$$p_{\text{QAM 64}} = \exp\left\{-\frac{N \cdot 10^{(l_4/10)}}{P}\right\} \tag{6.6}$$

$$\tag{6.7}$$

for BPSK, QPSK, Square 16 QAM and Square 64 QAM respectively. These values may be computed in order to confirm the average BPS performance, B, which was given in Equation 4.6. Wang's model is based upon Lee's Level Crossing Rate (LCR) theory [27], that was discussed in Chapter 2. It is assumed that the gradient of the channel amplitude is constant over the period T. For the adaptive speech and data modulation schemes that are considered the switching levels are not close to each other. Therefore, this assumption about the channel amplitude gradient lead Wang to assume that if there is a change in the

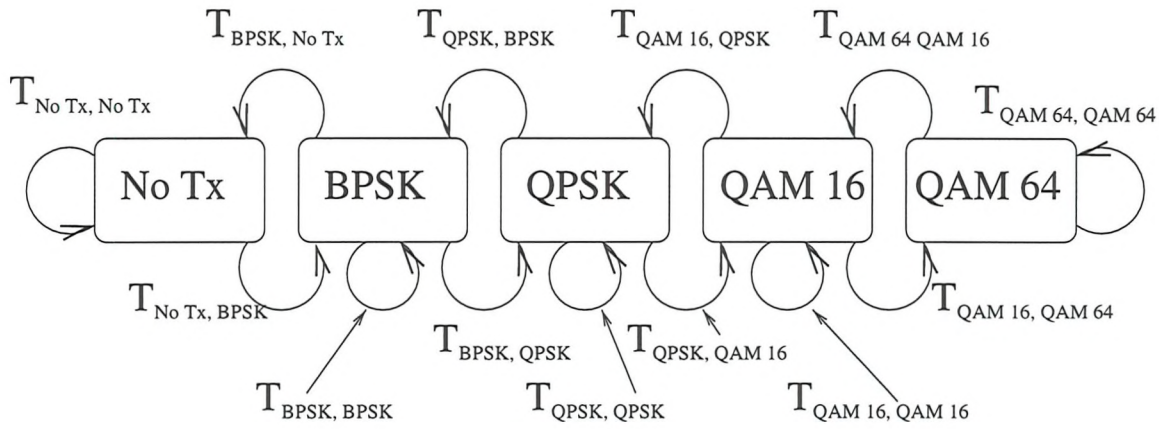

Figure 6.2: Markov model of where the rectangular states represent the modulation scheme employed with adaptive modulation in a Rayleigh fading channel assuming that adjacent frames employ the either the same, or adjacent, modulation schemes

transmission mode during the period T it may only be to an adjacent modulation scheme. For example, if BPSK is employed at time t then at $t+T$ the employment of Square 16 or 64 QAM will be excluded from the model. This is shown pictorially in Figure 6.2. The transition probabilities, $T_{j,k}$, from modulation scheme j to k, are given by Wang [150] as,

$$T_{\text{no tx,BPSK}} = \frac{f_d T \sqrt{\frac{2N\pi 10^{(l_1/10)}}{P}} \exp\left\{-\frac{N \cdot 10^{(l_1/10)}}{P}\right\}}{p_{\text{no tx}}}, \tag{6.8}$$

$$T_{\text{no tx,no tx}} = 1 - T_{\text{no tx,BPSK}}, \tag{6.9}$$

$$T_{\text{BPSK,no tx}} = T_{\text{no tx,BPSK}}, \tag{6.10}$$

$$T_{\text{BPSK,QPSK}} = \frac{f_d T \sqrt{\frac{2N\pi 10^{(l_2/10)}}{P}} \exp\left\{-\frac{N \cdot 10^{(l_2/10)}}{P}\right\}}{p_{\text{BPSK}}}, \tag{6.11}$$

$$T_{\text{BPSK,BPSK}} = 1 - T_{\text{BPSK,no tx}} - T_{\text{BPSK,QPSK}}, \tag{6.12}$$

$$T_{\text{QPSK,BPSK}} = T_{\text{BPSK,QPSK}}, \tag{6.13}$$

$$T_{\text{QPSK,QAM 16}} = \frac{f_d T \sqrt{\frac{2N\pi 10^{(l_3/10)}}{P}} \exp\left\{-\frac{N \cdot 10^{(l_3/10)}}{P}\right\}}{p_{\text{QPSK}}}, \tag{6.14}$$

$$T_{\text{QPSK,QPSK}} = 1 - T_{\text{QPSK,BPSK}} - T_{\text{QPSK,QAM 16}}, \tag{6.15}$$

$$\tag{6.16}$$

$$T_{\text{QAM 16,QPSK}} = T_{\text{QPSK,QAM 16}}, \tag{6.17}$$

$$T_{\text{QAM 16,QAM 64}} = \frac{f_d T \sqrt{\frac{2N\pi 10^{(l_4/10)}}{P}} \exp\left\{-\frac{N \cdot 10^{(l_4/10)}}{P}\right\}}{p_{\text{QAM 16}}}, \tag{6.18}$$

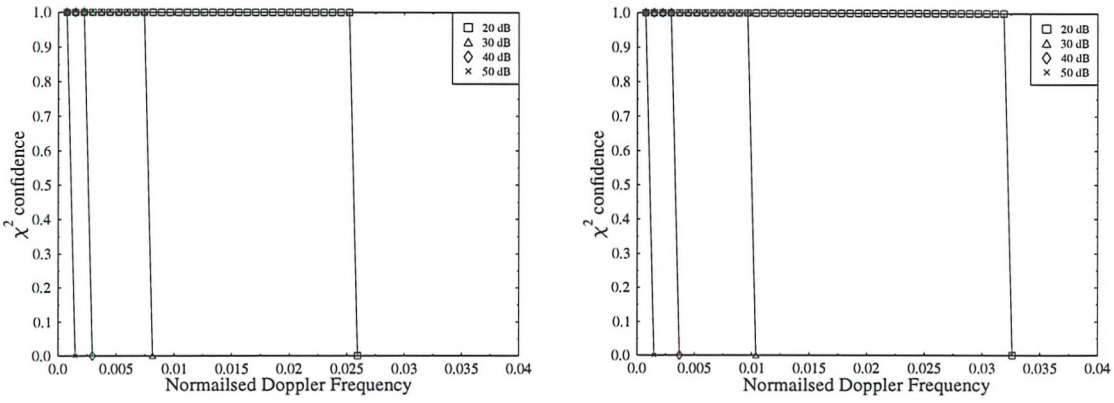

(a) Optimised Speech Switching Levels

(b) Optimised Computer Data Switching Levels

Figure 6.3: χ^2 confidence measure for Markov state transition probabilities for speech and computer data systems with average channel SNR of 20, 30 40 and 50 dB.

$$T_{\text{QAM 16, QAM 16}} = 1 - T_{\text{QAM 16,QPSK}} - T_{\text{QAM 16,QAM 64}}, \tag{6.19}$$

$$T_{\text{QAM 64,QAM 16}} = T_{\text{QAM 16, QAM 64}} \tag{6.20}$$

and

$$T_{\text{QAM 64, QAM 64}} = 1 - T_{\text{QAM 64,QAM 16}}. \tag{6.21}$$

$$\tag{6.22}$$

Values of T were evaluated exploiting Equations 6.8-6.22, with noise power, $N = 1$ and switching levels for the optimised speech and computer data systems from Table 4.1, at average channel SNRs of 20, 30, 40 and 50 dB, and with $f_d \cdot T$ values of $n \cdot 7.41 \times 10^{-4}$ where $n = 1 \ldots 100$. The transition probabilities were also evaluated by simulation under the same conditions. The simulated results were based upon the Rayleigh channels that were investigated in Chapter 2. The state transitions that resulted from the simulation were assumed to be correct as they were not based upon any assumptions as to the permitted state transitions and they were not constrained by constant amplitude gradients over the period T. The χ^2 test [15] was used to measure the significance of the comparison between the simulated transitions and those from Equations 6.8-6.22.

The results of the χ^2 confidence test are shown in Figure 6.3. There is a sharp cut-off where the confidence drops as a function of the normalised Doppler frequency. The normalised Doppler frequencies, where the χ^2 confidence level reflects the switch in acceptance of the Wang model are tabulated in Table 6.1. Inspection of this table reveals that, for both sets

	20 dB	30 dB	40 dB	50 dB
Speech	2.52×10^{-2}	7.41×10^{-3}	2.22×10^{-3}	7.41×10^{-4}
Computer Data	3.19×10^{-2}	9.64×10^{-3}	2.97×10^{-3}	7.41×10^{-4}

Table 6.1: Maximum normalised Doppler frequencies for which Wang's [150] Markov models show good correspondence with simulation

of switching levels, the maximum normalised Doppler frequency, for which Wang's model is acceptable increases with reduced average channel SNR; a phenomenon that is interpreted below. It is also apparent from the table that Wang's model is acceptable for higher normalised Doppler frequencies, when the computer data switching levels, rather than the speech switching levels, are employed. The Wang model becomes unacceptable at lower normalised Doppler frequencies, as the average channel SNR increases, because these conditions result in all the switching levels being deep in the fades. The fades are where the channel amplitude has the largest variation in gradient over the period T and, therefore, the state transitions predicted by Wang will become erroneous. The transition probabilities generated by the Wang model for the optimised speech switching levels are less acceptable at higher normalised Doppler frequencies, when compared to the optimised computer data levels. This is because the optimised computer data levels are further apart. Therefore, transitions from one modulation scheme to another non-adjacent scheme are less likely.

Adaptive modulation is likely to be implemented in a DECT-like system [29, 148], where the frame length is 10 ms, in an ATDMA environment [126] with 5 ms frame length or most likely within a proposed UMTS indoor environment [2], which has a frame length of 4.615 ms. Considering the 4.615 ms frame, if the Wang model is to be used for evaluation of the latency effects of adaptive modulation, for average channel SNRs up to 50 dB and for both computer data and speech models, the maximum Doppler frequency that can be successfully modelled is $3.19 \times 10^{-2}/4.615 \times 10^{-3} = 5.5$ Hz. Assuming the burst structure proposed by the pan-European FRAMES consortium, under the auspices of the Advanced Communications Technologies and Services (ACTS) programme, and a carrier frequency of 2 GHz, the maximum Doppler frequency of 5.5 Hz corresponds to a mobile velocity of 0.82 ms^{-1}, which is unacceptably low. Therefore, the Markov transition probabilities used to evaluate the latency are generated by simulation. Furthermore, these simulated transition probabilities include the finite probability of transition to and from non-adjacent transmission modes. The Markov transition probabilities for a Rayleigh channel were evaluated by simulation for average channel SNRs of 10, 20, 30, 40 and 50dB, and for normalised Doppler frequencies of 0.0042, 0.025, 0.054, 0.079 and 0.133, using both the peak and mean BER 1% and 0.01%

(speech and computer data system) switching levels.

6.4 Experimental Frame-work

In order to stipulate some parameters, the general issue of latency in adaptive modulation is considered complying with the FRAMES consortium approach. The current FRAMES proposal in the 2GHz band includes a TDD option with a 4.615 ms frame duration, up to 64 slots per frame for 2GHz transmission. Including adaptive modulation in this frame-work, and exploiting passive reception of the preceeding time-slot (Section 7.2.1) results in a temporal difference of 72μs between channel estimation and transmission. At 5 ms^{-1} this corresponds to 360 μm or 0.24 % of the carrier wavelength. Therefore, it is assumed that the the channel does not vary significantly between estimation and transmission.

Accordingly, every 4.615 ms the transmission scheme to be employed by a particular user will be evaluated. The Doppler frequency, normalised to the transmission frame rate, will determine how often the employed transmission scheme will actually vary. The transmission scheme for a particular user was modelled with a Markov model where the transition probabilities were evaluated by simulation for the values given in Section 6.3. At 2 GHz and at a frame duration of 4.615 ms the various models correspond to mobile velocities of 0.136, 0.812, 1.75, 2.57 and 4.32 ms^{-1}.

6.5 Single Slot performance

The initial evaluation of the latency considers a single user being allocated a single slot, within a TDMA/TDD frame, for the up-link, which is immediately followed by the down-link slot for the same user. It is assumed that the desired throughput for the up- and down-links are the same. Furthermore, because the channel is assumed to be reciprocal, the latency experienced by both the up- and down-link transmissions are the same. Every user may employ no transmission, BPSK, QPSK, Square 16 or 64 QAM in the slot allocated to them. The same modulation scheme must be employed over the full length of the slot. The duplex scheme is balanced, that is, the up- and down-links carry the same number of bits. It was also assumed that the buffer was initially empty.

If there was insufficient data in the buffer to exploit the full capacity of the channel at a given transmission instant then extra dummy bits would be added to fill the burst. The extra signalling to manage this is not considered here, although, it should be arranged such that

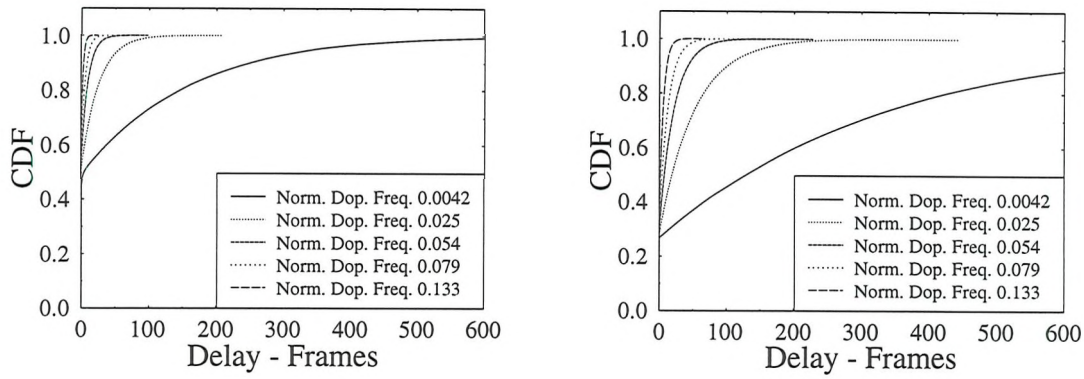

(a) Speech system

(b) Computer data system

Figure 6.4: CDF of delay expressed in terms of 4.165 ms frames for speech and computer data transmission with Ξ of 0.6 and various normalised Doppler frequencies.

no signalling bits are transmitted when the latency is close to the system specified maximum. One solution would be a control word or bit-stuffing.

The delay for a single user, that is allocated a single slot, transmitting through a Rayleigh fading channel was evaluated assuming the previously mentioned FRAMES configuration. Cumulative Distribution Functions (CDFs) of the number of frames, by which each bit was delayed, were evaluated for 2×10^6 frames, with Ξ of 0.6, 0.7 and 0.8, average channel SNR of 10, 20, 30 40 and 50 dB, normalised Doppler frequencies of 0.0042, 0.025, 0.054, 0.079 and 0.133, and for both the optimised speech and computer data transmission switching levels in the absence of interference. It should be noted that during this evaluation of latency there was no arbitrary limit upon the buffer length. However, in Section 6.9.3 where adaptive modulation is implemented in comparative study, the buffer is constrained to the maximum allowed latency. Figures 6.4(a) and 6.4(b) are examples of such delay CDFs, expressed in terms of the number of 4.615 ms frames for Ξ=0.6, for various normalised Doppler frequencies and for speech and data schemes, respectively.

Observe in the Figures that in both cases the delay increases with slower normalised Doppler frequencies. As expected, due to its more stringent BER, the computer data system also results in longer delays than the speech system. The effect of a lower normalised Doppler frequency is to prevent the transmission scheme changing very frequently and, therefore, there are relatively long periods where the transmission throughput is higher than the input rate, followed by relatively long periods of the reverse situation. This is what results in bursts

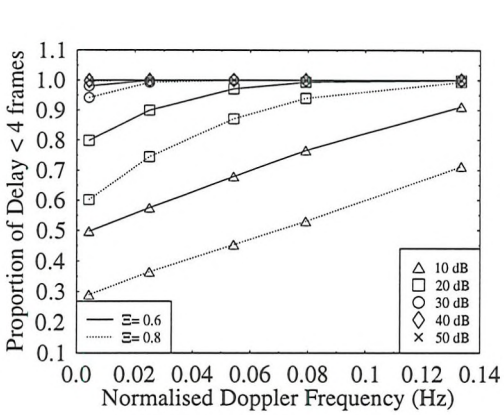

(a) Proportion of transmitted bits in speech system, experiencing four or fewer frames latency.

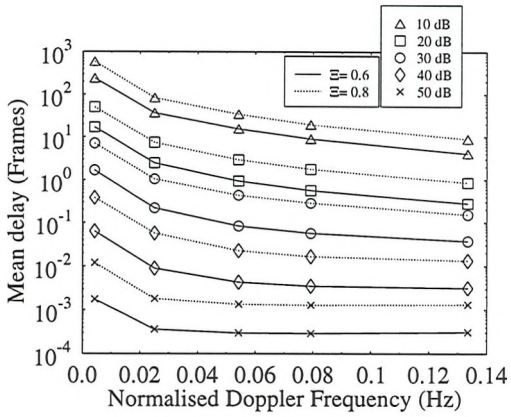

(b) Mean delay of bits expressed in terms of the number of frames for the computer data system

Figure 6.5: Delay through a Rayleigh fading channel as a function of normalised Doppler frequency for, Ξ of 0.6 and 0.8, and average channels SNRs of 10, 20, 30, 40 and 50 dB

of latency. At higher normalised Doppler frequencies the transmission scheme changes more frequently and the latency is reduced. The probability of the buffer becoming empty was also examined, which would result in a potential waste of channel capacity when the channel conditions are favourable. It was found that in all simulations the total throughput was only marginally less than the target value of $\Xi \cdot B$. The marginal difference was accounted for by the number of bits left in the buffer at the end of the simulation. Therefore, although lower normalised Doppler frequencies tend to result in greater latency, they do not affect the capacity of the channel, in terms of the number of bits transmitted for a particular average channel SNR.

For the speech system a maximum of four frames latency introduced by the modem was considered acceptable, which corresponded to less than 20 ms, or one typical linear predictive analysis speech coding frame duration [151]. The delay CDFs were processed in order to determine the proportion of bits that were transmitted within the acceptable four frame latency. For the computer data system no maximum delay was imposed, instead, the mean delay was considered. Figures 6.5(a), 6.5(b), 6.6(a) and 6.6(b) illustrate these measures of latency for both systems as a function of normalised Doppler frequency and average channel SNR.

Figure 6.5(a) shows that an increased normalised Doppler frequency reduces the latency, particularly when the average channel SNR is low. This improvement results from the reduced

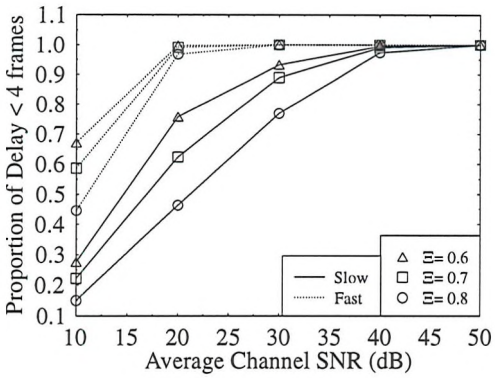

(a) Proportion of transmitted bits in speech system, experiencing four or fewer frames latency.

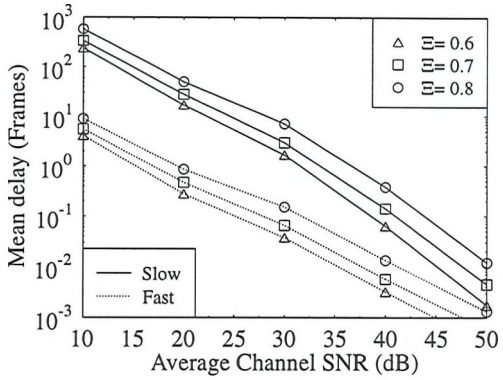

(b) Mean delay of bits expressed in terms of the number of frames for the computer data system

Figure 6.6: Delay over a Rayleigh fading channel as a function of average channel SNRs for Ξ values of 0.6, 0.7 and 0.8, and normalised Doppler frequencies of 0.004170 (Slow) and 0.133427 (Fast).

number of adjacent 'No Transmission' frames. At 30 dB, the probability of 'No Transmission' is very low and, therefore, even a highly correlated, slowly fading channel results in only a few adjacent 'No Transmission' frames. By considering the transition probabilities for the Markov model this can be confirmed. For example in a slow-fading channel, exhibiting a normalised Doppler frequency of 0.004170 at 10 dB average channel SNR, the probability of 'No Transmission' was 0.192 and the probability of remaining in 'No Transmission', given that this is the current transmission scheme is 0.980. By contrast at 30 dB these probabilities became 0.0021 and 0.775, respectively, which reflects the dramatic reduction in delay inferred from Figure 6.6.

At the average channel SNRs shown in Figure 6.5(a), in excess of 20 dB, the latency performance is nearly always acceptable for speech systems, irrespective of the Ξ value, when the normalised Doppler frequency is 0.025 or greater. However, at lower average channel SNRs the Ξ value has a greater bearing upon the latency. Therefore, in principle the speech codec could be re-configured depending upon the average channel SNR. This re-configuration would be similar to that proposed by Woodard [115]. However, rather than reducing the codec rate because of increased transmission error, it would be reduced on the basis of the latency ramifications resulting from lower average channel SNRs.

Observing Figure 6.5(b) reveals that the mean delay for the computer data system is also

reduced as the normalised Doppler frequency increases. It is interesting to note that for all Ξ values and all average channel SNRs the shape of the curves in the Figure is similar. Bearing in mind the logarithmic nature of the y-axis, this figure again shows that the increased de-correlation in the channel has greater effect upon the latency of systems under low average channel SNR conditions. Furthermore, most of the delay-reduction is observed due to the initial increases in normalised Doppler frequency, whereas for values in excess of about 0.02 the curves become more flat.

Figure 6.6(a) shows how the latency performance of the fast and slow fading channels, associated with Doppler frequencies of 0.004170 and 0.133427, respectively, converge at high average channel SNRs. This is because the instantaneous channel SNR is virtually always greater than l_4 and, therefore Square 64 QAM is always employed, irrespective of the normalised Doppler frequency. At 20 dB average channel SNR the latency is almost independent of Ξ for the faster fading channel, while for the lower fading rate there is nearly a factor of two performance difference between Ξ values of 0.6 and 0.8. This reflects the highly non-linear nature of the latency performance.

Figure 6.6(b) show the convergence in latency performance for both fading rates at high average channel SNRs. The Figure shows that an increased average channel SNR results in more significant benefits in latency performance for slower fading by having a steeper gradient for those results. However, the increased additional average channel SNR also increases the average BPS performance, $\bar{B}$, as shown in Figure 6.1(b). In this context increasing the average channel SNR reduces the latency while increasing the throughput.

The latency ramifications of adaptive modulation in a variety of scenarios have been considered. The following two sections consider techniques to mitigate the latency introduced by adaptive modulation.

6.6 Frequency Hopping

The results above show that reduced correlation in the fading channel reduces latency in an adaptive modulation scenario. Further, the correlation may be reduced by including frequency hopping into the system. This has no adverse effects upon the channel estimation when it is performed using the passive reception technique introduced in Section 7.2.1. The other advantage of de-correlating the fading is that the mean BER will tend towards the BER experienced in all the of source coded frames. This vindicates the decision to use the mean BER switching levels, from Section 4.3.6 for these experiments rather than the peak BER

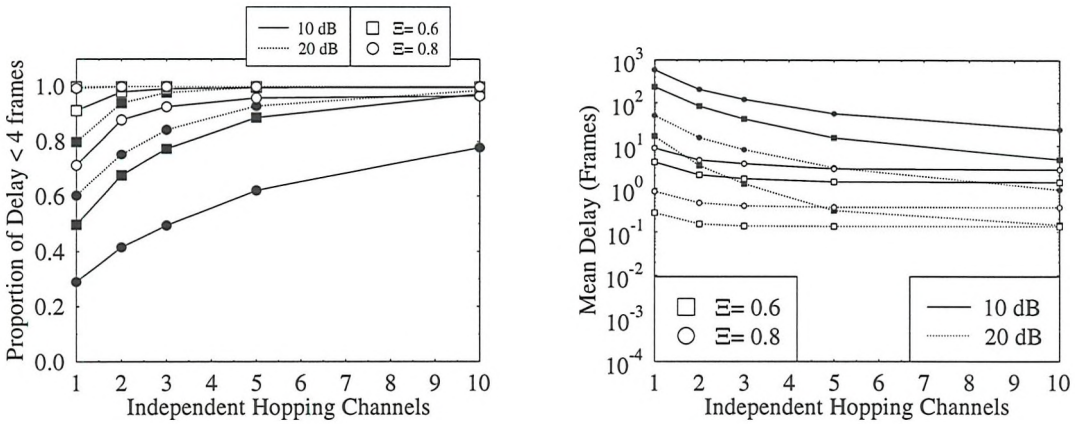

(a) Proportion of transmitted bits in speech system, experiencing four or fewer frames latency.

(b) Mean delay of bits expressed in terms of the number of frames for the computer data transmission system

Figure 6.7: Delay through independent frequency hopped channels for 10 and 20 dB average channel SNR, Ξ values of 0.6 and 0.8, and normalised Doppler frequencies of 0.004170 (Slow) and 0.133427 (Fast). Bold markers correspond to slow, hollow ones to fast fading.

switching levels from Section 4.4.

The frequency hopping was simulated assuming M independent fading channels, with a frequency hop every frame. All of the previous experiments were repeated employing $M = 2, 3, 5$ and 10 fading channels. Figures 6.7(a) and 6.7(b) show the effect of M independent frequency hopped channels upon the latency for the speech and computer data transmission systems, for 10 and 20 dB average channel SNR, Ξ values of 0.6 and 0.8, as well as for normalised Doppler frequencies of 0.004170 (Slow) and 0.133427 (Fast). These Figures reveal that significant reductions in delay may be achieved by introducing frequency hopping to an adaptive modulation scheme. Ten hopping frequencies allow virtually all bits under all circumstances in the speech system to exhibit less than four frames latency. Observe in Figure 6.7(b) for the computer data system that all mean delays are reduced below 20 frames, which is equivalent to 92 ms.

6.7 Statistical Multiplexing

From a base-band performance perspective frequency hopping offers a solution to the latency problems associated with adaptive modulation. Further, a careful frequency and hopping

Modulation Scheme	Slots Occupied
No Transmission	2
BPSK	8
QPSK	6
Square 16 QAM	4
Square 64 QAM	2

Table 6.2: Total number of up- and down-link slots in a frame for balance TDD with statistical multiplexing.

plan could be exploited to mitigate some interference effects [1, 136]. However, the FRAMES proposals support 32 duplex users per carrier with each carrier occupying 1.6 MHz. Therefore, 16 MHz would be required to support 10 carriers which would equate to a maximum 320 users. If less spectrum was available then frequency hopping would not be suitable for mitigating the delay. Also, there are complex practical radio issues associated with frequency hopping in terms of synthesiser design. Therefore, other techniques must be considered.

Pearce et al [152] considered allowing users to occupy a varying number of slots on the basis of the traffic, the modulation scheme, and path-loss that is experienced. In Asynchronous Transfer Mode [153] (ATM) systems the number of ATM cells transmitted increases with higher traffic demands. Williams et al [154] considered employing Packet Reservation Multiple Access (PRMA) combined with different modulation schemes to accommodate different average channel SNRs across a cell. These ideas are based on the bursty nature of speech data, assuming that a speech codec with Voice Activity Detection (VAD) is used [155, 156, 157, 158]. Here a different statistical multiplexing scheme is exploited to mitigate the delay in an adaptive modulation scheme. It is only considered for the speech switching levels because the computer data is less dependent upon system latency.

The number of slots allocated to a user is adaptively controlled in order to compensate for the variation in transmission scheme. Table 6.2 shows how many slots will be used for each scheme. As the channel conditions deteriorate, the modulation order is reduced and, therefore, the number of slots per frame is increased. These increases in demand for slots in a frame should be independent for all users and, therefore, with a sufficient number of users the variation in demand should be averaged. When the channel becomes so poor that transmissions will result in an unacceptable error-rate, that is the modem is in the 'no transmission' mode, no slots need to be occupied for transmission, however, 1 up- and 1 down-link slot is reserved for channel estimation.

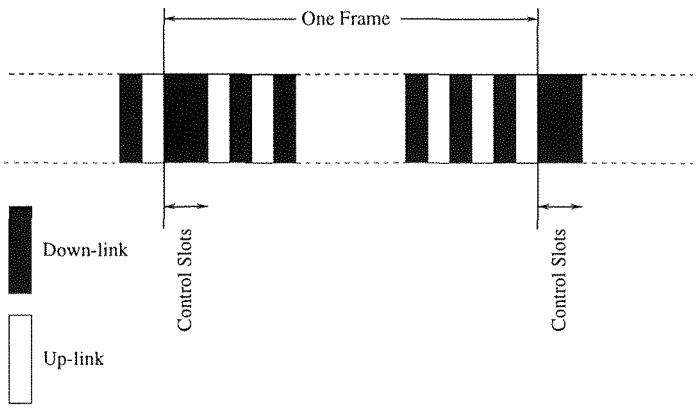

Figure 6.8: TDD/TDMA frame for employment of statistical multiplexing evaluation of latency in FRAMES TDD mode.

6.7.1 Implementation

With adaptive modulation the variation in throughput is bursty. Therefore, similar techniques, to those that have been used for speech multiplexing using VADs, may be used to statistically multiplex the transmission of adaptive modulation bursts. However, rather than a VAD determining whether a slot will be occupied or not, the number of slots used by each mobile will vary depending upon the channel conditions. Figure 6.8 shows a FRAMES TDD/TDMA frame. The number of slots that are occupied by each user in the frame will vary. If a user's channel improves, such that a more efficient modulation scheme may be employed, the mobile will not transmit in certain slots. This will de-allocate slots that were reserved for that user. Other users may contend for slots by transmitting in time slots that are not allocated to other users. All mobiles are aware of which slots are allocated to which user on the basis of the broadcast information contained in the control slots.

Without statistical multiplexing a slot is allocated to a user unconditionally. Therefore, if the user cannot completely fill that slot with information bits it is still worth transmitting the few information bits that are in the buffer along with some dummy bits as explained in Section 6.5. However, with statistical multiplexing a slot only partially filled with information bits by one user could have been completely filled with information bits by another user. Therefore, in the statistical multiplexing experiments a slot that would have only partially be filled with information bits is not transmitted and the bits are queued for the next frame. Figure 6.9 illustrates the operation of the base-station for employing statistical multiplexing. The processes in the flow-chart are now elaborated upon:

1. **Control slots**: The base-station occupies the first two of the 64 FRAMES slots. These

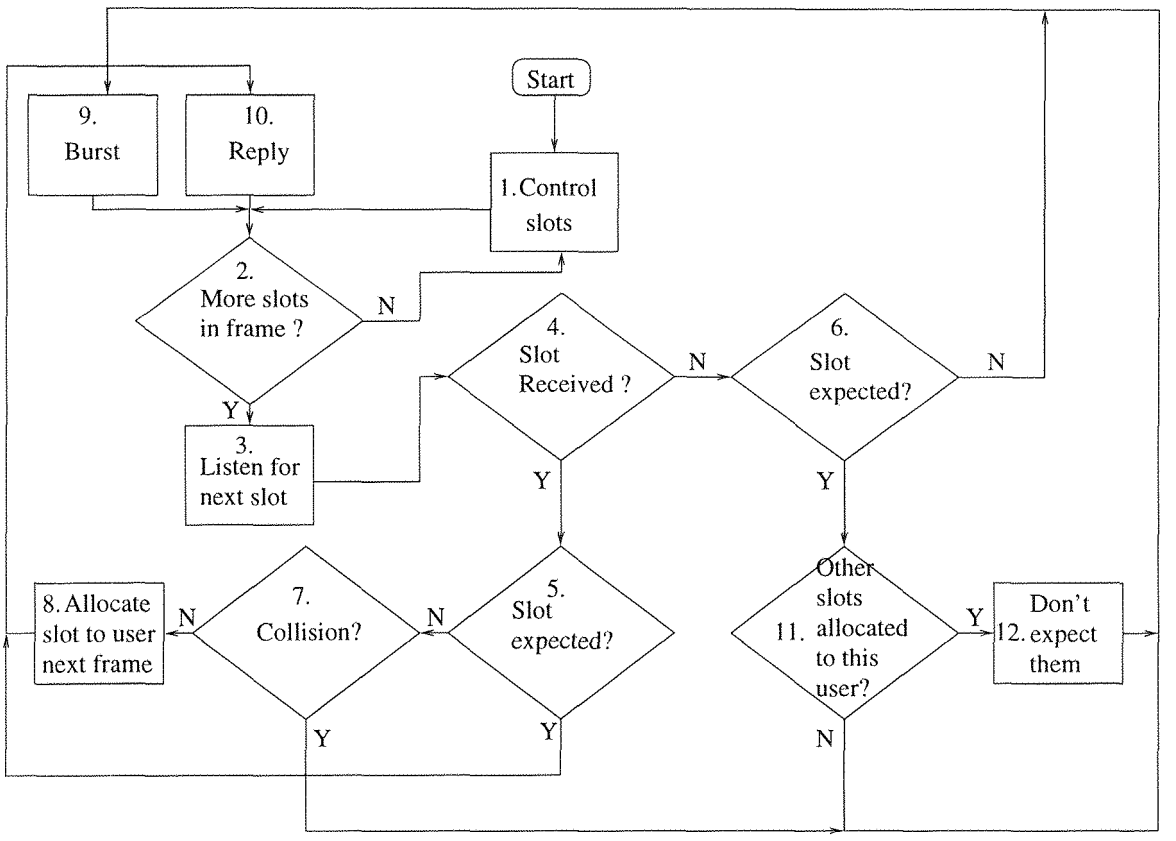

Figure 6.9: The base-station implementation of statistical multiplexing algorithm

slots communicate to each user which slots are allocated to them on the basis of their requirements in the previous frame. All users receive these slots and it is assumed that they are received error free. The slots are allocated so that for each user all of the pairs of up- and down-link slots in a particular frame are next to each another.

2. **More slots in frame?**: If there are any more slots in the frame (ie the last slot transmitted was not number 64) then they must be processed, otherwise, the base-station transmits another pair of control slots.

3. **Wait for next burst**: The base-station waits for a received burst.

4. **Burst received?**: The base-station determines whether a burst was transmitted by any mobile.

5. **Burst expected?**: If any mobile did transmit in the slot, was it the mobile that was allocated that slot in the control slots? An unexpected mobile transmission could only happen if the slot was not allocated to a specific user in the control slot. This, of course, is on the premise that the control slot is successfully received.

6. **Burst expected?**: If no mobile transmitted in the slot, was the slot allocated to a particular user? This would be the case, if a slot had been allocated to a user, but that user did not have sufficient data to make transmission worthwhile. Alternatively, the channel quality was so bad that the mobile decided not degrade the BER performance by transmitting.

7. **Collision?**:If more than one burst was received, then the received energy will be high but the data will be corrupted, which will result in a collision condition. In this evaluation no, so-called packet capture is considered, however, this is considered in Section 6.8.

8. **Allocate slot to user**: This slot is now allocated to the user in question for future frames.

9. **BS transmits Burst**: No users have used the previous up-link slot so the base-station transmits a burst as a beacon for any users, who wish to transmit in the next slot in order to obtain a measure of the channel quality.

10. **Reply**: One and only one user has transmitted in the previous up-link slot. On the basis of the channel quality the base-station replies using the appropriate modulation scheme. All users, who were permitted to transmit in the next up-link slot, will passively receive this down-link burst in order to estimate the channel.

11. **Other slots allocated to this user ?**: Were there any slots in positions after the current one in the frame allocated to the user who did not transmit in this one?

12. **Do not further bursts**: Other slots allocated to the user in the frame will be available for other users in this and following frames.

Having considered the base-station's actions, Figure 6.10 illustrates the operation of the mobile-station for using statistical multiplexing. The processes in the flow-chart are now elaborated upon:

1. **Get Bits from codec**: Every frame the source and channel codec supply the modem with $\Xi \cdot B$ bits to be transmitted, where B is dependent upon the average channel SNR.

2. **MS receive control bursts**: All mobiles receive the control slots and identify which slots they will be using. They also identify which slots are un-allocated so that they may contend for them if necessary. Furthermore, they identify which slots are used by other users because if a user does not use a slot that is allocated to them, any other

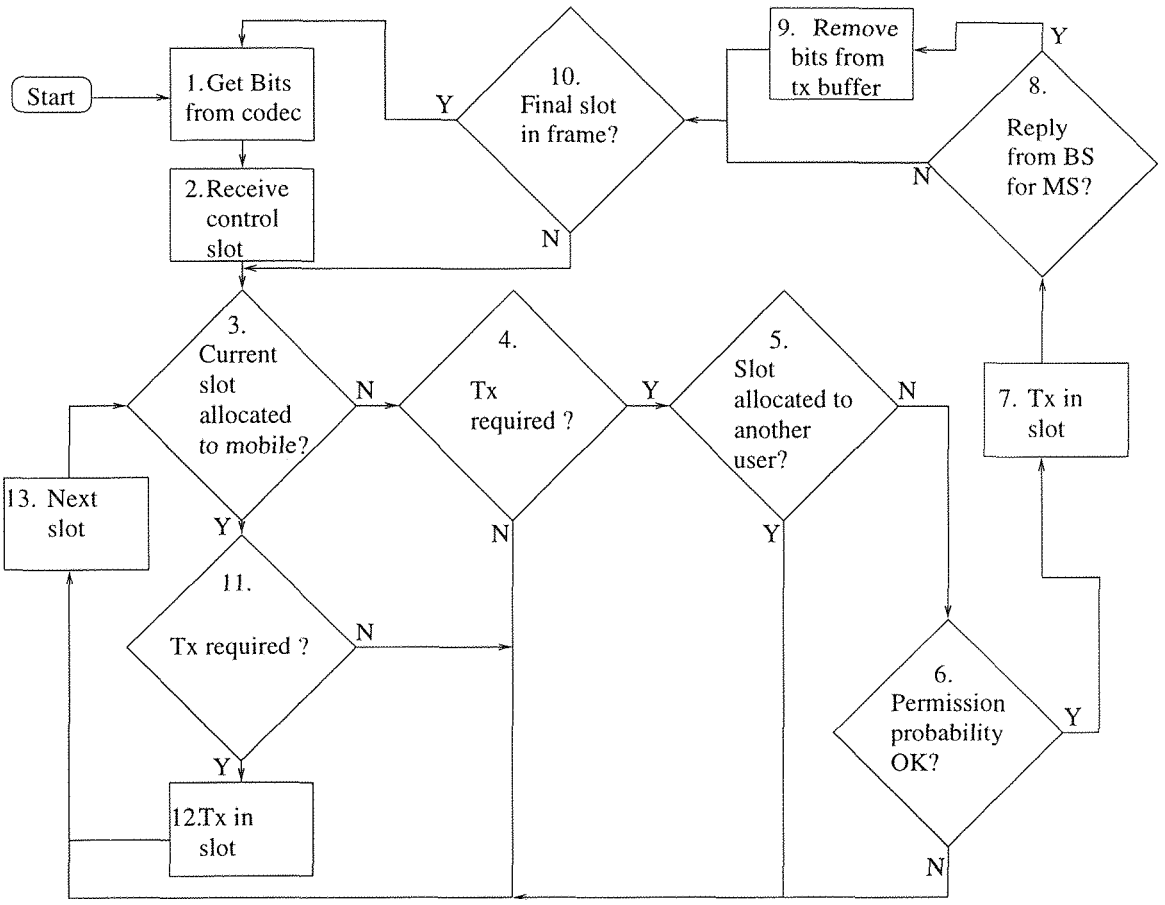

Figure 6.10: The mobile-station's statistical multiplexing algorithm

slots in the frame which were originally allocated to them are available to other mobiles. The received control bursts are also used for the first estimation of the instantaneous SNR.

3. **Current slot allocated to mobile?**: Determine whether the current slot is allocated to the user by referring to the received control burst.

4. **Tx Required?**:Are there sufficient bits in the buffer to fill a slot of symbols employing the current modulation scheme? The current modulation scheme is determined by evaluating the signal level of the burst received in the phases 'Receive control slots', 'Reply from BS to MS' or 'Next slot'.

5. **Slot allocated to another user?**: By referring to the received control slots determine if the current slot is allocated to another user? Even if the slot was allocated to a specific user in the control burst, the user may have forfeited an earlier slot in this frame which will mean that it will have implicitly de-allocated itself from this slot.

6. **Permit to contend?**: Generate a random number, and if this random number is below some system parameter then permission to contend is given. Otherwise it is not.

7. **Tx in slot**: The mobile acts as if the slot was allocated for their transmission but does not remove the transmitted bits from the buffer

8. **Reply from BS to MS?**: Receive the next burst from the base-station and estimate the instantaneous SNR. After decoding the header, determine if the response from the base-station was addressed to this mobile. If it was the burst (from Phase 7) was successful and that slot will be allocated to this mobile in the next frame.

9. **Remove bits from Tx buffer**: If the (phase 7) burst has successfully been received then the transmitted bits may be removed from the buffer.

10. **Final slot in frame?**: Determine if this is the final slot in the frame

11. **Tx Required?**: As phase 4.

12. **Tx in slot**: The slot is allocated to the user and therefore it transmits removing, the bits from the buffer.

13. **Next slot**: Use passive reception in order to determine the instantaneous SNR by receiving the down-link's burst.

Below it will be demonstrated that statistical multiplexing will result in reduced latency. This will allow the system throughput to be close to the mean theoretical BPS, that is, Ξ may be increased without introducing unacceptable delay. An alternative view is that statistical multiplexing mitigates the varying throughput that results from adaptive modulation. However, statistical multiplexing will result in the expected BER of a frame varying above and below the mean BER. This scenario is exemplified by the situation where the fading is extremely slow and transmission of several frames takes place when the SNR is either slightly above, or below, a switching level. Specifically, if the SNR is slightly above a switching level then an intolerable burst of errors may be experienced. Therefore, the peak BER switching levels that were discussed in Section 4.4 and shown in Table 4.4 will be used in the following experiments. This reduces the overall system capacity, as shown in Figure 4.16.

The statistical multiplexing scheme was evaluated for 5, 10, 15, 20, 25 and 30 users and 20, 30, 40 and 50 dB average channel SNRs. In all cases $\Xi = 0.8$, the peak BER switching levels were used and for each simulation all users were assumed to be receiving the same average channel SNR. The performance was only evaluated for the 1 % BER adaptive scheme and

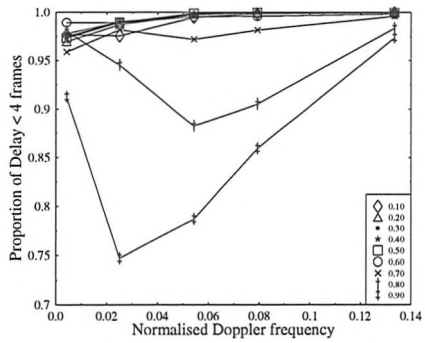

(a) 15 users with 20 dB average channel SNR

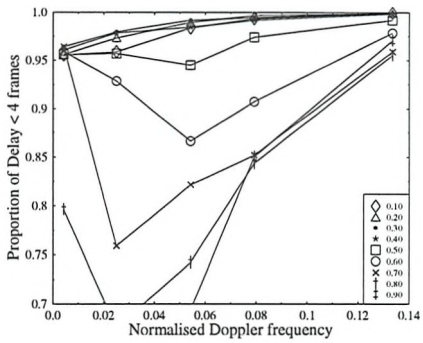

(b) 20 users with 20 dB average channel SNR

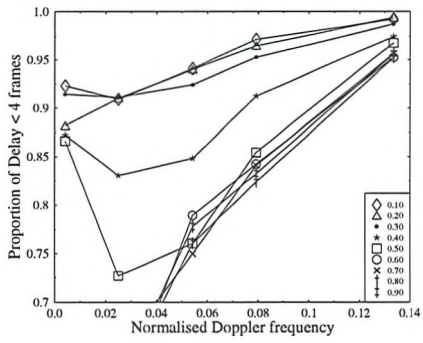

(c) 25 users with 20 dB average channel SNR

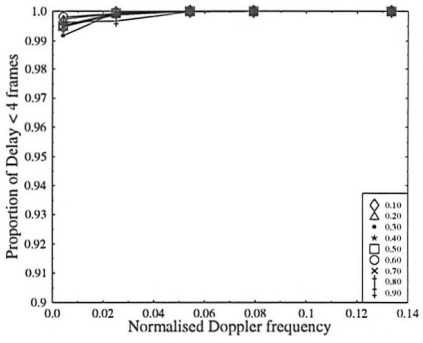

(d) 25 users with 30 dB average channel SNR

Figure 6.11: Proportion of speech frames delayed more than four frames for permission probabilities of $p = 0.1, 0.2, \ldots 0.9$, for a Ξ value of 0.8 with various average channel SNRs and a range of normalised Doppler frequencies.

results were obtained for normalised Doppler frequencies of 0.0042, 0.025, 0.054, 0.079 and 0.133, which correspond to mobile velocities of 0.136, 0.812, 1.75, 2.57 and 4.32 ms^{-1}.

Tables 6.3 and 6.4 summarise how many users may be accommodated on a single FRAMES carrier with a 99 % and 95 % probability of a four or fewer frame delay being incurred. When all users experience 40 or 50 dB average channel SNR, 30 balanced duplex users can be accommodated, assuming the FRAMES configuration. There is a limit of 31 duplexed users because the proposed statistical multiplexing algorithm maintains one pair of slots for each user, even if they are not transmitting, as was shown in Table 6.2. Furthermore, one pair of slots are used for sending the control information for the statistical multiplexing, as

SNR	50 dB	40 dB	30 dB	20 dB
Users Accommodated	30 users for all p.	30 users for all p.	25 users for all p. 30 users for $f_dT \geq 0.025$ and $p \neq 0.1$,0.7,0.8 or 0.9.	15 users for $f_dT \geq 0.025$ and $p \neq 0.1$,0.2,0.6 0.7,0.8 or 0.9.

Table 6.3: Number of users that can be accommodated in Rayleigh fading when all users are at the same average channel SNR for a range of normalised Doppler frequencies using statistical multiplexing with 99 % of frames being delayed less than the duration of 4 frames. The permission probability is p.

SNR	50 dB	40 dB	30 dB	20 dB
Users Accommodated	30 users for all p.	30 users for all p.	30 users for all p.	15 or 20 users for $p \neq 0.5$, 0.6, 0.7, 0.8 or 0.9.

Table 6.4: Number of users that can be accommodated in Rayleigh fading when all users are at the same average channel SNR for a range of normalised Doppler frequencies using statistical multiplexing with 95 % of frames being delayed less than the duration of 4 frames. The permission probability is p.

seen in Figure 6.8.

The performance of the statistical multiplexing scheme is considered in more detail at SNRs of 20 and 30 dB in Figure 6.11. Figure 6.11(a) shows that a high permission probability, p, increases the delay since there are too many collisions and renewed contentions. However, a large p has greater negative effect at 0.025 normalised Doppler frequency than at 0.0042. This is because at very low normalised Doppler frequencies the modulation scheme employed on a particular base-station to mobile-station link changes very infrequently. Therefore, extra slots are rarely required and consequently contention rarely occurs. However, as the normalised Doppler frequency increases slots in the frame are exchanged between users more frequently and the probability of contention increases. This increase in contention is superimposed on the effect that also as the normalised Doppler frequency increases the adaptive scheme's throughput varies less from the average throughput and therefore fewer symbols spend as much time in the buffer. Comparing Figure 6.11(a) with 6.11(b) shows how the probability of unacceptable delay increases as the number of users is increased by 33 %. The delay becomes worse at all normalised Doppler frequencies and p becomes a more critical parameter after this

increase of the number of users. A further increase by the same number of users is illustrated by Figure 6.11(c). Again, the delay performance becomes worse at all normalised Doppler frequencies. Also shown in this Figure is, with 20 dB average channel SNR and 25 users that the contention at very low normalised Doppler frequencies results in catastrophic delays if $p \geq 0.60$. From figures 6.11(a), 6.11(b) and 6.11(c) it was decided to use a permission probability of 0.3. Figure 6.11(d) shows the effect of increasing the SNR from 20 to 30 dB with respect to Figure 6.11(c).

6.8 Burst Capture and Assisted Capture

From Goodman's pioneering work on PRMA [155, 156] the principle of packet capture was identified and it may be applied to the statistical multiplexing techniques proposed here for adaptive modulation. Packet capture is defined as the situation where two or more users contend for the same slot, however, because of the relative strengths of the received signals at the base-station one user's burst may be received with considerably more power than the of the other. Therefore, it is possible that the slot received with the greatest power may be successfully decoded and the other contending slot(s) may be considered as interference.

An extension to this packet capture, a technique referred to as assisted packet capture, using similar interference cancellation algorithms to those proposed in Section 5.5 is considered. At least in principle, it is possible to successfully decode two simultaneous contending slots. This may be considered overly ambitious, however, decoding one user and identify which other user was contending for the slot is less demanding and conveniently fits into the statistical multiplexing protocol proposed. How this is achieved may be understood by considering block (7) in Figure 6.9. Rather than just dropping the bursts if there is a collision there are three alternatives:

1. One of the colliding bursts may be successfully decoded and the other completely lost, which is classic packet capture and flow will pass to block (8) in Figure 6.9.

2. One burst may be successfully decoded and the identity of the other may be extracted by the interference cancellation techniques. Therefore, the flow will pass to block (8) in Figure 6.9 but additionally the identity of the contenting user will be added to a list of users who have requested extra slots. Next time that the control slots are transmitted, in block (1) of Figure 6.9, users from this list will be selected for any available slots.

3. Neither capture nor the assisted capture are successful and therefore both packets are lost and neither users are allocated extra slots in the next frame.

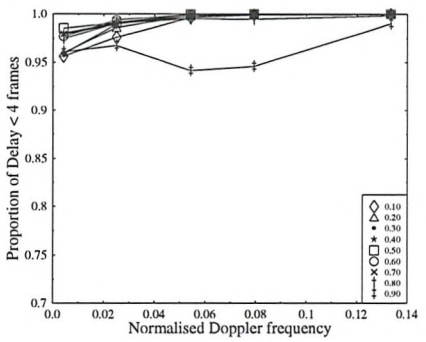

(a) 15 users with 20 dB average channel SNR

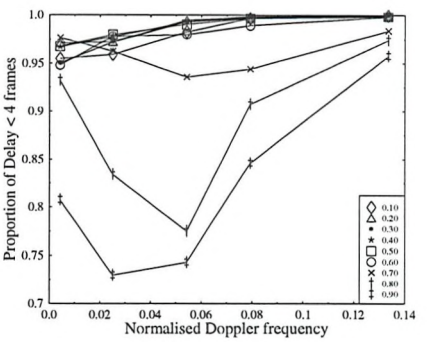

(b) 20 users with 20 dB average channel SNR

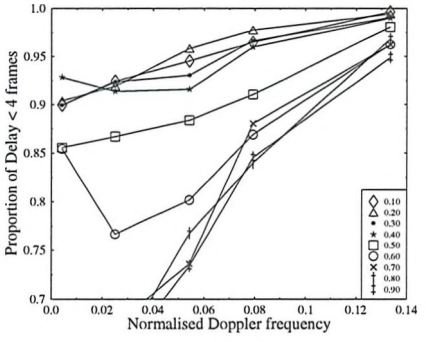

(c) 25 users with 20 dB average channel SNR

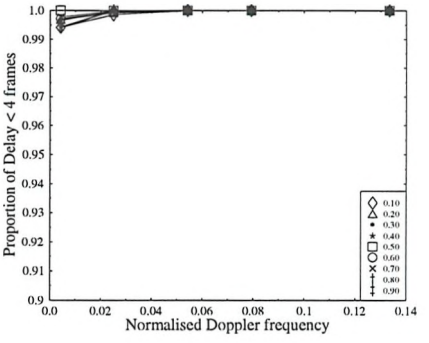

(d) 25 users with 30 dB average channel SNR

Figure 6.12: Proportion of speech frames delayed more than four frames, with capture and joint detection, for permission probabilities of $p = 0.1, 0.2, \ldots 0.9$, for a Ξ value of 0.8 with various average channel SNRs and a range of normalised Doppler frequencies.

The relative probabilities of these three events depend upon many factors, such as the distance of all the mobiles from the base-station, the transmitted power, the time and phase synchronisation, which are explained in Section 5.3.1. Therefore, in order to determine the potential gains of packet capture and assisted packet capture, the previous experiments conducted without capture were repeated. In the event of two and only two users contending for a slot, one of the three events above were chosen at random with each having the same probability. The results are shown in Figure 6.12. The primary observation, in comparison with Figure 6.11, is that at 20 dB, with 15 and 20 users, the performance of the worst case permission probabilities improves significantly. However, the performance of the best case permission probabilities only improve marginally. With 25 users the performance changes

only slightly and $p = 0.3$ is still the overall preferred permission probability.

The apparent small benefit of employing capture and assisted capture can be explained as follows. Both capture and assisted capture will reduce the effect of collision upon the delay if there is sufficient capacity in the TDD/TDMA frame by using the available slots with fewer contentions. This is the mechanism for improvements that are seen when p is high. However, neither technique can mitigate the delay caused when the capacity of the frame is insufficient to support all of the users, that is, when several users are transmitting using BPSK. It is for this reason that there is little significant improvement in the best case permission probability scenarios.

Therefore, it is concluded that both capture and assisted capture offer only marginal benefit to reducing the number of frames delay to fewer than four slots if capture and assisted capture are achieved 66 % and 33 % respectively for two user collisions.

6.9 Comparison with fixed modulation, using block coding

6.9.1 Background

In previous Sections the performance of adaptive and fixed modulation schemes have been discussed. The average BER performance has been discussed for both schemes in Rayleigh fading channels. The effects of latency for adaptive modulation have been investigated and two techniques have been discussed to mitigate the latency, namely frequency hopping and statistical multiplexing. It was shown in Figure 4.16 that the potential performance enhancement achieved by adaptive modulation over fixed modulation in a fading channel is higher for lower target BERs. These lower BERs are consistent with the quality of service for a data link, where latency is not a critical issue for transmission. Therefore, there is a very strong case to employ adaptive modulation for computer data communications. However, in this case study the performance of adaptive modulation in a latency constrained environment with a relatively high target BER is explored. There is a less obvious case to employ adaptive modulation in such an environment and will, therefore, represent a more rigorous test of the adaptive modulation technique, when compared with fixed modulation.

The adaptive and fixed modulation techniques are compared in terms of how many duplex users they can support on a single frequency at practical indoors velocities. Block coding is employed and an indoor propagation environment is assumed. The data frames are 4.615 ms in duration, they contain 64 slots each with a payload of 64 data symbols and because of ramp, guard and training symbols, the gross symbol rate is 1.3 MBd. A continuous balanced

Fixed Scheme	Bits Per Slot	Slots Per Frame	Bits Per Frame	Block Code	Codewords Per Frame	Info Bits Per Frame
BPSK	64	6	384	127,64,10	3	192
QPSK	128	3	384	127,64,10	3	192
QAM 16	256	2	512	127,50,13	4	200
QAM 64	384	1	384	127,64,10	3	192

Table 6.5: Summary of burst configurations of fixed modulation schemes to be used for comparison with adaptive modulation.

service is assumed with the data throughput of 41.6 kbit/s. The intended application for such a transmission scheme is a mixed video and speech service, for example speech encoded using a codec of the type standardised by the ITU as G.729 [159] and synchronised video encoded using a codec of the type that is also standardised by the ITU as H.263 [160]. For such a service the transmission Frame Error Rate (FER) should not exceed 1 %. The latency that can be afforded by the transmission is 30 ms. This is based upon a maximum 60 ms system delay (GSM [30] has a speech delay of 57.5ms), where for example 10 ms are the required for encoding and decoding of the source frames, and a further 10 ms are reserved for the so-called processing delay. The computational processing time could potentially be reduced, however, a faster processor would be required and there would be a consequential increase in power requirements. Interference is not considered at this stage.

6.9.2 Fixed Scheme

The performance of BPSK, QPSK, Square 16 and 64 QAM was evaluated separately over Rayleigh fading channels. The throughput was 41.6 kbit/s for all schemes and, therefore, they used six, three, two and one slots per user respectively. For Square 64 QAM, QPSK and BPSK this results in 384 bit/frame, and for Square 16 QAM 512 bit/frame. The 384 bits/frame, for Square 64 QAM, QPSK and BPSK, consists of three Bose-Chaudhuri-Hocquenghem (BCH)(127,64,10) block codes [1] where three transmitted bits will be waisted. The Square 16 QAM will use four BCH(127,50,13) block codes and waste four bits. The coding rates are close to 0.5; half rate codes are widely used in wireless communications. All of these values are summarised in Table 6.5.

For each of the fixed schemes the data was interleaved over four frames. If this is achieved in the most simple manner the total latency is 8×4.615 ms. However, it is possible to interleave over four frames and maintain the transmission delay below 30 ms. In this case, for the Square

64 QAM, QPSK and BPSK 12 BCH codewords will be interleaved over four TDD/TDMA frames and in the case of Square 16 QAM, 16 BCH codewords will be interleaved over four TDD/TDMA frames.

6.9.2.1 Interleaved Block-codes

In Section 3.3 the performance of rugged block codes for transmission over Gaussian channels was discussed. However, when the transmitted bits are interleaved over several transmission frames, the BER for bits from each of the frames will vary. The BCH(N,K,T) code is N bits long, it carries K data bits and can correct up to T bits. The codeword may be split over M frames where the probability of error and the number of bits in the m^{th} frame are respectively given by p_m and n_m, where $m = 1 \ldots M$. The probability of more than T errors in the N bits equates to the probability of the code being overloaded which is given by:

$$Y = \sum_{i_1=0}^{T} \sum_{i_2=0}^{T-i_1} \cdots \sum_{i_M=0}^{T-i_1-i_2 \ldots -i_{M-1}} \prod_{m=1}^{M} y(p_m, n_m, i_m). \tag{6.23}$$

where the function

$$y(p, n, t) = \sum_{e=0}^{t} \begin{pmatrix} n \\ e \end{pmatrix} \cdot p^e \cdot (1-p)^{(n-e)} \tag{6.24}$$

is the probability of t or fewer errors in n bits, assuming a constant probability of error p, which was derived Equation 3.11. The validity of Equation 6.23 was verified by simulation and gave very close correspondence.

6.9.2.2 Performance Evaluation

Full bit-level simulation of fixed modulation with block coding was undesirable because simulation times become prohibitive for accurate results. However, full analysis is complicated and therefore the following quasi bit level simulation was performed. The fading was assumed to be constant over the length of a slot because of the propagation environment and mobile velocities concerned. This assumption holds also for the adaptive modulation analysis. The PSD of the noise was assumed to be constant for the duration of the experiment. A correlated Rayleigh fading profile was invoked to yield a received power profile. The quotient of this faded received power and the noise power gave an instantaneous SNR, which depending upon the modulation scheme, was substituted into Equations 3.1-3.10 in order to obtain the BER for the slot. The BER was substituted into Equation 6.24 to determine the probability that the code was not overloaded and the average FER may be evaluated over a minimum of 10000 frames.

	Slow		Fast	
Modulation Scheme	Not Interleaved	Interleaved	Not Interleaved	Interleaved
BPSK	20.0	20.0	20.3	17.7
QPSK	23.0	23.0	23.1	20.7
QAM 16	27.7	27.7	28.0	23.7
QAM 64	33.9	33.9	34.2	30.5

Table 6.6: Average Channel SNR (dB) required to obtain 1% FER when using the fixed modulation schemes described in Table 6.5 under Slow (0.136 ms^{-1}) and Fast (4.32 ms^{-1}) Rayleigh fading conditions.

The FER was evaluated for the four fixed schemes shown in Table 6.5 through Rayleigh fading channels for normalised Doppler frequencies of 0.0042, 0.025, 0.054, 0.079 and 0.133, which correspond to mobile velocities of 0.136, 0.812, 1.75, 2.57 and 4.32 ms^{-1}. The FERs were evaluated with and without interleaving and the SNR where the 1% FER was achieved was recorded. The SNR required for lowest and highest normalised Doppler frequencies are shown in Table 6.6. Under slow fading conditions the interleaving had no effect upon the required average SNR, however, for the fastest fading it resulted in a reduction in required average SNR between 2.6 and 4.3 dB.

6.9.3 Adaptive Scheme

In adaptive modulation a frame error can occur for two reasons, either as a result of the noise corrupting a sufficient number of bits that the codeword is overloaded, or, alternatively the frame experiences too high a delay and is therefore not transmitted. The frames lost due to corruption yield the FER, the frames lost because of delay result in a Delay Error Rate (DER) and the total rate of corrupted frames is the Total Error Rate (TER). For the fixed schemes the DER was zero and therefore TER equals FER.

An ideal adaptive modulation scheme balances the DER and FER in order to minimise the TER and this is analogous to the trade-off in BER and BPS that was discussed in Section 4.2.1. From the frequency hopping investigation in Section 6.6 it is that DER can be reduced for no cost in FER. However, the intention of this case study is to employ adaptive modulation under the most demanding conditions and therefore a single frequency statistical multiplexing is used to reduce the DER.

Current Transmission Mode	Codewords Per Slot	Information Bits Per Slot	Desired Multiplexed Slots	Info Per Frame
No Transmission	0	0	1	0
BPSK	1	39	5	195
QPSK	2	78	2.5	195
QAM 16	4	156	1.25	195
QAM 64	6	234	$0.8\dot{3}$	195

Table 6.7: Transmission rate for statistically multiplexed adaptive modulation scheme showing the desired number of slots to achieve a throughput comparable with the fixed scheme in Table 6.5

6.9.3.1 Performance Evaluation

The switching levels to be used for the adaptive modulation scheme were the speech system's optimised mean BER levels and the speech system's peak BER levels from Tables 4.1 and 4.4 respectively. The block code BCH(63,39,4) was chosen because it was the most rugged code from the $n = 63$ family that the results in Section 6.7 implied would achieve the 41.6 kbit/s without the resulting Ξ value becoming too large for average channel SNRs of approximately 20 dB. Depending upon which mode the adaptive modem was in, 0, 1, 2, 4 or 6 codewords could be transmitted per frame as exemplified by Table 6.7.

The performance of the adaptive scheme was evaluated using the statistical multiplexing algorithm from Section 6.7, without capture and assisted capture. The ratio Ξ was no longer fixed, that is the performance of the adaptive modulation and statistical multiplexing presented here is not dependent upon the re-configurable codecs that are discussed in Section 6.5. Here, the adaptive modulation and statistical multiplexing support 195 bits/frame for every users that is accommodated and therefore irrespective of the average channel SNR each user adds five BCH(63,39,4) codewords to its queue. This yields a throughput of 42.25 kbit/s, which is in excess of the target value of 41.6 kbit/s. Frames that were in the transmission buffer longer than 30 ms were removed from the buffer and were not transmitted. The relative frequency of this event gave the DER estimate. Perfectly coherent detection and channel estimation was assumed, as it had been for the fixed modulation, and the SNR was assumed to be constant over a 72μs slot. The FER was evaluated using the same technique as was used for fixed modulation and the results were obtained for the same Slow and Fast fading rates. All users transmitting in the frame had the same throughput requirements, average

channel SNR and fading statistics. Table 6.8 shows the DER, FER and TER for both sets of switching levels, in both the Slow and Fast Rayleigh fading channels, for various numbers of users at average channel SNRs when all the users are generally achieving the desired performance.

Several observations may be made from Table 6.8:

- The DER with mean BER switching levels is greater than DER with peak BER switching levels. This is because the peak BER switching levels are higher and, therefore, the throughput is on average lower. This means that there is more possibility of frames being dropped from the transmission buffer due to delayed transmission.
- The FER with mean BER switching levels is less than the FER with peak BER switching levels. This is the reverse situation compared to above, since the higher switching levels result in greater integrity for the data transfer.
- The FER is the same for the equivalent Fast and Slow scenarios, however the DER reduces with increased mobile speed. The FER is constant as a function of mobile speed because the modulation scheme that is used depends upon the instantaneous SNR only, however, the lower speeds incur higher DER and this is for the reasons outlined in Section 6.2.
- When the number of users increases for the same average channel SNR the DER increases. This is a result of the extra contention for slots.
- When the average channel SNR increases for the same number of users the DER reduces. This is because all users will on average require fewer slots or experience fewer 'no transmission' instances.

From the table it can be observed that combined adaptive modulation and statistical multiplexing can support 5, 10, 15, 20, 25 or 30 TDD users at 20, 20, 22, 26, 28 and 30 dB average channel SNRs, respectively, at either velocity or either set of switching levels. The number of users supported for the fixed modulation schemes can be calculated by taking the 32 duplex slot pairs and dividing them by the number of slots required per frame, as given in Table 6.5. The results are shown in Figure 6.13 for the Fast and Slow environments, with and without interleaving. The adaptive performance is also shown, however it should be noticed that the line given is for the Slow fading channel and better performance is achieved by the Fast fading channel, hence the label 'Worst Case'.

Figure 6.13 shows that the adaptive scheme can support at least as many, and often 25 % more multi-media users the the BPSK, QPSK and Square 16 fixed modulation schemes through

		Normalised Doppler Frequency 0.0042 (velocity 0.136 ms^{-1})						Normalised Doppler Frequency 0.133 (velocity 4.32 ms^{-1})					
		Mean BER switching levels			Peak BER switching levels			Mean BER switching levels			Peak BER switching levels		
Users	SNR (dB)	FER	DER	TER	FER	DER	TER	FER	DER	TER	FER	DER	TER
5	18	3.0×10^{-3}	9.5×10^{-3}	1.3×10^{-2}	4.4×10^{-5}	1.4×10^{-2}	1.4×10^{-2}	3.0×10^{-3}	1.8×10^{-3}	4.8×10^{-3}	4.4×10^{-5}	2.9×10^{-3}	2.9×10^{-3}
5	20	2.3×10^{-3}	5.8×10^{-3}	8.1×10^{-3}	4.1×10^{-5}	7.2×10^{-3}	7.2×10^{-3}	2.3×10^{-3}	1.0×10^{-3}	3.3×10^{-3}	4.1×10^{-5}	1.4×10^{-3}	1.4×10^{-3}
10	20	2.3×10^{-3}	6.1×10^{-3}	8.4×10^{-3}	4.1×10^{-5}	7.6×10^{-3}	7.6×10^{-3}	2.3×10^{-3}	1.1×10^{-3}	3.4×10^{-3}	4.1×10^{-5}	3.4×10^{-3}	3.4×10^{-3}
10	22	1.7×10^{-3}	2.0×10^{-3}	3.7×10^{-3}	3.3×10^{-5}	3.4×10^{-3}	3.4×10^{-3}	1.7×10^{-3}	2.2×10^{-4}	1.9×10^{-3}	3.3×10^{-5}	3.7×10^{-4}	4.0×10^{-4}
15	22	1.7×10^{-3}	3.0×10^{-3}	4.7×10^{-3}	3.3×10^{-5}	5.5×10^{-3}	5.5×10^{-3}	1.7×10^{-3}	2.9×10^{-4}	2.0×10^{-3}	3.4×10^{-5}	4.1×10^{-4}	4.4×10^{-4}
15	24	1.2×10^{-3}	9.3×10^{-4}	2.1×10^{-3}	2.4×10^{-5}	1.5×10^{-3}	1.5×10^{-3}	1.2×10^{-3}	6.7×10^{-5}	1.3×10^{-3}	2.4×10^{-5}	1.0×10^{-4}	1.2×10^{-4}
20	26	8.7×10^{-4}	1.1×10^{-3}	2.0×10^{-3}	1.7×10^{-5}	1.7×10^{-3}	1.7×10^{-3}	9.0×10^{-4}	7.3×10^{-5}	9.7×10^{-4}	1.7×10^{-5}	1.0×10^{-4}	1.2×10^{-4}
20	28	4.6×10^{-4}	6.6×10^{-4}	1.1×10^{-3}	1.2×10^{-5}	1.0×10^{-3}	1.0×10^{-3}	4.8×10^{-4}	3.5×10^{-5}	5.2×10^{-4}	1.2×10^{-5}	7.4×10^{-5}	8.6×10^{-5}
25	28	4.6×10^{-4}	8.6×10^{-4}	1.3×10^{-3}	1.1×10^{-5}	8.4×10^{-3}	8.4×10^{-3}	4.7×10^{-4}	2.5×10^{-4}	7.2×10^{-4}	1.2×10^{-5}	3.7×10^{-4}	3.8×10^{-4}
25	30	3.8×10^{-4}	5.4×10^{-4}	9.2×10^{-4}	7.0×10^{-6}	6.2×10^{-3}	6.2×10^{-3}	3.8×10^{-4}	2.1×10^{-5}	4.0×10^{-4}	7.0×10^{-6}	3.6×10^{-5}	4.3×10^{-5}
30	30	4.0×10^{-4}	2.0×10^{-3}	2.4×10^{-3}	7.0×10^{-6}	1.2×10^{-2}	1.2×10^{-2}	4.1×10^{-4}	1.8×10^{-3}	2.2×10^{-3}	8.0×10^{-6}	4.4×10^{-3}	4.4×10^{-3}
30	32	2.4×10^{-4}	6.4×10^{-4}	8.8×10^{-4}	6.0×10^{-6}	3.1×10^{-3}	3.1×10^{-3}	2.5×10^{-4}	4.1×10^{-5}	2.9×10^{-4}	6.0×10^{-6}	4.8×10^{-5}	5.4×10^{-5}

Table 6.8: The Frame Error Rate (FER) due to noise, Dropped Error Rate (DER) and Total Error Rate (TER) for statistically multiplexed, block coded adaptive modulation scheme using the peak and mean BER switching values at two velocities

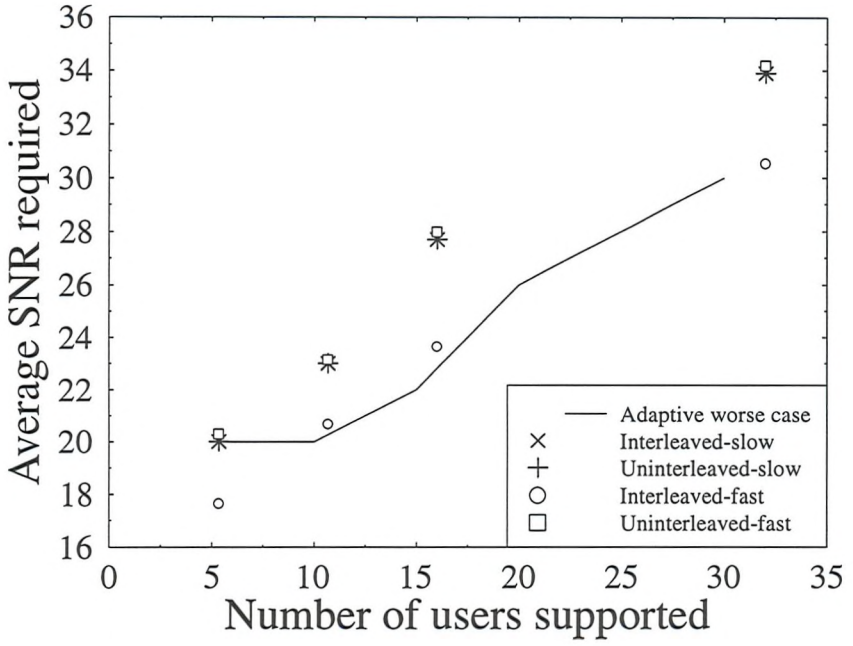

Figure 6.13: The average channel SNR required to support a given number of users with fixed and adaptive modulation on the basis of the comparison case study. Adaptive performance is for the 'Slow' channel and is hence labelled 'Worst Case'.

the Slow fading channel. Through the Fast fading channel, with the exception of 5 users, the adaptive modulation can match the performance all the fixed schemes but at slightly lower average channel SNRs.

There are however, two key points have not been expressed which further improve the performance of adaptive modulation over fixed which are elaborated on below:

- The overall effect of a given DER and FER upon the quality of a wireless service is not the same. With a fixed scheme the DER is zero and therefore all errors are caused by corruption. This has the advantage that since systematic block codes are used the decoder can output the received information bits, rather than erroneously decoding then when the code is overloaded. Alternatively, the overloaded block may be ignored at the receiver. Either way, without the use of Automatic Repeat Request techniques which exhibit an associated delay, redundancy and additional complexity, the transmitting encoder does not know the condition of the received block. With adaptive modulation and the peak switching levels the FER can become very low, as seen Table 6.8, and the DER approximates the TER. As a consequence of this it possible for the source encoder

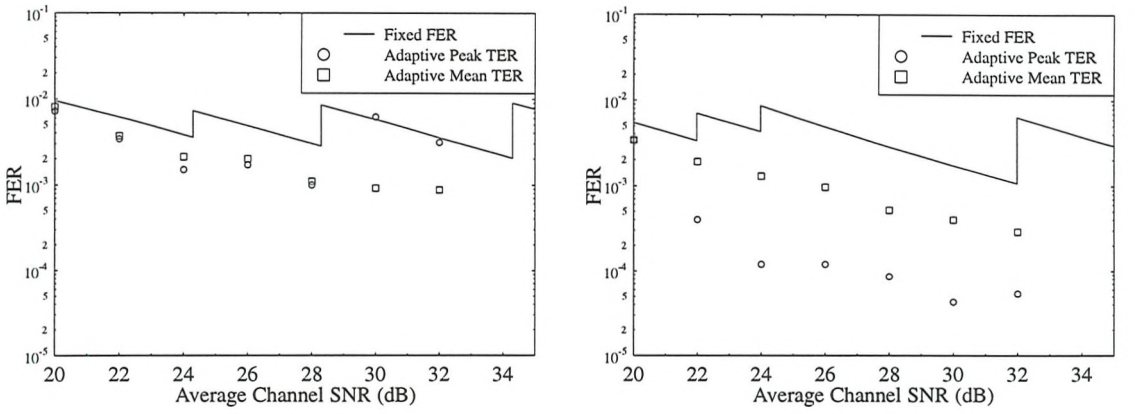

(a) Slow Channel

(b) Fast Channel

Figure 6.14: Total Error Rate for adaptive and interleaved fixed modulation schemes at normalised Doppler frequencies of 0.004170 (Slow) and 0.133427 (Fast). The Adaptive schemes shown with both mean and peak BER switching levels and the number of users that are supported can be inferred from Figure 6.13.

to have near perfect knowledge of what is received at the decoder. This is extremely useful in preventing the propagation of errors resulting from the encoder ignorantly assuming that its local decoded state is the same as the decoded state at the other end of the link.

- The results for the fixed modulation were evaluated using BPSK, QPSK, square 16 and 64 QAM. They are based around a particular operating average channel SNR. If the average channel SNR increases the BER performance will improve, and if the average channel SNR reduces the BER performance will deteriorate. There is no capacity for reassigning the number of slots to a user as the average channel SNR varies. Without this reassignment every fixed modulation user will potentially require a margin of SNR to protect it against reducing average channel SNRs. Furthermore, as the average channel SNR increases, the lack of capacity to reassign slots results in fewer users being supported than possible. Slot reassignment is possible for the fixed modulation schemes [154], however, it incurs an additional transceiver reconfiguration capability beyond the scope of this work.

Figure 6.13 shows that adaptive modulation increases the number of users that can be supported at a given average channel SNR over a Rayleigh fading channel, when compared with

fixed modulation combined with perfect channel reassignment. Although all of the points in Figure 6.13 achieve the TER of 1% the illustration does not show by what margin this target is achieved. To rectify this, Figure 6.14 considers the TER for the adaptive and fixed modulation schemes from Figure 6.13. The number of users is, therefore, a variable in Figure 6.14, however, the number of users supported by the adaptive schemes is always equal or greater than the number of users supported by the fixed schemes, as was shown in Figure 6.13.

Considering Figure 6.14(a) it can be seen, in the Slow fading channel, that with the exception of one value the adaptive scheme results in a better channel quality than the fixed scheme. Also, for the slow fading channel there is no advantage of using either the peak or mean BER adaptive switching levels. At the higher speed, Figure 6.14(b), both sets of switching levels show even greater improvements over the fixed schemes and there is a marked advantage with the peak BER switching levels. The mean and peak switching levels, result respectively, in up to a factor of three or 30 reduction in TER respectively. The peak BER switching levels are so much better than the mean BER switching levels because the DER becomes negligible in both cases as the channel becomes the less correlated channel. Therefore, the TER tends to the FER which is much lower with the peak BER switching levels.

The net result of Figures 6.13 and 6.14 is that adaptive modulation, improves the quality of the link expressed in terms of FER while accommodating these additional users.

6.10 Conclusions

Previous work has shown that adaptive modulation can mitigate the effects of fading and maintain an arbitrary target mean BER. In this Chapter a Markov model has been used to simulate the varying states of an adaptive modem. Two techniques for generating the model were considered. One, originally proposed by Wang [150], and a more empirical approach. It was concluded that the latter technique was more suitable for the normalised Doppler frequencies that were encountered in this work.

A buffer was proposed between the source and channel encoder and the modulator to accommodate the variation in throughput in an adaptive scheme. This introduced latency and how the latency varies with normalised Doppler frequency and average channel SNR was considered in Figures 6.5 and 6.6, for various values of Ξ. It was also demonstrated that frequency hopping could be employed to overcome this latency in Figure 6.7. However, the hardware and network considerations involved in employing frequency hopping may prevent

the technique from being a practical solution. A more sophisticated technique, using statistical multiplexing was proposed. The results of statistical multiplexing were first considered neglecting packet capture and assisted packet capture and are shown in Figure 6.11. These results identified the permission probability p, to be optimum around 0.3. Packet capture and assisted packet capture were included in the results shown in Figure 6.12 and from these experiments it was determined that the performance of adaptive modulation with statistical multiplexing was mainly unaffected by Packet capture and assisted packet capture if p was approximately 0.3.

Adaptive modulation has a strong case to be used for computer data, where data integrity is much more important than latency. Without loosing sight of that, a case study of adaptive modulation versus fixed modulation in a low-delay, interactive mobile multi-media scenario was considered in Section 6.9. The fixed modulation and BCH schemes shown in Table 6.5 were compared with the adaptive, statistical multiplexing scheme shown in Table 6.7. The comparison identified that adaptive modulation and statistical multiplexing could increase the number of users in a system by 25% without an increase in average channel SNR, this was shown in Figure 6.13. Furthermore, the quality of service in terms of the TER offered to the users would be increased by a maximum of a factor of 30, as shown in Figure 6.14. These features provide further justification for the inclusion of adaptive modulation within a multi-mode UMTS air interface tool-box.

Chapter 7

Modulation Scheme Selection and Signalling

7.1 Introduction

The efficiency of adaptive modulation is dependent upon employing the appropriate modulation scheme for the given channel conditions. The modulation scheme employed may be determined by an estimate of the level of signal power with which the particular transmission burst will be received. The effect of the error in this estimation is considered and a system-level technique is proposed to mitigate inaccuracies.

It is essential in an adaptive modulation scheme that the receiver can determine the modulation scheme employed in each frame by the transmitter. At the receiver a decision is made regarding the modulation scheme employed on the basis of decoding the control information included in the frame and this is referred to as 'pre-decoding frame type decision'. This Chapter includes a review of techniques for performing 'pre-decoding frame type decision' and proposes an optimised technique for the mean BER schemes introduced in Chapter 4.

7.2 Modulation Scheme Selection

In Section 4.3.1 it was assumed that exploiting the reciprocity of a TDD channel would result in a perfect channel estimate. There are two problems associated with this assumption that are considered here:

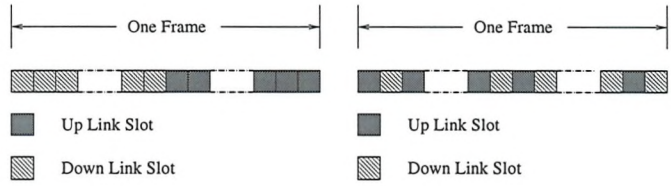

(a) Sub-frame TDD (b) Slot-TDD

Figure 7.1: Different configurations of up and down-link slots

- The channel conditions between the time of channel estimation and transmission will vary. This is dependent upon the time separation between channel estimation and transmission. The variation is also dependent upon the rate at which the channel fluctuates.
- The estimation of the channel, like the successful detection of the data symbols, requires accurate measurement of the channel and is dependent upon the instantaneous SNR. Therefore, when the received signal power is very low, the received signal strength is dependent upon the receiver noise power.

These two issues are considered separately below and their combined effect is portrayed in Figures 7.3 and 7.4, as discussed in the proceeding text.

7.2.1 Channel variation between estimation and transmission

Initially, the variations in channel conditions are addressed by discussing the TDD/TDMA frame construction. When considering the slots in a TDD/TDMA frame, usually all the down-link slots are in the first half of the frame and each of the up-link slots in the second half of the frame. This configuration is shown in Figure 7.1(a) and will be referred to as sub-frame TDD. An alternative to this, which will be referred to as slot-TDD, is shown in Figure 7.1(b). In this case the down-link slot is transmitted immediately after the up-link slot. This increases the correlation between the channel conditions during the base-station receiving a slot from a given mobile and the transmission to the same mobile but imposed tight constraints upon switching. It is therefore likely that the base-station will select a more appropriate modulation scheme. However, the correlation in the channel between the mobile receiving its slot and then transmitting will be reduced. This may be mitigated by the mobile passively receiving the base-station's transmission intended for another mobile, however, there will be consiquences for battery life. Figure 7.2 illustrates passive reception,

in Figure 7.2(a) a slot in the 5 ms TDD/TDMA frame is used for the up-link transmission from mobile n. The base-station can estimate the channel quality for the return down-link very accurately on the basis of this transmission. In Figure 7.2(b) the next slot in the 5 ms TDD/TDMA is used by the base-station to transmit to the mobile n, however the next mobile in the sequence, $n+1$, passively receives this slot. This will result in mobile $n+1$ having an up to date estimation of the channel before, in Figure 7.2(c), transmitting to the base-station. Figure 7.2(d) continues the sequence with the base-station transmitting to mobile $n+1$ and mobile $n+2$ passively receiving the signal. The penalty paid for employing slot-TDD is the need for more expensive hardware at the base-station, because under this scheme the transceiver has to switch more quickly between transmit and receive modes.

There are also penalties paid for a mobile passively receiving slots that are intended for other mobiles. Firstly, there would be complications with the down-link power control, should the operator wish to implement it. Explicitly, when a mobile passively receives the frame before transmitting, it would have to be aware of the base-station transmitter power. However, power control in the base-station is considerably less critical for interference characteristics than power control in the mobile. A second problem is that the base-station has to transmit a signal in every slot before a mobile a mobile is due to transmit, even if there is no mobile actively receiving that slot. This could have some undesirable effects upon the interference characteristics of the system, although down-link interference is typically less critical than up-link. The third penalty is increased power consumption at the base-station due the lack of power control flexibility and the need to transmit in some slots that could have been left empty.

The burst structure proposed by the pan-European FRAMES [2] consortium, also used in Section 6.3, assuming a 2 GHz carrier, 4.615 ms frame duration with 32 duplex users supported in 64 time slots at a multi-user symbol rate of 1.3 MBd was used to evaluate the performance of sub-frame TDD and slot-TDD. With the burst configuration described above the FRAMES proposals relate to the indoors propagation environment so performances were evaluated for mobile velocities of 0.136, 0.812, 1.75, 2.57 and 4.32 ms^{-1}. A worst case scenario was simulated assuming Rayleigh fading. The performance of the most decorrelated, worst case, channel, that with mobile velocity of 4.32 ms^{-1}, is shown in Figures 7.3 and 7.4, for the mean BER switching levels, for the speech (1×10^{-2}) and computer data (1×10^{-4}) systems, respectively. In this Section it is assumed that the measurements of the received power, used to estimate the channel conditions for the next transmission, are not corrupted by noise, and these results are represented by the hollow markers in the figures. Observe in the Figures that the hollow markers are often 'eclipsed' by the bold markers. The Figures show

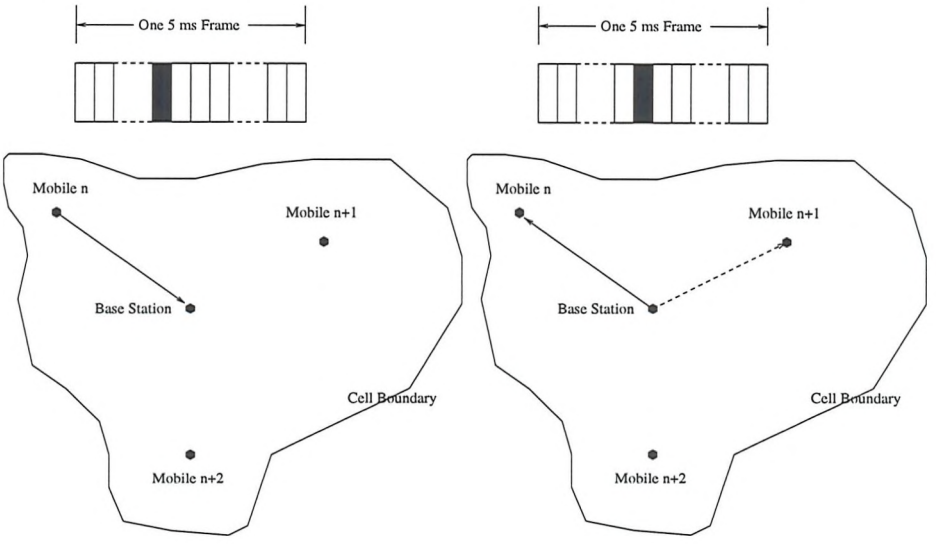

(a) Mobile n transmits to the Base-station and link quality is evaluated

(b) Base-station transmits to Mobile n, mobile n+1 uses this to evaluate channel quality

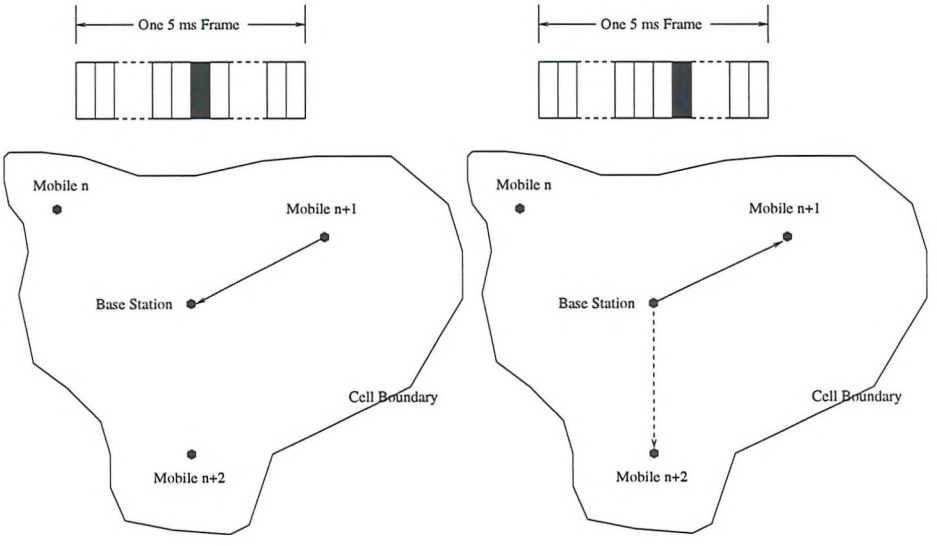

(c) Mobile n+1 transmits to the Base-station and link quality is evaluated

(d) Base-station transmits to Mobile n+1, mobile n+2 uses this to evaluate channel quality

Figure 7.2: Slot-TDD in an arbitrary cell; solid lines show active reception and dotted lines show the passive communication which is used to evaluate channel quality. The frame slot is also identified.

the upper-bound performance based on the assumptions in Section 4.3.1, the performance of sub-frame TDD and slot-TDD with passive reception. In the case of the speech system sub-frame TDD with noise-less channel estimations, the BER performance is above the target by a factor of two, when the average channel SNR is less than 20 dB. Furthermore, when the average channel SNR is sufficient for the sub-frame TDD BER to be below the target, the performance penalty, compared to the upper-bound, equates to seven dB SNR. However, by employing slot-TDD with passive reception, and noise-less channel estimations, the BER performance is the same as the upper-bound average channel SNRs below 30 dB. Between 30 and 50 dB average channel SNR the performance difference between the slot-TDD with passive reception and the upper-bound reaches a maximum of five dB. Importantly, it should be noted that slot-TDD with passive reception results in the BER performance always being below 1×10^{-2}.

Similar observations may be made about the computer data system, however, the effects of the channel estimation error are more significant. With sub-frame TDD the BER is maximum at 17.5 dB average channel SNR. Under these channel conditions the BER is 3.4×10^{-3} which is 34 times the target BER and equates to an average channel SNR penalty of approximately 30 dB, compared with the upper-bound. The slot-TDD with passive reception never exceeds the target BER, however, it does experience a residual BER above 30 dB average channel SNR.

For both the speech and computer data systems, and both sub-frame TDD and, slot-TDD with passive reception, the BPS performance remains the same. This is because, although channel estimates may select a sub-optimum modulation scheme for given channel conditions, on average the throughput remains unchanged.

7.2.2 Channel measurement

Webb et al [148, 6] and Steele et al [104] proposed exploiting TDD to determine which modulation scheme would be most appropriate for the symbols in a particular frame. They proposed using either the Received Signal Strength Indicator (RSSI), or the number of errors detected by the channel coder in, the incoming frame as a measure of the channel quality.

The RSSI varies with the fading profile of the channel, however, it is also affected by the receiver noise power and, in the case of multi-level modulation, by the transmitted symbol sequence. Within the FRAMES proposals there is a 24-symbol mid-amble; because this is a sequence of known symbols, it is proposed to exploit it for the measurement of the channel attenuation. The same experiments that were conducted in Section 7.2.1 were repeated using

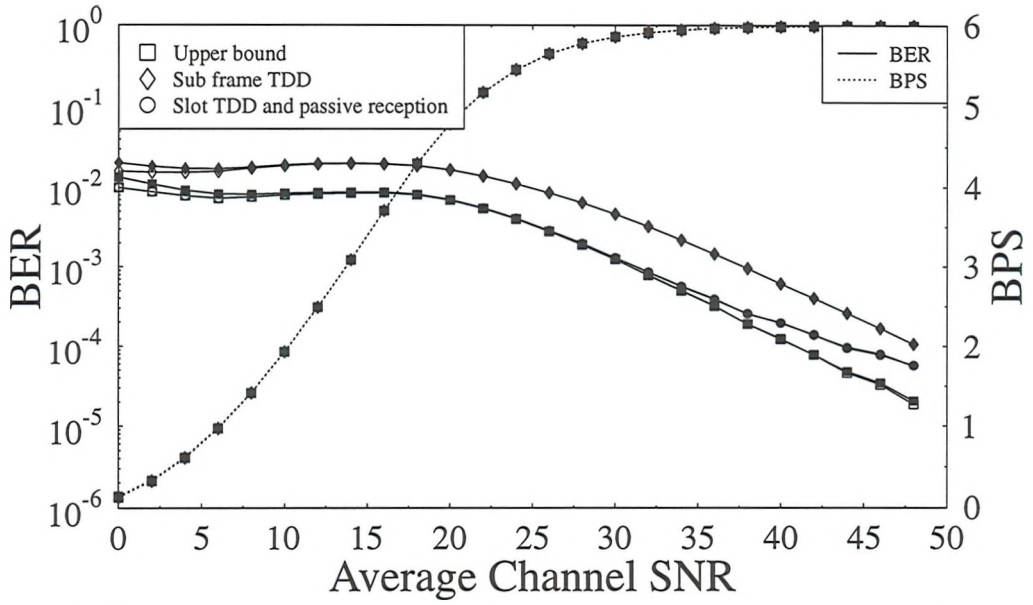

Figure 7.3: Simulated performance of the 1×10^{-2} mean BER adaptive modulation through a Rayleigh fading channel at 1.3 MBd symbol rate and mobile velocity of 4.32 ms^{-1}, using noise-less estimation of the received power (hollow markers) and a 24-symbol mid-amble (bold markers) for received power estimation.

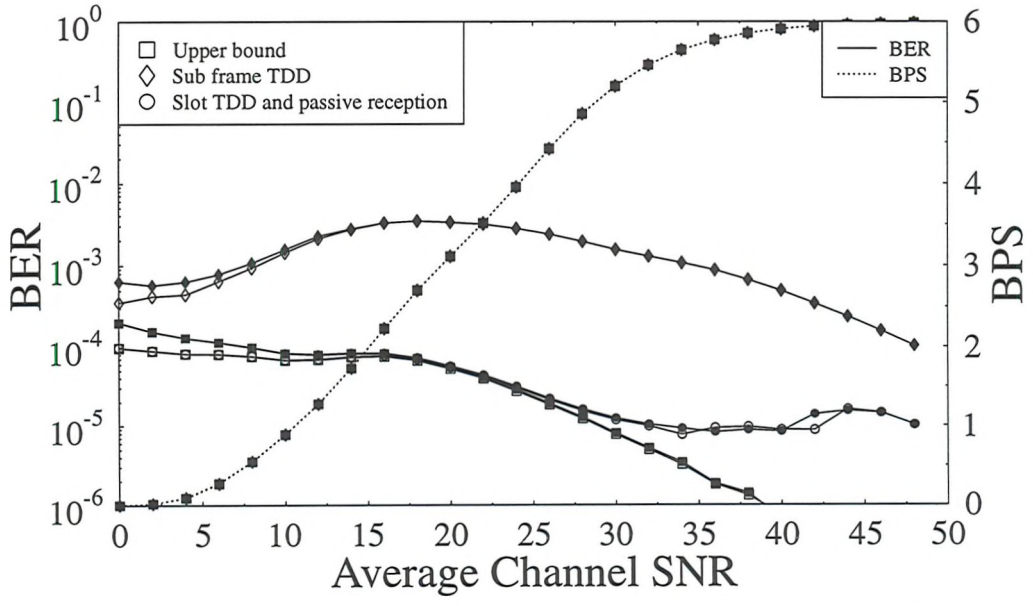

Figure 7.4: Simulated performance of the 1×10^{-4} mean BER adaptive modulation through a Rayleigh fading channel at 1.3 MBd symbol rate and mobile velocity of 4.32 ms^{-1}, using noise-less estimation of the received power (hollow markers) and a 24-symbol mid-amble (bold markers) for received power estimation.

the mid-amble, corrupted by noise, in order to estimate the channel. The results are shown, with bold markers, in Figures 7.3 and 7.4. The effect of the noise corruption experienced by the channel measurement, and its consequential effect on the error of the channel estimation, results in poorer BER performance at low average channel SNRs than experienced when the measurement is conducted in a noise-less environment. In the case of the speech system, the BER is increased by a maximum factor of 1.2 compared with the noise-less measurement performance, at an average channel SNR of 0 dB. As the average channel SNR increases the effect of the noisy channel measurement becomes negligible and above 10 dB average channel SNR there is no resolvable difference between the performance of the noisy and the noise-less channel measurements. For the computer data system, the BER is increased by a maximum factor of two compared with the noise-less measurement performance, again at 0dB average channel SNR. For the computer data system there is no resolvable difference between the noisy and noise-less channel measurements above 16 dB average channel SNR.

A technique to mitigate the small effects of noise upon the channel measurements at low average channel SNR is now considered. It involves using the errors detected in the received codeword [148, 6, 104] which, in theory, can be exploited in conjunction with slot-TDD and passive reception.

7.2.2.1 Error Detection

When a channel is subject to Rayleigh fading, there are signal variations up to 80dB excluding the path-loss. Webb and Steele suggest invoking an interleaved channel codec for channel quality estimation. This technique could have latency ramifications, beyond those investigated in Chapter 6, although it would have some benefits dicussed in Section 5.5.4.

An additional problem associated with evaluating the channel condition on the basis of the errors detected in a channel codeword occur when this technique is used in conjunction with slot-TDD and passive reception. In such a system the channel codeword would have to be decoded almost instantaneously in order for the channel conditions of the previous user's down-link slot to be exploited for channel estimation. While this is possible, it would result in more processing power required in the hand-set, and therefore increased power consumption. From Figures 7.3 and 7.4 it can be observed that slot-TDD and passive reception offer more gain than can be achieved by making noise-less estimation of the channel with sub-frame-TDD. Therefore, it is proposed that error-rate estimation is reserved for systems without significant mid-ambles or where down-link power control is essential.

7.3 Pre-decoding frame type decision

In Section 7.2.2 techniques for determining the modulation scheme employed in a particular frame were discussed. However, it is imperative that the receiver is aware of which modulation scheme has been selected by the transmitter and the process of identifying the correct modulation scheme is referred to as pre-decoding. It is assumed that any pre-decoding error is fatal for the whole frame but calculating the effect upon the BER is not clear and depends upon other system parameters. Specifically, when a frame is pre-decoded incorrectly, the number of bits decoded is wrong. However, whether the erroneous bits counted should be the number of bits transmitted or the number of bits which were thought to have been transmitted is not clear. Furthermore, an erroneous pre-decoding decision results in the bit stream requiring re-synchronisation. Therefore, it is not clear whether a pre-decoding error by over estimating the number of transmitted bits is any better or any worse than underestimating the number of bits.

7.3.1 Single PSK Symbol

A possible approach to signalling the transmitter's modulation scheme to the receiver is to replace some of the data symbols in the outgoing frame with control symbols. These symbols would communicate the modulation scheme employed for the data symbols. Initially a single Phase Shift Keyed (PSK) symbol is considered to communicate this information, where each phasor identifies a different modulation scheme from the set of possible schemes that could have been used for the data symbols. The Symbol Error Rate (SER) of the control symbols, at a given SNR, will represent the probability of the receiver demodulating the data symbols within a frame with the wrong modulation scheme. The SER of an M-phasor PSK modulation scheme in a Gaussian channel is given in Proakis [25] as

$$P_{M1\,g}(\gamma) = 1 - \int_{-\pi/M}^{\pi/M} \frac{1}{2\pi} e^{-\gamma} \left(1 + \sqrt{4\pi\gamma}\cos\theta e^{\gamma\cos^2\theta} \frac{1}{\sqrt{2\pi}} \int_{-\infty}^{\sqrt{2\gamma}\cos\theta} e^{-x^2/2} dx \right) d\theta \quad (7.1)$$

where γ and M are the SNR and the number of symbols in the corresponding regular maximum-minimum constant amplitude constellation. The 1 suffixed to the M is used to differentiate this relationship from Equation 7.2. The outer integral in Equation 7.1 may easily be solved numerical by using Romberg's method [15]. However, the inner integral is improper and may be computed using the *Second Euler-Maclaurin summation formula* as described by Press et al [15]. In the case of $\gamma > 40$ and $M \geq 2$ Equation 7.1 is approximated by [25]:

$$P_{M2\,g}(\gamma) = 2Q(\sqrt{2\gamma}\sin\frac{\pi}{M}), \tag{7.2}$$

where $Q(x)$ was defined by Equation 3.3. Therefore, generally Equations 7.1 and 7.2 may be written:

$$P_{M\,g}(\gamma) = \begin{cases} P_{M1\,g}(\gamma) & \text{if } \gamma < 40 \\ P_{M2\,g}(\gamma) & \text{otherwise.} \end{cases} \tag{7.3}$$

The general expression for M-PSK BER, Equation 7.3 may be put in to Equation 4.4 to give the upper bound performance of a M PSK symbol in a Rician channel as seen below:

$$P_{M\,r}(S/N) = \int_0^\infty P_{M\,g}(s/N) \cdot F(s,S)\,ds, \tag{7.4}$$

where the variables are defined as in Section 4.3.2, specifically s, S and N are the instantaneous received power, average received power and average noise power respectively. Furthermore, $F(s,S)$ may be defined as a Rician channel, or more specifically as a Rayleigh channel, by employing the expressions in Equations 4.2 and 4.3. Numerical evaluation of the performance of PSK, where $M = 5$ corresponding to No Transmission, BPSK, QPSK, Square 16 and 64 QAM, is given in Figure 7.5 for K factors of 0, 4 and 16. These results were derived by solving Equation 7.4 using the trapezium rule, with limits of [-80 dB, 20 dB] and steps of 0.1 dB. The logarithmic SNRs were relative to the mean signal level. The same procedure as adopted in Section 2.4.1.2 was employed to evaluate the infinite summation in the Rician CDF. Figure 7.5 also shows the simulated performance of 5 PSK at the same K values. Good correspondence between the simulated and numerical results is achieved. It can be observed that the SER reduces with increased average channel SNR and increased K factor. However, for the speech- and data-optimised schemes, developed in Section 4.3.6, acceptable SERs would be approximately 1×10^{-2} and 1×10^{-4}, respectively. It should be noted that SERs of 1×10^{-2} and 1×10^{-4} are equivalent to the Frame Error Rate (FER), but correctly pre-decoded frames have non-zero BER. The acceptable SER may only be approximated because the independence between control symbol errors and BER in the data symbols has not been established. It can be seen from the Figure that in a Rayleigh channel ($K = 0$), SERs of 1×10^{-2} and 1×10^{-4} are achieved at average channel SNRs of approximately 20 and 40 dB, respectively.

7.3.2 Majority Decision

Steele et al [104] proposed an adaptive modulation scheme that employed one of four fixed differential modulation schemes depending upon the instantaneous channel conditions. It

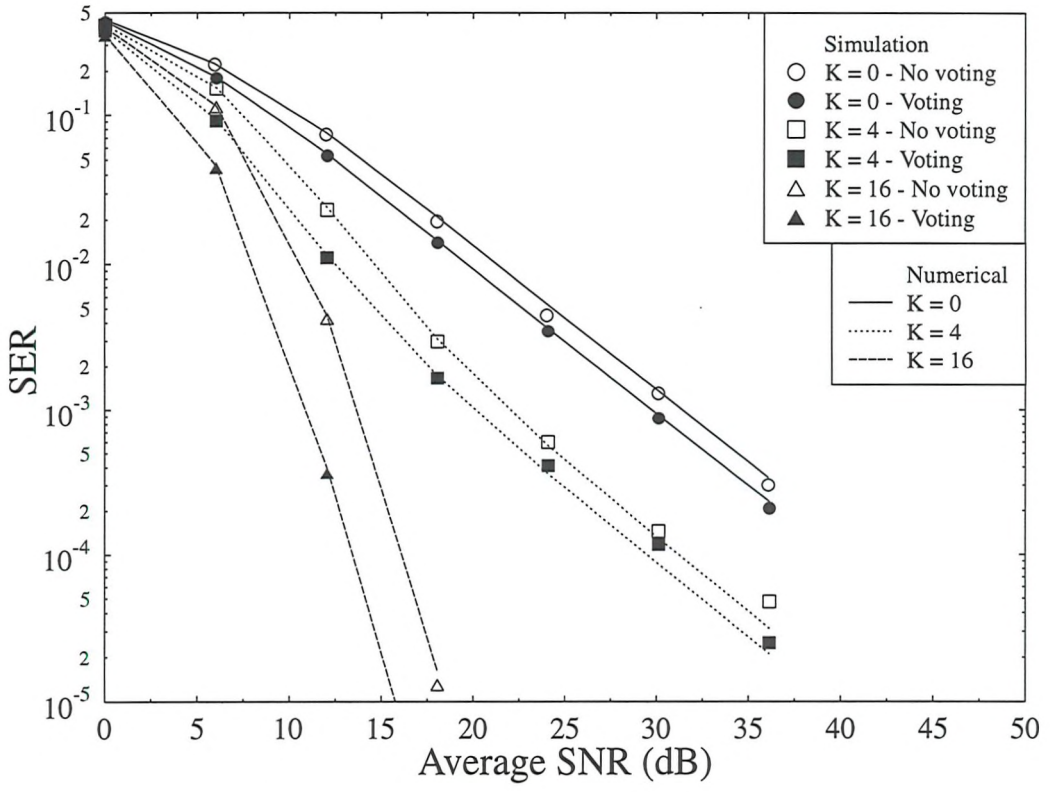

Figure 7.5: Simulated and Numerical Upper Bound Performance of 5 Symbol PSK in Fading Channels with varying K factors with 3 Symbol Majority voting disabled and enabled

was proposed to use DPSK control symbols to communicate to the receiver which particular modulation scheme was used for the incoming frame. Three identical control symbols were transmitted and a majority decision was made upon the basis of the decoded control symbols. This scheme has been modified to use coherent detection of non-differential encoded symbols. However, irrespective of whether differential or non-differentially encoding are used, this voting scheme can be represented by a binomial distribution. Exploiting this binomial relationship Equation 7.4 may be modified to,

$$P_{M\,r\,b}(S/N) = \int_0^\infty P_{M\,g\,b}(s/N) \cdot F(s,S)\, ds, \tag{7.5}$$

where

$$P_{M\,g\,b}(s/N) = \sum_{n=0}^{n=1} \left(\begin{array}{c} 3 \\ n \end{array} \right) (P_{M\,g}(s/N))^n (1 - P_{M\,g}(s/N))^{3-n} \tag{7.6}$$

and $P_{M\,r\,b}(S/N)$ is the upper bound SER of three-symbol M-PSK in a Rayleigh channel after majority decision voting.

Steele et al [104] had proposed an adaptive modulation scheme that could transmit with one of any four fixed modulation schemes and therefore the control symbols were quantised to four levels, that is $M = 4$ was used. The adaptive modulation scheme considered here employs one of five fixed modulation schemes and therefore $M = 5$. Figure 7.5 shows the numerical solution of Equation 7.5 for K factors of 0, 4 and 16 and $M = 5$. Simulated results are also shown and these correspond well to the numerical results. The improvements that result from majority voting over the single control symbol transmission are approximately 1.6 dB, 2.1 dB and 2.7 dB for $K = 0$, $K = 4$ and $K = 16$ channels, respectively. The explanation for the increase in differential between the majority voting and single control symbol transmission as K increases is reduction in deep fades. Specifically, as K increases, the probability of one control symbol being overcome by noise reduces, however, the probability of more than one in three control symbols being overcome by noise reduces much faster. However, the majority voting scheme adds more redundancy to the transmitted signal.

7.3.3 Discrete Walsh Codes

Otsuki et al [105] proposed using control symbols to identify at the receiver, which modulation scheme had been employed by the transmitter for the data symbols. As an alternative, they proposed using a four symbol Walsh code and to use maximum likelihood detection to decode the Walsh codes. They suggested using simple orthogonal codes and transmitting them using BPSK, exploiting the maximum amplitude displacement in the 1^{st} and 3^{rd} quadrants. When Walsh codes are used in such a way there should be 2^n [161] ($n = 1, 2, \ldots$) fixed modulation schemes in order to avoid coding redundancy. A, so-called, binary Walsh code that can signal 2^n different modulation schemes requires at least n chip intervals. Otsuki et al [105] proposed an adaptive modulation scheme that could transmit with one of any four fixed modulation schemes (QPSK, 16, 64 and 256 Square QAM) and therefore they opted for $n = 2$. Following Otsuki et al [105] the duration of four symbols were used to transmit the code. The performance of the Walsh codes, as control symbols, was simulated in channels with K factors of 0, 4 and 16. As a comparison, the performance of a single 4 PSK control symbol, through a Rayleigh channel was calculated numerically from Equation 7.4. Both the Walsh function and the single 4 PSK control symbol performance are plotted in Figure 7.6. This Figure also re-plots the performance of a single 5 PSK control symbol from Figure 7.5.

As expected, the single QPSK control symbol is slightly more robust than the single 5-PSK control symbol. The difference is about 1.5 dB under Rayleigh channel conditions. The Walsh code in a Rayleigh channel appears to be considerable better than the QPSK symbol, although they both signal the same information. However, the Walsh function occupies four

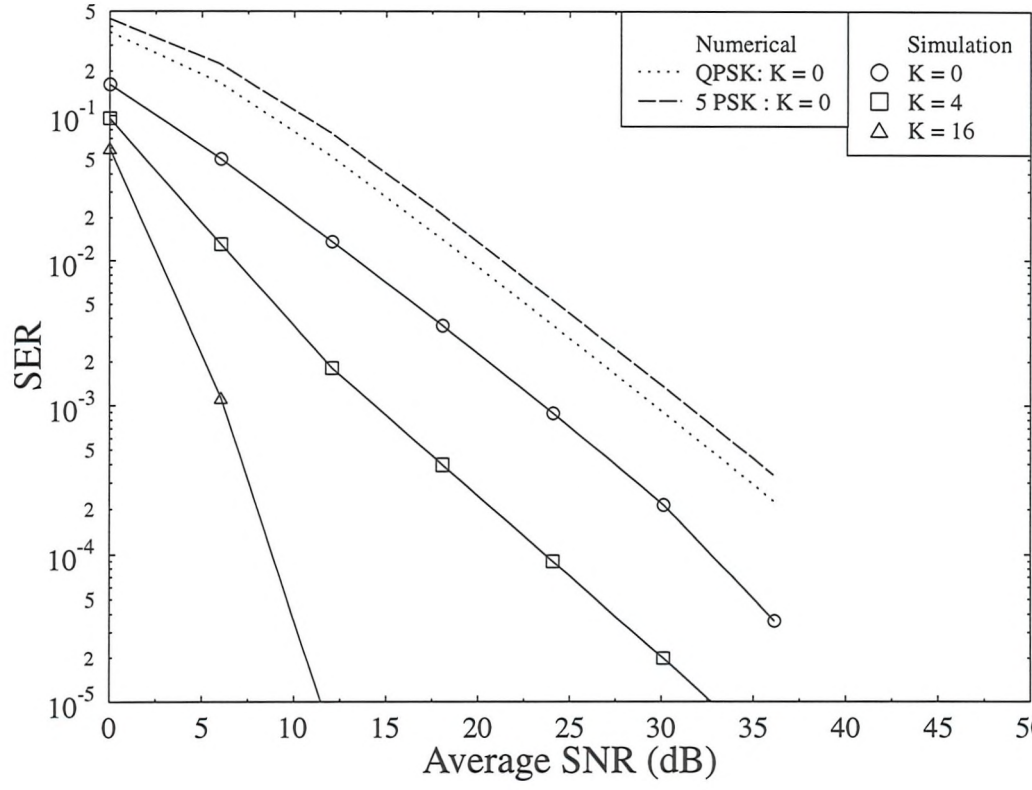

Figure 7.6: Simulated and numerical upper-bound performance of, 4- and 5-PSK in a slow Rayleigh fading channel, and 4 symbol duration, 2 code Walsh control sequences in fading channels with K values of 0, 4 and 16

symbol spaces. Gfeller [162] states that each time the number of samples of the same symbol is doubled and the resulting received signal is averaged, the effective received SNR increases by $10\log_{10}(2) \approx 3$ dB. That is doubling the number of measurements of an value, in the presence of noise effectively increases the SNR by approximately 3 dB, assuming the noise at the two measurement points is independent. This would suggest that transmitting the same single QPSK control symbol four times would result in a 6 dB improvement over the single symbol performance given in Figure 7.6. Therefore, the effective SER of a burst of four identical QPSK control symbols, averaged at the receiver and the de-mapped, would be coincident with the error-rate of the Walsh code. When only four fixed modulation schemes may be employed for the transmission of data symbols, Walsh codes and averaging a repeated QPSK symbol have equivalent performance as control techniques. However, when there are not 2^n fixed modulation schemes that may be employed for the transmission of data symbols,

the additional flexibility of the multi-PSK symbols makes it more attractive than the Walsh code for transmitting control information.

7.3.4 Uneven Error Protection

A novel approach to the problem of pre-decoding frame type decision is to use modulation symbols that have uneven error protection [149]. Consider a coherent PSK modulation constellation with M complex vectors, $C_1 \ldots C_M$, and M decision boundaries at $\theta_1 \ldots \theta_M$. Conventional thinking would result in maximising the minimum distance between each of the M vectors. This maximisation would result in the vectors being equally distributed around a circle and the decision boundaries also spaced evenly with the same separation as the constellation points. This is the case for conventional M-PSK because there is no correlation between the symbol transmitted and the instantaneous channel conditions. However, when M-PSK symbols are used to transmit control information about the fixed modulation scheme that has been employed for the data in the frame, there will be a strong correlation between the channel conditions and the symbol transmitted. It is therefore proposed to use a more robust symbol communicate that there is no data in the frame and accept a more noise sensitive symbol, when the data is encoded with square 64 QAM. For an adaptive modulation scheme that can employ, No Transmission, BPSK, QPSK and 16 or 64 square QAM this uneven error protection 5 PSK symbol is shown in Figure 7.7.

7.3.4.1 Optimisation

Assuming that only noise noise could corrupt the control symbol [163] and given that noise is modelled by a zero mean process each of the transmitted phasors were restricted to be in the centre of their decision thresholds. Other than that, no constraint was placed upon the values of C_m. Again assuming slow fading, Equation 7.4 may be modified to obtain the SER of different, uneven protection M-PSK schemes. In the case of the 5-phasor PSK, the upper-bound SER,

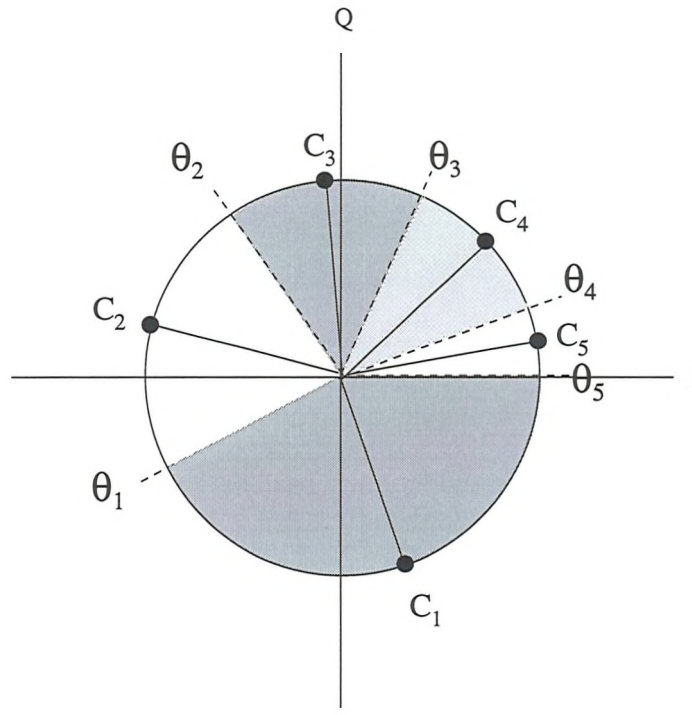

Figure 7.7: An uneven error protection 5 PSK symbol with complex symbol phasors at $C_1, C_2 \ldots C_5$, and decision boundaries at $\theta_1, \theta_2 \ldots \theta_5$

$$P_u(S/N) = \begin{bmatrix} & \int_0^{l_1} P_{M=\left(\frac{\pi}{\theta_1-\theta_5}\right)_g}(s/N) \cdot F(s,S) \quad ds \\ + & \int_{l_1}^{l_2} P_{M=\left(\frac{\pi}{\theta_2-\theta_1}\right)_g}(s/N) \cdot F(s,S) \quad ds \\ + & \int_{l_2}^{l_3} P_{M=\left(\frac{\pi}{\theta_3-\theta_2}\right)_g}(s/N) \cdot F(s,S) \quad ds \\ + & \int_{l_3}^{l_4} P_{M=\left(\frac{\pi}{\theta_4-\theta_3}\right)_g}(s/N) \cdot F(s,S) \quad ds \\ + & \int_{l_4}^{\infty} P_{M=\left(\frac{\pi}{\theta_5-\theta_4}\right)_g}(s/N) \cdot F(s,S) \quad ds \end{bmatrix}, \tag{7.7}$$

The values for θ_m are dependent upon the switching levels l_m. Considering the mean BER speech and computer data systems that were introduced in Section 4.3.6 and summarised in Table 4.1 it is possible to minimise the SER in Equation 7.7 by finding optimum values of θ_n for given ranges of average channel SNRs. This was achieved using Powell's [15] optimisation, where the cost function was $P_u(S/N)$ and the initial conditions were $\theta_1 - \theta_5 = \theta_2 - \theta_1 = \theta_3 - \theta_2 = \theta_4 - \theta_3 = \theta_5 - \theta_4 = 0.2\pi$. The optimisation was conducted for average SNRs of 10, 15, 20, 25, 30, 35 and 40 dB and for each average channel SNR value the optimisation was terminated, when the iteration improvement was less than 1%. The optimal values for θ_m

SNR	$\theta_1 - \theta_5$	$\theta_2 - \theta_1$	$\theta_3 - \theta_2$	$\theta_4 - \theta_3$	$\theta_5 - \theta_4$	SER
10	1.225421	0.810571	0.699682	0.405919	0.000000	0.057126
15	1.003984	0.744393	0.697061	0.459929	0.236226	0.025976
20	0.951273	0.732170	0.701014	0.479739	0.277396	0.009043
25	0.935256	0.729485	0.703069	0.484734	0.289048	0.002946
30	0.930156	0.728621	0.703645	0.486559	0.292611	0.000941
35	0.928734	0.727877	0.703650	0.487460	0.293872	0.000298
40	0.928416	0.727716	0.703569	0.487669	0.294223	0.000094

Table 7.1: Optimised θ_n values, for the adaptive speech system switching levels, through a slow Rayleigh channel, shown in Radians/2

SNR	$\theta_1 - \theta_5$	$\theta_2 - \theta_1$	$\theta_3 - \theta_2$	$\theta_4 - \theta_3$	$\theta_5 - \theta_4$	SER
10	1.800873	0.670482	0.524380	0.145857	0.000000	0.022975
15	1.569406	0.712817	0.568780	0.290590	0.000000	0.009813
20	1.454808	0.693972	0.577136	0.322835	0.092842	0.003765
25	1.416545	0.688705	0.579114	0.332477	0.124751	0.001263
30	1.404741	0.689835	0.579317	0.334870	0.132831	0.000406
35	1.401966	0.689263	0.579969	0.335848	0.134547	0.000129
40	1.402039	0.686365	0.579678	0.336431	0.137079	0.000041

Table 7.2: Optimised θ_n values, for adaptive computer data system switching levels, through a slow Rayleigh channel, shown in Radians/2

in the range of average channel SNRs investigated are given in Table 7.1 for the optimised speech scheme and in Table 7.2 for the computer optimised schemes.

The results of the phase optimisation are also plotted in Figures 7.8 and 7.9. Both these Figures show that the control symbol transmitted at high SNRs require smaller decision thresholds compared with the symbols transmitted at lower SNRs. In the case of the speech system characterised in Figure 7.8, it can be seen that the variation in decision threshold angles amongst the different phasors is less than that for the computer data system of Figure 7.9. This results from the greater dynamic range, and higher valued switching levels employed after the BER optimisation of the computer data system that was reported in Chapter 4. Since there is less variation in the speech system decision threshold angles than there is with the computer data system, there is less overall benefit from employing an unequal protection control system compared with uniform 5-PSK. Conveniently, however, there is also less need, because the acceptable BER in the speech system is higher and therefore

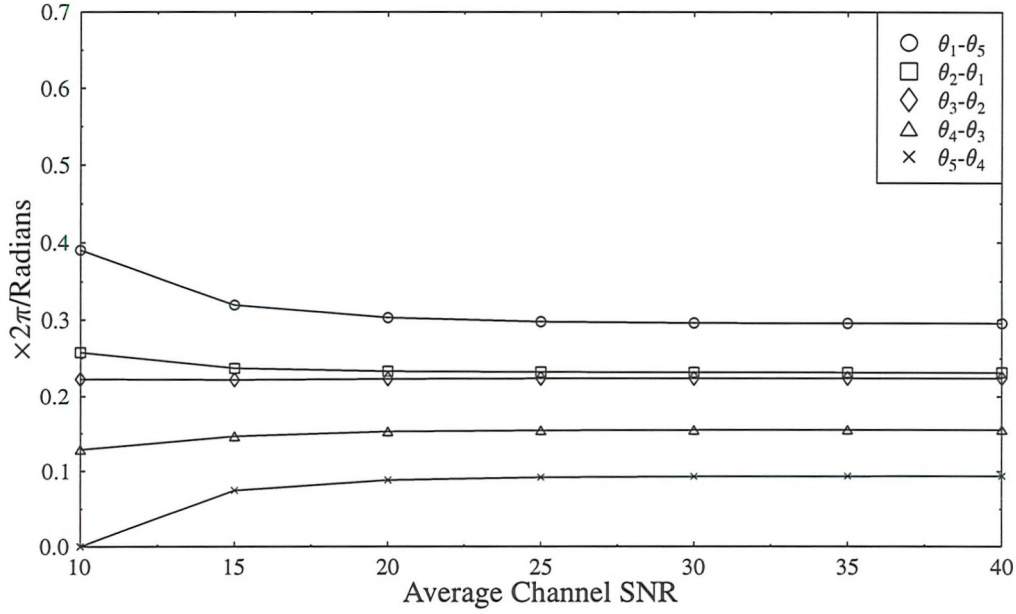

Figure 7.8: Five-PSK decision boundaries with SER optimised for transmission of control symbols of the adaptive modulation speech system in a slow Rayleigh channel calculated at SNRs of 10, 15, 20, 25, 30, 35 and 40 dB

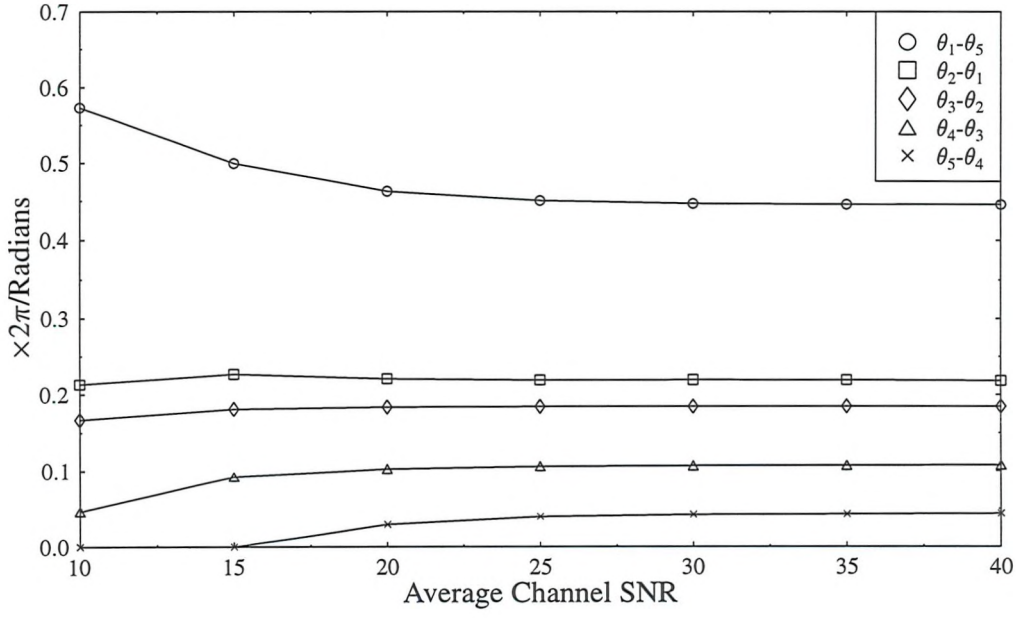

Figure 7.9: Five-PSK decision boundaries with SER optimised for transmission of control symbols of the adaptive modulation computer data system in a slow Rayleigh channel calculated at SNRs of 10, 15, 20, 25, 30, 35 and 40 dB

control errors are also more acceptable.

Figures 7.8 and 7.9 also show that once the average channel SNR exceeds about 25 dB, there is little change in the optimum phasor decision threshold angles. Therefore, it is likely that there is little benefit in changing the decision threshold angles on the basis of the long term signal level. Results are shown in Figure 7.10 for the simulated and numerical solution of the SER using the decision threshold angles which were optimum at 30dB. It can be seen that the penalty for using the 30-dB-optimised angles is small amounting to at most 1 dB and 2 dB for the speech and computer data systems, respectively. However, the total benefit of using unequal protection PSK is in excess of 5 dB for the computer data system and 1 dB for the speech system over slow Rayleigh fading channels. This is virtually a zero cost improvement and sets an upper-bound on the performance for a single control symbol. Multi-symbol performance can easily be determined by exploiting Gfeller's [162] expression.

The performance of pre-decoding frame type decisions could be enhanced, for all signalling methods, by the receiver taking into account the instantaneous SNR with which a frame was received. Given the transmitters estimation of the channel was reasonable this would give further information about which modulation scheme was likely to have been used at the transmitter. Moreover, if appropriate FEC coding were used for the data symbols, then the frame could be decoded once for each of the possible modulation schemes. Then, depending upon which demodulation processes gave valid codewords, the bits corresponding data bits could be selected.

7.4 Conclusions

In this chapter sub-frame TDD and slot-TDD have been discussed. It has been shown that slot-TDD in conjunction with passive reception justifies the assumption of perfect channel estimation, made in Section 4.3.1, for an indoors system similar to that proposed by the FRAMES consortium. It has been shown that assuming noise-less channel measurements and Rayleigh fading, for a mobile velocity up to, at least, 4.32 ms^{-1}, employing slot-TDD and passive reception target mean BERs of 1×10^{-2} and 1×10^{-4} may be achieved using adaptive modulation and the switching levels presented in Table 4.1, in the range of average channel SNRs from 0 to 50 dB. It has also been shown that using a 24-symbol mid-amble to measure the received signal power, the target mean BERs of 1×10^{-2} and 1×10^{-4} may also be achieved when the measurement experiences noise for average channel SNRs in excess of 2.5 dB and 7.5 dB for the speech and computer data systems, respectively.

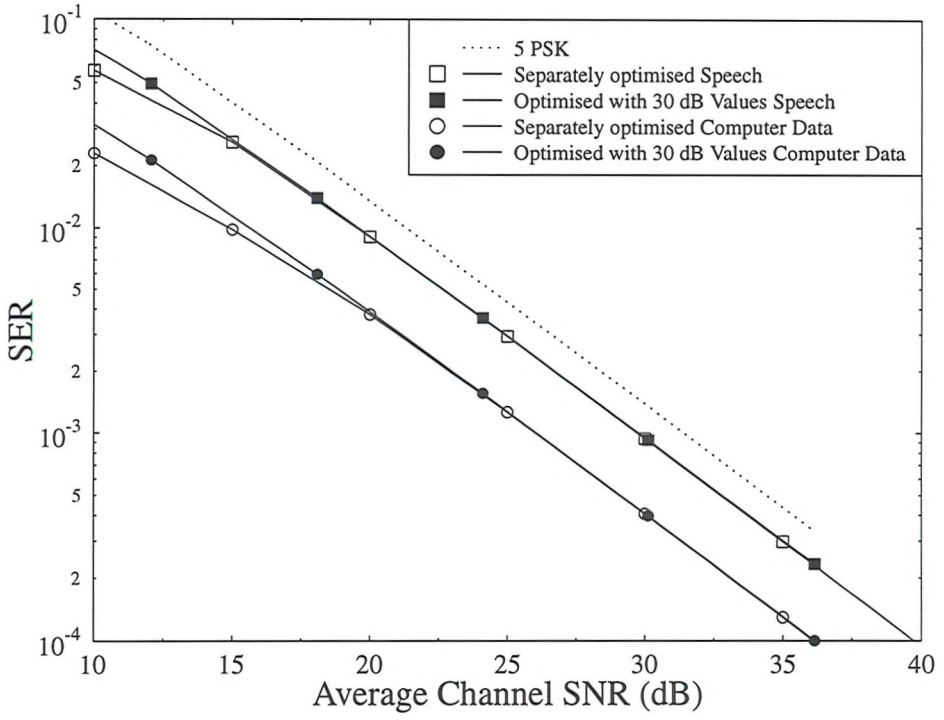

Figure 7.10: SER through a slow Rayleigh channel for both speech and computer data optimised systems, where results are shown using the optimum thresholds for specific average channel SNRs and using the 30-dB-optimised values for all SNRs. The markers represent the simulated and lines the numerical results. 5-PSK numerical results are shown for comparison.

Exploiting the number of errors experienced in a received frame for channel quality estimation was deemed inconvenient for use with the type of system that is proposed by the FRAMES consortium. This was because adaptive modulation intrinsically introduces system latency as shown in Chapter 6. The type of interleaving and FEC coding required to achieve sufficient channel quality dynamic range resolution, that would enable the FEC codeword to identify the number of errors in a frame, without employing an excessively strong channel code, would compound the intrinsic latency of adaptive modulation beyond a level acceptable to that permitted by a FRAMES type system. Furthermore, using this technique to estimate the channel conditions is not necessarily compatible with passive reception.

Also discussed in this Chapter was how the transmitter should communicate the modulation scheme that has been employed in a particular slot to the receiver. The performance of the a single PSK symbol, majority decision, Walsh codes and an uneven protection PSK scheme were considered. The uneven protection PSK scheme offers the greatest flexibility and up

to 5 dBs improvement in performance over other schemes, as shown in Figure 7.10. The overall effect of pre-decoding frame type decision errors upon BER is very dependent on the specific system. Uneven protection PSK schemes may not be suitable, when the effect of co-channel interference, emanating from an adaptive source, is to be reduced using the interference cancellation techniques discussed in Section 5.5.

Chapter 8

Conclusions and Suggestions for Further work

8.1 Introduction

This concluding chapter will summarise the results that were presented in this thesis. These results are discussed in the context of UMTS, as outlined in Chapter 1, and suggestions for further work are outlined.

8.2 Summary and Conclusions

Narrow-band mobile radio channels were discussed. Gaussian and Rayleigh channels have been defined as the best and worst case scenarios for narrow-band mobile radio communications. Correlated Rayleigh channels were simulated using the QNS and Jakes' methods and the resulting channels were compared in terms of their Amplitude PDF in Figures 2.6-2.7, their phase PDF in Figures 2.8-2.9, their LCR in Figure 2.10, their MFD in Figure 2.11, their spectral properties in Figures 2.12-2.13 and their equivalent auto-correlation in Figures 2.14-2.15. It was concluded that the QNS method is more appropriate for the channels used in the simulations associated with this thesis.

A model was proposed to simulate the channel from a leaky feeder to an omni-directional receiver antenna in an indoors environment. This was verified by simulated results generously provided by Thomas Keller and Professor Steele. Figures 2.18-2.19 showed a good correspondence between the simulated and modelled results.

The performance of differential and non-differential encoded QAM constellations was considered with non-coherent and coherent detection. The various modulation schemes were evaluated in Gaussian and Rayleigh fading channels. Figure 3.3 compares the performance of coherently detected non-differential QAM schemes with their analytical performance, which was given by Equations 3.1-3.10. Figure 3.4 showed that the performance gain at 1×10^{-4} BER was 1.25, 2 and 7 dB respectively for BPSK, QPSK and 16 QAM when non-differential encoding and perfect coherent detection are employed over Gaussian channels rather than differential and non-coherent detection. The performance gains associated with coherent detection increase with constellation complexity. Coherent detection is also required for interference cancellation as was discussed in Section 5.5 and therefore was used, in conjunction with the square constellations shown in Figure 3.1, throughout the thesis.

The analytical and simulated performance of block codes transmitted via BPSK were presented in Figure 3.5 and these results were used in the comparison of fixed and adaptive schemes in a latency bounded system, which was discussed in Figure 6.9. PSAM was proposed as a technique for maintaining coherent detection in narrow-band fading channels. Linear, Polynomial, Cavers and Low-pass interpolation were evaluated for estimating the channel between pilots and it was concluded that polynomial interpolation was the most appropriate for cellular systems. In Section 4.3.1 it was assumed that the detection is close to perfectly coherent and this was realistic based upon exploiting the mid-amble for channel estimate, as was explained in Section 5.5 and Section 7.2.1, and assuming a slow fading profile channel.

Adaptive modulation was introduced, based upon the seminal work by Steele and Webb [104, 148] as well as by Sampei et al [98, 164]. The numerical upper-bound was given for adaptive modulation in Section 4.3, based on the instantaneous SNR determining the most appropriate modulation scheme, as given in Equation 4.1. A set of optimised switching levels was derived which were used throughout the thesis. They were given in Table 4.1 and referred to as the optimised speech and optimised computer data mean BER switching levels. These names were used as the switching levels were optimised to obtain mean BER and BPS targets, over Rayleigh fading channels, based on the assumptions in Section 4.3.1, pertinent for speech and computer data transmission, which were explicitly given in Section 4.3.6. Peak BER switching levels were given for the same systems in Table 4.4; these switching levels insured that the peak BER did not exceed the target BER, and therefore the average BER was below the target. This resulted in a more resilient and less bandwidth-efficient system. Figure 4.16 showed, that the performance gain of adaptive modulation over fixed schemes in slow Rayleigh fading channels was up to 7 dB E_b/N_0 at BERs of 1×10^{-2} and, 18 dB E_b/N_0 at BERs of 1×10^{-4}, when the mean BER optimised switching levels are employed.

Figure 4.17 represented how the performance of adaptive modulation, due to the channel estimate degradation, reduced as the normalised Doppler frequency became too high. It also showed how it was proposed to switch between an adaptive modulation air-interface and one based upon coding and interleaving.

ATDMA requires a Nyquist filter roll-off factor, $\alpha = 0.35$. It was shown in Figure 5.2 that such a filter could be implemented in an ATDMA-type system, such that the ISI introduced by truncated filter impulse responses had only a negligible affect on BPSK, QPSK, and Square 16 and 64 QAM performance for BERs down to 1×10^{-4}. The effect of CCI upon BPSK, QPSK, and Square 16 and 64 QAM was given numerically and by simulation. Figure 5.5 and Figure 5.8 showed the close correspondence between numerical and simulated results. ACI was addressed, and Figure 5.11(a) showed the carrier to interference ratio as a function of the excess band-width and carrier separation to symbol rate ratio, which was derived from Equations 5.44-5.50. Figure 5.12 revealed that ACI was more hostile to BER performance than CCI over Gaussian channels, for a given SIR. However, the difference became negligible, when the performance was evaluated over Rayleigh channels, as was shown in Figure 5.13.

The effect of CCI upon adaptive schemes was evaluated and the results were based upon different independently fading interferers at the base-station and mobile-station. Figures 5.16 and 5.17 revealed that the effect of CCI upon the channel measurement, and the consequential employment of a modulation scheme other than the optimum, had a significant detrimental effect upon the BER, even if there was no CCI corruption upon the received symbols. This difficulty was overcome, when interference cancellation was employed, as explained in Section 5.5.4, because both the signal and interferer channels were resolved orthogonally, by the separate mid-ambles. CCIs effects were also considered, when the optimum modulation scheme was employed, that is the effects of the interference upon the received symbols were considered, assuming the transmitter had prefect knowledge of the channel. These results were shown in Figure 5.18 and 5.19, and by modifying the switching levels to the values shown in Tables 5.7 and 5.8 the performance is improved to that shown in Figures 5.20 and 5.21. These results did still not achieve the BER target, hence manual adjustment of the switching levels was considered.

In Section 5.5 interference cancellation was considered. The performance of fixed modulation schemes was evaluated, and the benefit of employing interference cancellation is summarised in Table 5.10. Interference cancellation was also considered in conjunction with adaptive modulation. Figure 5.29 and Figure 5.30 showed how adaptive modulation with interference cancellation, using the appropriate switching levels, could deliver BERs of 1×10^{-2} and 1×10^{-4} in Rayleigh fading channels, with single independent Rayleigh fading interferers at

the mobile- and base-stations for average channel SNRs from 0 to 50 dB, with a range of SIRs. Figures 5.31 and 5.32 revealed that such systems offer more flexibility than any one fixed scheme. Furthermore, the capacity of adaptive modulation was greater than that of the most appropriate fixed scheme under most circumstances, when the target BER is 1×10^{-2}, and for all values measured with a target BER of 1×10^{-4}.

The performance of adaptive modulation was considered in a FRAMES-type environment. The speech and the computer data systems were considered. For the former the proportion of frames delayed more than 20 ms, and the latter the mean frame delay, resulting from continuous poor channel conditions manifesting prolonged employment of low order modulation schemes, was evaluated. The results were shown with respect to the Normalised Doppler frequency in Figure 6.5, the average channel SNR in Figure 6.6 and the number of independent hopping channels in Figure 6.7. A statistical multiplexing scheme was proposed in Section 6.7 and the performance of this in conjunction with adaptive modulation, without burst capture or assisted capture, were compared with fixed modulation. Block coding was employed with and without interleaving and comprehensive results were given in Table 6.8 and Figures 6.13 and 6.14. They showed that when adaptive modulation was used in a latency-constrained system, with a target BER of 1×10^{-2} adaptive modulation supported 25 % additional users in comparison to fixed modulation. As well as increasing system capacity, it was shown that adaptive modulation and statistical multiplexing reduced the TER by a maximum of a factor of 50.

The issue of measuring the instantaneous signal level and estimating the SNR value at the other end of the link was investigated. Slot-TDD and passive reception were proposed in Section 7.2.1. Their performance was compared with sub-frame-TDD, at 4.32 ms^{-1} in a Rayleigh fading environment with a FRAMES-compatible air-interface exploiting adaptive modulation, in Figure 7.3 and 7.4. The plots showed that slot-TDD and passive reception result in a maximum reduction in the BER performance by a factor of five and 34 for the speech and computer data systems, respectively. It was shown in Section 7.2.2 that above 10 dB average channel SNR the training sequence proposed by the FRAMES consortium would be sufficient to obtain channel estimates resulting in an indistinguishable performance from those for perfect estimations. Below 10 dB, the non-perfect estimates resulted in the BER being increased by a maximum of two.

The performance of the control symbols, which inform the receiver of the modulation scheme employed at the transmitter, were considered in Section 7.3. Uneven error protection was selected as the preferred technique, if interference cancellation was not employed. It offered one or five dB extra protection, in a slow Rayleigh fading channel, for speech and computer

data systems respectively, when compared with conventional PSK.

In terms of UMTS, adaptive modulation could be employed in indoors environments where TDD is intended to be used. It has been shown in this thesis, in Section 6.9.3.1, that latency limited multimedia services can be delivered through adaptive modulation more efficiently than with a fixed scheme. Furthermore, Figure 4.16 and 5.31-5.32 show that adaptive modulation will offer considerably greater benefits, when the uncoded target BER is lower, for example 1×10^{-4}. The gains are greater still, when the service being delivered is not latency constrained, and interference cancellation is employed. A UMTS modulation tool-box would be enhanced with the inclusion of adaptive modulation, to deliver multimedia services and in indoor cellular environments.

8.3 Suggestions for further work

In Section 4.4, 5.7 and 6.9.3.1 it was shown that adaptive modulation could offer significant benefits over fixed modulation schemes, when compared under a variety of different circumstances. However, all these comparisons were based on the most appropriate fixed modulation scheme, for the average channel conditions, being compared with the adaptive scheme. Therefore, implicitly the comparison is based upon a fixed scheme that is slowly adaptive, that is the particular fixed modulation scheme was changed on the basis of the average propagation statistics. The control and network issues associated with this would make an interesting comparison with the results for the fast adaptive modems that have been the subject of this thesis.

Optimisation of communications systems is based upon the mutual optimisation of source and channel coder with the modulation scheme. In Section 6.9.3.1 it was observed that a coder could exploit the knowledge of the frames dropped, due to excessive delay in the transmission buffer and therefore dropped frames would have less impact upon the service quality than frames that are lost due to transmission errors. Investigation into such coders and coders that could rapidly vary the bit-rate would be complementary to the advancement of adaptive modulation.

Interference cancellation was discussed in Section 5.5, based upon the assumption that the information and interfering symbols were temporally aligned. The difference in performance, when this is not the case should be considered and how a receiver would be modified to cope with this situation. A possible approach could be to exploit over-sampling and use maximum likelihood detection to estimate the timing delay. Furthermore, the interference cancellation

algorithm could be extended to cancel ACI.

The planning of cell-clusters changes, when interference cancellation is employed should be considered. Rather than trying to reduce the levels of CCI from all interferers, the objective would be to arrange the network so that there was only one source of CCI. Considering such a system, a planning tool would offer the possibility of evaluating the spectral efficiency [134] benefits of interference cancellation, as well as the bandwidth efficiencies shown in Figures 5.31 and 5.32. This would also involve selection of mid-ambles that were suitable for equalisation, where necessary, and sufficiently orthogonal to allow channel estimation of the signal and interferer.

There is scope to expand upon the research reported in Chapter 7. It is possible that the FEC could be used to determine the modulation scheme employed in a particular frame as well as estimating the channel conditions. Furthermore, the control strategy and interference cancellation could be incorporated with power control to obtain an optimum adaptive scheme.

Finally the issues mentioned in Section 1.4 should be addressed. Clock and carrier recovery are more difficult, when channel conditions are poor and less difficult, when channel conditions improve, yet when adaptive modulation is employed, the accuracy required is lower when the channel conditions are poor and higher when channel conditions improve. That is, the most accurate clock and carrier recovery is required for Square 64 QAM but such a scheme is only employed when the channel conditions are better. This suggests the clock and carrier recovery for adaptive schemes, in fading channels, should be easier than for fixed Square 64 QAM.

Glossary

ACTS	Advanced Communications Technologies and Services. The 4th Framework for European Research (1994-98). A series of consortia consisting of universities and industrialists considering future communications systems.
AM	Amplitude Modulation.
ATDMA	Advance Time Division Multiple Access - Project R2084 sponsored by the European Community to consider the evolution of TDMA systems for mobile broad-band communications.
ATM	Asynchronous Transfer Mode - 155 MBPS data rate system supporting Multi-media transmission conceived mainly for fixed networks.
AWGN	Additive White Gaussian Noise.
BER	Bit Error Rate.
BCH	Bose-Chaudhuri-Hocquenghem - Type of linear, cyclic, block code.
BPS	Bits Per Symbol.
BPSK	Binary Phase Shift Keying.
BS	Base Station.
ACI	Adjacent Channel Interference.
C1,C2 and C3	Sub-channels in multi-level modulation schemes, where C1 is the most protected.
CCI	Co-Channel Interference.
CDF	Cumulative Distribution Function.

CDMA Code Division Multiple Access.

CODIT COde DIvision Testbed - Project R2020 sponsored by the European Community to consider the evolution of CDMA systems for mobile broad-band communications.

DBPSK Differential BPSK.

DCS 1800 A personal commination system based around GSM but delivered via a 1.8 GHz carrier.

DECT Digital European Cordless Telephony - 1152 kBPS cordless telephone system.

DQPSK Differential QPSK.

DSP Digital Signal Processing.

E_b/N_0 The Quotient of the Energy per Bit and the Noise Power.

FDD Frequency Division Duplex.

FDMA Frequency Division Multiple Access.

FEC Forward Error Correction.

FER Frame Error Rate.

FFT Fast Fourier Transform.

FH Frequency Hopping.

FIR Finite Impulse Response.

FIRST Flexible Integrated Radio Systems Technology, ACTS Project AC005 with partners ERA Technology Ltd United Kingdom, Bosch Telecom GmbH, Germany, CSEM F Dassault Electronique, Switzerland, Motorola ECID, United Kingdom, Motorola SPS, France Orange PCS Ltd, United Kingdom, Thomson CSF, France, University of Bristol, United Kingdom and University of Southamptom, United Kingdom.

FLMPTS Future Land Mobile Personal Telephone Service.

FM Frequency Modulation.

FRAMES Future Radio Wideband Multiple Access Systems, ACTS project AC090 with partners Siemens AG, Germany, Nokia Corporation, Finland, Ericsson Radio Systems AB, Sweden, Centre Suisse d'Electronique et de Microtechnique CSEM, Switzerland, France Telecom CNET, France, Instituto Superior Tecnico, Portugal, University of Kaiserslautern, Research Group for RF Communications & Center for Microelectronics (ZMK), Germany, Delft University of Technology, The Netherlands, University of Oulu, Finland, The Royal Institute of Technology, Sweden, Chalmers University of Technology, Sweden, Roke Manor Research, United Kingdom, and Swiss Federal Institute of Technology (ETHZ), Communication Technology Laboratory, Switzerland.

GSM Groupe Speciale Mobile or Global System of Mobile Communications.

IS 54 TDMA-based replacement for US analogue cellular telephone system.

ISI Inter-Symbol Interference.

ITU International Telecommunications Union.

K factor Ratio of power in dominant path to other received power.

LAN Local Area Networks.

LCR Level Crossing Rate.

MAE Mean Absolute Error.

MFD Mean Fade Duration.

MS Mobile Station.

PDF Probability Density Function.

PN Pseudo Noise.

PM Phase Modulation.

PRMA Packet Reservation Multiple Access.

PSAM Pilot Symbol Assisted Modulation.

PSD	Power Spectral Density.
PSK	Phase Shift Keyed.
QAM	Quadrature Amplitude Modulation.
QNS	Quadrature Noise Source.
QPSK	Quarternary Phase Shift Keying.
RACE	Research and development in Advanced Communications technologies in Europe. Running from June 1987 to December 1995 (including Phases I & II and extension).
RBER	Residual BER.
RMS	Root Mean Squared.
RSSI	Received Signal Strength Indicator.
TCM	Trellis Coded Modulation.
TER	Total Error Rate.
TTIB	Transparent Tone In Band.
SER	Symbol Error Rate.
SIR	Signal to Interference Ratio.
SNR	Signal to Noise Ratio.
STDCC	Swept Time Delay Cross Correlator.
TDD	Time Division Duplex.
TDMA	Time Division Multiple Access.
UMTS	Universal Mobile Telecommunications System.
VAD	Voice Activity Detection.

Bibliography

[1] R. Steele, ed., *Mobile Radio Communications.* IEEE Press - Pentech Press, 1994.

[2] Francois de Ryck, Hakan Persson, Tom Leskinen, Tero Ojanpera and Werner Mohr, "FRAMES contibution to the standardisation of the UMTS air interface," in *ACTS Mobile Telecommunications Summit*, pp. 244–249, IEEE, November 27-29, 1996.

[3] Vialen Jukka, Beming Per, Vermuyten Guido, Verrier David, Hernandez and von Allmen Laurent, "High layer air interface protocols for FRAMES," in *ACTS Mobile Telecommunications Summit*, pp. 61–66, IEEE, November 27-29, 1996.

[4] K. David, P. Blanc, J. Irvine, T. Kassing, M.I. Lopez-Carrillo, R. Maddelena, W. Mohr and P.Ranta, "First results of ATDMA's test campaigns," in *RACE Mobile Telecommunications Summit*, pp. 468–472, 1995.

[5] P. Walter, "Codit macro diversity and handover performance in an outdoor environment," in *RACE Mobile Telecommunications Summit*, pp. 206–211, 1995.

[6] W. T. Webb and L. Hanzo, *Modern Quadrature Amplitude Modulation.* Pentech Press, 1994.

[7] S.P. Stapleton and Le Quach, "Reduction of adjacent channel interference using postdistortion," in *IEEE* 42^{nd} *IEEE Vehicular Technology Conference*, pp. 915–918, IEEE, 1992.

[8] A. R. Mansell and A. Bateman, "Adaptive predistortion with reduced feedback complexity." Electronics Letters, June 1996. pp 1153 - 1154.

[9] Majid Boloorian and Joseph McGeehan, "The frequency-hopped cartesian feedback linear transmitter," *IEEE Transactions on Vehicular Technology,* vol. 45, no. 4, pp. 688–706, 1996.

[10] Frances A. Jenkins and Harvey E. White, *Fundamentals of Optics.* McGraw-Hill, 1950.

[11] T. Young, "On the theory of light and colours," *Philosphical Transactions of the Royal Society of London*, pp. 12–48, 1802.

[12] J. C. Maxwell, "Dynamic theory of electromagnetic fields," *Philosphical Transactions of the Royal Society of London*, pp. 459–512, 1865.

[13] A. Einstein, "Uber einen die erzeugung und verwandlung des lichtes betreffenden heuristischen gesichtspunkt," *Annalen Physics*, vol. 7, p. 132, 1905.

[14] Bernard Sklar, *Digital Communications: Fundamentals and Applications.* McGraw-Hill, 1988.

[15] W. H. Press, S. A. Teukolsky, W. T. Vetterling and B. P. Flannery, *Numerical Recipes in C.* Cambridge University Press, 1994.

[16] Grigorios A. Kalivas, M El-Tanany and S. Mahmoud, "Millimeter-wave channel measurements with space diversity for indoor wireless communications," *IEEE Transactions on Vehicular Technology*, vol. 44, no. 3, pp. 494–505, 1995.

[17] Akram M. Hammoudeh and Graham Allen, "Millimeter wavelength radiowave propagation for line-of-sight indoor microcellular mobile communications," *IEEE Transactions on Vehicular Technology*, vol. 44, no. 3, pp. 449–460, 1995.

[18] Takeshi Manabe, Katsuyoshi Sato, Hiroshi Masuzawa, Kazumasa Taira, Toshio Ihara, Yoshinori Kasashima and Katsunori Yamaki, "Polarization dependence of multipath propagation and high-speed transmission characteristics of indoor millimeter-wave channel at 60 GHz," *IEEE Transactions on Vehicular Technology*, vol. 44, no. 2, pp. 268–274, 1995.

[19] Raymond Steele, "The cellular environment of lightweight handheld portables," *IEEE Communications Magazine*, vol. 27, no. 7, pp. 20–29, 1989.

[20] Henry L. Bertoni, Walter Honcharenko, Leandro Rocha Maciel and Howard H. Xia, "UHF propagation prediction for wireless personal communications," *Proceedings of the IEEE*, vol. 82, no. 9, pp. 1333–1359, 1994.

[21] A. J. Motley and J. M. P. Keenan, "Personal communication radio coverage in buildings at 900 MHz and 1700 MHz." Electronics Letters, June 1988. pp. 763-764.

[22] Homayoun Hashemi, "The indoor radio propagation channel," *Proceedings of the IEEE*, vol. 81, no. 7, pp. 943–968, 1993.

[23] D. M. Devasirvatham, "Multi-frequency propagation measurements and models in a large metropolitan commercial building for personal communications," in *IEEE PIMRC*, pp. 98–103, IEEE, 1991.

[24] D. Åkerberg, "Properties of TDMA pico cellular office communication system," in *IEEE Globecom*, pp. 1343–1349, IEEE, 1988.

[25] J. G. Proakis, *Digital Communications.* McGraw-Hill, 1989.

[26] S. O. Rice, "Mathematical analysis of random noise," *Bell System Technical Journal*, pp. 282–335 and 46–159, 1945/6.

[27] W. C. Y. Lee, *Mobile Communications Engineering.* McGraw-Hill, 1982.

[28] Gibson, ed., *The Mobile Radio Handbook.* CRC Press - IEEE Press, 1995.

[29] "Digital European Cordless Telecommunications interface part 2: Physical layer." prETS 300 175-172, 1992.

[30] "Groupe speciale mobile (GSM) recommendation," April 1988.

[31] A. R. Potter, "Personal communications networks," in 4^{th} *Nordic Seminar of Digital Mobile Radio Communications*, 1990.

[32] Faramaz Davarian, "Channel simulations to facilitate mobile-satellite communications research," *IEEE Transactions on Communications*, vol. 35, no. 1, pp. 47–56, 1987.

[33] William. C. Jakes, *Microwave Mobile Communications.* John Wiley and Sons, Inc, 1974.

[34] Gaston A. Arredondo, William H. Chriss and Edward H. Walker, "A multipath fading simulator for mobile radio," *IEEE Transactions on Vehicular Technology*, vol. 22, no. 4, pp. 241–244, 1973.

[35] Eduardo Casas and Cyril Leung, "A simple digital fading simulator for mobile radio," *IEEE Transactions on Vehicular Technology*, vol. 39, no. 3, pp. 205–212, 1990.

[36] W. R. Bennett, "Distribution of the sum of randomly phased components," *Quarterly Applied Maths*, vol. 5, pp. 385–393, 1948.

[37] M. Slack, "The probability of sinusoidal oscillations combined in random phase," *Journal of IEEE - Part III*, vol. 93, pp. 76–86, 1946.

[38] R.A. Comroe, "All-digital fading simulator," in *Proceedings of the National Electronics Conference*, pp. 136–139, 1978.

[39] J. R. Ball, "A real-time fading simulator for mobile radio," *The Radio and Electronic Engineer*, vol. 52, no. 10, pp. 475–478, 1982.

[40] R. Agusti, J.Argimon and D. Vila, "Digital fading simulator for mobile radio," in *Proc. Melecon (Mediterranean Electrotech. Conference*, pp. 403–406, 1985.

[41] R.A. Goubran, H.M. Hafez and A.U.H. Sheikh, "Real-time programmable land mobile channel simulator," in 36^{th} *IEEE Vehicular Technology Conference*, pp. 215–218, IEEE, 1986.

[42] Steven M. Kay, *Fundamentals of Statistical Signal Processing Estimation Theory.* Prentice-Hall, 1993.

[43] Peter Hoeher, "A statistical discrete-time model for the WSSUS multipath channel," *IEEE Transactions on Vehicular Technology*, vol. 41, no. 4, pp. 461–468, 1992.

[44] Pedro M. Crespo and Jose Jimenez, "Computer simulation of radio channels using a harmonic decomposition technique," *IEEE Transactions on Vehicular Technology*, vol. 44, no. 3, pp. 414–419, 1995.

[45] Krzysztof Wesolowski, "Computer generation of a slowly varying pseudorandom process," *IEE Proceedings*, vol. 130, no. f, pp. 314–316, 1983.

[46] J. D. Parsons, D. A. Demery, A. M. Turkmani, "Sounding techniques for wide-band mobile radio channels: A review," *IEE Proceedings-I*, vol. 138, no. 5, pp. 437–446, 1991.

[47] P. A. Bello, "Characterisation of randomly time-variant linear channels," *IEEE Transactions Communications Systems*, vol. 11, pp. 360–393, 1963.

[48] Justin C-I Chuang, "The effects of time delay spread on portable radio communications channels with digital modulation," *IEEE Journal on Selected Areas in Communications*, vol. 5, no. 5, pp. 879–889, 1987.

[49] Edgar L. Caples, Khalil E. Massad and Timothy R. Minor, "A UHF channel simulator for digital mobil radio," *IEEE Transactions on Vehicular Technology*, vol. 29, no. 2, pp. 281–289, 1980.

[50] N. Monk and H. S. Wingbier, "Communications with moving trains in tunnels," *IRE Transactions Vehic. Comm.*, vol. PGVAC-7, p. 2128, 1956.

[51] Ronald J. Jakubowski, "Results of distributed antenna and leaky feeder systems tests at 800 MHz in washington d.c. metro system tunnels," in 44^{th} *IEEE Vehicular Technology Conference*, pp. 1113–1116, IEEE, 1994.

[52] Rolf Klingler, "Radio coverage for road and rail tunnels in the frequency range 75 to 1000 MHz," in 41^{st} *IEEE Vehicular Technology Conference*, pp. 433–438, IEEE, 1991.

[53] D. J. R. Martin, "A general study of the leaky-feeder principle," *The Radio and Electronic Engineer*, vol. 45, no. 5, pp. 205–214, 1975.

[54] A. A. M. Saleh, A. J. Rustako and R. S. Roman, "Distributed antennas for indoor radio communications," in *International Conference on Communications*, pp. 76–80, 1987.

[55] Adel A. M. Saleh, A. J. Rustako and R. S. Roman, "Distributed antennas for indoor radio communications," *IEEE Transactions on Communications*, vol. 35, no. 12, pp. 1245–1251, 1987.

[56] D. A. Palmer and A. J. Motley, "Controlled radio coverage within buildings," *British Telecom Journal*, vol. 4, no. 4, 1986.

[57] Kevin J. Bye, "Leaky-feeders for cordless communication in the office," in *IEEE Eurocon*, pp. 387–390, IEEE, 1988.

[58] A. J. Motley and D. A. Palmer, "Reduced long range signal reception with leaky feeders." Electronics Letters, September 1983. pp. 714-715.

[59] P.L. Camwell and J.G. McRory, "Experimental results of in-building anisotropic propagation at 835 MHz using leaky feeders and dipole antennas," in *Proceeding MONTECH '87 Conference on Communications*, pp. 213–216, 1987.

[60] Thoms Keller, "Tripartite project report leaky feeder measurements and analysis," tech. rep., University of Southampton, 1995.

[61] J. M. Torrance T. Keller and L. Hanzo, "Multi-level modulation in the indoors leaky-feeder environment," in 46^{th} *Vehicular Technology Conference*, pp. 1554–1558, IEEE, 1996.

[62] Y.T.Lo and S.W.Lee, *Antenna Handbook - Theory, Applications and Design.* Van Nostrand Reinhold Company, 1988.

[63] Chun Loo and Norman Secord, "Computer models for fading channels with applications to digital transmission," *IEEE Transactions on Vehicular Technology*, vol. 40, no. 4, pp. 700–707, 1991.

[64] J. D. Balcomb, H. B. Demuth and E. P. Gyftopoulos, "Cross-correlation method for measuring the impulse response of reactor systems," *Nuclear Science and Engineering*, vol. 11, pp. 159–166, 1961.

[65] L. B. Lopes, "Performance of the DECT system in fading dispersive channels." Electronics Letters, August 1990. pp. 1416-1417.

[66] R. W. Lucky and J. C. Hancock, "On the optimum performance of n-ary systems having two degrees of freedom," *IRE Trans. Comms.*, vol. CS-10, pp. 185–192, June 1962.

[67] J. G. Smith, "Odd-bit quadrature shift keying," *IEEE Trans Comms*, vol. COM-23, pp. 385–389, 1975.

[68] C-E. W. Sundberg, W. C. Wong and R. Steele, "Logarithmic pcm weighted qam transmission over gaussian and rayleigh fading channels," in *IEE Proc. Pt. F*, vol. 134, pp. 557–570, Oct 1987.

[69] R. Steele, C-E. W. Sundberg and W. C. Wong, "Transmission of log–pcm via qam over gaussian and rayleigh fading channels," in *IEE Proc. Pt. F*, vol. 134, pp. 539–556, Oct 1987.

[70] J. K. Cavers, "An analysis of pilot symbol assisted modulation for Rayleigh fading channels," *IEEE Transactions on Vehicular Technology*, vol. 40, no. 4, pp. 686–693, 1991.

[71] William T. Webb, Lajos Hanzo and Raymond Steele, "Bandwidth-efficient QAM schemes for Rayleigh fading channels," *IEE Proceedings Part I*, vol. 138, no. 3, pp. 169–175, 1991.

[72] P.M. Fortune, L. Hanzo and R.Steele, "On the computation of 16-QAM and 64-QAM performance in Rayleigh fading channels," *IEICE Transactions on Communications*, vol. E75-B, no. 6, pp. 466–475, 1992.

[73] G. Wade, *Signal Coding and processing.* Cambridge University Press, 1994.

[74] J. M. Torrance and L. Hanzo, "Comparative study of pilot symbol assisted modem schemes," in *IEE Conference on Radio Receivers and Associated Systems*, pp. 36–41, IEE, 1995.

[75] H. K. Lau and S. W. Cheung, "A pilot symbol-aided technique used for digital signals in multipath environments," in *IEEE International Conference on Communications*, pp. 1126–1130, IEEE, 1994.

[76] Ronald E. Crochiere and Lawrence R. Rabiner, "Interpolation and decimation of digital signals - a tutorial review," *Proceedings of the IEEE*, vol. 69, no. 3, pp. 300–331, 1975.

[77] M. L. Moher and J. H. Lodge, "TCMP-A modulation scheme and coding strategy for rician fading channels," *IEEE Journal on Selected Areas in Communications*, vol. 7, no. 9, pp. 1347–1355, 1989.

[78] S. Gurunathan and K. Feher, "Pilot symbol aided QPRS for digital land mobile applications," in *IEEE International Conference on Communications*, pp. 760–764, IEEE, 1992.

[79] C. Liu and K. Feher, "Pilot-symbol aided coherent M-ary PSK in frequency selective fast Rayleigh fading channels," *IEEE Transactions on Communications*, vol. 42, no. 1, pp. 54–62, 1994.

[80] Norm W.K. Lo, David D. Falconer and Asrar U.H. Sheikh, "Channel interpolation for digital mobile radio communications," in *International Conference on Communications*, pp. 773–777, IEEE, 1991.

[81] S. Sampei and T. Sunaga, "Rayleigh fading compensation method for 16-QAM in digital land mobile radio channels," in 39^{th} *Vehicular Technology Conference*, pp. 640–646, IEEE, 1989.

[82] S. Sampei, Y. Kamio and H. Sasaoka, "Field experiments on pilot symbol aided 16 QAM modems for land mobile communications." Electronics Letters, November 1992.

[83] S. Sampei and T. Sunaga, "Rayleigh fading compensation for QAM in land mobile radio communications," *IEEE Transactions on Vehicular Technology*, vol. 42, no. 2, pp. 137–147, 1993.

[84] T. Sunaga and S. Sampei, "Performance of multi-level QAM with post-detection maximal ratio combining space diversity for digital land-mobile radio communications," *IEEE Transactions on Vehicular Technology*, vol. 42, no. 3, pp. 294–301, 1993.

[85] Y.Kamio and S. Sampei, "Performance of Trellis-Coded 16QAM/TDMA System for Land-Mobile Radio Communications," *IEEE Transactions on Vehicular Technology*, vol. 43, no. 3, pp. 294–301, 1994.

[86] K.Y. Tsie and A.H. Aghvami, "Performance of concatenated trellis-coded 16QAM with pilot symbol aided technique in the presence of fading," in *IEE Conference Publication*, pp. 352–356, IEE, 1993.

[87] Geerd Oetken, Thomas W. Parks and Hans W. Schussler, "New results in the design of digital interpolaters," *IEEE Transactions on Acoustics, Speech and Signal Processing*, vol. 23, no. 3, pp. 301–309, 1975.

[88] J. K. Cavers, "Pilot symbol assisted modulation in fading and delay spread," in 43^{rd} *IEEE Vehicular Technology Conference*, pp. 13–16, IEEE, 1993.

[89] Aldo N. D'Andrea, Antonello Diglio and Umberto Megali, "Symbol-aided channel estimation with nonselective Rayleigh fading channels," *IEEE Transactions on Vehicular Technology*, vol. 44, no. 1, pp. 41–49, 1995.

[90] Kai-Yiu Tsie and A. Hamid Aghvami, "High level trellis-coded modulation with slow frequency hopping for land mobile communications," *IEEE Transactions on Vehicular Technology*, vol. 43, no. 1, pp. 147–155, 1994.

[91] Floyd M. Gardner, "Interpolation in digital modems - part i: Fundamentals," *IEEE Transactions on Communications*, vol. 41, no. 3, pp. 502–508, 1993.

[92] Lars Erup, Floyd M. Gardner and Robert A. Harris, "Interpolation in digital modems - part ii: Implementation and performance," *IEEE Transactions on Communications*, vol. 41, no. 6, pp. 998–1008, 1993.

[93] R. Steele and F. Benjamin, "Sample reduction and subsequent adaptive interpolation of speech signals," *The Bell System Technical Journal*, vol. 62, no. 6, pp. 1365–1398, 1983.

[94] Michel C. Jeruchim, Philip Balaban and K. Sam Shanmugan, *Simulation of Communications Systems.* Plenum Press, 1992.

[95] P. M. Martin, A. Bateman, J. P. McGeehan and J. D. Marvill, "The implementation of a 16-QAM mobile data system using TTIB- based fading correction techniques," in 38^{th} *IEEE Vehicular Technology Conference*, pp. 71–76, IEEE, 1988.

[96] J. K. Cavers and M. Liao, "A comparison of pilot tone and pilot symbol techniques for digital mobile communication," in *IEEE GlobeCom*, pp. 915–921, IEEE, 1992.

[97] R. Calderbank and J. E. Mazo, "A new description of trellis codes," *IEEE Transactions on Information Theory*, vol. 30, no. 6, pp. 784–791, 1984.

[98] Seiichi Sampei, Shozo Komaki and Norihiko Morinaga, "Adaptive modulation/TDMA scheme for large capacity personal multi-media communication systems," *IEICE Transactions on Communications*, vol. 77, no. 9, pp. 1096–1103, 1994.

[99] C. Mourot, J. DeVile, P.Ranta, P. Diaz and M.E. Gerboles, "Low delay transmission over the ATDMA air interface," in *RACE Mobile Workshop, Amsterdam May 17-19*, pp. 75–79, EU, 1994.

[100] Leandro Fernandes, "Developing a system concept and technologies for mobile broadband communications," *IEEE Personal Communications Magazine*, vol. 2, no. 2, pp. 54–59, 1995.

[101] Alistair Urie, Malcolm Streeton and Christophe Mourot, "An advanced TDMA mobile access system for UMTS," *IEEE Personal Communications Magazine*, vol. 2, no. 2, pp. 38–47, 1995.

[102] Ferandes Bosco Eduardo, "A further exploitation of ATDMA," in *RACE Mobile Telecommunications Summit*, pp. 43–54, 1995.

[103] Alistair Urie, "Link layer of the adaptive transport architecture proposed for the ATDMA system," in *RACE Mobile Telecommunications Summit*, pp. 282–287, 1995.

[104] R. Steele and W.T. Webb, "Variable rate QAM for data transmission over Rayleigh fading channels," in *Wireless '91, Calgary, Alberta*, pp. 1–14, IEEE, 1991.

[105] S. Otsuki, S. Sampei and N. Morinaga, "Square-QAM adaptive modulation TDMA/TDD systems using modulation level estimation with walsh function." Electronics Letters, November 1995. pp 169-171.

[106] Norihiko Morinaga, "Advanced wireless communication technologies for achieving high-speed mobile radios," *IEICE Transactions on Communications*, vol. 78, no. 8, pp. 1089–1094, 1995.

[107] Hidehiro Matsuoka, Seiichi Sampei, Norihiko Morinaga and Yukiyoshi Kamio, "Adaptive modulation systems with punctured convolutional code for high quality personal communications systems," in *Fourth IEEE International Conference on Universal Personal Communications Record*, pp. 22–26, IEEE, 1995.

[108] Takashi Suzuki, Seiichi Sampei and Norihiko Morinaga, "Directive antennas diversity reception for an adaptive modulation system in land mobile communications," in *Fourth IEEE International Conference on Universal Personal Communications Record*, pp. 595–599, IEEE, 1995.

[109] Seiichi Sampei, Norihiko Morinaga and Yukiyoshi Kamio, "Adaptive modulation/TDMA with BDDFE for 2 mbit/s multi-media wireless communication systems," in 45^{th} *Vehicular Technology Conference*, pp. 311–315, IEEE, 1995.

[110] Toyoki Ue, Seiichi Sampei and Norihiko Morinaga, "Symbol rate and modulation level controlled adaptive modulation/TDMA/TDD for personal communication systems," in 45^{th} *Vehicular Technology Conference*, pp. 306–310, IEEE, 1995.

[111] Toyoki Ue, Seiichi Sampei and Norihiko Morinaga, "Symbol rate controlled adaptive modulation/TDMA/TDD for wireless personal communication systems," *IEICE Transactions on Communications*, vol. 78, no. 8, pp. 1117–1124, 1995.

[112] Yukiyoshi Kamio, Seiichi Sampei, Hideichi Sasaoka and Norihiko Morinaga, "Performance of modulation-level-control adaptive-modulation under limited transmission delay time for land mobile communications," in 45^{th} *Vehicular Technology Conference*, pp. 221–225, IEEE, 1995.

[113] M-S. Alouini, A. Goldsmith, "Capacity of nakagami multipath fading channels," in 47^{th} *Vehicular Technology Conference*, pp. 652–656, IEEE, 1997.

[114] Lajos Hanzo and Jason P. Woodard, "An intelligent multimode voice communications system for indoor communications," *IEEE Trans. on Vehicular Technology*, vol. 44, no. 4, pp. 735–748, 1995.

[115] J.P. Woodard J.M. Torrance and L. Hanzo, "A low delay multi-mode speech terminal," in 46^{th} *Vehicular Technology Conference*, pp. 213–217, IEEE, 1996.

[116] J. Streit and L. Hanzo, "A fractal video communicator," in 44^{th} *IEEE Vehicular Technology Conference*, pp. 1030–1034, IEEE, 1994.

[117] J. M. Torrance and L. Hanzo, "Upper bound performance of adaptive modulation in a slow Rayleigh fading channel." Electronics Letters, April 1996. pp 169-171.

[118] Laura Dossi, Guido Tartara and Fiorenzo Tallone, "Statistical analysis of measured impulse response functions of 2.0 GHz indoor radio channels," *IEEE Journal on Selected areas in Communications*, vol. 14, no. 3, pp. 405–410, 1996.

[119] Giovanni Santella and Elio Restuccia, "Analysis of frequency domain wide-band measurements of the indoor radio channel at 1, 5.5, 10 and 18 GHz," in *IEEE GlobeCom*, pp. 1162–1166, IEEE, November 18-22, 1996.

[120] W. C. Wong, R. Steele and C-E. W. Sundberg, *Source-Matched mobile Communications.* Pentech Press, 1995.

[121] K. A. Stroud, *Further engineering mathematics.* MacMillan Education Ltd, 1988.

[122] J. M. Torrance and L. Hanzo, "Performance upper bound of adaptive QAM in slow Rayleigh fading environments," in *IEEE International Conference on communication systems and IEEE International workshop on intelligent signal processing and communications systems*, pp. 1653–1657, IEEE, October 25-29, 1996.

[123] W. C. Y. Lee, "Estimate of channel capacity in Rayleigh fading environment," *IEEE Trans. on Vechicular Technology*, vol. 39, pp. 187–189, Aug 1990.

[124] Hidehiro Matsuoka, Seiichi Sampei, Norihiko Morinaga and Yukiyoshi Kamio, "Adaptive modulation system with variable coding rate concatenated code for high quality multi-media communications systems," in 46^{th} *Vehicular Technology Conference*, pp. 487–491, IEEE, 1996.

[125] J. M. Torrance D. Didascalou, and L. Hanzo, "The potential and limitations of adaptive modulation over slow rayleigh fading channel," in *IEE Colloquium on The Future of Mobile Multimedia Communications*, pp. 10/1–10/6, IEE, December 6, 1996.

[126] Bernd Friedrichs, "Report to FIRST partners on ATDMA proposal," tech. rep., Bosch Telecom GmbH, 1996.

[127] H. Nyquist, "Certain factors affecting telegraph speed," *Bell System Technical Journal*, p. 617, 1928.

[128] N. Kingsbury, "Transmit and receive filters for QPSK signals to optimise the performance on linear and hard-limited channels," *IEE Proceedings*, vol. 133, no. f, pp. 345–335, 1986.

[129] E. A. Lee and G. G. Messerchmitt, *Digital Communications.* Kluwer Academic Publishers, Boston, 1988.

[130] I. Korn, *Digital Communications.* Van Nostrand Reinhold, New York, 1985.

[131] David J. DeFatta, Joseph G. Lucas, William S. Hodgkiss, *Digital Signal Processing: A System Design Approach.* Wiley, 1988.

[132] J. M. Torrance and L. Hanzo, "Optimisation of switching levels for adaptive modulation in a slow Rayleigh fading channel." Electronics Letters, June 1996. pp 1167 - 1169.

[133] William C. Y. Lee, "Spectrum efficiency in cellular," *IEEE Transactions on Vehicular Technology*, vol. 38, no. 2, pp. 69–75, 1989.

[134] William Webb, "Spectrum efficiency of multilevel modulation schemes in mobile radio communications," *IEEE Transactions on Communications*, vol. 43, no. 8, pp. 2344–2349, 1995.

[135] R. Steele and V. K. Prabhu, "High-user-density digital cellular mobile radio systems," *IEE Proc. on Communications, Radar and Signal Processing*, vol. 132, no. 5, pp. 396–404, 1985.

[136] C.-C. Lee and R. Steele, "Signal-to-interference calculations for modern TDMA cellular communications systems," *IEE Proceeding on Communications*, vol. 142, no. 1, pp. 21–30, 1995.

[137] Esa Malkamaki, "Binary and multilevel offset QAM, spectral efficient modulation schemes for personal communications," in 42^{nd} *IEEE Vehicular Technology Conference*, pp. 325–328, IEEE, 1992.

[138] A. G. Burr, "Bounds and estimates of the uplink capacity of cellular systems," in 44^{th} *IEEE Vehicular Technology Conference*, pp. 1480–1484, IEEE, 1994.

[139] Norma C. Beaulieu, Adnan A. Abu-Dayya, "Bandwidth efficient qpsk in cochannel interference and fading," *IEEE Transactions on Communications*, vol. 43, no. 9, pp. 2464–2474, 1995.

[140] Marco Chiani, "Performance of BPSK and GMSK with multiple cochannel interferers," in 7^{th} *Personal, Indoor and Mobile Radio Communications (PIMRC) Conference*, pp. 833–837, IEEE, 1996.

[141] Athanasios Papoulis, *Probability Random Variables, and Stochastic Processes, Third Edition.* McGraw-Hill, 1991.

[142] Shahram Golestaneh, H. M. Hafez, and Samy A. Mahmound, "The effect of adjacent channel interference on the capacity of FDMA cellular systems," *IEEE Transactions on Vehicular Technology*, vol. 43, no. 4, pp. 946–954, 1994.

[143] Kazuhiko Fukawa and Hiroshi Suzuki, "Blind interference cancelling equalizer for mobile radio communications," *IEICE Transactions on Communications*, vol. E77-B, no. 5, pp. 580–588, 1994.

[144] S. W. Wales, "Technique for cochannel interference suppression in TDMA mobile radio systems," *IEE Proceeding on Communications*, vol. 142, no. 2, pp. 106–114, 1995.

[145] P. Bo Hagerman, "Downlink relative co-channel interference power in cellular radio systems," in 45^{th} *Vehicular Technology Conference*, pp. 366–370, IEEE, 1995.

[146] Hidekazu Murata, Atsushi Fujiwara and Susumu Yoshida, "Computational complexity reduction of trellis-coded co-channel interference canceller," *IEICE Transacations on Communications*, vol. E79-B, no. 3, pp. 342–351, 1996.

[147] Reza Berangi, Patrick Leung and Michael Faulkner , "Cochannel interfernce cancellation for mobile communication systems," in *Proceedings of IEEE ICUPC Conference*, pp. 438–442, IEEE, September 27-29, 1996.

[148] William Webb and Raymond Steele, "Variable rate QAM for mobile radio," *IEEE Transactions on Communications*, vol. 43, no. 7, pp. 2223–2230, 1995.

[149] J. M. Torrance and L. Hanzo, "Adaptive modulation in a slow Rayleigh fading channel," in *Proceedings of the* 7^{th} *Personal, Indoor and Mobile Radio Communications (PIMRC) Conference*, pp. 497–501, IEEE, 1996.

[150] Hong Wang and Nader Moayeri, "Finite-state markov channel-a useful model for radio communication channels," *IEEE Transactions on Vehicular Technology*, vol. 44, no. 1, pp. 163–171, 1995.

[151] Jason Paul Woodard, *Digital coding of speech using code excited linear prediction.* PhD thesis, University of Southampton, 1995.

[152] D. A. Pearce, A. G. Burr and T. C. Tozer, "Comparison of counter-measures against slow Rayleigh fading for TDMA systems," in *Colloquium on Advanced TDMA Techniques and Applications*, pp. 9/1–9/6, IEEE, 1996.

[153] Antony Acampora, "Wireless ATM: A perspective on issues and prospects," *IEEE Personal Communications Magazine*, vol. 3, no. 3, pp. 8–17, 1996.

[154] J. Williams, L. Hanzo and R. Steele, "Channel adaptive modulation," in *Proceedings of IEE Conference on Radio Receivers and Associated Systems*, pp. 144–147, IEE, 1995.

[155] D. J. Goodman, R. A. Valuenzuela, K. T. Gayliard and B. Ramamurthi, "Packet reservation multiple access for local wireless communications," *IEEE Transactions on Communications*, vol. 37, pp. 885–890, 1989.

[156] D. J. Goodman and S. X. Wei, "Efficiency of packet reservation multiple access," *IEEE Transactions on Vehicular Technology*, vol. 40, no. 1, pp. 170–176, 1991.

[157] Sanjiv Nanda, David J. Goodman and Uzi Timor, "Performance of PRMA: A packet voice protocol for cellular systems," *IEEE Transactions on Vehicular Technology*, vol. 40, no. 3, pp. 584–598, 1991.

[158] Wai-Choong Wong, "Dynamic allocation of packet reservation multiple access carriers," *IEEE Transactions on Vehicular Technology*, vol. 42, no. 4, pp. 385–392, 1993.

[159] "Recommendation G. 729: Coding of speech at 8 kbits/s using conjugate-structure algebraic-code-excited-linear-prediction (CS-ACELP)," tech. rep., ITU-T, 1996.

[160] "Recommendation H. 263: Video coding for low bitrate communications," tech. rep., ITU-T, 1996.

[161] K. G. Beauchamp, *Walsh functions and their applications.* Academic Press, 1975.

[162] Fritz Gfeller, Walter Hirt, Martin de Lange and Beat Weiss, "Wireless infrared transmission: How to reach all office space," in 46^{th} *Vehicular Technology Conference*, pp. 1535–1539, IEEE, 1996.

[163] J. M. Torrance and L. Hanzo, "Demodulation level selection in adaptive modulation." Electronics Letters, September 1996. pp 1751 - 1752.

[164] Soon-Ghee Chua and Andrea Goldsmith, "Variable-rate variable-power MQAM for fading channels," in 46^{th} *Vehicular Technology Conference*, pp. 815–819, IEEE, 1996.